High Resolution Photoelectron Studies of Polyatomic Molecules

Neil Angus Macleod

Doctor of Philosophy
University of Edinburgh
2000

Abstract.

High resolution photoelectron spectra of a number of polyatomic molecules have been obtained using Zero-Kinetic-Energy Pulsed-Field-Ionisation (ZEKE-PFI) spectroscopy. The molecules studied were trifluoromethyl iodide (CF_3I), all three geometric isomers of the aminobenzotrifluorides ($CF_3C_6H_4NH_2$) and 4-fluorobiphenyl ($C_6H_5C_6H_4F$).

The ground ionic state ($^2E_{3/2}$) of CF_3I^+ has been studied by two separate excitation schemes. The first involved a direct two-photon (one-colour) process from the neutral ground state. The spectrum observed was found to be very similar to that of the conventional photoelectron spectrum with progressions being observed in all three totally symmetric normal modes reflecting the direct Franck-Condon overlap between the two states. The spectrum is very different to that seen for CH_3I where long vibrational progressions were observed due to the stretching of the C-I bond at the one-photon level caused by the presence of dissociative states. The lack of such effects in CF_3I is ascribed to the weakness of the one-photon absorption at the wavelength required for two-photon ionisation. A second excitation scheme involved a two colour ($2 + 1'$) process via the [$^2E_{3/2}$]6p Rydberg states. The ZEKE-PFI spectra obtained allowed the assignment of the majority of the vibrational structure of the intermediate. This structure, assigned to normal mode ν_3 (the C-I stretch), has a vibrational frequency far lower (144 cm^{-1}) than either the neutral (286 cm^{-1}) or ionic (205 cm^{-1}) ground states. This is ascribed to interactions between the 6p Rydberg states and an ion-pair state.

The aminobenzotrifluorides have been studied in a two-colour ($1 + 1'$) scheme via the S_1 valence state. The high resolution of ZEKE-PFI spectroscopy allows the torsional structure of the ion to be resolved for all three isomers. This structure could be simulated using a one-dimensional rigid rotor model. Trends in barriers to internal rotation were in line with previous studies on other toluenes but some noticeable

differences were found. 2-ABTF shows substantial activity in both the CF_3 and NH_2 torsions indicating a substantial interaction between the two substituents. The electron withdrawing nature of the CF_3 makes the formation of an intramolecular hydrogen bond possible. For all three isomers considerable activity was observed in torsional transitions which are forbidden by symmetry selection rules. The appearance of such transitions is attributed to the coupling of the torsional motion to that of the high-*n* Rydberg states upon which pulsed-field-ionisation depends. That these transitions have a large intensity relative to allowed transitions is caused by the high density of torsional levels in the ion which is a consequence of the heavy CF_3 rotor.

Similar transitions have been found in an analogous experiment on 4-fluorobiphenyl. The ZEKE-PFI spectrum of this molecule is the first photoelectron study of a biphenyl for which torsional resolution has been obtained. Calculations indicate that the ionic ground state is planer but with a very flat bottomed potential. The barriers to internal rotation for three electronic states (S_0, S_1 and D_0) are found to depend upon a subtle balance between steric and electronic effects.

Acknowledgments.

The work presented in this thesis could not have been carried out with the help and support of a great many people. Firstly my supervisors, Robert Donovan and Kenneth Lawley for all their advice and support throughout my three years in their group. To the other members of the group, both past and present, for making the lab and office a pleasurable place. So thanks to Trevor, Andy, Dave, Alistair, Shiliang, Pat, John, Sandy and Robert. To the other members of the laser group (Neil, Alison, Colin, Craig and everybody else) for lots of good nights out and for any equipment I may have borrowed. Finally thanks to the secretarial staff (Margaret, Annette and Terri).

Beyond Edinburgh my family have been of great support both financial and emotional. To my mum and dad and my brother and his family, Colin, Catriona and Connor.

Finally thanks to both the EPSRC and the University of Edinburgh for providing the money to make it all possible.

Let a certain note be struck, let this or that corn be trodden on - and it may be a corn whose very existence has been unsuspected hitherto - and the most fair-minded and sweet-tempered person may suddenly be transformed into a vicious partisan, anxious only to score over his adversary and indifferent as to how many lies he tells or how many logical errors he commits in doing so.

Eric Blair (1945).

Table of Contents

Chapter 1

Introduction

This thesis presents high resolution photoelectron spectra of a number of polyatomic molecules. Previous work using the apparatus[1-4] had concentrated on diatomic molecules, particularly the halogens and their complexes with rare-gas atoms. The aim of the research presented here was to extend the range of molecules to larger more complex systems. The first of these, trifluoromethyl-iodide (CF_3I), was chosen partly because of its simplicity and its similarities with the diatomic halogens but also to assign the complicated vibronic structure of the $[^2E_{3/2}]6p$ Rydberg states. Later work focuses on the study of large amplitude motion (particuarly internal rotation) in molecular ions with substituted toluenes and biphenyls as examples. These studies are made possible by the resolution afforded by Zero-Kinetic-Energy Pulsed-Field-Ionisation (ZEKE-PFI)[5-7] which allows the torsional structure of the ion to be resolved.

The thesis is laid out in the following manner; chapter 2 presents an overview of the theory behind photoelectron spectroscopy and internal rotation while chapter 3 provides a description of the experimental arrangement. The remaining chapters present the results obtained; chapter 4 presents ZEKE-PFI spectra of CF_3I^+ ($^2E_{3/2}$) excited both directly from the neutral ground state and from the $[^2E_{3/2}]6p$ Rydberg states in a two-colour process; chapter 5 is a study of the torsional structure of the aminobenzotrifluorides excited via the S_1 valence state and chapter 6 is a similar study for 4-fluorobiphenyl. The final chapter (chapter 7) provides a brief summary and overview of the experimental work with some discussion for future work.

References.

1. J.G. Goode. PhD thesis. University of Edinburgh. 1995.
2. D.A. Beattie. PhD thesis. University of Edinburgh. 1998.
3. M.C.R. Cockett. *J.Phys.Chem.* 1995, **99**, 16228.
4. D.A. Beattie, M.C.R. Cockett, K.P. Lawley & R.J. Donovan. *J.Chem.Soc.Faraday Trans.* 1997, **93**, 4245.
5. K. Muller-Dethlefs, M. Sander & E.W. Schlag. *Chem.Phys.Lett.* 1984, **112**, 291.
6. High Resolution Laser Photoionization and Photoelectron Studies. Edited by I. Powis, T. Baer & C.Y. Ng. John Wiley & Sons (London). 1995.
7. K. Muller-Dethlefs & E.W. Schlag. *Angew.Chem.Int.Ed.* 1998, **37**, 1346.

Chapter 2

Theoretical Principles

2.1. Introduction

An understanding of the theory behind the experimental work presented in this thesis is vital. This chapter gives an overview of such theory and covers the basics of molecular spectroscopy (section 2.2.), ionic and photoelectron spectroscopy (2.3.). More detailed information is given for the directly applicable ideas behind ZEKE-PFI (2.4.) and internal rotation (2.5.).

2.2. Molecular Spectroscopy

2.2.1. Introduction

The work presented in this thesis relies on a basic understanding of the nature of electronic states and the selection rules which connect them. This section gives a brief outline of these for valence states (the example used is benzene) and Rydberg states (Hunds coupling cases).

2.2.2. Valence states

A large part of this thesis is concerned with the valence states of substituted benzenes (most importantly the first excited singlet state, S_1). This section introduces the concept of bonding in such molecules and the selection rules by using benzene itself as an example[1-5].

The carbon framework of benzene is taken as a perfect hexagon and only the six p_z orbitals are considered. The molecular orbital diagram of the interaction of these orbitals is shown schematically in figure 2.1.

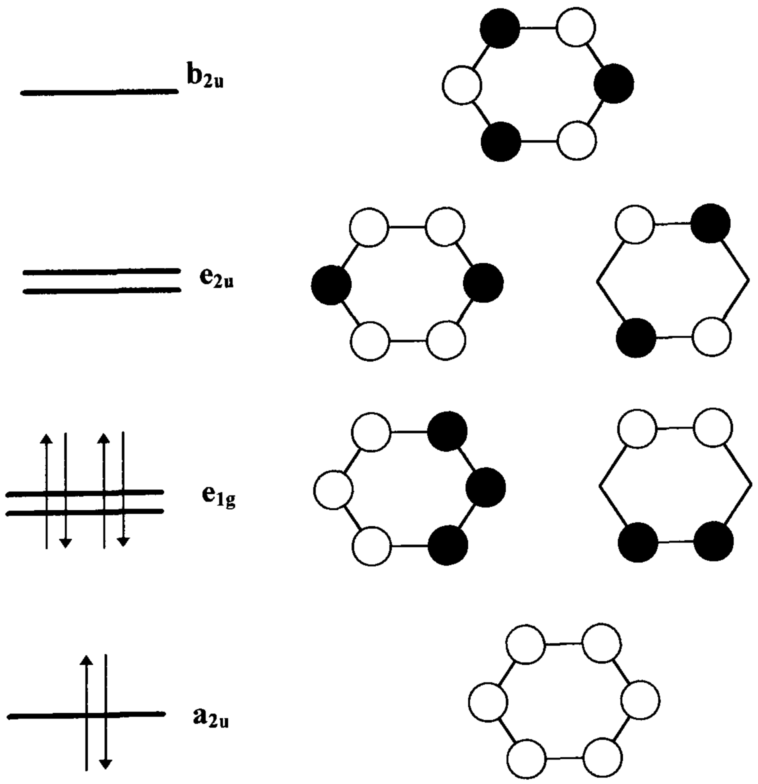

Figure 2.1. Schematic of the molecular orbitals of benzene. The electron configuration is that of the neutral ground state ($^1A_{1g}$).

The neutral ground state of benzene can be classified as having $\mathbf{a_{1g}}$ symmetry under the D_{6h} point group (for substituted benzenes the HOMO is no longer degenerate but is split into two different symmetry states due to the lower symmetry of the molecule[2]). Excitation of an electron from the e_{1g} to the e_{2u} orbital results in states that can be classified as having $\mathbf{e_{1g} \otimes e_{2u} \equiv b_{1u} + b_{2u} + e_{1u}}$ symmetry. The first selection rule is that the overall spin of the system cannot change. Since the ground state is a singlet state only transitions to singlet states are allowed. Furthermore group theory can be used to decide whether a electronic transition is allowed or forbidden. This can be done by considering the product of the symmetry of the initial and final states with that of the x, y and z axes. If the result of any one of these three products contains the totally symmetric representation of the point group ($\mathbf{a_{1g}}$ for benzene) the transition is symmetry allowed and is polarised along that particular axis. Such polarisation can have a large effect on the rotational band contour of a transition[6]. Hence for the π-π^* transition in benzene there are three transitions of which all three are spin allowed. In terms of symmetry the product of the three symmetry states with the x, y ($\mathbf{e_{1u}}$) and z ($\mathbf{a_{2u}}$) axes are $\mathbf{b_{2g} + e_{2g}}$ for the $\mathbf{b_{1u}}$ state, $\mathbf{b_{1g} + e_{2g}}$ for the $\mathbf{b_{2u}}$ state and $\mathbf{a_{1g} + a_{2g} + e_{1g} + e_{2g}}$ for the $\mathbf{e_{1u}}$ state. Thus the $\mathbf{b_{1u}}$ and $\mathbf{b_{2u}}$ states are symmetry forbidden while the $\mathbf{e_{1u}}$ state is allowed. The ultra-violet absorption spectrum of benzene vapour[7,8] shows three absorption bands which can be assigned to the three transitions; 260 nm ($\mathbf{b_{2u}}$) 200 nm ($\mathbf{b_{1u}}$) and 180 nm ($\mathbf{e_{1u}}$). The 260 nm band is assigned as the $S_1 \leftarrow S_0$ transition and appears with considerable intensity despite being symmetry forbidden. This is due to coupling of the electronic and vibrational degrees of freedom[9].

A similar scheme can be followed for monosubstituted benzenes where the S_1 transition is allowed due to the lower symmetry of the molecule (C_{2v})[2]. Vibrations can also be considered using group theory if the symmetries of the normal modes are known.

2.2.3. Rydberg states

Rydberg states are defined as states which have a higher principal quantum number than the valence orbitals and can be fitted to equation 2.1. where E is the term energy of the Rydberg state, I.E. is the ionisation threshold to which the Rydberg series converges, R is the Rydberg constant, *n* is the principal quantum number and δ is a measure of the interaction of the Rydberg electron with the ionic core and is called the quantum defect[10,11].

$$E = \mathrm{I.E.} - \frac{R}{(n-\delta)^2} \qquad \mathbf{(2.1)}$$

Each Rydberg state can be defined by three quantum numbers, *n*, the principal quantum number; *l*, the angular momentum quantum number and m_l, the magnetic quantum number. The quantum defect is *l* dependent with Rydberg states with $l > 3$ having $\delta \cong 0$. Such states have little interaction with the ionic core.

Both the Rydberg electron and the ionic core can have spin and orbital angular momentum. These couple together in different ways depending on the molecule and the exact nature of the Rydberg state. The majority of coupling cases can be described by Hunds cases which are covered in Herzbergs book[12]. As an example of this figure 2.2. shows Hunds case (c) which is relevant to low-*n* Rydberg states in molecules which have substantial spin-orbit coupling. This applies to molecules containing heavy atoms such as I_2 and methyl iodide[13,14] and is relevant to the work on CF_3I in chapter 4[15]. The other cases are given in appendix 1.

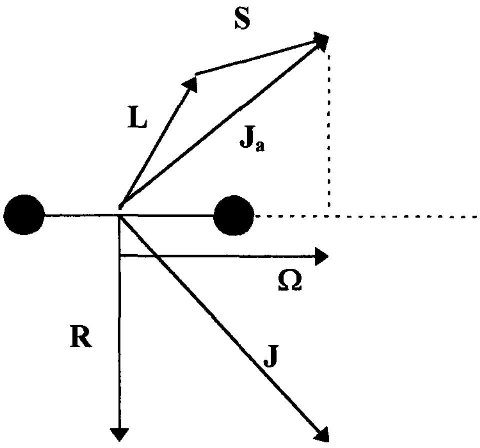

Figure 2.2. Hunds coupling case (c).

The interaction of the total spin (S) and orbital (L) angular momentum with each other is far greater than with the internuclear axis. Thus L and S form a resultant angular momentum (J_a) which in turn couples to the axis to form the total angular momentum without nuclear rotation (Ω). When the rotation of the molecule (angular momentum R) is considered the total angular momentum (J) is formed by Ω + R. Selection rules[12] for a one-photon transition are shown in equation 2.2.

$$\begin{gathered}\Delta S = 0 \\ \Delta J = 0, \pm 1 \\ \Delta\Omega = 0, \pm 1 \qquad \textbf{(2.2)} \\ 0^+ \leftrightarrow 0^+, 0^- \leftrightarrow 0^- \\ g \leftrightarrow u\end{gathered}$$

The terms 0^+ and 0^- represent the $\Omega = 0$ state where the wavefunction can be symmetric (+) or antisymmetric (-) with respect to a mirror plane along the internuclear axis (σ_v). The gerade and ungerade labels apply only to molecules which possess a centre of symmetry such as homonuclear diatomics[13].

2.3. Ionic Spectroscopy

2.3.1. Introduction

Ions are ubiquitous in nature and impact on virtually every facet of chemistry[16-18]. Given this, it is perhaps surprising that the study of ionic states has lagged behind that of neutral molecules both in the quantity of species studied and the quality of results found. The last four decades have seen rapid developments in techniques in studying ionic states of molecules. The purpose of this section is to describe ionic spectroscopy up to the mid 1980's covering both early experimental methods and the development of conventional and threshold photoelectron spectroscopy.

2.3.2. Photoionisation Selection Rules

Selection rules for ionisation[19,20] are similar to those for neutral states in that the product of the wavefunctions of the two states must contain the totally symmetric representation of the point group when multiplied by the representation of the x, y and z vectors. There is one major difference in that the photoelectron takes with it both spin and angular momentum so that the spin state of molecule can change. The spin of an electron (±1/2), means that the spin of the molecule can change (i.e. $\Delta S = \pm 1$). This allows triplet and singlet states to be accessed, for example, when the neutral state is a doublet.

2.3.3. Early Studies

The fact that ions had discernible and resolvable energy levels grew out of optical measurements of the sun and other stars whose emission and absorption lines could not be completely assigned to known neutral species[21-23]. In the early part of this century electric discharges were used to produce emission spectra that matched some astronomical observations. The emitting species were found to be small ionic species such as N_2^+, CO^+ etc. Emission was from an excited electronic state of the ion to the ionic ground state. Spectroscopic examination of the light produced allowed the determination of molecular constants for both states. Such methods continue to be applied[24] but it is almost a universal fact that only small (most commonly diatomic) molecules can be examined. Few larger ions have excited electronic states which decay by fluorescence. For example benzene does not produce any useful emission spectrum although perfluorinated benzene (C_6F_6) does. Non-radiative decay through the vibrational and rotational degrees of freedom of the molecule increases dramatically as the size of the molecule increases[25].

A different method, developed by Watanabe in the 1950's, involved a more universal property of molecules, namely their ability to be ionised by light of high enough energy[26-35]. By combining a tunable vacuum ultraviolet light source with charged particle detection Watanabe and co-workers were able to determine the ionisation energies of a wide range of molecules. The experiment is shown schematically in figure 2.3.

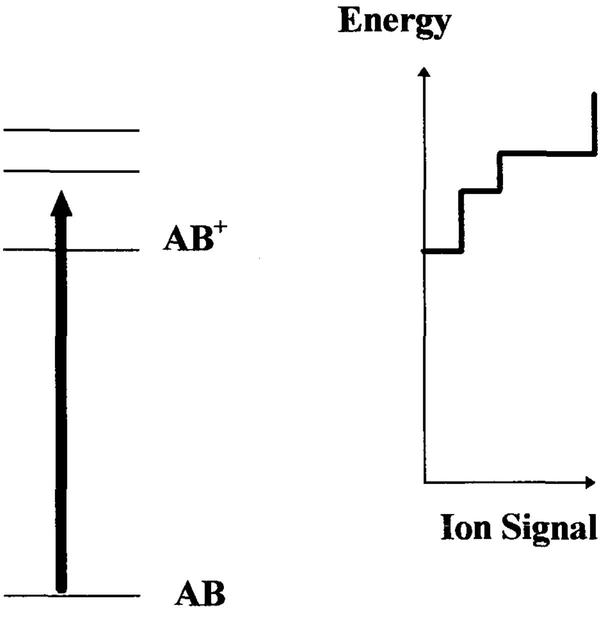

Figure 2.3: Schematic of photoionisation.

Determination of the vibrational and rotational structure of the ion proved more difficult to achieve. Although numerous examples[28,29] exist where a stepped pattern was observed in the photoionisation spectrum indicating additional ionisation channels (i.e. the vibrational structure of the ion) opening up, a large number of molecules do not show such structure. For example the CF_3 radical has a very long and gradual threshold indicating a large change in molecular geometry following ionisation[30].

The development of intense tunable laser sources allows photoionisation studies to be carried out from states other than the neutral ground state. In particular the S_1 state of molecules containing a benzene ring has been heavily used for such experiments[31-33]. These multiphoton ionisation (MPI) schemes allow the determination of ionic structure (in favourable cases) and are specific to one molecule if mass selection is used. Notable examples include aniline[32] (where there is a large change in the geometry of the NH_2 group on ionisation from the S_0 state but very little from the S_1 state) and m-cresol[33] (3-hydroxytoluene) where the torsional structure of the ion can be found by photoionisation measurements alone.

In addition a sizeable number of molecules display widespread features around the ionisation region which cannot be assigned to the vibrational structure of the ion but instead are Rydberg states of the neutral molecule converging on higher states of the ion. As such they lie above the first ionisation energy and thus can ionise into the continua of lower states of the ionic core. This obscures the ionisation threshold making photoionisation useless for determining either the ionisation energy or the structure of the ion.

The presence of Rydberg states can be used to determine the ionisation energy and the structure of the ion if enough such states are observed by use of equation 2.1. Thus measurements of VUV absorption spectra can also be useful in determining the structure of ions. Excellent examples of long Rydberg series are NO[36] and acetaldehyde[37] (CH_3CHO) for which ionisation energies can be found with an accuracy better than one wavenumber. Multiphoton techniques are also useful and such work has been carried out for benzene via the S_1 state at high resolution by Neusser[38].

None of the methods outlined in this section have the benefit of being universally applicable. A solution to this is photoelectron spectroscopy which is outlined in the next section.

2.3.4. Photoelectron Spectroscopy

Ionisation is an universal phenomenon. A technique which can use this fact and circumvent the problems limiting photoionisation and Rydberg extrapolation would be able to study any ionic species. Such a technique is photoelectron spectroscopy (PES) which was developed in the 1960's by several groups (Turner in England[39], Vilasov[40] in the Soviet Union and Siegbahn[41] in Sweden).

The principles underlying the technique are straightforward. If a photon of high enough energy interacts with a molecule electrons are produced. These photoelectrons can only be produced with a limited number of discrete kinetic energies since the energy levels of the ion are quantised. By conservation of energy and linear momentum the kinetic energy of the electron (KE) can be related to the ionisation energy of a specific rovibronic state of the ion (IE) by equation 2.3. where hν is the energy of the ionising radiation. This ionisation energy can be related to the binding energy of the molecular orbital (BE) by Koopmans theorem[42] as shown in equation 2.4. This ignores any rearrangement of the molecular orbitals following the removal of an electron but is a useful guide to the relative energies of the MO's of the molecule.

$$KE = h\nu - IE \qquad \textbf{(2.3)}$$

$$IE = -BE \qquad \textbf{(2.4)}$$

The ionisation process is shown in figure 2.4. All that is required to obtain the spectrum of the ion is the measurement of the kinetic energy of the photoelectron.

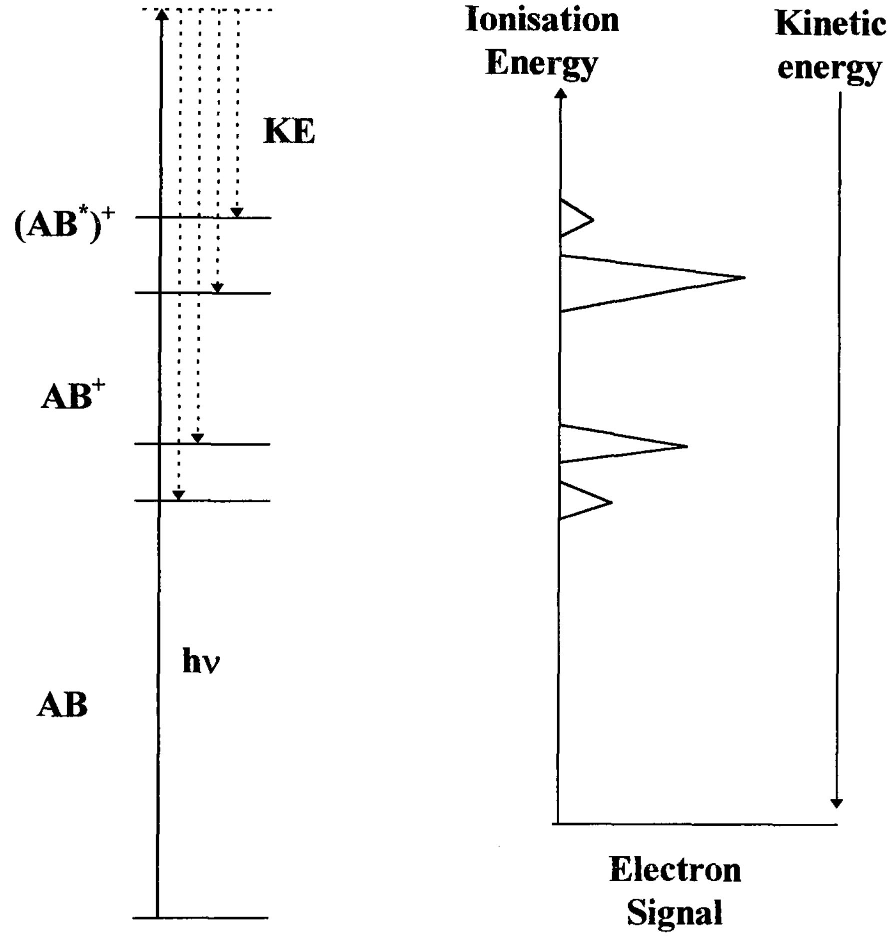

Figure 2.4: Schematic of photoelectron spectroscopy.

Two basic methods for measuring the kinetic energy of photoelectrons have been developed. The first involves use of a retarding electric field which can be adjusted in steps to only allow electrons with more than a certain energy to pass while the second method uses a 108^0 magnetic sector to separate the different kinetic energies[19-20]. It is here that the greatest drawback of conventional PES occurs and this is detailed in the next section.

2.3.5. Disadvantages of Conventional PES

In the decade after its inception photoelectron spectroscopy developed into a widely used technique and was applied to a vast number of molecules[19,20,43,44]. However several important, and ultimately limiting, drawbacks were found. Firstly the ionisation wavelength used (usually the He(I) resonance line at 584 Å although other noble gases could be used) resulted in the ionisation of all molecules present in the spectrometer. For stable molecules this presents no problems since vigorous purification methods will yield the required molecule with 100 % purity. For unstable and short-lived species such as radicals and weakly bound clusters which generally cannot be purified the interference from other species can mask the photoelectron transitions of the species of interest[45]. In addition only those states of the ion directly accessible from the neutral ground state could be detected.

With the development of tunable laser systems it is possible to ionise molecules using ultra-violet radiation by multiphoton ionisation. Combined with mass selective detection this allows one particular species in a mixture to be selectively ionised. Measurement of the photoelectron kinetic energy can then be performed[46-48]. The degree of excitation (vibrational or rotational) in the intermediate can also be selected. This time-of-flight PES method has been extensively used to study radical species. The group of de Lange in Amsterdam[47,48] have studied the hydride radicals XH where X is O, N and S. Such radicals are produced by laser photolysis of suitable precursers. Electrons are collected using a magnetic bottle spectrometer. However TOF-PES still suffers from the remaining two drawbacks of PES.

The first of these is the absolute energy calibration. This is generally carried out by placing a small quantity of calibrant gas in the spectrometer and measuring the PES. The most common calibrants are the noble gases (e.g. Ar, Ne etc.) since these provide sharp photoelectron spectra[19,20]. However this calibration must be performed at regular intervals due to build up of charge on insulating surfaces. These contact potentials can lead to a drift in the measured kinetic energy over time resulting in a poor degree of accuracy.

Much more limiting is the final drawback which is the measurement of the kinetic energy distribution of the photoelectrons. Current methods[49,50] do not allow the kinetic energy to be measured at a resolution better than approximately 25 cm^{-1} with 80 cm^{-1} being far more common[43,44]. This effectively limits conventional PES and TOF-PES to vibrational resolution although for diatomic hydrides (e.g. H_2, D_2, OH etc.) some degree of rotational resolution can be achieved since the rotational spacing is greater than the resolution of the spectrometer[51,52,47]. For large polyatomic molecule such as substituted benzenes, which have a large number of vibrational modes, even vibrational transitions may not be fully resolved[53,54]. Thus conventional PES is a universally applicable technique which suffers from a lack of resolution and cannot provide the high-resolution data that is common for neutral state techniques. A slightly different approach is required to improve the resolution of PES to such a degree that the resolution is limited by the bandwidth of the light source and is detailed in the next section.

2.3.6. Threshold PES

Conventional PES commonly uses discharge lamps containing a noble gas (He or Ne for example) which provide discrete wavelengths for photoionisation and hence are not broadly tunable. It was known that if a stream of charged particles (e.g. electrons) was accelerated in a circle by magnets that broad band photoemission occurs. This forms the basis of a light source capable of producing photons from the infra-red to the extreme ultra-violet. Such synchrotron sources[55,56] have found widespread use in chemistry, physics and biology. For photoelectron spectroscopy a tunable monochromatic light source can be produced by the addition of a monochromator. As the wavelength of such a light source is scanned over an ionisation threshold electrons are produced. At, or a few wavenumbers above, the threshold these electrons have zero (or only a small amount of) kinetic energy. By application of a small d.c. electric field and by carefully constructing the geometry of the ionisation region such threshold electrons can be preferentially detected. This technique of Threshold Photoelectron Spectroscopy (TPES) was first developed in the late 1960's and continues to be used[57-60]. A schematic of the technique is shown in figure 2.5.

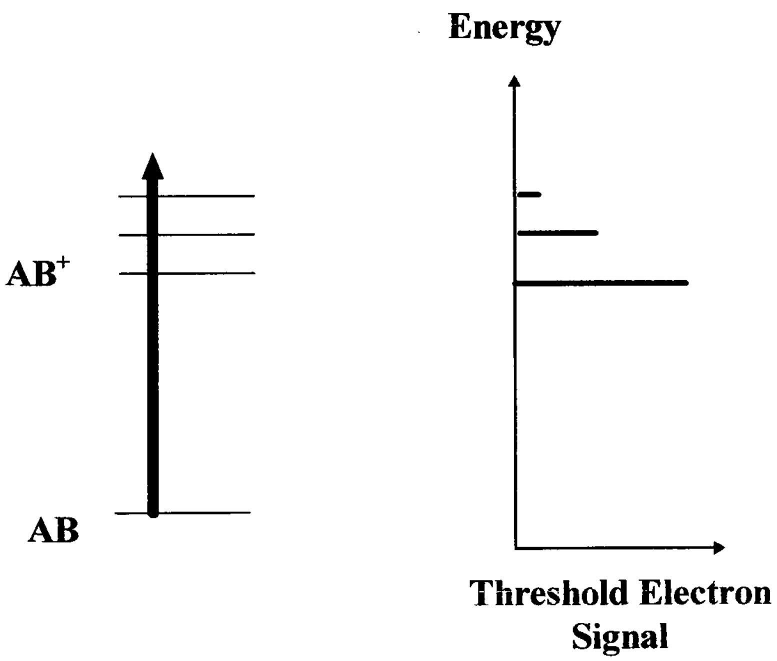

Figure 2.5: Schematic of TPES.

The resolution of TPES should therefore be limited only by the bandwidth of the light source. The emission of the synchrotron is broad band and must be wavelength dispersed to be spectroscopically useful. The bandwidth of the monochromatic beam cannot be arbitrarily reduced since there exists a minimum bandwidth beyond which the beam has too low an intensity to be useful. With early synchrotrons this generally limited resolution to a few tens of wavenumbers. However a new generation of synchrotrons are currently in use which provide far higher intensities of light and can be used to generate light with a bandwidth approaching that of a typical nanosecond pulsed dye laser (a few wavenumbers). Photoelectron studies using such light sources are in the early stages of development[61,62] but one group has reported spectra using the Advanced Light Source in Berkely with a bandwidth of 4 cm^{-1} at 12 eV. Although this is beginning to approach typical nanosecond pulsed dye laser resolution (~0.1 cm^{-1}) it is still too poorly resolved to study rotational resolution for bigger molecules (such as benzene). In addition the expense of constructing and maintaining a synchrotron facility means that beamtime is very limited. In order to solve these problems it is necessary to use a different approach, namely ZEKE spectroscopy which is described in the next section.

2.4. ZEKE-PFI Spectroscopy

2.4.1. Introduction

Pulsed nanosecond dye lasers provide a tunable light source with a relatively narrow bandwidth (typically 0.1 cm^{-1}) and, in contrast to synchrotron sources, are readily available. By combining such a light source with threshold PES it should be possible to resolve the rovibronic structure of molecular ions at a resolution limited only by the laser bandwidth. In addition the pulsed nature (typically 10 Hz) of dye lasers allows easy discrimination between electrons with and without kinetic energy. The high intensity of lasers also allow the use of multiphoton excitation schemes so overcoming the non-selectivity of conventional PES. This was the method first used in 1984 by Muller-Dethlefs, Sander and Schlag in Munich[63] to study the rotational structure of the ground ionic state of NO. This section will describe the basic ideas underpinning ZEKE PES including the somewhat surprising fact that ZEKE relies on a different mechanism to TPES, namely the delayed field ionisation of high-*n* Rydberg states converging on the ionic thresholds.

2.4.2. The Initial Concept

The initial thought behind the first ZEKE experiment was that it was essentially using pulsed lasers to measure the threshold photoelectron spectrum. In contrast to the pseudocontinuous emission of synchrotron sources a dye laser produces nanosecond pulses at a relatively slow repetition rate (typically 5 or 10 Hz). Thus the detection of threshold electrons was slightly different from that of TPES and is outlined in figure 2.6. The principle is simple. By simply waiting for a few microseconds any electrons with kinetic energy will have moved away from the focus of the laser (an electron with 1 cm^{-1} of kinetic energy will move ~0.7 cm in one microsecond). Pulsing an electric field on after this delay will result in different flight times for zero-kinetic energy (ZEKE) electrons and those with kinetic energy. In practice a long enough delay time will result in all non-ZEKE electrons leaving the extraction region and not being detected (typical ionisation regions are only a few cm across). Using such a scheme Muller-Dethlefs and coworkers were able to fully resolve the rotational structure of the ionic ground state of NO where the spacing is of the order of a few wavenumbers[63]. This was a vast improvement over previous PES studies[64].

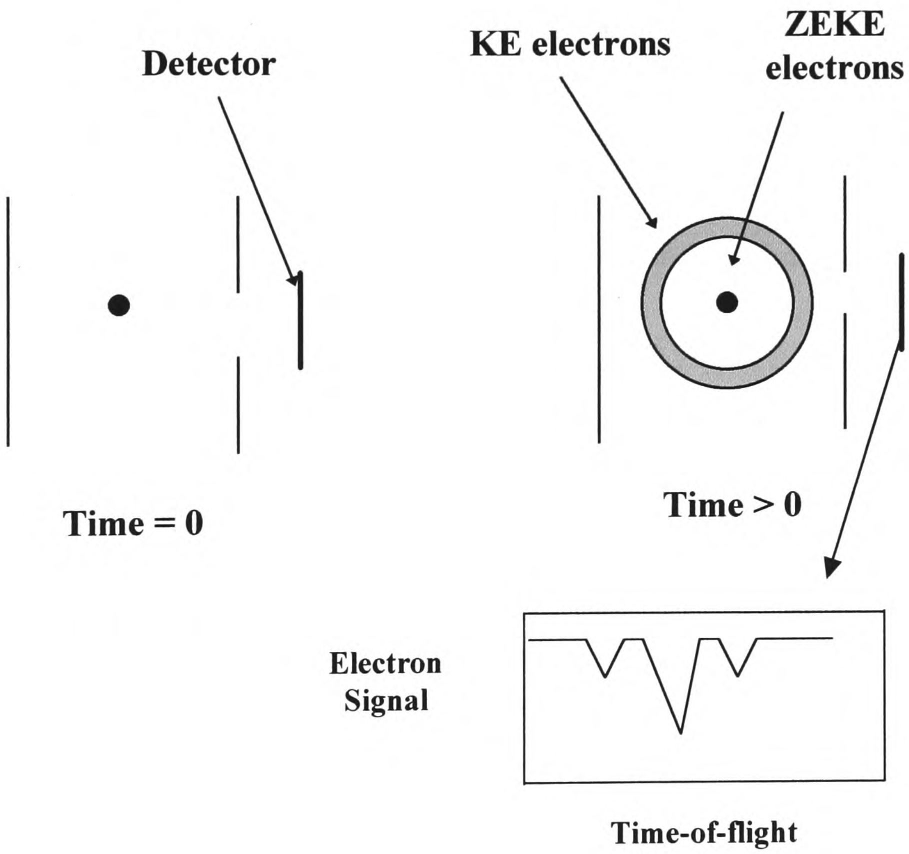

Figure 2.6: Schematic of discrimination of ZEKE electrons.

2.4.3. Pulsed Field Ionisation

In addition to the rotational structure the ionisation energy of NO could also be measured (74719 cm^{-1})[65]. This could be compared to the value obtained by extrapolation of Rydberg series[36,66] converging on the ground rotational state of the ion (74722 cm^{-1}) leading to a discrepancy far beyond even the worst case error bars. This discrepancy could not be ascribed to rotational effects since full rotational resolution was obtained for both the Rydberg states and the ion. In addition the Rydberg series were very long and had been interpreted by a multi-channel quantum defect approach. The conclusion that was reached was that the ZEKE experiment does not involve direct ionisation but consists of excitation to high-*n* Rydberg states converging on the various rotational states of the ionic core. During the delay time any prompt photoelectrons will disperse while the neutral Rydberg states remain in the excitation volume. The application of an electric field after the delay ionises the Rydberg neutrals to produce electrons which are detected at the same time-of-flight as true ZEKE electrons[65,67].

Since the value of *n* is so high the Rydberg state can be considered as two distant point charges so the interaction between them can be approximated by a coloumbic potential as shown by the lighter curve in figure 2.7. This potential is symmetric about the ionic core. Application of a homogeneous electric field (E) tilts this potential (bolder curve) to form a saddle point which lies at an energy proportional to the square root of the electric field.. The Rydberg states lying above this saddle point are no longer bound to the core and can ionise. To obtain a field-free value for the ionisation energy it is necessary to measure the transition energy at a variety of extraction voltages and extrapolate to zero field[68]. This can be done in a succession of scans or in one scan by programming a stepped voltage pulse. Figure 2.8. shows the origin band of CF_3I^+ ($^2E_{3/2}$) at a variety of extraction voltages. As the voltage is lowered the band shifts to higher energy. This mechanism also allows the detection of the ion produced with the result that a mass-resolved ZEKE spectrum can be obtained. This technique (Mass Analysed Threshold Ionisation or MATI) is particuarly useful for studying the fragmentation dynamics of molecular clusters[69,70].

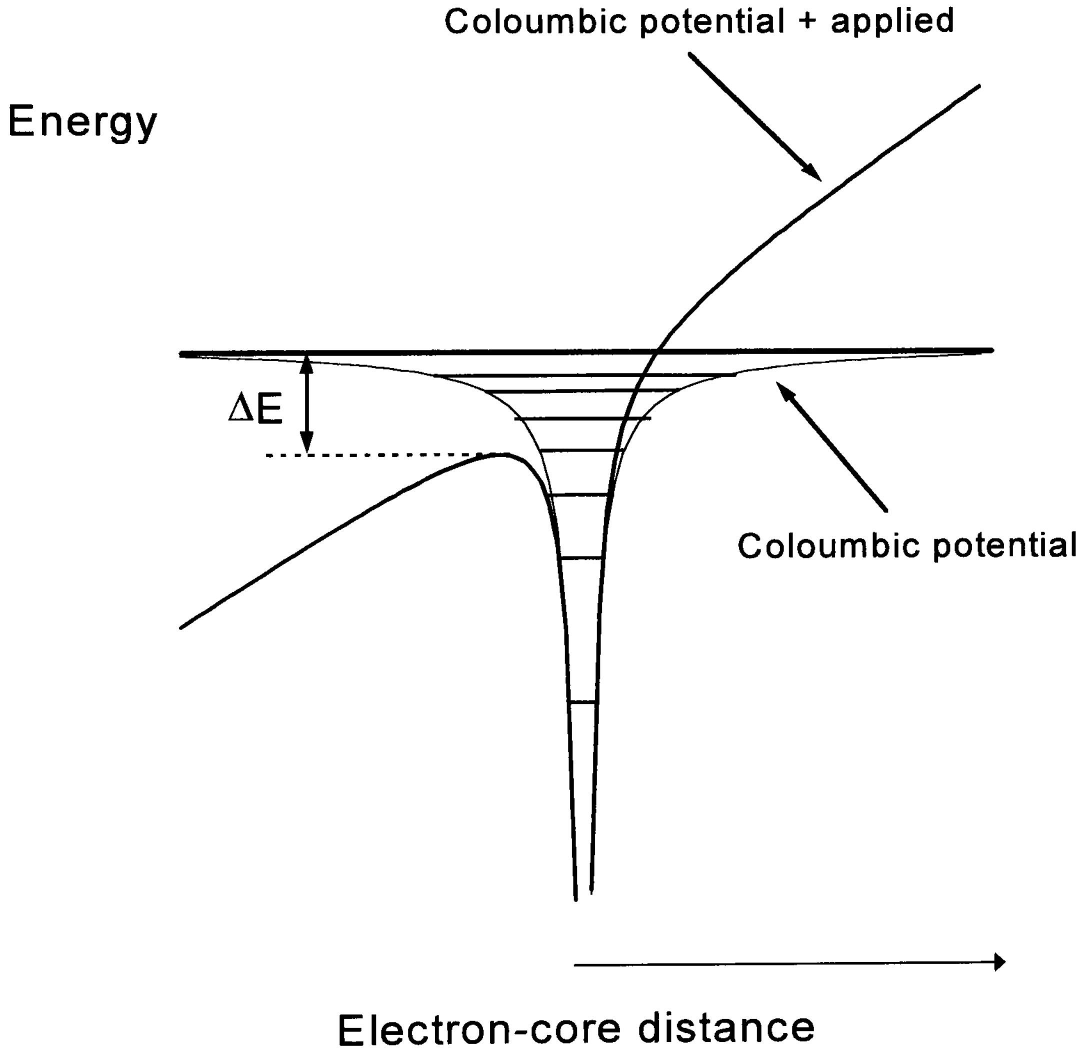

Figure 2.7: Pulsed Field Ionisation. The lighter curve represents the coulombic potential between the electron and the ionic core. The bold curve shows the effects of an electric field imposed on such a potential. The energy from the saddle point to the ionisation threshold (ΔE) is proportional to the square-root of the applied electric field.

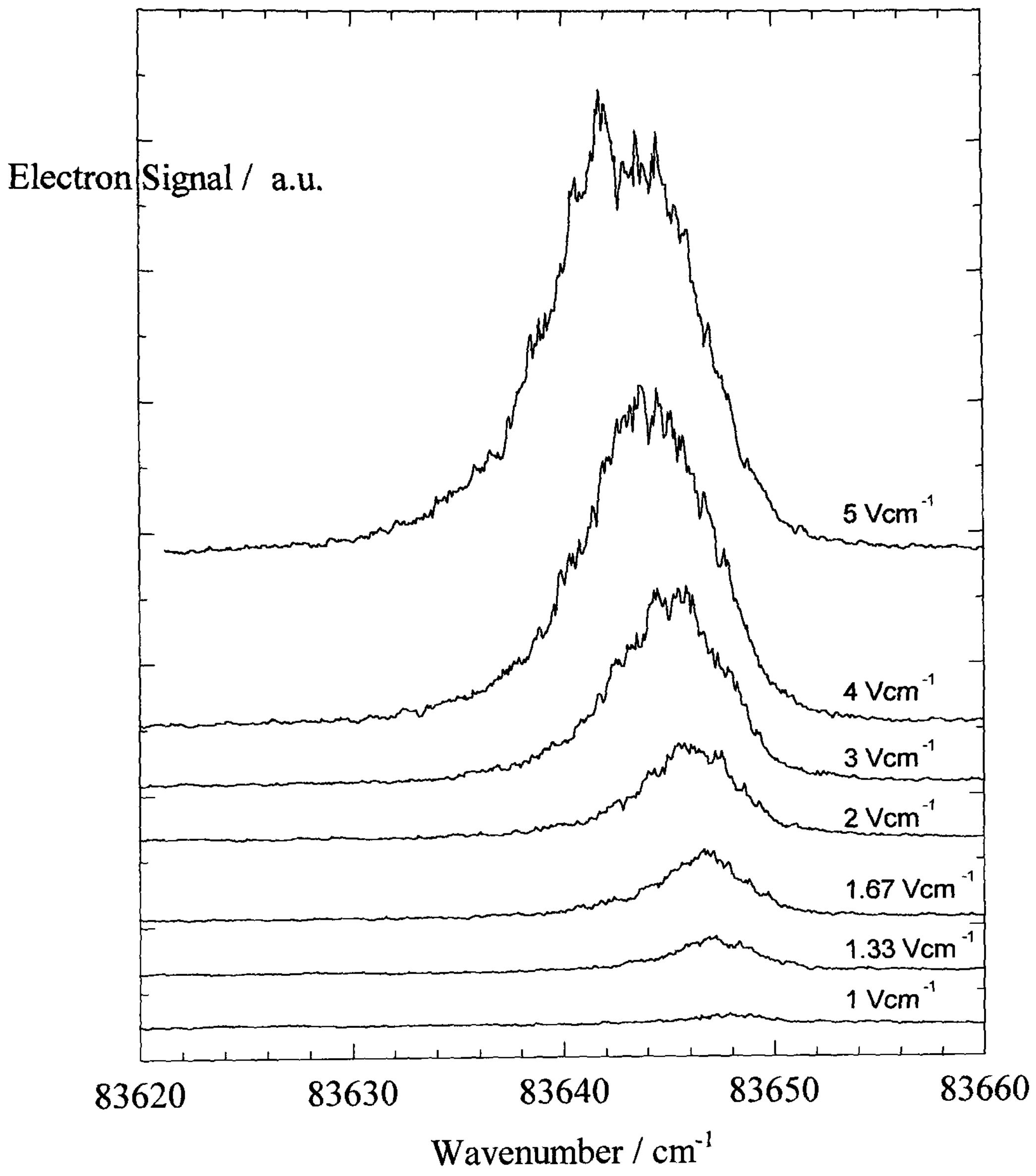

Figure 2.8: The origin band of CF_3I^+ ($^2E_{3/2}$) obtained at a variety of extraction voltages in a (2+1') process via the [$^2E_{3/2}$] 6p Rydberg states. The intermediate state was the origin band of the second Ω = 2 Rydberg state (see chapter 4).

Although the mechanism accounts for the observed discrepancy between the two ionisation energies there remains one major problem in that the Rydberg states populated have lifetimes of typically only a few nanoseconds[65,68] and would not be expected to be detected after a delay of a microsecond (recent studies have shown that in some molecules and under the right conditions the Rydberg states can survive for tens of microseconds[71,72]). As an example of this figure 2.9. shows the origin band of CF_3I^+ ($^2E_{3/2}$) scanned after different delay times. A photoelectron spectrum is still detectable after 24 μs. The next section describes the means by which such states survive for much longer than predicted.

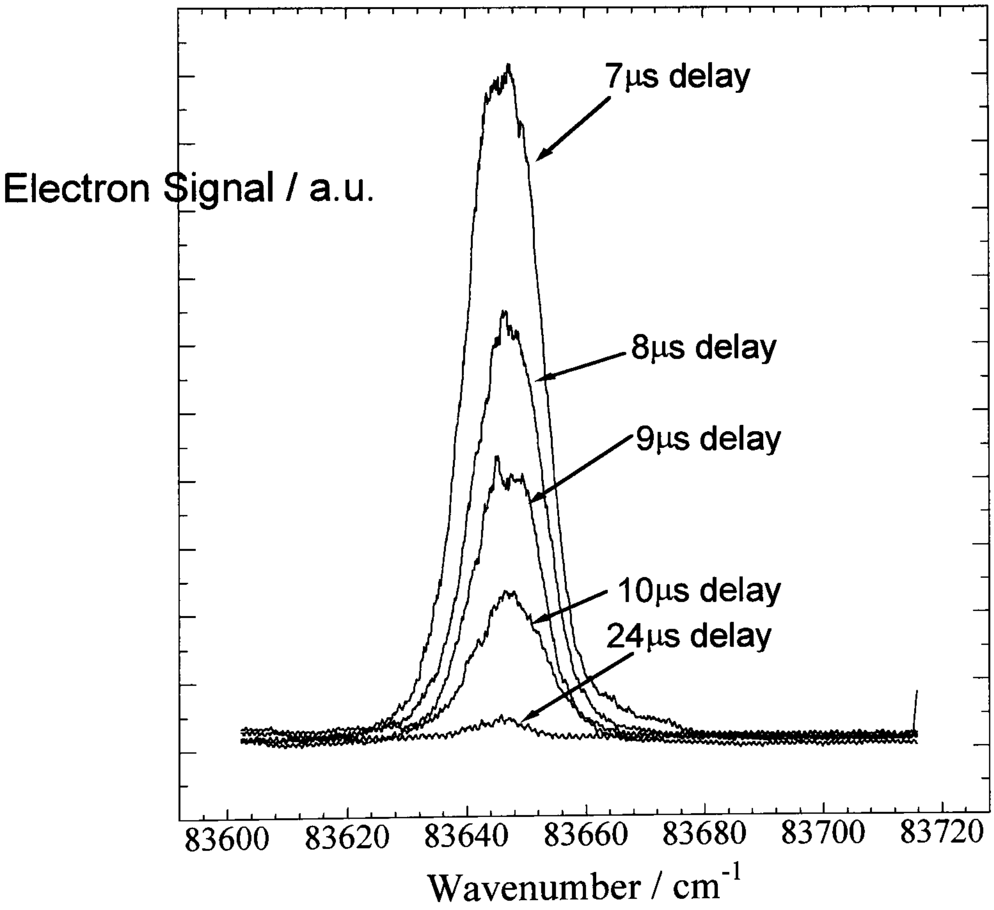

Figure 2.9: The origin band of CF_3I^+ ($^2E_{3/2}$) at a number of delay times. The intermediate used was the same as in figure 2.8.

2.4.4. Stabilisation of high-*n* Rydberg states

The dependence of various properties of Rydberg states on principal quantum number[73] is shown in table 2.1. Of these the most relevant is the lifetime which scales as n^3 in the absence of any other effects. Extrapolation of measured lifetimes for relatively low-*n* Rydberg states leads to a lifetime for n~200 of only a few nanoseconds[67]. Due to the selection rules the angular momentum of the system can only be changed by one unit per photon[12] so the Rydberg states accessed in typical ZEKE-PFI experiments can only have relatively low values of l. Such Rydberg states have large quantum defects and interact readily with the ionic core. Decay mechanisms such as predissociation can only occur in the region of the core[72]. Therefore any Rydberg state which penetrates near to the core can undergo rapid decay and would not be detected in a ZEKE-PFI experiment. The conclusion must be that the field-ionised Rydberg states are not those which are initially populated by the laser but instead are more stable states formed from the initial states.

Property.	Dependence.
Lifetime	n^3
radius	n^2
polarisability	n^7
energy spacing	n^{-3}

Table 2.1: Dependence of properties of Rydberg states on principal quantum number, *n*.

Several ideas have been suggested but the one which explains the experimental observations most satisfactory is the mechanism first suggested by Chupka[74] in 1993.

This involves the initial population of low angular momentum Rydberg states by the laser pulse followed by the formation of high angular momentum states. Such states have zero quantum defects and hence do not penetrate to the core. Thus their lifetimes are far longer than the low-*l* states first populated.

Chupka identified two complimentary sources of such Rydberg state mixing, homogeneous and inhomogeneous electric fields. Although such fields have been measured to be relatively small (~50 mVcm^{-1}) they can have a huge effect due to the nature of Rydberg states. For high values of *n* the Rydberg electron can be considered to have three separate regions[75] as shown in figure 2.10.

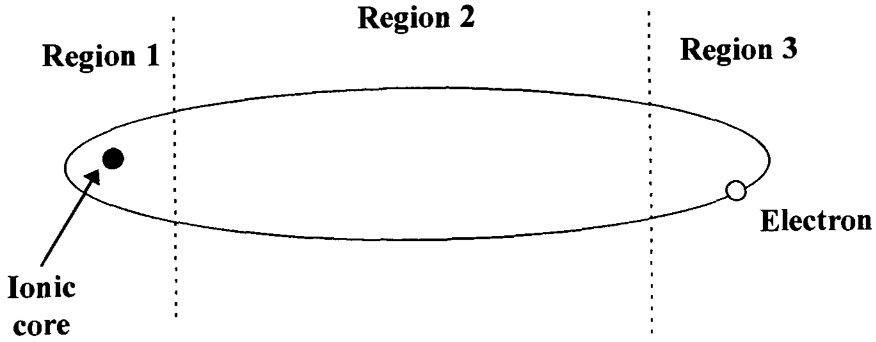

Figure 2.10: Rydberg electron.

Region 1 is where the electron passes close to and interacts with the ionic core. Region 2 is the Coulombic area where the core and electron can be considered as two distant point charges and hence have a 1/r potential. The final region is the point at which external fields have a similar or greater magnitude than the coulombic attraction of the ionic core. It is this region which is important for ZEKE-PFI spectroscopy since the polarisability of a Rydberg state scales as n^7. For ZEKE the principal quantum number is of the order of 200 so such states are very susceptible to electric fields (in addition the density of Rydberg states at this value of n is also very high ($\propto n^3$)).

The mechanism of Chupka can be quantitatively understood by considering first the action of homogeneous fields followed by inhomogeneous. The coulombic potential has spherical symmetry[68,76,77]. When a homongeneous electric field is present the symmetry is reduced to cylindrical with the long axis of the cylinder aligned with the electric vector of the field. This means that l is no longer a good quantum number and the state now consists of a mixture over all possible l states. The projection of l onto the axis remains defined so m_l is a good quantum number. The net result of this is that each of the Rydberg states initially populated have now gained substantial high-l character and have a greatly extended lifetime. Since l can take the values of 0 up to n-1 and because states with $l > 3$ have essentially infinite lifetimes the increase in lifetime is approximately a factor of n resulting in a lifetime dependence of n^4.

Even this degree of enhancement does not account for experimental observations. The effect of an inhomogeneous field is to further reduce the overall symmetry of the system such that m_l is no longer a good quantum number. Hence mixing of m_l states can occur. High m_l states do not have any inherent lifetime effects but their effect on the lifetime can be explained by reference to figure 2.11. A state with angular momentum l can have m_l values of l, l-1,........-l giving a total of $2l + 1$ levels. Thus if m_l is mixed by inhomogeneous fields statistical effects will favour the high-l states. The net result is that the lifetime is extended by another factor of n to n^5 which is more in accord with experimental observations[76,77].

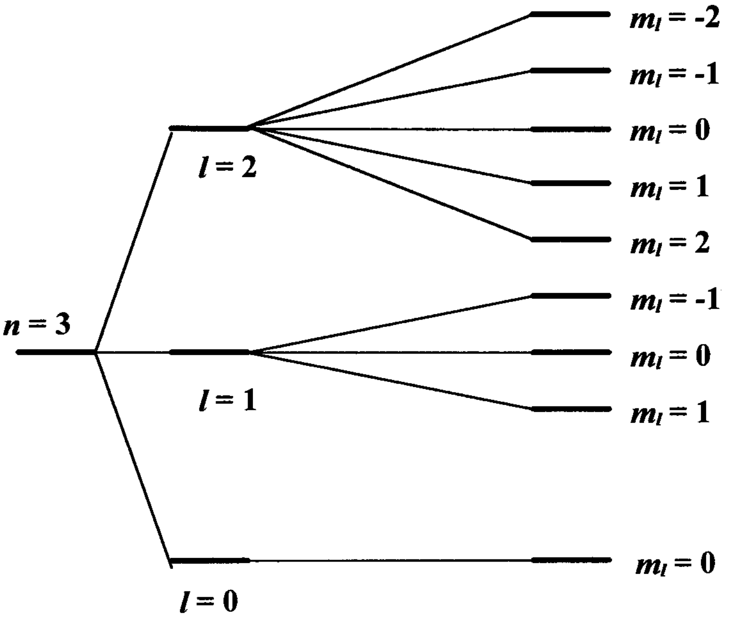

Figure 2.11. The n, l and m_l levels of a Rydberg state for n = 3.

The effects of electric fields on a Rydberg state can be considered more quantitatively by the Stark effect[78-82]. For the hydrogenic case, where the quantum defect is zero, the situation can be described by the linear Stark effect if the field is small. This is shown in atomic units in equation 2.5. where F is the electric field, n is the principal quantum number and n_1, n_2 are parabolic quantum numbers which vary from n-1 to 0. These follow the sum given in equation 2.6. where m is the magnetic quantum number.

$$E = -1/2n^2 + 3/2\,F(n_1 - n_2)n \quad \textbf{(2.5.)}$$

$$n = n_1 + n_2 + |m| + 1 \quad \textbf{(2.6.)}$$

Hence the Rydberg state is now defined by the quantum numbers, n, n_1, n_2 and m with l no longer a good quantum number and is replaced by n_1-n_2 which is a combination of l states. As an example of this the n = 3 Rydberg manifold has l = 2, 1 and 0 and m = 2, 1, 0, -1 and -2. In the presence of a small electric field these are split into states with n_1 - n_2 = 2, 1, 0, -1 and -2. These are shown in figure 2.12.

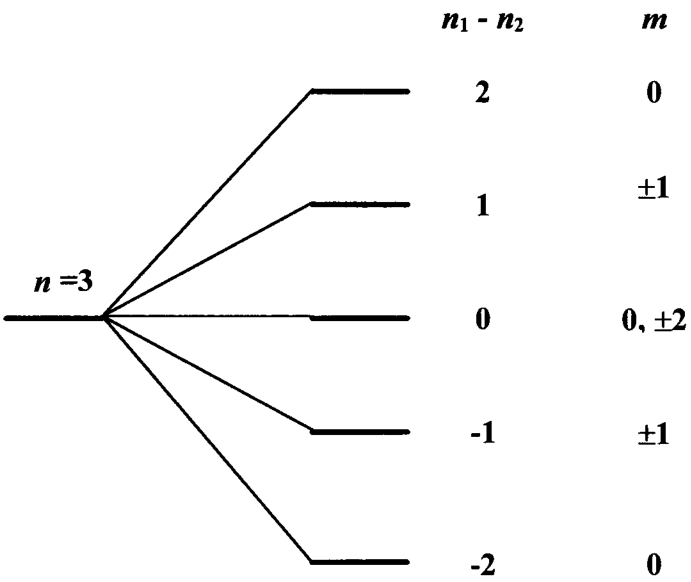

Figure 2.12. Linear Stark effect on an n = 3 hydrogenic Rydberg manifold.

For higher fields second or higher order effects must also be considered. For the type of Rydberg states (n > 100) examined in ZEKE-PFI interactions between Stark levels of different n manifolds are also a factor since typical laser bandwidths cover several different values of n. This is even more crucial in non-hydrogenic atoms[80,81] where the Rydberg states of the same n are not degenerate although states with l > 3 which have zero quantum defects can be treated in this way. States with quantum defects have to be treated using second order Stark splitting. This leads to considerably more complicated energy maps (see references 80-82 for examples) with multiple avoided crossings of states. The situation is even more complicated for molecular systems which have Rydberg series converging on different vibrational and rotational states of the ion.

Experimental proof for such effects remain of interest to several groups[72,83-85] and it is now widely accepted that the two mechanisms outlined in this section are the cause of the extended lifetimes of high-n Rydberg states. Prior to the development of ZEKE, Rydberg states of the alkali metals[80-82] with n in the range 10-40 were studied with regard to the Stark effect. For states with n more in line with those used in ZEKE experiments recent work on NO (n = 70-130) the states undergo a significant increase in lifetime[83] when a d.c. field of 50 mVcm^{-1} is applied. However the opposite effect has been observed for fields greater than 200 mVcm^{-1} where a decrease in lifetime has been observed for several molecules including NO[86] and benzene[72]. This has a particularly large effect on the lower n states (at the red end of the ZEKE band, $n \approx 150$) and has been attributed to increased coupling of the Rydberg states to the dissociative channels by the electric field.

The effects of ions on ZEKE lifetimes has been more difficult to establish experimentally with several early studies[87,88] reporting no change in lifetime with ion density. More recent studies have shown that only very small ion densities[72,84] are necessary for lifetime enhancement and that the early studies were carried out at densities where the effect was saturated.

The behavior of the ionisation mechanism has also been studied[68,74] and found to be overwhelmingly diabatic for typical ZEKE conditions (field shift of approximately $4\sqrt{E}$ in wavenumbers where E is in Vcm^{-1}) in line with the prediction of Chupka[74]. He ascribed this to the combined effects of a fast rising extraction pulse and extensive m-mixing by the effects of ions. This has a crucial effect on the resolution obtainable using ZEKE-PFI spectroscopy. Simply applying a smaller extraction field to maximise resolution is not feasible since a field of approximately 1 mVcm^{-1} is required to obtain a resolution of 0.1 cm^{-1}. Such small fields result in a great reduction in electron signal and limit the minimum field useable. In addition the stray electric fields[83] present in most ZEKE-PFI spectrometers have been estimated to be of a similar magnitude (~ 10-50 mVcm^{-1}). A more practical method uses more than one field to obtain a resolution of 0.1 cm^{-1}. This slicing method[68] uses two fields of similar magnitude (V_1 and V_2). The first field (V_1) removes the high-*n* Rydberg states down to a depth of $4\sqrt{V_1}$ while the second (V_2) which is slightly greater than the first pulse extracts the remaining Rydberg states down to $4\sqrt{V_2}$. The limit of resolution is $\Delta E = 4\sqrt{V_2} - 4\sqrt{V_1}$. Using such a scheme it is possible to obtain ZEKE spectra with a resolution[68] of 0.1-0.2 cm^{-1} which allows the full rotational structure of the benzene cation to be resolved. An alternative technique is to use a very high resolution laser system which is capable of resolving the individual Rydberg states[38]. Extrapolation of these Rydberg series to infinity by use of equation 2.1. yields very accurate ionisation energies of both the ground state and the rovibronic levels of the ion.

2.4.5. Intensities of Photoelectron Transitions

Conventional photoelectron spectra are an excellent example of two of the most important principles of molecular spectroscopy; the Born-Oppenheimer approximation and the Franck-Condon principle[19,20]. The first of these states that an electronic transition occurs on such a rapid timescale that the much heavier (and slower) nuclei have no time to adapt to the new geometry of the molecule. The transition is considered to be vertical. The Franck-Condon principle makes use of this to say that the transition probability is proportional to the square of the overlap intergral of the wavefunctions of the two states. This is shown in equation 2.7. where ψ_1 and ψ_2 are the wavefunctions of the two states and $d\tau$ represents integration over all space[89].

$$P \propto \left[\int \Psi_1 \Psi_2 d\tau\right]^2 \qquad \textbf{(2.7)}$$

The wavefunctions have both electronic and vibrational components. The Born-Oppenheimer approximation allow the separation of these components so that equation 2.8. is now appropriate where ψ^1_{vib} and ψ^2_{vib} are the wavefunctions of the vibrational motion and G is the electronic transition moment.

$$P \propto [G\int \psi_{1\mathrm{vib}}\psi_{2\mathrm{vib}}dt]^2 \qquad \textbf{(2.8.)}$$

Hence P depends on G which varies slowly with the internuclear coordinates. For a conventional photoelectron experiment the relative kinetic energies of the bands are different so G is different[19-20]. Over the vibrational sub-structure of a photoelectron band this will not vary a great deal and so can be treated as a constant.

These approximations have been a great success for conventional PES with the vast majority of spectra showing intensities consistent with calculated Franck-Condon factors. However there are a few cases in which the approximations appear to break down. The best example of this is the spectrum of molecular oxygen where the photoelectron spectrum observed agrees with Franck-Condon factors when the ionising radiation is the He(I) line[90] at 22.22 eV. When a lower energy line (the Ne(I) line at 16.84 eV) is used the spectrum observed[91] is very different with many more vibrational states observed. This can be attributed to the presence of a broad autoionising resonance around 17 eV. The photoelectron spectrum is a combination of the direct FCF from the neutral ground state and the indirect ones from the autoionising state. The appearance of Franck-Condon forbidden transitions by such a mechanism has been found to be more prevalent for threshold techniques[57-60, 68,92,93].

For TPES any autoionising state which lies near (within the bandwidth of the light source) a state of the ion can produce photoelectrons which are detected as threshold electrons. Typical bandwidths for synchrotron sources are several tens of wavenumbers so the likelihood of a coincidence is very high[59,60,68]. Hence most threshold photoelectron spectra show extensive activity in Franck-Condon forbidden transitions[94,95].

For ZEKE-PFI the situation is a little different since the bandwidth of the light source is much smaller (typically less than a wavenumber) and the mechanism involves the excitation of neutral states and not direct ionisation. This means that an autoionising state (usually a low-*n* Rydberg state converging on a higher state of the ion) must lie within a few wavenumbers of the high-*n* Rydberg (or ZEKE) states which are detected by pulsed-field ionisation. The mechanism is termed field-induced (or forced) autoionisation[96,97] and is shown in figure 2.13.

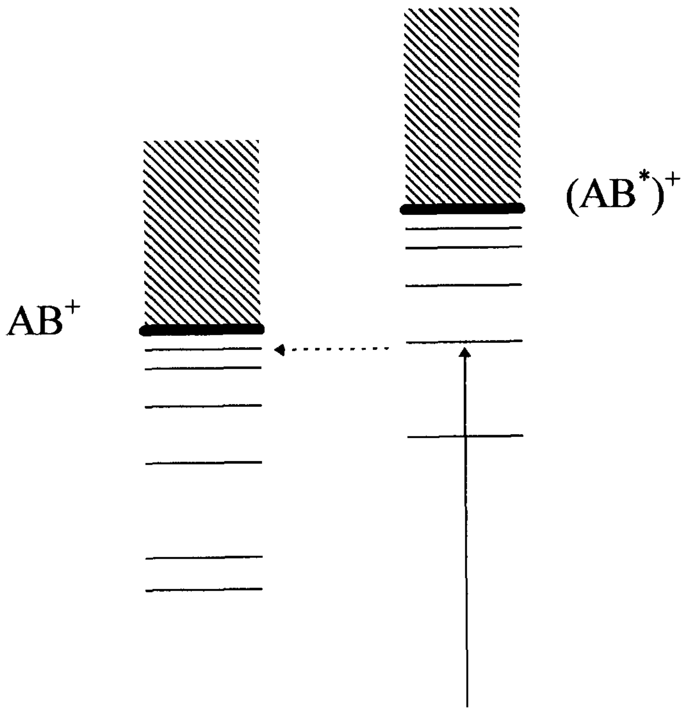

Figure 2.13. Field-induced autoionisation.

Such a mechanism requires that the two states lie close in energy, that there is efficient coupling between them on a timescale comparable to that of the decay of the low-*n* state and that the transition probabilities to the two states are different. If the first two conditions are met then there are two possible outcomes of such interaction. If the transition probability to the ZEKE states is greater than that of the low-*n* state then the ZEKE states will be depleted and so appear weaker than predicted. This has been observed for H_2 by Softley and co-workers[98] but such depletion is more common when the ZEKE states interact with a continuum and can occur for every state of the ion above the first ionisation threshold. For halogen containing molecules[99,100] (e.g. I_2, IBr, HCl etc.) the ground ionic state is split into two components by spin-orbit coupling. It has been found that the ZEKE-PFI spectrum of the upper state is generally weaker than the lower due to the depletion of the ZEKE states of the upper state into the continuum of the lower.

For the second case where the transition to the low-*n* Rydberg state is far more intense than that of the ZEKE states transitions to Franck-Condon forbidden levels of the ion can occur. Such non Franck-Condon behavior has been found for many molecules[92,93]. In general this mechanism appears to require the coincidence of the low-*n* states with the ZEKE states. Guyon and co-workers have proposed a mechanism[101] where the states are coupled through a neutral repulsive state. Recent work on O_2 by Hepburn[102] has found that a low-*n* Rydberg state is not always necessary and coupling can be direct between the ZEKE states and the repulsive state.

In conclusion it can be said that transition intensities in ZEKE-PFI can be easily distorted from direct Franck-Condon factors by autoionisation and as such care must be taken when assigning spectra on this basis alone.

2.5. Internal Rotation

2.5.1. Introduction

Low frequency (large amplitude) vibrations such as internal rotations or inversions are a subject of intense interest to chemists both in terms of theory and in the practical determination of the conformation of larger molecules[103-130]. Such vibrations display very different characteristics to those of higher energy vibrations and as such require a different approach. The purpose of this section is to describe the theoretical methods necessary to study the internal rotation problem. This covers the symmetry of the energy levels involved and the various selection rules for transitions between torsional states as well as a summary of the methods used to calculate barriers to internal rotation. The main example used is that of a threefold rotor (e.g. CH_3) attached to a system which has no other symmetry elements about the internal rotation axis such as propene and ortho and meta substituted toluenes. This is one of the simplest and clearest examples and has been extensively studied[103-130].

2.5.2. Non Rigid Molecules

For a rigid molecule conventional group theory is adequate to describe the normal modes of vibration and classify their symmetry species. However, for a molecule which has a low frequency vibration that alters the point group of the molecule, this is no longer adequate to describe the molecule. For example figure 2.14. shows the staggered and eclipsed forms of ethane. In conventional point group theory the staggered form has D_{3d} symmetry while the eclipsed is classified under D_{3h}. In order to analyse the molecule correctly a rigid model is no longer useful.

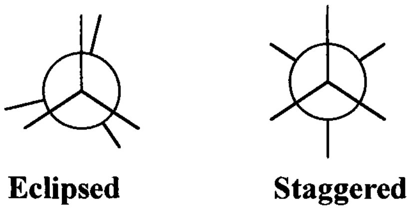

Figure 2.14: Conformations of ethane. The eclipsed conformer has been moved slightly to allow the second methyl group to be observed.

A new way of treating such molecules was developed by Longuet-Higgins[103] and others[104] by considering symmetry operations which swap (or permute) identical nuclei and those which invert the molecule through the center of mass. Such operations leave the overall geometry of the molecule unchanged. The entire set of operations is called the complete nuclear and permutation (CNPI) group. This contains all valid permutations and inversions and can be a very large and clumsy construct. To simplify the situation it is only necessary to consider only those operations that are energetically feasible on the scale of the experiment. The resulting operations are called the molecular symmetry group[104].

An example of this is a methyl rotor in molecules such as propene or ortho substituted toluenes[105,106]. Although interchange of the protons and carbon nuclei of the alkene or benzene parts of the molecule is a valid permutation such a change requires the breaking of molecular bonds. Hence such operations are not energetically feasible and can be ignored. This leaves the permutations and inversions of the methyl group which shown in figure 2.15. E is the identity while (123) denotes the rotation of the rotor such that proton 1 moves to position 2, 2 moves to 3 and 3 to1. $(12)^*$ indicates the interchange of protons 1 and 2 followed by inversion of the whole molecule. Of these operations E^* is the inverse of E as are (123) and (321). The operations (12), (23), (31) and E^* change the handedness of the rotor in that the rotor has a clockwise rotation from 1 to 2 to 3 while the original molecule is anticlockwise as drawn in figure 2.15. These operations require the breaking of bonds and hence are not energetically feasible. The remaining operations E, (123), (321), $(12)^*$, $(23)^*$ and $(31)^*$ can be counted into three separate classes (E, (123) + (321) and $(12)^*$, $(23)^*$ and $(31)^*$ to form the molecular symmetry group G_6. This group is isomorphous with the rigid point group C_{3v} (symmetry elements E, C_3 and σ_v) and the symmetry labels remain the same (**a**$_1$, **a**$_2$ and **e**). The G_6 group is shown in table 2.2. For the situation where the rest of the molecule has some permutation/inversion symmetry (for example toluene where the ring has a C_2 axis) each of the operations listed above exists but in addition there are new operations which are a combination of the C_2 axis of the ring (denoted (AB)) with the symmetry of the rest of the molecule. Such molecules are classified under the G_{12} group (isomorphous with D_{3h}) which is shown in table 2.3.

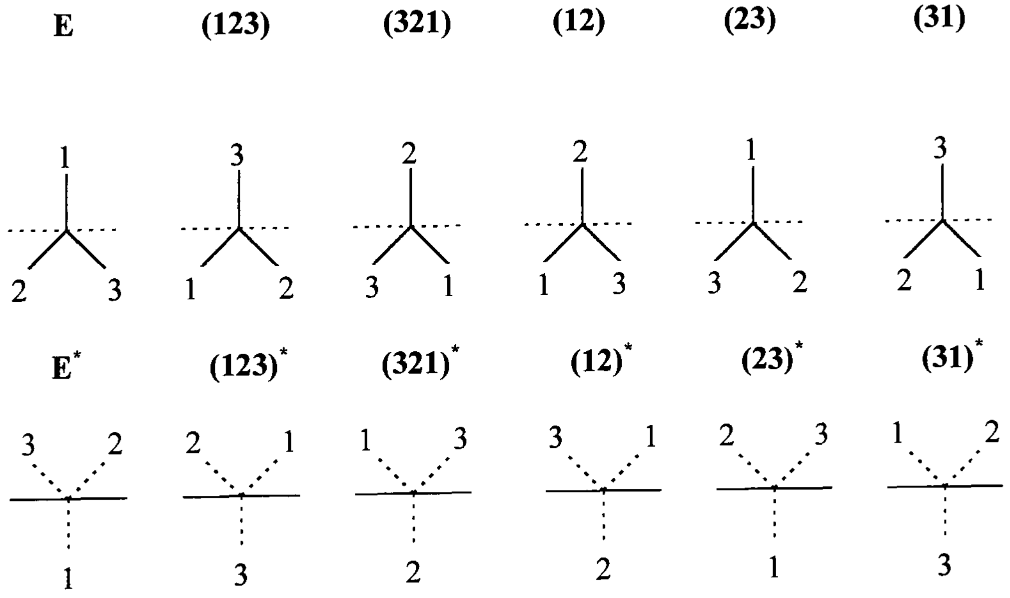

Figure 2.15. Permutation and inversion symmetry operations for a methyl rotor.

Symmetry label.	**E** **[1]**	**(123)** **[2]**	**(23)*** **[3]**
A_1	1	1	1
A_2	1	1	-1
E	2	-1	0

Table 2.2: The G_6 molecular symmetry group.

Symmetry label	**E** **[1]**	**(123)** **[2]**	**(23)*** **[3]**	**(45)** **[1]**	**(123)(45)** **[2]**	**(23)(45)*** **[3]**
A_1'	1	1	1	1	1	1
A_2'	1	1	-1	1	1	-1
E'	2	-1	0	2	-1	0
A_1''	1	1	1	-1	-1	-1
A_2''	1	1	-1	-1	-1	1
E''	2	-1	0	-2	1	0

Table 2.3: The G_{12} molecular symmetry group.

2.5.3. Symmetry of Torsional Energy Levels

Using the symmetry operations outlined in the previous section it is possible to assign symmetry labels to the torsional levels. This can be done for a free rotor[105,106] by considering the effect of each symmetry operation on the free rotor basis function, exp(imβ), where m is the internal rotation quantum number (m = 0, ±1, ±2 etc.) and β is a reference angle (see figure 2.16.) between proton 1 and B in an anticlockwise fashion (i.e. in the direction of proton 2). For a free rotor this can be expressed as cos(mβ). Since cos(x) is equivalent to cos(-x) all states except m = 0 can be expressed as 2cos(mβ). The effect of each symmetry operation on β is shown in figure 2.17.

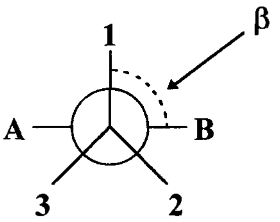

Figure 2.16: Reference diagram for the determination of the symmetry levels of a G_6/G_{12} rotor.

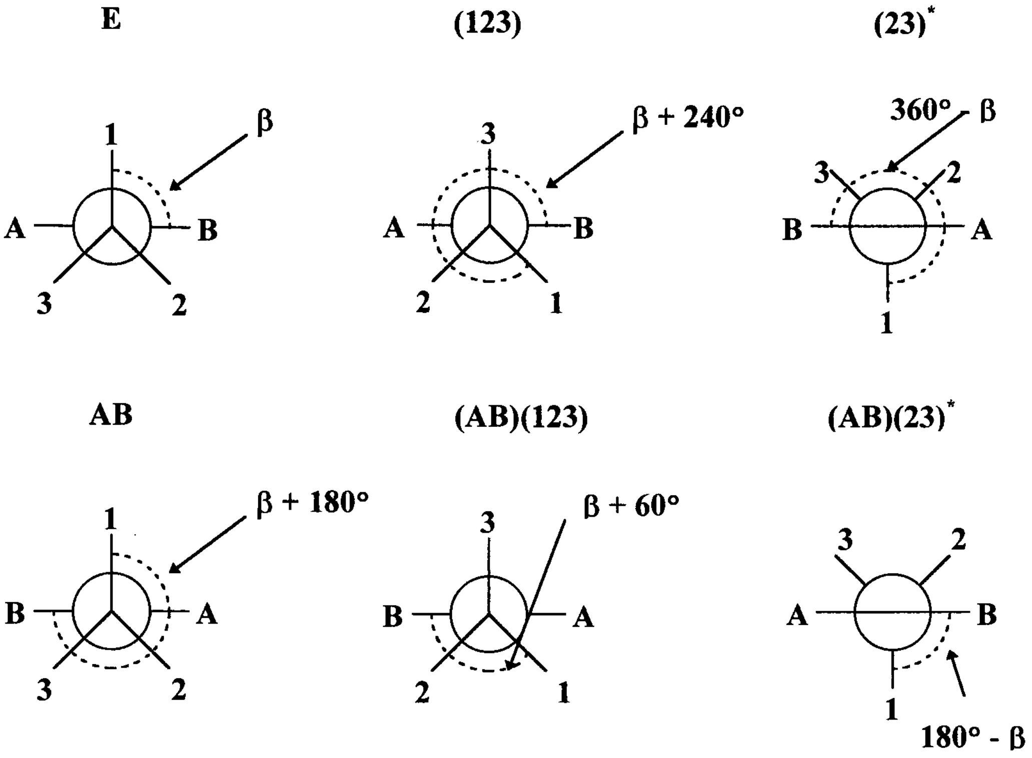

E

(123)

$(23)^*$

AB

(AB)(123)

$(AB)(23)^*$

Figure 2.17: Effects of symmetry operations for a G_6/G_{12} rotor.

Thus for each value of the internal rotation quantum number (m) it is possible to find the reducible representation as shown in table 2.4. For the $(23)^*$ and $(AB)(23)^*$ operations the effect is to interchange the positive and negative m values. Hence for all values of m except m = 0 the reducible representation for these operations is zero. Using the same methods as conventional group theory it is possible to reduce these to the appropriate symmetry labels. These are given in table 2.5.

Symmetry operation	**E**	**(123)**	**$(23)^*$**	**(AB)**	**(AB)(123)**	**$(AB)(23)^*$**
m	**cos(0)**	**cos(m4π/3)**		**cos(mπ)**	**cos(mπ/3)**	
0	1	1	1	1	1	1
±1	2	-1	0	-2	1	0
±2	2	-1	0	2	-1	0
±3	2	2	0	-2	-2	0
±4	2	-1	0	2	-1	0
±5	2	-1	0	-2	1	0
±6	2	2	0	2	2	0

Table 2.4: Reducible representations for the G_6 and G_{12} molecules.

Torsional quantum number (m)	**Symmetry label (G_6)**	**Symmetry label (G_{12})**
0	a_1	a_1'
±1	e	e''
±2	e	e'
±3	a_1, a_2	a_1'', a_2''
±4	e	e''
±5	e	e'
±6	a_1, a_2	a_1', a_2'

Table 2.5: Irreducible representation of the torsional energy levels of G_6 and G_{12} rotors.

Thus for a molecule with G_6 symmetry the torsional energy levels are **0a_1**, **1e**, **2e**, **3a_1/3a_2**, **4e** and so on for a free rotor. The presence of a potential of the type shown in equation 2.9. where ϕ is the angle of the rotor results in the m = 3 levels no longer being degenerate.

$$V = \frac{V_3}{2}(1 - \cos 3\phi) \qquad \textbf{(2.9)}$$

Figure 2.18. shows the torsional energy levels for three limiting cases, free rotation, rotation hindered by a typical potential (V_3 = 500 cm^{-1}, rotor = CH_3)[68] and rotation hindered by an infinite potential[105].

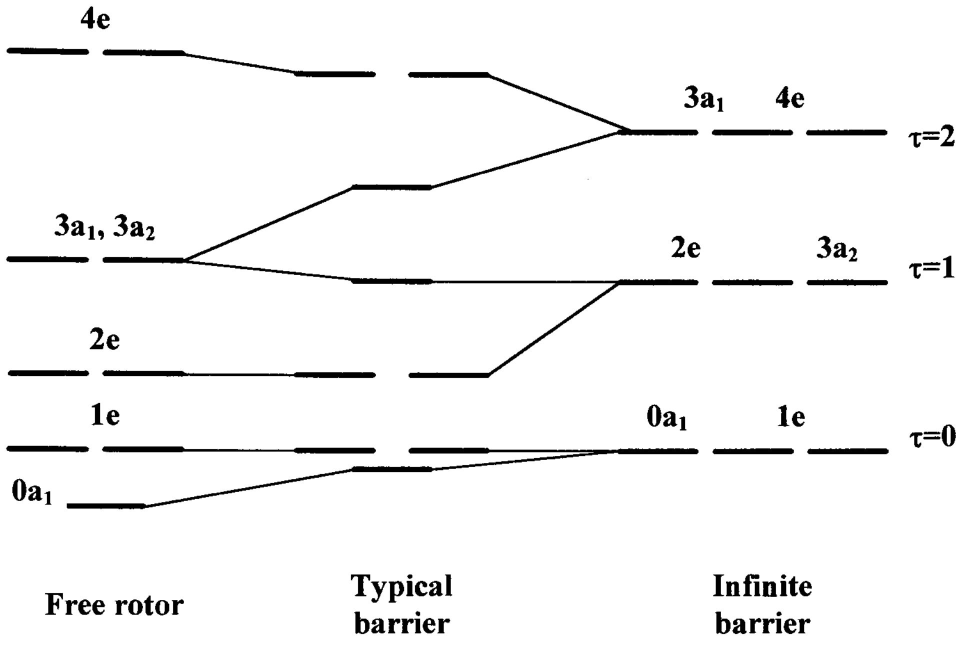

Figure 2.18: Energy diagram of torsional states for a molecule of G_6 symmetry for three magnitudes of barriers. The typical barrier case corresponds to $V_3 = 500$ cm^{-1} for a methyl rotor ($F = 5$ cm^{-1})

For a typical barrier the spacing between **a** type and **e** type symmetry levels increases as the barrier is approached. This is due to tunneling through the potential. The **0a₁** and **1e** states are very similar in energy and are not always resolved experimentally[68]. For an infinite barrier (or for a very heavy rotor such as CF_3) the **a** and **e** symmetry levels are degenerate since tunneling through the barrier is negligible and torsional motion is better described as a vibration rather than as true internal rotation. This is indicated in figure 2.18. by τ. The threefold degeneracy is a result of the threefold nature of the hindering potential. Splitting between the **a** and **e** states becomes greater as the top of the barrier is approached. For G_{12} molecules the potential is sixfold and the torsional vibrations are sixfold degenerate[107].

The existence of different symmetries of torsional levels has major implications for the spectroscopy of such species. Firstly **a** and **e** type symmetries have different nuclear spin statistics[108,109] and hence different weightings when considering Franck-Condon factors. Because of this the two symmetry types cannot relax into each other with the result that even in a cold molecular beam (vibrational temperatures of only a few tens of Kelvins) there will be a substantial population in both the $\mathbf{0a_1}$ and **1e** states. The selection rules for transitions from such states are different (see the next section) and so two distinct progressions are present[105-115]. Finally, the interaction with other degrees of freedom of the molecule may be dependent on the symmetry of the torsional level, hence the **e** levels may show different effects than those of $\mathbf{a_1}$ symmetry. For example, interaction with the overall rotation of the molecule is far more substantial for **e** type levels than for $\mathbf{a_1}$ levels[106].

2.5.4. Selection Rules

The application of symmetry to the problem of internal rotation as outlined in the previous section allows the experimental observation of internal rotation to be modeled. For this it is necessary to understand the selection rules for transitions between torsional levels of different electronic states. Such rules have been outlined by several groups[105-115].

The transition dipole moment for a transition between two electronic states can be expressed as the product of the wavefunctions of the vibrational, internal rotation and overall rotation of the molecule in the two electronic states. This is shown in equation 2.10. where Ψ_m is the wavefunction of the molecule and Ψ_e, Ψ_v, Ψ_t and Ψ_r are the wavefunctions of the electronic, vibrational, torsional and overall rotational motions of the molecule.

$$\Psi_m = \Psi_e \Psi_v \Psi_t \Psi_r \quad \textbf{(2.10.)}$$

The vibrational effect can be removed by only considering the vibrationless level of the electronic state. For an electronic transition the direct product of the symmetry states is shown in equation 2.11. where Γ_{el} is the symmetry of the electronic state, Γ_{tor} is the same for the torsional motion, Γ_{rot} for the overall rotation of the molecule, $\Gamma(T_j)$ is the irreducible representation of translation along the j = a, b or c direction i.e. the electric vector of the photon polarised along the a, b or c axes and Γ_{tot} is the totally symmetric representation of the molecular symmetry group. The prime indicates a different electronic state.

$$\Gamma_{el} \otimes \Gamma_{el}' \otimes \Gamma_{tor} \otimes \Gamma_{tor}' \otimes \Gamma_{rot} \otimes \Gamma_{rot}' \otimes \Gamma(T_j) \equiv \Gamma_{tot} \qquad \textbf{(2.11.)}$$

If any coupling between the degrees of freedom is small equation 2.11. can be factored into separate electronic, torsional and rotational parts. The result is that for an allowed electronic transition the product of the two torsional symmetries must retain symmetry i.e. for G_6 this must be $\mathbf{a_1}$. The consequence of this is that transitions between states of the same torsional symmetry are fully allowed while those between states of different symmetries are forbidden. This is summarised in equations 2.12., 2.13. and 2.14. for the G_6 case. All other transitions are forbidden.

$$\mathbf{a_1 \leftrightarrow a_1} \qquad \textbf{(2.12.)}$$

$$\mathbf{a_2 \leftrightarrow a_2} \qquad \textbf{(2.13.)}$$

$$\mathbf{e \leftrightarrow e} \qquad \textbf{(2.14.)}$$

In the more general case the selection rule is that allowed transitions are those between levels of the same torsional symmetry. For example in the G_{12} case transitions of the type $\mathbf{a_1'} \leftrightarrow \mathbf{a_1'}$ are allowed.

Such selection rules have been found to be extremely useful in the spectroscopy of neutral states[105-116]. However, in many cases, there are transitions which cannot be assigned to such transitions and most therefore be assigned to symmetry forbidden transitions. For techniques used to study neutral species (such a MPI or LIF) such transitions are generally only weakly observed indicating that coupling between the various degrees of freedom is fairly weak[114,116]. However, for the pulsed-field-ionisation variant of ZEKE-PES, there exists an additional complication in that the transition is not to the ionic state itself but to the Rydberg states converging on it[68]. Equation 2.11. can be modified to compensate for this. Equation 2.15. shows this with the rotational and vibrational contributions ignored. Γ_{ryd} is the symmetry of the Rydberg state used in the ZEKE-PFI method[107].

$$\Gamma_{el} \otimes \Gamma_{el}^{+} \otimes \Gamma_{ryd} \otimes \Gamma_{tor} \otimes \Gamma_{tor}^{+} \otimes \Gamma(T_j) \equiv \Gamma_{tot} \quad \textbf{(2.15.)}$$

Thus if there is any interaction between the torsional motion and the Rydberg state it is possible for transitions which are forbidden to a first approximation to gain some intensity. For a molecule like toluene the Rydberg states can be assigned a symmetry label by applying the operations of the molecular symmetry group to the Rydberg state which is based at the center of mass of the molecule. This is shown in figure 2.19. for the *n*s and *n*p Rydberg states. For a G_6 molecule the only operation that affects the Rydberg orbitals is the $(23)^*$ operation since this involves an inversion of the whole molecule through the center of mass. This has no affect on the *n*s, $n\text{p}_z$ and $n\text{p}_y$ orbitals hence these can be classified as $\mathbf{a_1}$ symmetry but it does invert the $n\text{p}_x$ Rydberg orbital which is classified as $\mathbf{a_2}$. It is not possible to find a Rydberg state with **e** symmetry.

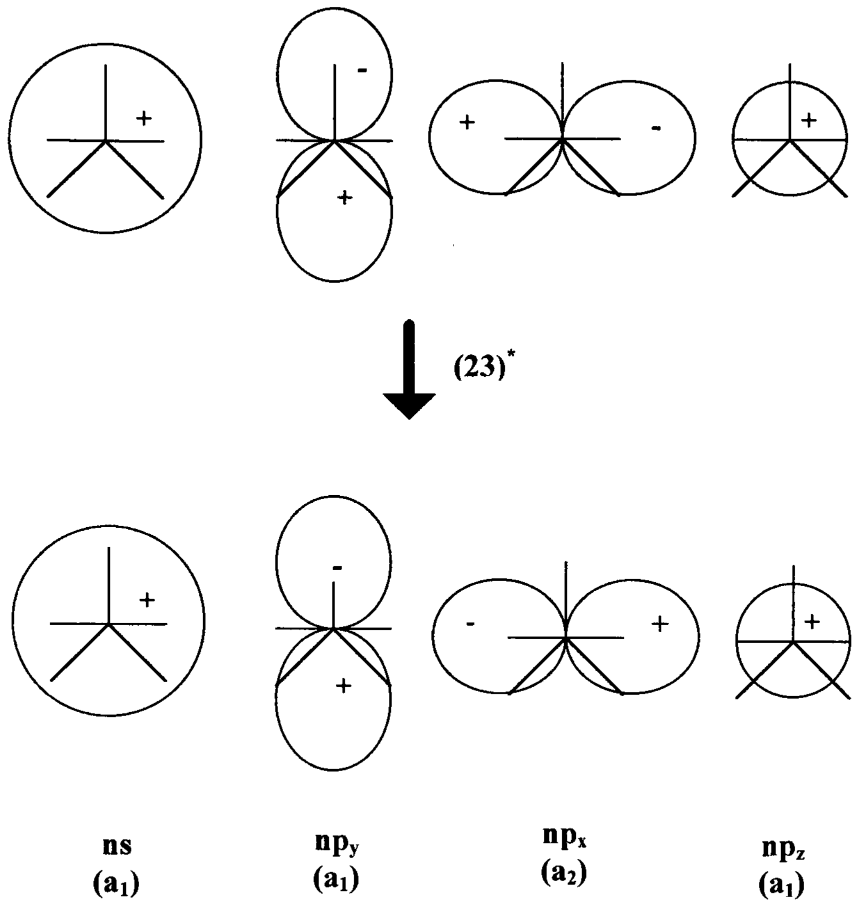

Figure 2.19: Rydberg orbitals of a substituted toluene.

If there is coupling between the torsional motion and the Rydberg states then it is possible for $\mathbf{a_1}$ ↔ $\mathbf{a_2}$ transitions to gain some intensity (transitions of the type $\mathbf{a_1}$ ↔ **e** remain forbidden under this mechanism). From previous work[107,110-115] it has been observed that such a situation is common in ZEKE-PFI spectroscopy with forbidden transitions having considerable intensity particularly when the forbidden transition lies close in energy to an allowed transition. The effect is considerably more apparent than for the coupling of other degrees of freedom with the torsion which is the cause of forbidden transitions in neutral state techniques[116].

2.5.5. Calculational Methods

A potential barrier to internal rotation can be found from experimental torsional energies by calculating torsional energy levels and fitting them to the observed values. The model commonly used is a one-dimensional rigid rotor approximation where only the internal rotation is considered.

Such a model is identical to the problem of a particle on a ring[105,106]. In the absence of a hindering potential the Hamiltonian is shown in equation 2.16. where F is the internal rotation constant and ϕ is the angle of the rotor relative to some defined zero.

$$H = -F\partial^2/\partial\phi^2 \quad \textbf{(2.16.)}$$

The solutions to this are the same as for the particle on a ring. The eigenvalues are $E = m^2F$ where m is the internal rotation quantum number (0, ±1, ±2 etc.). The eigenfunctions are of the form $\varphi = \exp(im\phi)$.

The presence of a hindering potential changes the Hamiltonian as shown in equation 2.17. where V is the potential.

$$H = -F\partial^2/\partial\phi^2 + V(\phi) \quad \textbf{(2.17.)}$$

In principle any potential can be used but the one which is most common is shown in equation 2.18. For a methyl rotor (such as in 2 substituted toluenes) the relevant terms are n = 3, 6, 9 etc. while for a two-fold rotor such as biphenyl the terms are n = 2, 4, 6 etc.

$$V = \sum \frac{V_n}{2}(1 - \cos n\phi) \qquad \textbf{(2.18.)}$$

The effects of such a potential on the energy levels of the rotor have been discussed in section 2.5.3. and figure 2.18. Using this it is possible to calculate the torsional energy levels.

Several methods have been developed to do this. Early methods used solutions of Mathieu equations to generate tables of energy levels[117] for various values of V_n and F. The drawback of such a scheme was that only one value of n could be considered. Small perturbations could be added to the system to simulate the presence of higher order terms[117,118] but these could not have a magnitude greater than 5 % of the main term.

The method developed by Lewis and co-workers[119] in the early 1970's was a breakthrough which allowed the calculation of torsional barriers in a straightforward and versatile manner. Using a basis set of sin and cosine functions it is possible to obtain both the energies and the wavefunctions of the torsional states. This method is particularly simple for calculating Franck-Condon factors which derive directly from the coeffecients of the basis set. In addition the relative phase of the potentials can be easily varied and the value of F can be allowed to change as a function of rotation angle[106,119].

The main drawback of this method is that it is restricted to potentials of the type shown in equation 2.18. Recent work by Lawley[122] has shown the usefulness of applying discrete variable formalism to the internal rotation problem. The advantage of this method is that an arbitrary potential can be chosen and the energy levels calculated. This allows the potential to be modified over one region while another portion is held constant. This spline fitting method should be very useful for potentials which are not well described by equation 2.18. However for the work presented in this thesis only the conventional form of the potential was used. The programs for both a threefold (e.g. the aminobenzotrifluorides in chapter 5) and a twofold rotor (4-fluorobiphenyl in chapter 6) are given in appendix 2.

2.5.6. Sources of Barriers to Internal Rotation

The discovery, in the first half of this century, that the internal rotation of the methyl groups in ethane[123] was hindered (barrier of ~1000 cm^{-1}) was something of a surprise given that such motion requires no bond breaking. In addition the steric interaction of the rotors is not enough to account for the barrier so the effect must be electronic in origin. Such interaction (termed hyperconjugation) can best be seen for the case of propene where a single methyl rotor interacts with an isolated double bond[124-128]. This has been described in detail by several groups[105,106]. The C-C double bond has bonding and anti-bonding π orbitals of which the bonding MO is filled in the ground state. For the methyl rotor the overlap of a p-type orbital on the carbon with the s-type of the protons result in the formation of bonding and anti-bonding π orbitals. These are shown in figure 2.20. Four possible interactions between the orbitals exist and are labeled A, B, C and D. It is these interactions that determine the conformation of the rotor and the barrier between conformations.

For the neutral ground state of propene both bonding orbitals are filled. Interaction D is between two unfilled orbitals and can be ignored. B and C involve a two electron interaction but are between energetically very different orbitals. Hence these are small effects. The main interaction is thus A which is repulsive since it is an interaction between fully occupied orbitals..

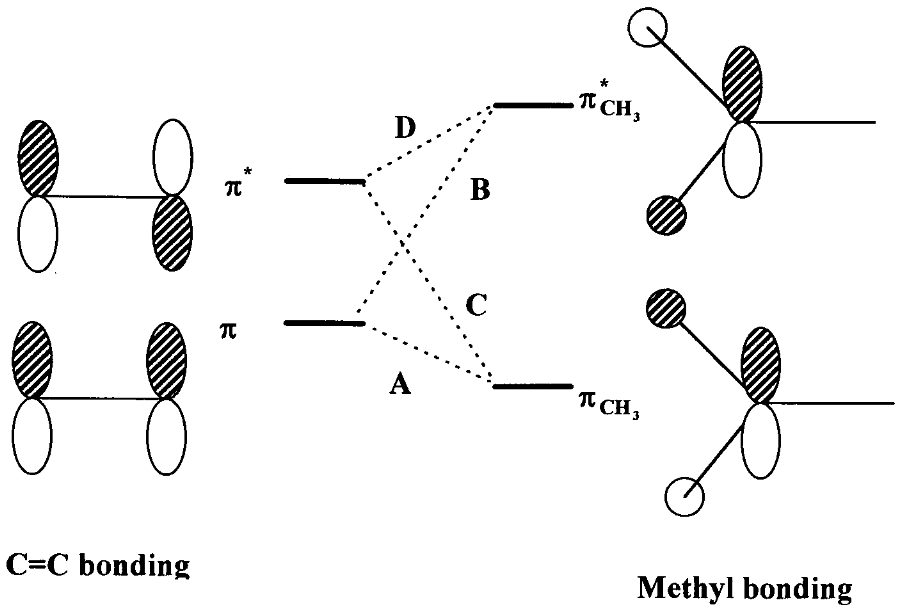

Figure 2.20: Molecular orbitals for propene.

Hence the energetically favourable conformation will be that which minimises the overlap of the two orbitals. This is shown in figure 2.21. for the eclipsed and staggered conformers.

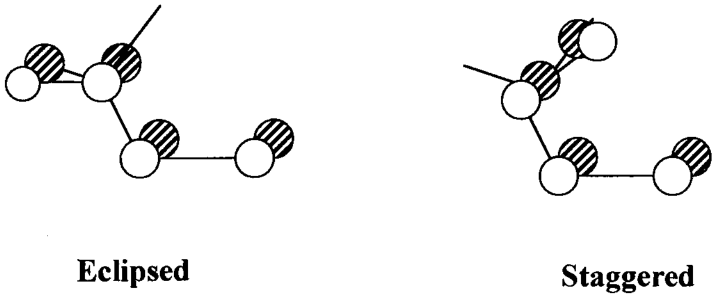
Eclipsed

Staggered

Figure 2.21. Eclipsed and staggered conformations of propene.

It is clear that the eclipsed conformer has less interaction between the two orbitals than the staggered. Hence propene adopts the eclipsed conformation in the neutral ground state[124].

Excitation or removal of an electron radically alters the conformation of the molecule. The S_1 state is formed by excitation of an electron from the π bond of the double bond to its antibonding counterpart with the result that interactions A and C are now three electron problems while B and D are one electron interactions. Of these A is weak and favours the staggered form, B and C involve orbitals energetically very different and hence are weak but favour the eclipsed form and D is large and favours greater overlap between the antibonding orbitals as found by the staggered conformer. Hence the S_1 state favours the staggered conformation[124]. A similar argument can be made for the ground ionic state corresponding to removal of an electron from the bonding orbital of the double bond. A, B and C are the interactions with B and C much weaker than A. Hence the staggered conformation is preferred. This state of propene has not been studied at a high enough resolution to confirm this. Table 2.6. lists the effects of each interaction in each electronic state.

Interaction	**Electrons (S_0)**	**Conf.**	**Electrons (S_1)**	**Conf.**	**Electrons (D_0)**	**Conf.**
A	4	eclipsed	3	staggered	3	staggered
B	2	eclipsed	1	eclipsed	1	eclipsed
C	2	eclipsed	3	eclipsed	2	eclipsed
D	0	-	1	staggered	0	-

Table 2.6. Interaction of MO's for propene in three electronic states.

The process outlined above has been found to be very useful for molecules such as propene and other molecules with an isolated double bond[124-128]. Extending it to molecules with delocalised double bonds such as in toluene has been difficult. However, the ideas behind the mechanism are useful.

Wiesshaar and co-workers[68,114,115,129] have explored the origins of barriers to internal rotation in substituted toluenes using both experimental results and ab-initio calculations. Two effects have been found to be important. Steric effects[129] only occur for ortho substituted toluenes and change very little with electronic state. The second, and more interesting, contribution to the barrier arises from electronic effects caused by the substituent on the geometry of the ring[68,115]. It was found that the local geometry of the ring around the rotor had a large effect on the barrier. For para substituted toluenes the substituent has an equal effect on both sides of the ring as the ring has local C_{2v} symmetry at the carbon bonded to the methyl rotor. Hence only very small barriers to internal rotation are found for such molecules. Examples include para-aminotoluene[130] and toluene itself[107]. For the neutral ground state of toluene there are two main resonance structures as shown in figure 2.22. These have a double bond on opposite sides of the ring relative to the methyl group. Hence each resonance structure has a large three-fold barrier to internal rotation which is exactly 180° out of phase with each other. The relative weighting of the two structures is 1:1 with the result that the two barriers cancel each other out. Weaker interactions such as steric repulsion now dominate the potential which is small and sixfold.

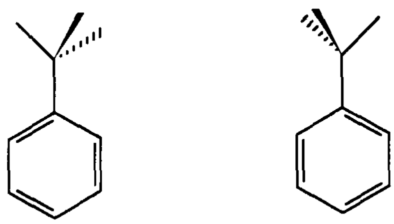

Figure 2.22. The resonance structures of toluene.

Ortho and meta substituted toluenes, on the other hand, display changes in the local geometry of the ring which varies from state to state[109-116]. Wiesshaar's calculation could only be performed on ground states (both neutral and ionic) but the idea could be extended to the S_1 state. It was found that the preferred conformation was one in which one of the C-H bonds of the rotor lies in the same plane as the C-C bond of the ring with the highest double-bond character. This is shown in figure 2.23.

Favoured **Unfavoured**

Figure 2.23: Conformations of substituted toluenes. The difference in double bond character has been exaggerated for clarity.

It was possible for Wiesshaar to use this model to explain the observed dependence of the barrier to internal rotation on electronic state. For ortho substituted toluenes the neutral ground state has a large barrier[68] which is greatly reduced in the S_1 state but increases again in the ion. Steric effects between the protons of the rotor and the substituent result in the large barrier in the S_0 and ionic ground states but the electronic effect of the S_1 state would prefer the molecule to adopt a conformation opposite to that which minimises steric repulsion[115]. This is called the pseudo-trans conformation as shown in figure 2.24. The near cancellation of the two effects results in internal rotation which is nearly unhindered.

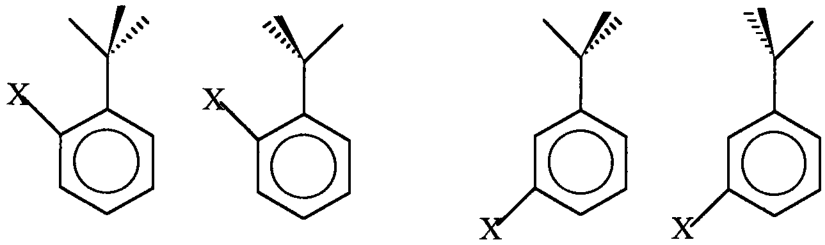

Ortho. **Meta.**

Pseudo cis. **Pseudo trans.** **Pseudo cis.** **Pseudo trans.**

Figure 2.24. Cis and trans conformers of ortho and meta toluenes.

For meta substituted toluenes the picture is much clearer since there are no (or at least very small) steric effects and the variation of barrier with electronic state can be attributed purely to electronic effects. A small barrier exists in the S_0 state and increases greatly in both the S_1 and D_0 states[68]. The equilibrium conformation of the rotor also changes by 60° from the S_1 to D_0 states. Ab-initio calculations[115] show that the S_0 state has C_{2v} symmetry around the rotor but that both the S_1 and D_0 states do not. In addition the D_0 geometry has the bond with greater double bond character on the opposite side of the molecule to that of the S_1 state. The net result of this is that the barrier changes conformation following ionisation from the S_1 state.

It is clear from all the previous work that the major causes of barriers to internal rotation are steric and electronic effects. Although the examples given here are propene and the toluenes it is possible to extend such ideas to other molecules such as biaryl species such as biphenyl and its derivatives. Such work is discussed in chapter 6.

2.6. References

1. J.N. Murrell, S.F.A. Kettle & J.M. Tedder. Valence Theory. John Wiley & Sons (London). 1965.
2. M.B. Robin. Higher Excited States of Polyatomic Molecules Volume 1. Academic Press (New York). 1974.
3. J. Berkowitz. Photoabsorption, Photoionisation and Photoelectron Spectroscopy. Academic Press (New York). 1979.
4. T.E. Peacock. *Mol.Phys.* 1960, **3**, 453.
5. S. Nagakura, M. Kojima & Y. Maruyama. *J.Mol.Spectrosc.* 1964, **13**, 174.
6. P.W. Joireman, R.T. Kroemer, D.W. Pratt & J.P.Simons. *J.Chem.Phys.* 1996, **105**, 6075.
7. H.H. Jaffe & M. Orchin. Theory and Applications of Ultraviolet Spectroscopy. John Wiley & Sons (London). 1962.
8. K. Kimura & S. Nagakura. *Mol.Phys.* 1965, **9**, 117.
9. J.I. Steinfeld. *An Introduction to Modern Molecular Spectroscopy.* MIT Press (Cambridge, Massachusetts). 1985.
10. R.F. Stebbings & F.B. Dunning. Rydberg States of Atoms and Molecules. Cambridge University Press (Cambridge). 1983.
11. T.F. Gallagher. Rydberg Atoms. Cambridge University Press (Cambridge). 1994.
12. G. Herzberg. Molecular Spectra and Molecular Structure. Volume 1: Spectra of Diatomic Molecules. Krieger Publishing (Florida). 1989.
13. J.G. Goode. PhD Thesis. University of Edinburgh. 1995.
14. M.R. Dobber, W.J. Buma & C.A. de Lange. *J.Chem.Phys.* 1993, **99**, 836.
15. N.A. Macleod, S. Wang, J. Hennessy, T. Ridley, K.P. Lawley & R.J. Donovan. *J.Chem.Soc.Faraday Trans.* 1998, **94**, 2689.
16. R. Glaser, S. Rayat, M. Lewis, M.S. Son & S. Meyer. *J.Am.Chem.Soc.* 1999, **121**, 6108.
17. A. Halama, J. Kavalek, V. Machacek & T. Weidlich. *J.Chem.Soc.* 1999, **13**, 1839.

18. N. Arun, P. Jeevanandam, S. Vasudevan & K.V. Ramanathan. *J.Chem.Phys.* 1999, **111**, 1231.
19. D.W. Turner, C. Baker, A.D. Baker & C.R. Brundle. Molecular Photoelectron Spectroscopy. Wiley-Interscience (London). 1970.
20. C.R. Brundle & A.D. Baker. Electron Spectroscopy: Theory, Techniques and Applications Volume 1. Academic Press (London). 1977.
21. T.A. Miller & V.E. Bondybey. Molecular Ions: Spectroscopy, Structure and Chemistry. North Holland Publishing (Amsterdam). 1983.
22. F.P. Huberman. *J.Mol.Spectrosc.* 1966, **20**, 29.
23. I. Dabrowski & G. Herzberg. *J.Mol.Spectrosc.* 1978, **73**, 183.
24. C.V.V. Prasad, D. Lacombe, K. Walker, W. Kong, P. Bernath & J. Hepburn. *Mol.Phys.* 1997, **91**, 1059.
25. C. Cossart-Magos, D. Cossart & S. Leach. *Mol.Phys.* 1979, **37**, 793.
26. K. Watanabe. *J.Chem.Phys.* 1959, **26**, 542.
27. K. Watanabe. *J.Chem.Phys.* 1954, **22**, 1564.
28. J.P. Morrison, H. Hurzeler, M.G. Inghram & H.E. Stanton. *J.Chem.Phys.* 1960, **33**, 821.
29. K. Watanabe & T. Nakayama. *J.Chem.Phys.* 1958, **29**, 48.
30. C. Lifshiftz & W.A. Chupka. *J.Chem.Phys.* 1967, **47**, 3439.
31. M.A. Duncan, T.G. Dietz & R.E. Smalley. *J.Chem.Phys.* 1981, **75**, 2118.
32. M.A. Smith, J.W. Hager & S.C. Wallace. *J.Chem.Phys.* 1984, **80**, 3097.
33. H. Mizuno, K. Okuyama, T. Ebata & M. Ito. *J.Phys.Chem.* 1987, **91**, 5589.
34. Y. Tanaka. *Can.J.Phys.* 1962, **40**, 1596.
35. K.Watanabe & T. Namioka. *J.Chem.Phys.* 1956, **24**, 915.
36. E. Miescher. *Can.J.Phys.* 1976, **54**, 2074.
37. L. Singleton & P. Brint. *J.Chem.Soc.Faraday Trans.* 1997, **93**, 11.
38. R.G. Neuhauser, K. Siglow & H.J. Neusser. *J.Chem.Phys.* 1997, **106**, 896.
39. M.I. Al-Joboury & D.W. Turner. *J.Chem.Soc.* 1963, 5141.

40. F.I. Vilesov, B.C. Kurbatov & A.N. Terenin. *Dokl.Akad.Nauk.SSSR.* 1961, **138**, 1329.
41. K. Siegbahn, C, Nordling, G. Johansson, J. Hedman, P.F. Heden, K. Hamrin, U. Gelius, T. Bergmark, L.O. Werme, R. Manne & Y. Baer. *ESCA applied to free molecules.* North-Holland (Amsterdam). 1971.
42. T.A. Koopmans. *Physica.* 1933, **1**, 104.
43. J.W. Rabalais. Principles of Ultraviolet Photoelectron Spectroscopy. John Wiley & Sons (London). 1977.
44. C.R. Brundle & A.D. Baker. Electron Spectroscopy: Theory, Techniques and Applications Volume 2. Academic Press (London). 1978.
45. J.D. Barr, A. De Fanis, J.M. Dyke, S.D. Gamblin, A. Morris, S. Stranges, J.B. West, T.G. Wright & A.E. Wright. *J.Chem.Phys.* 1998, **109**, 2737.
46. J.B. Milan, W.J. Buma, C.A. de Lange, K. Wang & V. McKoy. *J.Chem.Phys.* 1997, **107**, 2782.
47. E. de Beer, M.P. Koopmans, C.A. de Lange, Y. Wang & W.A. Chupka. *J.Chem.Phys.* 1991, **94**, 7634.
48. S.G. Clement, M.N.R. Ashfold, C.M. Western, E. de Beer, C.A. de Lange & N.P.C. Westwood. *J.Chem.Phys.* 1992, **96**, 4963.
49. G. Ohrwall & P. Baltzer. *Chem.Phys.Lett.* 1999, **308**, 199.
50. D. Edvardsson, P. Baltzer, L. Karlsson, M. Lundqvist & B. Wannberg. *J.Electron Spectrosc.Relat.Phenom.* 1995, **73**, 105.
51. L. Asbrink. *Chem.Phys.Lett.* 1970, **7**, 549.
52. W. Peatmann, F.P. Wolf & R. Unwin. *Chem.Phys.Lett.* 1983, **95**, 453.
53. A.D. Baker, D.P. May & D.W. Turner. *J.Chem.Soc.B.* 1968, 22.
54. P. Baltzer, L. Karlsson, B. Wannberg, G. Ohrwall, D.M.P. Holland, M.A. MacDonald, M.A. Hayes & W. von Niessen. *Chem.Phys.* 1997, **224**, 95.
55. U. Becker & D.A. Shirley. VUV and Soft X-Ray Photoionization. Plenum Press (New York). 1996.
56. A. Robinson. *Chem.Brit.* 1997, **33**(4), 50.

57. D. Villarejo, R.R. Helm & M.G. Inghram. *J.Chem.Phys.* 1967, **46**, 4995.
58. A.Y. Yencha, A.J. Cormack, R.J. Donovan, A. Hopkirk & G.C. King. *Chem.Phys.* 1998, **238**, 109.
59. A.Y. Yencha, A.J. Cormack, R.J. Donovan, K.P. Lawley, A. Hopkirk & G.C. King. *Chem.Phys.* 1998, **238**, 133.
60. T. Tanaka, H. Yoshii, Y. Morioka, T. Hayaishi, K. Ito & R.I. Hall. *J.Chem.Phys.* 1998, **108**, 6240.
61. C.W. Hsu, P. Heimann, M. Evans, S. Stimson, P.T. Fenn & C.Y. Ng. *J.Chem.Phys.* 1997, **106**, 8931.
62. T. Akahori, Y. Morioka, T. Tanaka, H. Yoshii, T. Hayaishi & K. Ito. *J.Chem.Phys.* 1997, **107**, 4875.
63. K. Muller-Dethlefs, M. Sander & E.W. Schlag. *Chem.Phys.Lett.* 1984, **112**, 291.
64. C.R. Brundle. *Chem.Phys.Lett.* 1970, **5**, 410.
65. M. Sander, L.A. Chewter, K. Muller-Dethlefs & E.W. Schlag. *Phys.Rev.A.* 1987, **36**, 4543.
66. S. Fredin, D. Gauyacq, M. Horani, C. Jungen & G. Lefevre. *Mol.Phys.* 1987, **60**, 825.
67. G. Reiser, W. Habenicht, K. Muller-Dethlefs & E.W. Schlag. *Chem.Phys.Lett.* 1988, **152**, 119.
68. High Resolution Laser Photoionization and Photoelectron Studies. Edited by I. Powis, T. Baer & C.Y. Ng. John Wiley & Sons (London). 1995.
69. K.T. Lu & P. Johnson. *J.Chem.Phys.* 1991, **94**, 5769.
70. G. Lembach & B. Brutschy. *J.Phys.Chem.* 1996, **100**, 19758.
71. A. Held, L.Y. Baranov, H.L. Selzle & E.W. Schlag. *Chem.Phys.Lett.* 1998, **291**, 318.
72. A. Held, L.Y. Baranov, H.L. Selzle & E.W. Schlag. *J.Chem.Phys.* 1997, **106**, 6848.

73. R. Signorell F. Merkt. *Artifacts in PFI-ZEKE Photoelectron Spectroscopy.* The Role of Rydberg States in Spectroscopy and Photochemistry. Edited by C. Sandorfy. Kluwer Academic (Amsterdam). 1999.
74. W.A. Chupka. *J.Chem.Phys.* 1993, **98**, 4520.
75. G. Herzberg & C. Jungen. *J.Mol.Spectrosc.* 1972, **41**, 425.
76. J.W. Hepburn. *Chem.Soc.Rev.* 1996,281.
77. K. Muller-Dethlefs & E.W. Schlag. *Angew.Chem.Int.Ed.* 1998, **37**, 1346.
78. F. Merkt & H. Schmutz. *J.Chem.Phys.* 1998, **108**, 10033.
79. G.D. Stevens, C.H. Iu, T. Bergeman, H.J. Metcalf, I. Siepp, K.T. Taylor & D. Delande. *Phys.Rev.A.* 1996, **53**, 1349.
80. J.F. Baugh, C.E. Burkhardt, J.J. Leventhal & T. Bergeman. *Phys.Rev.A.* 1998, **58**, 1585.
81. M. Ciocca, C.E. Burkhardt, J.J. Leventhal & T. Bergeman. *Phys.Rev.A.* 1992, **45**, 4720.
82. F. Merkt. *Annu.Rev.Phys.Chem.* 1997, **48**, 675.
83. M.J.J. Vrakking & Y.T. Lee. *J.Chem.Phys.* 1995, **102**, 8818.
84. M.J.J. Vrakking & Y.T. Lee. *J.Chem.Phys.* 1995, **102**, 8833.
85. M.J.J. Vrakking. *J.Chem.Phys.* 1996, **105**, 7336.
86. S.T. Pratt. *J.Chem.Phys.* 1993, **98**, 9241.
87. C.Alt, W.G. Scherzer, H.L. Selzle & E.W. Schlag. *Chem.Phys.Lett.* 1995, **240**, 457.
88. C.Alt, W.G. Scherzer, H.L. Selzle & E.W. Schlag. *Chem.Phys.Lett.* 1994, **224**, 366.
89. P.W. Atkins. Physical Chemistry. Oxford University Press (Oxford). 1990.
90. O. Edqvist, E. Lindholm, L.E. Selin & L. Asbrink. *Phys.Scr.* 1970, **1**, 25.
91. A.L. Smith. *Phil.Trans.Roy.Soc.Lond.A.* 1970, **268**, 169.
92. S.T. Pratt. *J.Chem.Phys.* 1998, **108**, 7131.
93. C. Jungen & S.T. Pratt. *J.Chem.Phys.* 1997, **106**, 9529.
94. A.J. Cormack. Phd Thesis. University of Edinburgh. 1998.

95. A.J. Cormack, A.J. Yencha, R.J. Donovan, K.P. Lawley, A. Hopkirk & G.C. King. *Chem.Phys.* 1996, **213**, 439.
96. M.C.R. Cockett, R.J. Donovan & K.P. Lawley. *J.Chem.Phys.* 1996, **105**, 3347.
97. M.C.R. Cockett, J.G. Goode, K.P. Lawley & R.J. Donovan. *J.Chem.Phys.* 1995, **102**, 5226.
98. F. Merkt & T.P. Softley. *J.Chem.Phys.* 1992, **96**, 4149.
99. N.P.L Wales, W.J. Buma, C.A. de Lange & H. Lefebvre-Brion. *J.Chem.Phys.* 1996, **105**, 5702.
100. M.C.R. Cockett. *J.Phys.Chem.* 1995, **99**, 16228.
101. P.M. Guyon, T. Baer & I. Nenner. *J.Chem.Phys.* 1983, **78**, 3665.
102. W. Kong & J.W. Hepburn. *Can.J.Phys.* 1994, **72**, 1284.
103. H.C. Longuet-Higgins. *Mol.Phys.* 1963, **6**, 445.
104. P.R. Bunker. *Mol.Phys.* 1965, **9**, 257.
105. L.H. Spangler. *Annu.Rev.Phys.Chem.* 1997, **48**, 481.
106. L.H. Spangler & D.W. Pratt. *Internal rotation dynamics from electronic spectroscopy in supersonic jets and beams.* Jet Spectroscopy and Molecular Dynamics. Edited by J.M. Hollas & D. Phillips. Blackie Academic (London). 1995.
107. K.T. Lu, G.C. Eiden & J.C. Weisshaar. *J.Phys.Chem.* 1992, **96**, 9742.
108. L.H. Spangler & D.W. Pratt. *J.Chem.Phys.* 1986, **84**, 4789.
109. R.D. Gordon, J.M. Hollas, P.J.A. Ribeiro-Claro & J.J.C. Teixeira-Dias. *Chem.Phys.Lett.* 1991, **183**, 377.
110. K. Takazawa, M. Fujii & M. Ito. *J.Chem.Phys.* 1993, **99**, 3205.
111. H. Ikoma, K. Takazawa, Y. Emura, J. Ikeda, H.Abe, H. Hayashi & M. Fujii. *J.Chem.Phys.* 1996, **105**, 10201.
112. R.A. Walker, E.C. Richard, K.T. Lu & J.C. Weisshaar. *J.Phys.Chem.* 1995, **99**, 12422.
113. R.A. Walker, E.C. Richard & J.C. Weisshaar. *J.Phys.Chem.* 1996, **100**, 7333.

114. R.A. Walker, E. Richard, K.T. Lu, E.L. Sibert & J.C. Weisshaar. *J.Chem.Phys.* 1995, **102**, 8718.
115. K.T. Lu, F.Weinhold & J.C. Weisshaar. *J.Chem.Phys.* 1995, **102**, 6787.
116. Z.Q. Zhao, C.S. Parmenter, D.B. Moss, A.J. Bradley, E.W. Knight & K.G. Owens. *J.Chem.Phys.* 1992, **96**, 6362.
117. D.R. Herchbach. *J.Chem.Phys.* 1959, **31**, 91.
118. A.V. Cunliffe. *The calculation of barriers to internal rotation from torsional frequencies.* Internal Rotation in Molecules. Edited by W.J. Orville-Thomas. John Wiley & Sons (London). 1974.
119. J.D. Lewis, T.B. Malloy, T.H. Chao & J. Laane. *J.Mol.Struct.* 1972, **12**, 427.
120. D.W. Wertz. *J.Chem.Phys.* 1969, **51**, 2133.
121. L.A. Carreira & R.C. Lord. *J.Chem.Phys.* 1969, **51**, 3225.
122. K.P. Lawley. *J.Mol.Spectrosc.* 1997, **183**, 25.
123. J.D. Kemp & K.S. Pitzer. *J.Chem.Phys.* 1936, **4**, 749.
124. W.J. Hehre, J.A. Pople & A.J.P. Deuaquet. *J.Am.Chem.Soc.* 1976, **98**, 664.
125. D. Cremer, J.S. Binkley, J.A. Pople & W.J. Hehre. *J.Am.Chem.Soc.* 1974, **96**, 6900
126. D.R. Lide & D.E. Mann. *J.Chem.Phys.* 1957, **27**, 868.
127. M.H. Whangbo, H.B. Schlegel & S. Wolfe. *J.Am.Chem.Soc.* 1977, **99**,1296.
128. A.E. Dorigo, D.W. Pratt & K.N. Houk. *J.Am.Chem.Soc.* 1987, **109**, 6591.
129. J.K. Badenhoop & F. Weinhold. *J.Chem.Phys.* 1997, **107**, 5406.
130. X.Q. Tan & D.W. Pratt. *J.Chem.Phys.* 1994, **100**, 7061.

Chapter 3

Experimental Methods

3.1. Introduction

The ZEKE-PFI spectrometer and laser system has been established in the department for several years now[1-4]. The purpose of this chapter is to describe the basic experimental arrangement and operating conditions and to detail the changes which were made to the system to provide a more versatile system.

3.2. The ZEKE-PFI Spectrometer

3.2.1 General Outline

A cross-section of the ZEKE-PFI spectrometer is shown in figure 3.1. It consists of a differentially-pumped vacuum chamber, a pulsed nozzle source with a conical skimmer, ion-optics and a 40 cm time-of-flight tube with a microchannel plate (MCP) detector. The main chamber and flight-tube are pumped by a Turbomolecular pump (Balzers TPU 510S, pumping speed 500 l s^{-1}) while the molecular beam source is pumped by an oil-based diffusion pump (Edwards 160-700, pumping speed 700 l s^{-}

^{1}) both of which are backed by rotary oil pumps. Base pressures are typically 3×10^{-7} rising to 6×10^{-7} mbar when the nozzle is operated with an atmosphere of helium.

The nozzle (General Valve, 300 μm orifice diameter) driven by a control unit (General Valve Iota one) operates at a repetition rate of 10 Hz to produce a jet-cooled molecular beam which is collimated by a conical skimmer (Beam Dynamics, 0.49 mm diameter). The use of helium or argon as the backing gas allows the formation of rotationally and vibrationally cold molecules resulting in greatly simplified spectra[5]. For molecules with a low vapour pressure at room temperature a heated nozzle source can be used[1]. The sample reservoir is upstream from the valve and can be heated up to 130°C. To avoid the sample condensing onto and blocking the nozzle the valve itself is kept at a higher temperature than the reservoir.

The ion/electron optics consist of two copper grids spaced 3 cm apart. In positive ion-mode a dc voltage of +2.5 kV is applied to the top plate and a positive or negative dc voltage of 0-2 kV to the lower grid. For ZEKE-PFI experiments a fast rising (?? ns) negative voltage of 3-21 V is applied to the upper grid at a variable delay time (0-25 μs). In addition a smaller pulse (0-5 V) of positive or negative voltage can be applied to the lower grid to act as a discrimination pulse and to improve resolution and sensitivity (see chapter 2 and section 3.2.3.). The minimum delay time for these fields is 70 and 170 ns respectively. The flight tube and the ionisation region itself are surrounded by a single layer of mu-metal shielding to reduce the effects of the earth's magnetic field. The molecular beam and laser beams pass through small (2 cm diameter) holes in the shielding.

Timing is controlled by the Q-switch of the laser through a digital delay generator (EG&G model 9650) to provide timed pulses for the nozzle, electric fields and data acquisition system. The detection system consists of a microchannel plate for detection of both positive and negative species. Data is collected unamplified by a gated integrator/averager (Stanford Research Systems SR250) for display on a digital oscilloscope (LeCroy model 9310) and stored on a PC. Data manipulation was carried out using Microcal Origin™ versions 3.7. and 4.1.

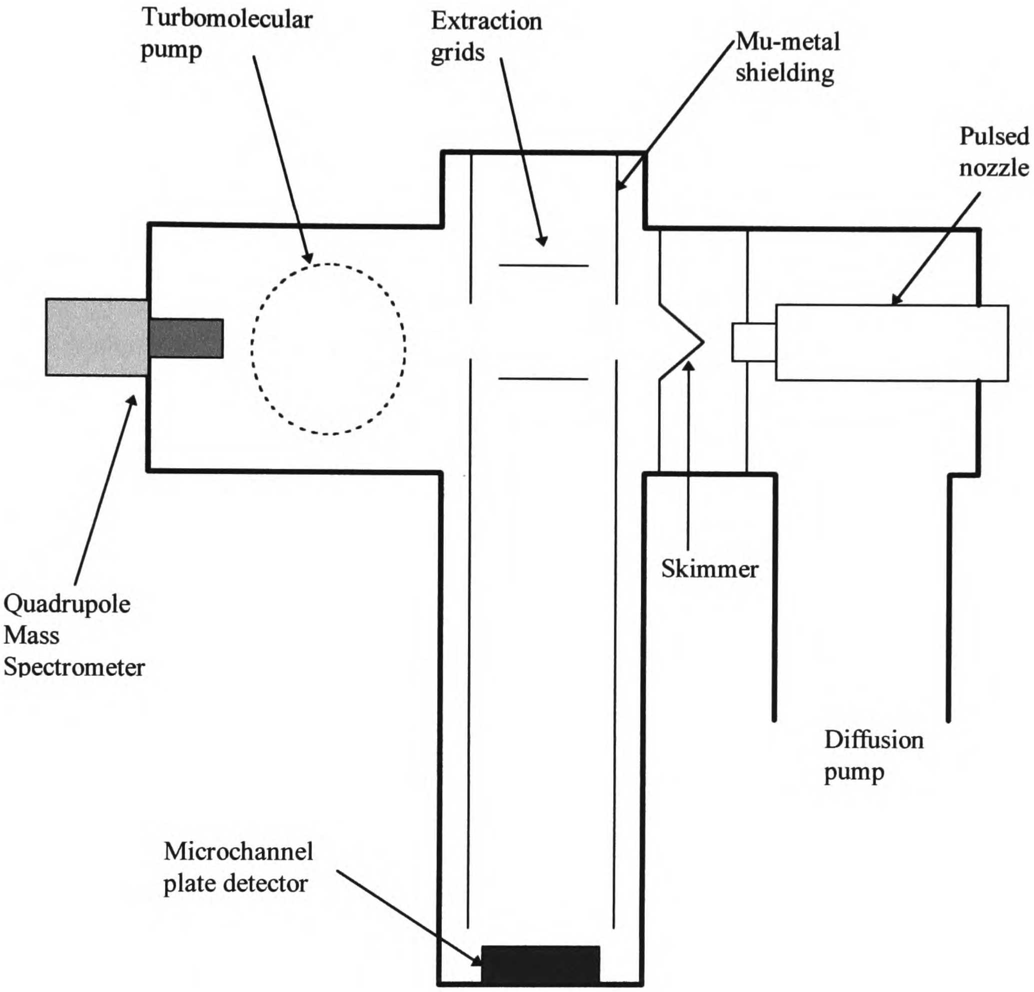

Figure 3.1: Cross section of the ZEKE-PFI spectrometer.

3.2.2. Molecular Beam and Jet Cooling

A vital part of the experimental arrangement oulined in figure 3.1 is the pulsed nozzle and skimmer. This allows the production of a collimated molecular beam of inert gas (usually helium or argon). By entraining a small percentage of the molecule of interest in such a beam vibrationally and rotationally cold molecules can be produced by jet cooling[5]. Vibrational temperatures are of the order of 100 K while rotational temperatures are typically around 10 K. Typical operating conditions involve an atmosphere of inert gas (760 Torr) with a few Torr of sample.

Such a procedure has two major consequences. Firstly, more highly resolved spectra can be obtained by the elimination of hot band transitions and the narrowing of rotational band contours. Figure 3.2. shows the (1+1) MPI spectrum of the S_1 state of 3-Aminobenzotrifluoride at two different backing pressures of helium (300 Torr and 700 Torr). Transitions from excited torsional levels of the neutral ground state (S_0) increase in intensity at the lower backing pressure[6].

The second effect of jet cooling is that the low temperature of the beam allows the formation (and survival) of weakly bound molecular clusters[7,8]. Examples of these which have been studied with this spectrometer include the van der Waals clusters between molecular iodine and the rare gases argon and krypton[3,4]. More strongly bound examples are the hydrogen bonded complexes examples of which include phenol with water or methanol, studied by Muller-Dethlefs and co-workers[9].

A final advantage of a pulsed molecular beam source is the convenience with which it can be used in cooperation with pulsed laser systems and time-of-flight mass spectrometry.

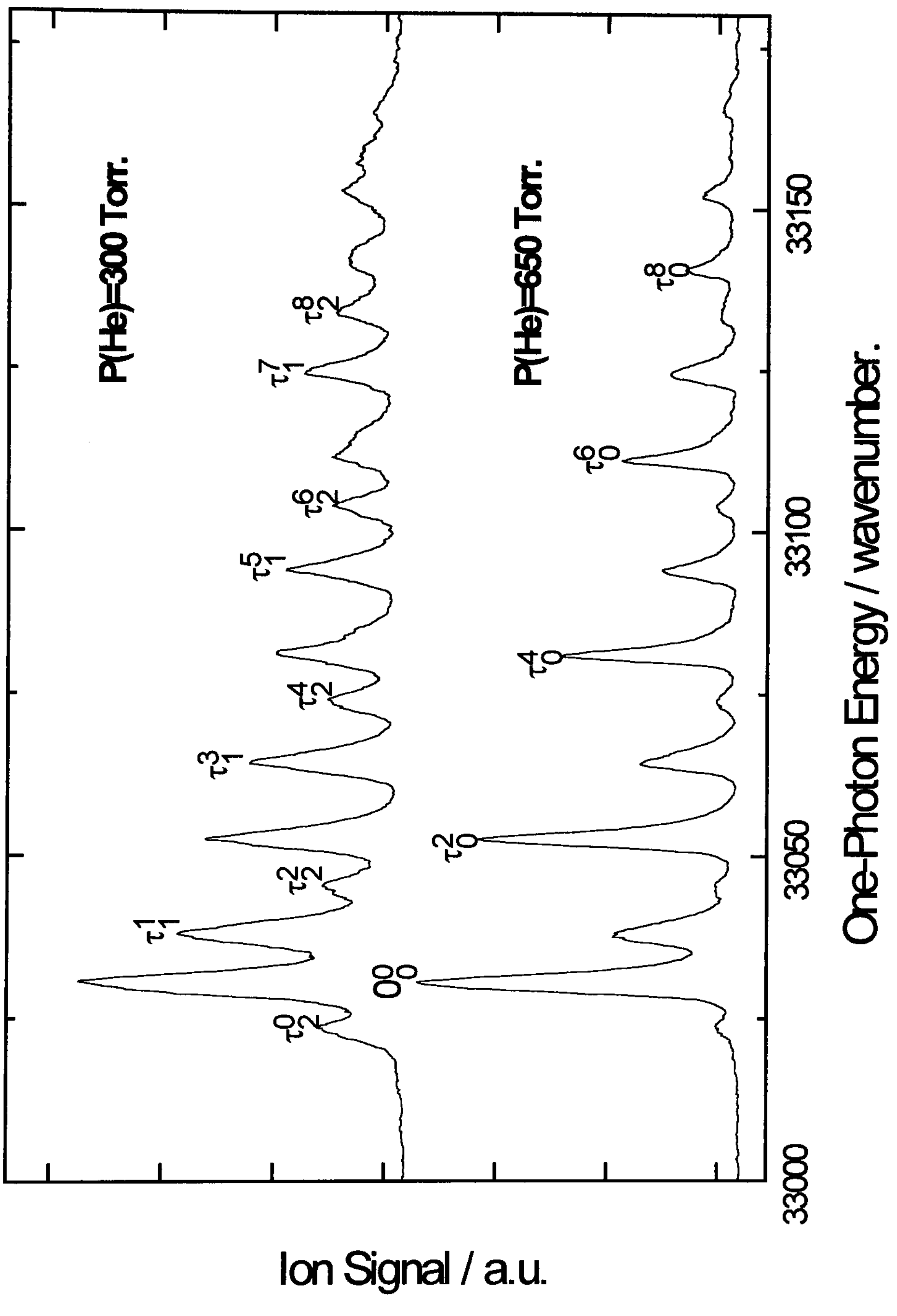

Figure 3.2: The (1+1) MPI spectrum of the S_1 state of 3-ABTF using different beam conditions.

3.2.3. Fields used in ZEKE-PFI Spectroscopy

The pulsed-field-ionisation variant of ZEKE spectroscopy relies on careful application of electric fields to obtain maximum resolution[10]. In this case two fields can be applied at variable times and with adjustable magnitudes. The first of these, the extraction pulse, can be varied from -0.3 to -7 V cm^{-1} with an application time of 0 to 25 μs and has the effect of ionising the high-*n* Rydberg states (the energy range in wavenumbers studied is ~$4\sqrt{V}$ where V has units of V cm^{-1}). The second pulse, termed the discrimination pulse, is generally applied before the extraction pulse and acts both to remove low kinetic energy photoelectrons from the ionisation region[11] and as an aid to resolution by reducing the width of Rydberg states ionised by the extraction field[12] (see chapter 2). This technique is known as slicing and reduces the range of Rydberg states detected to $4\sqrt{V_1} - 4\sqrt{V_2}$ where V_1 is the extraction pulse and V_2 is the discrimination pulse.

Previous work on establishing the spectrometer showed the capability of rotational resolution in favourable cases[1] (for example the coherent two-photon one-colour ZEKE-PFI spectrum of NO displayed a FWHM of 1.3 cm^{-1}). None of the spectra presented in this thesis require this resolution since the rotational constants are considerably smaller than for first-row diatomic molecules. Typical values of the FWHM found are 5-7 cm^{-1}. However, as an example of the crucial nature of the choice of fields the origin band of the cation of 4-Aminobenzotrifluoride using two separate field conditions is shown in figure 3.3. The torsional structure of this ion consists of three closely spaced peaks (approx. 7 cm^{-1} apart). At high values of the extraction field (7 V cm^{-1}) one featureless peak is observed with a full width at half maximum of 20 cm^{-1}. With a smaller field (3 V cm^{-1}) three peaks become visible with FWHM of 7 cm^{-1}.

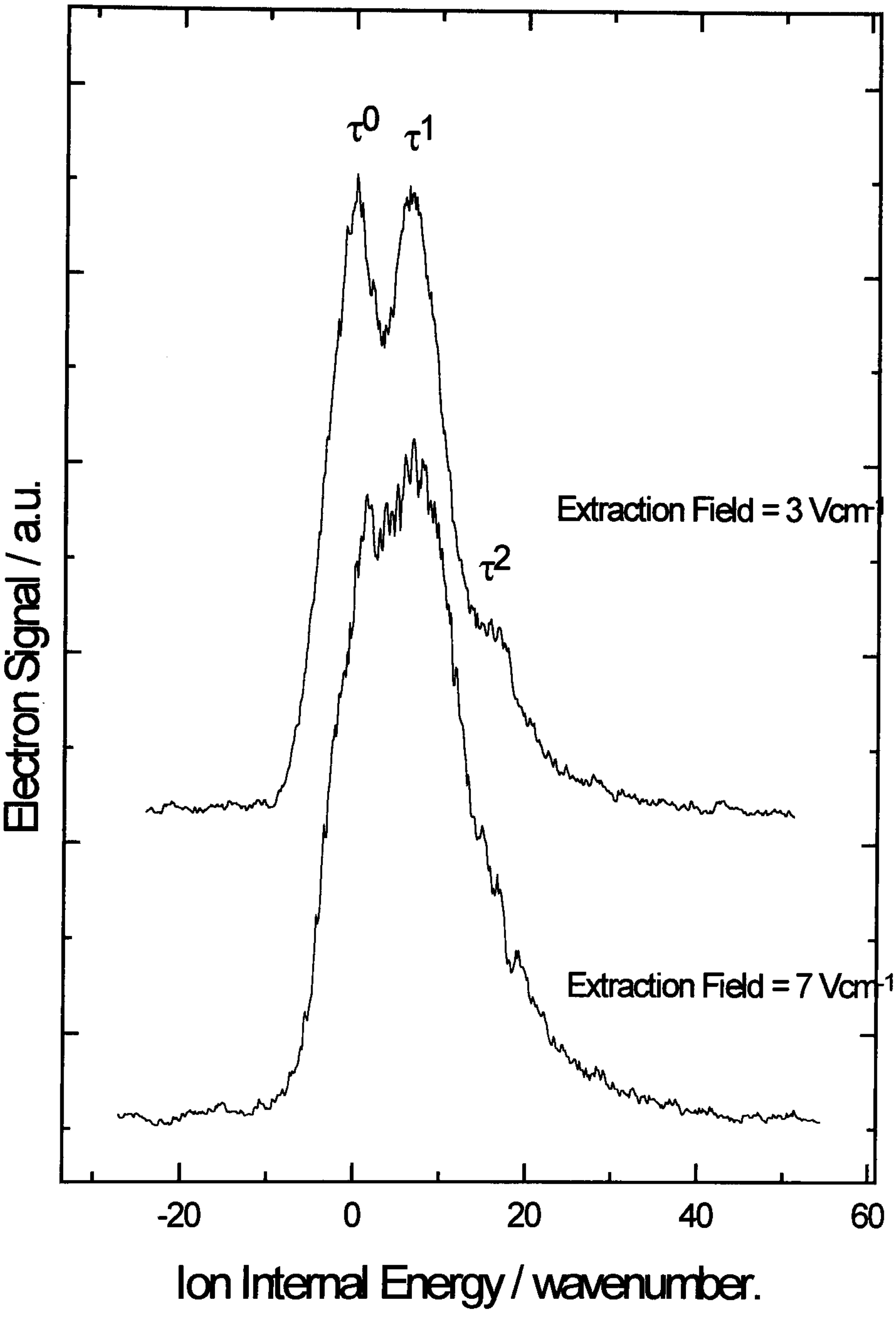

Figure 3.3: (1+1') ZEKE-PFI spectrum of 4-ABTF under different field conditions.

3.3. Laser System

3.3.1. General Outline

The laser system consists of two dye lasers (Spectra-Physics PDL-3 and PDL-2) pumped by the second (532 nm) and third (355 nm) harmonics of a Nd:YAG laser (Spectra-Physics DCR2A), as shown in figure 3.4. The output from either laser could be frequency doubled or mixed with the 1064 nm output of the YAG using KDP or BBO crystals. This allows coherent light in the range 220-900nm to be generated. Separation of the doubled output from fundamental was done by coloured filters or by a home built separator using two Pellin-Broca crystals.

Automatic tracking of the crystal angle for frequency doubling was carried out by a wavelength extension unit (Spectra-Physics WEX-1) for wavelengths down to 270nm. For light of shorter wavelength manual tracking of the angle was necessary using a photodiode. For experiments requiring two UV photons the pump wavelength was obtained by manually setting the doubling crystal to the correct angle for frequency doubling.

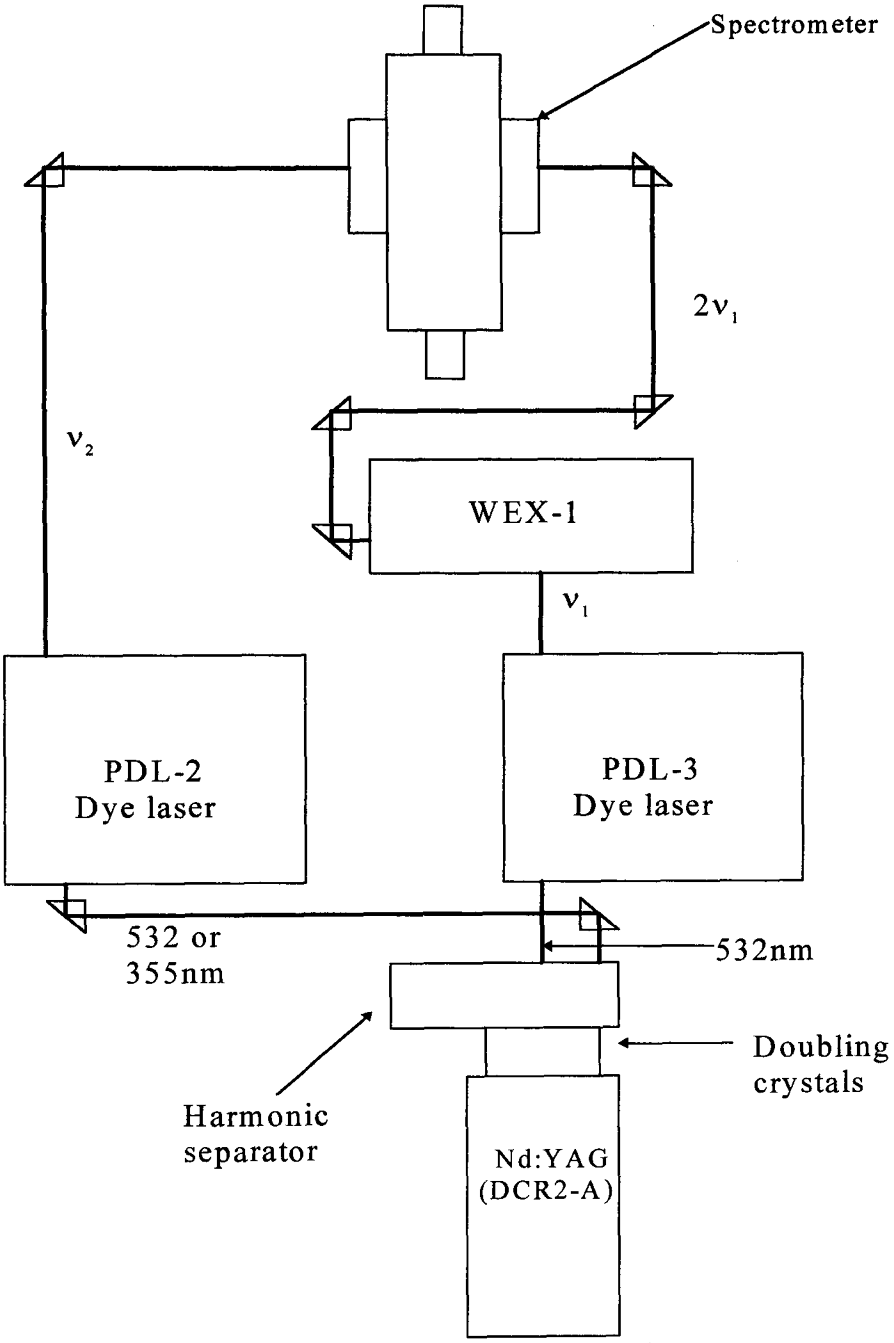

Figure 3.4: Outline of the laser system.

3.3.2. Calibration and Bandwidth of Lasers

Calibration of dye fundamentals was made by use of the optogalvanic effect in a neon lamp[13,14]. Figure 3.5. shows the calibration data for Rhodamine 640 laser dye using the PDL-3 laser. Table 3.1. lists the calibrated and literature frequencies. The residual difference between these is less than 1 cm^{-1}. The two dye-lasers have specified bandwidths[15] of 0.1-0.2 cm^{-1} (PDL-3) and 0.5-1.0 cm^{-1} (PDL-2). Both lasers can be scanned by a home-built stepper motor controlled using a PC (Elonex 486) running Stanford Systems SR245 software with typical step-sizes of 0.2-0.3 cm^{-1}. For experiments involving the use of two frequency-doubled photons the PDL-3 was used as the probe wavelength with the PDL-2 providing the pump photon. When a fundamental wavelength was required the opposite configuration was used.

Calibrated Frequency. (cm^{-1})	**Literature Frequency. (cm^{-1})**	**Difference. (E_{lit} - E_{cal}) / cm^{-1}**
16404.2	16403.8	-0.4
16462.5	16462.7	+0.2
16583.6	16583.8	+0.2
16734.7	16734.9	+0.2
16821.4	16821.3	-0.1
16941.9	16941.1	-0.8
16953.2	16953.7	+0.5

Table 3.1. Calibrated and literature frequencies for neon optogalvanic transitions using the PDL-3 dye-laser with Rhodamine 640 dye.

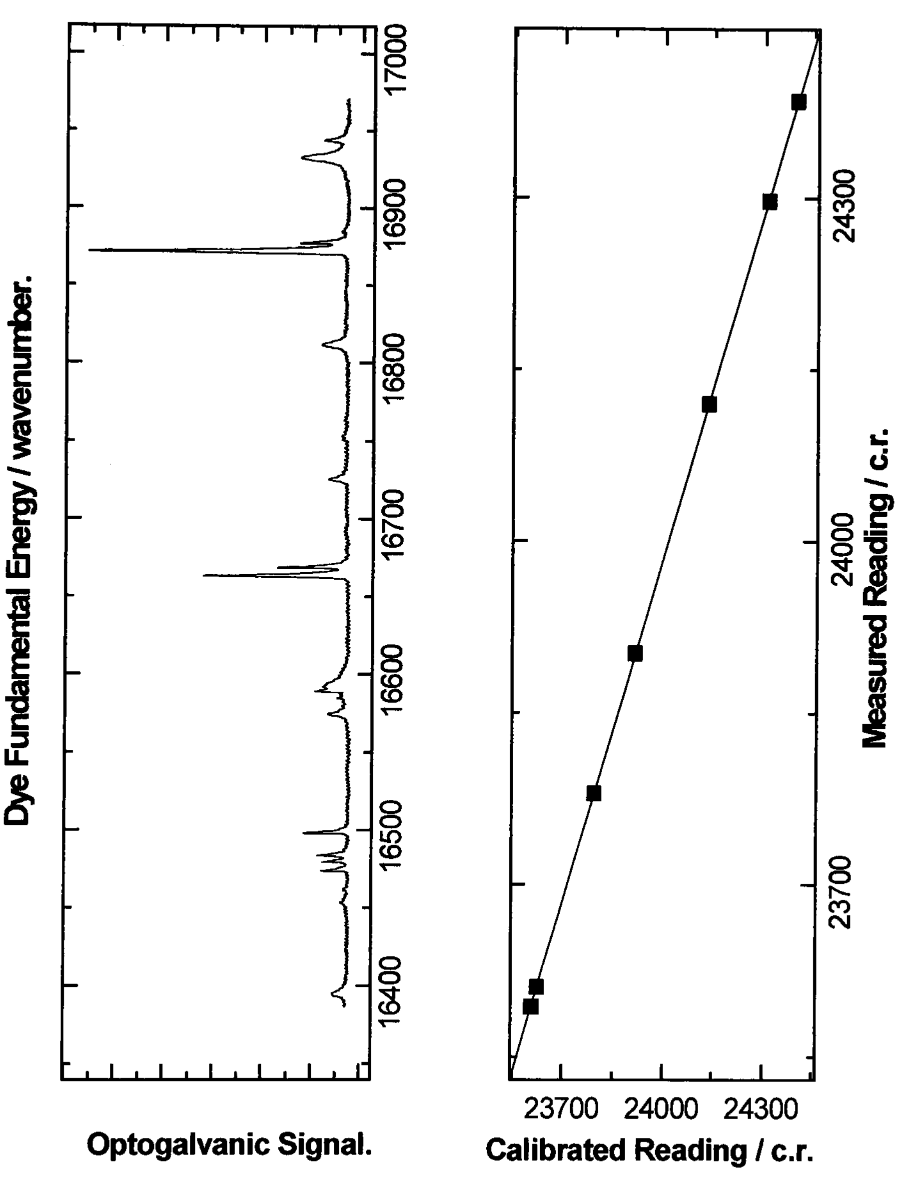

Figure 3.5: Frequency calibration of dye laser. Upper panel is the optogalvanic spectrum of Neon, lower panel is the calibration fit.

3.4. Recent Modifications

3.4.1. Introduction

In the original design[1] of the system light entered the chamber through 7.6 cm focal length fused silica lenses which were fixed in position and formed part of the vacuum seal. Changing the lens involved bringing the system up to atmospheric pressure and there was only limited control over the precise positioning of the focal point. The work on CF_3I presented in chapter 4 was carried out using this system.

To increase the versatility and ease of use of the system a new lens system was designed in which both lenses can be manipulated in the x, y and z directions. This is shown in figure 3.6. and consists of three orthogonal translators (Parker Hannifin), which allow movement of up to 15 mm in the x and y planes and 25 mm along the z-axis, inside a re-entrant port. Fused silica lenses (of variable focal length) were held in a home made brass holder which could be moved in the z direction as a coarse alignment. The presence of the mu-metal shielding around the excitation region limits the minimum distance of the lens from the geometric centre of the ionisation region to 80 mm.

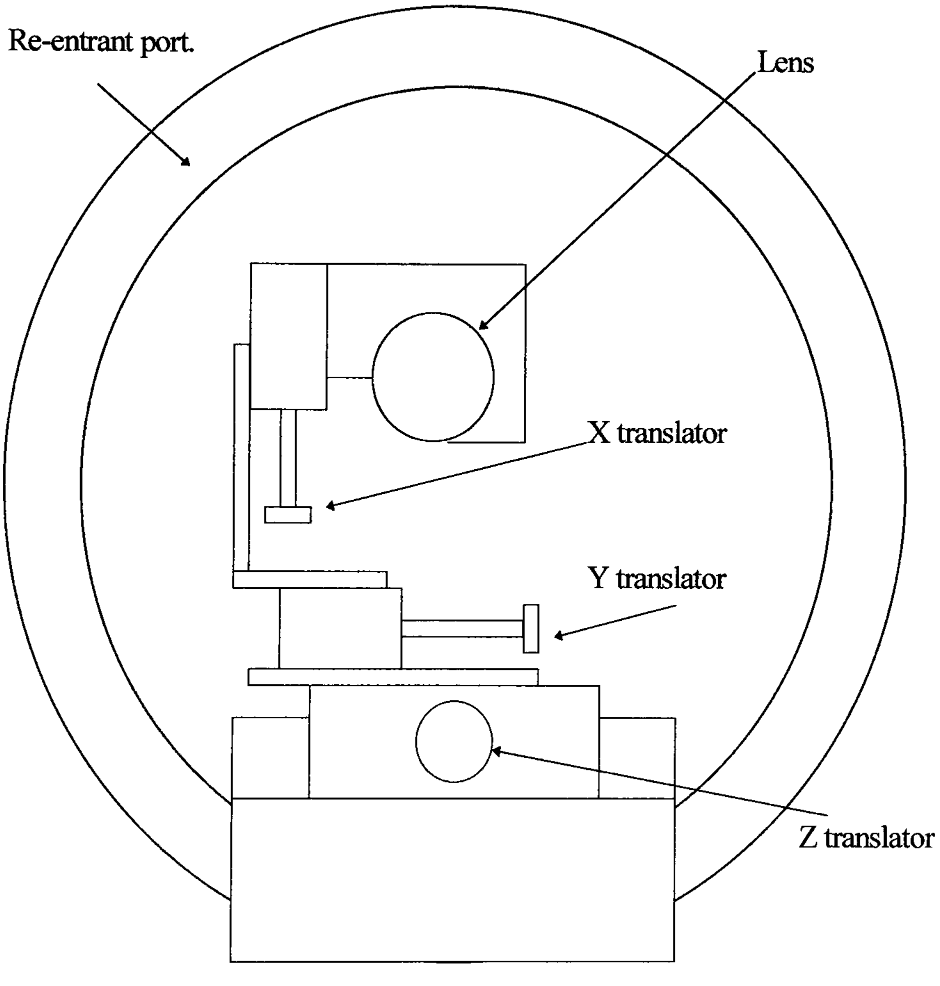

Figure 3.6: New lens system.

3.4.2. Dependence of Focal Length on Wavelength

The reasons for making this change to the system was to allow finer control and adjustment of the focusing conditions and to increase the ease of two-colour alignment. The dependence of focal length on refractive index (and hence the wavelength of light) is particularly acute in the ultra-violet region[16]. The ratio of focal length for two different wavelength is given by equation 3.1. where f_1 and f_2 are the focal lengths and n_1 and n_2 are the refractive indices at the respective wavelengths.

$$\frac{f_1}{f_2} = \frac{n_2 - 1}{n_1 - 1} \qquad \textbf{(3.1.)}$$

The result of this is that a lens will have a considerably shorter focal length in the ultra-violet compared to visible and infra-red. Figure 3.7. shows the variation in refractive index and focal length for a fused silica lens with a focal length of 75 mm at 588 nm (this is typical of the lenses used previously[17]). For experiments involving two ultra-violet photons it is clear that control over the focus will be important.

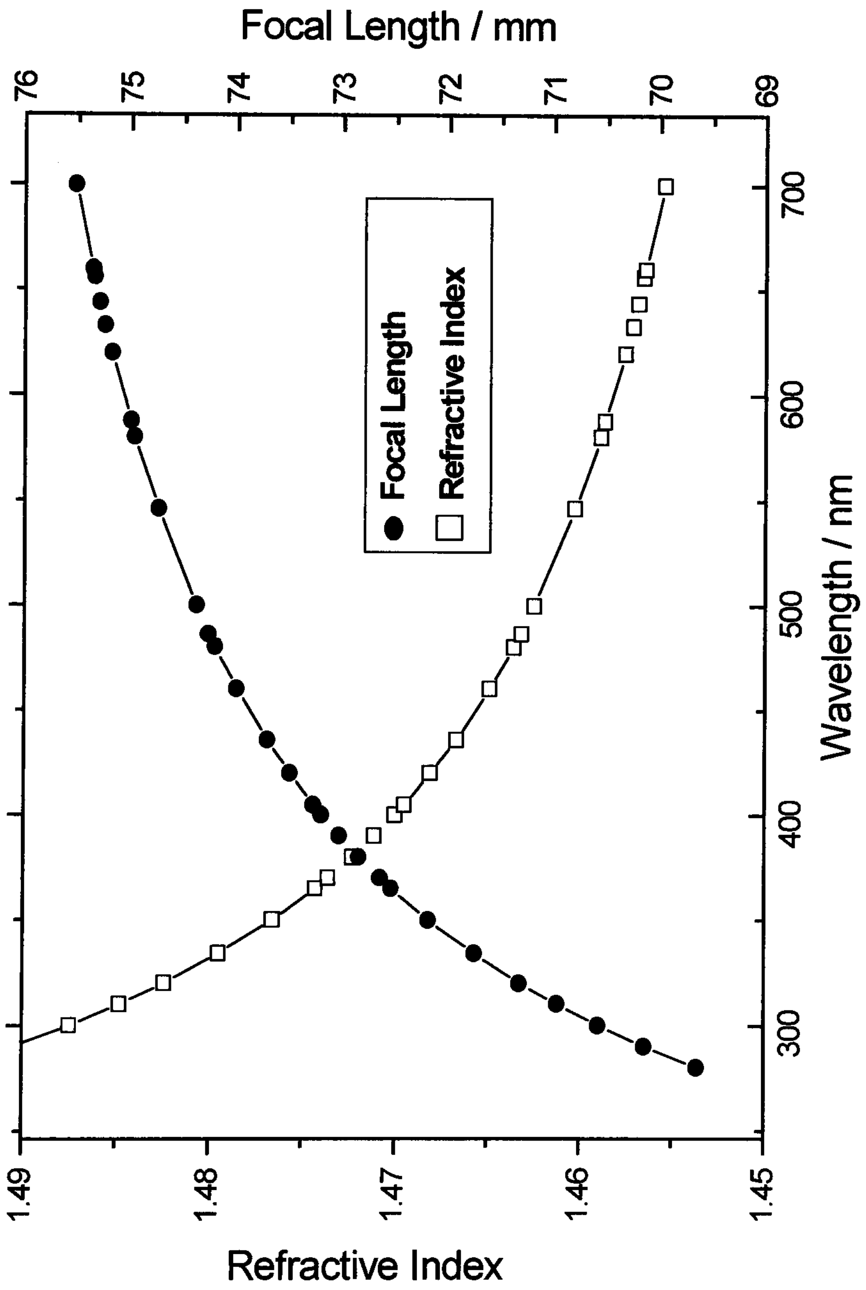

Figure 3.7: Variation of refractive index and focal length with wavelength for fused silica.

3.4.3 Example of the new arrangement

The overall effect of the modifications was to make it considerably easier to change the focusing conditions both in terms of lens position and in the focal length of lens used. As a test of the new arrangement the two-colour (1+1') ZEKE-PFI spectrum of aniline via the first excited singlet state (S_1) was obtained. The aniline cation has been previously studied by several groups by both two-colour photo-ionisation and ZEKE-PFI spectroscopy[18,19]. In addition, aniline displays similar characteristics (both chemical and spectroscopic) to the aminobenzotrifluorides (see chapters 5 and 6).

The excitation route was as follows. The transition from the ground state to the origin band of the first excited state (S_0 to S_1) was pumped by approximately 200 μJ of UV radiation while the probe was 500 μJ. The pump photon was directed *unfocused* into the spectrometer (approximate spot size 4 mm) while the probe was focused with a fused silica lens of focal length 20 cm, although an identical spectrum could be obtained using a 10 cm lens (quoted focal lengths are from the manufacturers catalogue[17] and are for light of wavelength 600 nm). The ZEKE-PFI spectrum obtained is shown in figure 3.8. Assignments are from previous work[18,19].

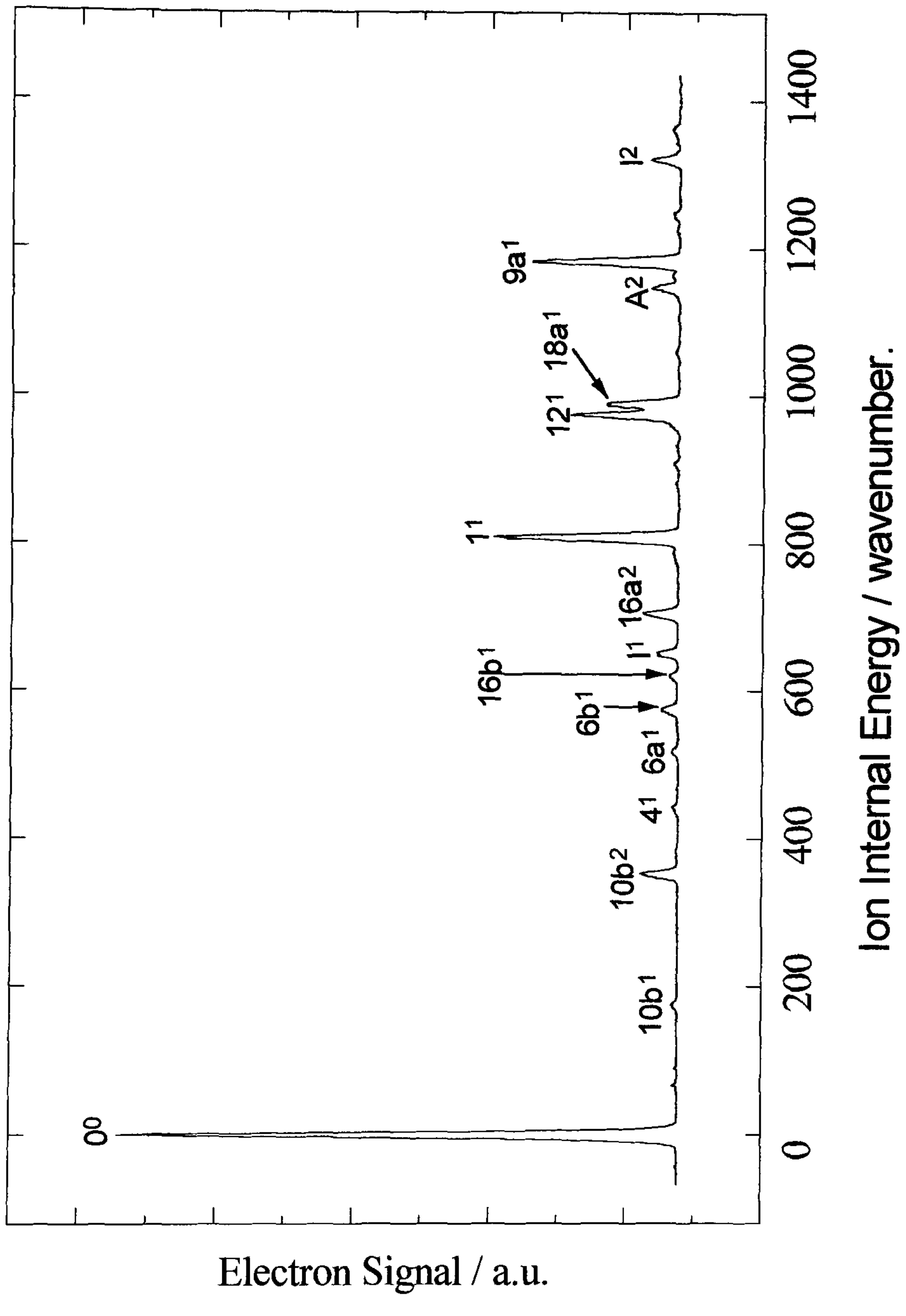

Figure 3.8: The (1+1') ZEKE-PFI spectrum of aniline. The resonant intermediate used was the origin band of the S_1 state.

3.5. References

1. J.G. Goode. PhD Thesis. University of Edinburgh. 1995.
2. M.C.R. Cockett, J.G. Goode, K.P. Lawley & R.J. Donovan. *J.Chem.Phys.* 1995, **102**, 5226.
3. M.C.R. Cockett, J.G. Goode, K.P. Lawley & R.J. Donovan. *Chem.Phys.Lett.* 1994, **231**, 521.
4. D.A. Beattie, M.C.R. Cockett, K.P. Lawley & R.J. Donovan. *J.Chem.Soc. Faraday Trans.* 1997, **93**, 4245.
5. Jet Spectroscopy and Molecular Dynamics. Edited by J.M. Hollas & D. Phillips. Blackie (London). 1995.
6. P.J.A. Ribeiro-Claro, J.C.C. Texeira-Dias, R.D. Gordon & J.M. Hollas. *J.Mol.Spectrosc.* 1991, **150**, 46.
7. K. Muller-Dethlefs, O. Dopfer & T.G. Wright. *Chem.Rev.* 1994, **94**, 1845.
8. K. Muller-Dethlefs & E.W. Schlag. *Angew.Chem.Int.Ed.* 1998, **37**, 1346.
9. T.G. Wright, E. Cordes, O. Dopfer & K. Muller-Dethlefs. *J.Chem.Soc.Faraday Trans.* 1993, **89**, 1609.
10. A. Held, L.Y. Baranov, H.L. Selzle & E.W. Schlag. *J.Chem.Phys.* 1997, **106**, 6848.
11. High Resolution Laser Photoionization and Photoelectron Studies. Edited by I. Powis, T. Baer & C.Y. Ng. John Wiley & Sons (London). 1995.
12. S.I. Sato & K. Kimura. *J.Chem.Phys.* 1997, **107**, 3376.
13. W. Demtroder. *Laser Spectroscopy. Basic Concepts and Instrumentation.* Springer-Verlag (Berlin). 1982.
14. D.L. Andrews & A.A. Demidov. *An Introduction to Laser Spectroscopy.* Plenum Press (New York). 1995.
15. Spectra-Physics. PDL-3/PDL-2 user manuals.

16. M. Nelkon & P. Parker. Advanced Level Physics. Heinemann books (London). 1979.
17. Spindler & Hoyer. Optics/Mechanic catalogue (Gottingen, Germany). 1995.
18. X. Song, M. Yang, E.R. Davidson & J.P. Reilly. *J.Chem.Phys.* 1993, **99**, 3224.
19. X Zhang, J.M. Smith & J.L. Knee. *J.Chem.Phys.* 1992, **97**, 2843.

Chapter 4

ZEKE-PFI of Trifluoromethyl-Iodide (CF_3I)

4.1. Introduction

Substituting fluorine for hydrogen can have a dramatic effect on the spectroscopic properties of a molecule. Brundle and co-workers, in the 1970's, using conventional He(I) photoelectron spectroscopy (PES) compared a wide number of fluorinated and unfluorinated species[1,2]. They found dramatic increases in the ionisation energies and the extent of vibrational structure of photoelectron bands for the fluorinated species relative to the unfluorinated analogues. This was termed the "perfluoro" effect. For a subset of molecules (including planer and aromatic species) the magnitude of this effect was considerably greater for ionisation from σ-type orbitals (increase in I.E. of up to 4 eV) than from π-orbitals (increase of 1 eV) since the σ-type orbitals were more directly involved with the orbitals of the fluorine atoms than the π-orbitals. This was of use in the assignment of photoelectron bands. For non-planer molecules the increase in ionisation energy was not linked to the orbital symmetry and was of the order of 1-2 eV. The overall conclusion was that, for perfluorinated molecules, all non-bonding orbitals were stabilised by the presence of the fluorine atoms.

One of the most experimentally accessible series of molecules in which to study the perfluoro effect are the alkyl halides. The unfluorinated series, starting with the methyl halides, represent some of the most studied species in molecular spectroscopy (see for example references 3-6 and references therein). In the 1970's Boschi and Salahub studied both the VUV absorption and He(I) photoelectron spectra of a substantial number of fluorinated and unfluorinated alkyl iodides[7,8]. The first two photoelectron bands of such molecules correspond to ionisation from a non-bonding orbital based predominately on the iodine. As such any geometry change following ionisation would be expected to be minimal resulting in the observation of only limited vibrational structure in the photoelectron spectrum. This is the case for the alkyl iodides (i.e. CH_3I, C_2H_5I etc.) which do indeed display sharp photoelectron bands dominated by origin transitions. Perfluorination results in considerably wider bands, with unresolved vibrational structure, shifted to higher energy by up to 1 eV. Later, higher resolution (~80 cm^{-1}), work on the He(I) and He(II) photoelectron spectra of the trifluoromethyl halides (CF_3X where X = Cl, Br and I) by Cvitas and co-workers[9,10] partially resolved this structure. They observed progressions (up to 3 or 4 quanta) in two of the symmetric normal modes (ν_1 and ν_3) of the molecules.

Of the trifluoromethyl halides the most experimentally tractable is the iodide (CF_3I). This chapter presents the ZEKE-PFI spectrum of the ionic ground state of CF_3I by two separate ionisation schemes. The first involves a direct two-photon one-colour excitation scheme while the second uses the $[^2E_{3/2}]_c6p$ Rydberg states as resonant intermediates in a two-colour scheme. The data obtained from both these schemes, in conjunction with polarisation measurements, allow the identification of the vibronic structure of the $[^2E_{3/2}]_c$ 6p Rydberg states.

4.2. Previous work on CF_3I

4.2.1. Neutral states

The ground state of CF_3I ($X\ ^1A_1$) has been studied by vibrational spectroscopy and frequencies for all six fundamental vibrations are known[11,12]. Of these ν_1, ν_2 and ν_3 are classified as totally symmetric (**a_1**) while ν_4, ν_5 and ν_6 are non-totally symmetric and degenerate (**e**) under the C_{3v} point group.

Electronically excited states of CF_3I were first studied by absorption spectroscopy[13]. The first excited state (the A state) lies in the ultra-violet (absorption maximum at 270 nm) and gives rise to a broad featureless continuum. Magnetic circular dichroism (MCD) has been used to determine the presence of three repulsive states ($^3Q_1$, $^3Q_0$ and ^1Q) and their relative contributions to the overall absorption spectrum[14].

The Rydberg states of CF_3I were first studied by Sutcliffe and Walsh[15], using vacuum-ultra-violet (VUV) absorption, who identified a Rydberg series converging to 83984 cm^{-1} (10.41 eV). This was assigned to an *ns* series (n = 6, 7 & 8) based on the ground ionic state ($^2E_{3/2}$). Some vibrational structure was seen and assigned to the three symmetric normal modes with frequencies in the range 950-1000 cm^{-1} (ν_1), 680-720 cm^{-1} (ν_2) and 200-230 cm^{-1} (ν_3). The components of the first member of this series, the $[^2E_{3/2}]_c$ 6s states, (energy around 57000 cm^{-1}) were studied in more detail by Herzberg[12,16] as an example of the Jahn-Teller effect[17]. This manifested itself as a small splitting into A and E components (~8 cm^{-1}) of the hot band transition (6_1^1) from the lowest energy degenerate normal mode (ν_6) of the neutral ground state.

More recently this region has been studied by resonance enhanced multiphoton ionisation spectroscopy (REMPI). Taatjes and co-workers[18], using (2+1) REMPI, studied both the $[^2E_{3/2}]_c6s$ states and the corresponding spin-orbit states, the $[^2E_{1/2}]_c6s$ states.

Utilising both ion fragmentation patterns and polarisation measurements they were able to assign two Rydberg states to each spin-orbit component of the ionic core. For all four states the origin band was the dominant feature with weaker vibrational structure. The $[^2E_{1/2}]_c6s{:}0$ Rydberg state displayed considerably broader peaks than its counterparts. This was ascribed to state-selective predissociation by a repulsive state.

To higher energy (~65000 cm^{-1}) considerably more intense Rydberg transitions were observed by Waits and co-workers[19]. They assigned these to a 6p Rydberg system built on a $^2E_{3/2}$ core using time-of-flight photoelectron spectroscopy (TOF-PES). However, they were unable to make any vibrational assignments due to the complexity of the vibronic structure. Assuming a similar spin-orbit splitting as the 6s cluster (~5000 cm^{-1})[18] the $[^2E_{1/2}]_c6p$ states should lie in the region of 70000 cm^{-1}. No features that could be attributed to the molecular species could be seen due to the presence of a repulsive state at the one-photon level.

Recently the Rydberg states of CF_3I have been extensively studied by a variety of excitation schemes[20]. Using one-colour two-photon techniques no Rydberg states higher than the $[^2E_{3/2}]_c6p$ cluster have been observed. The 6p region itself has been studied by two-colour (1+1`+1) REMPI with the first photon on or off resonance with the repulsive A band. No substantial difference was noted between these spectra and the one-colour two-photon experiments thus excluding intermediate bond stretching as a possible explanation for the unusual vibrational structure of the 6p region.

Rydberg states with principal quantum numbers higher than 6 can be observed by one-colour three-photon excitation routes ((3+1) REMPI). These states displayed vibrational spacings more in line with the ionic values (e.g. ν_3 = 215 cm^{-1} for the $[^2E_{3/2}]5d$ state[20]). In addition three-photon excitation to the 6p region in conjunction with polarisation studies has shown the presence of an $\Omega=1$ Rydberg state. This state shows only one very weak transition and lies towards the red end of the observed structure (two-photon energy 65496 cm^{-1}). The remaining structure has not yet been assigned.

4.2.2. Ionic states

The CF_3I cation has been extensively studied by both photoelectron[8,9,21] and photoionisation/photofragmentation[22] techniques. The main interest has been the assignment of the various photoelectron bands to localised molecular orbitals by varying the ionisation wavelength. The first two bands (ionisation energies of 10-11 eV) have been assigned to the spin-orbit components ($^2E_{3/2}$ and $^2E_{1/2}$) resulting from the removal of an electron from an iodine "lone-pair" orbital. These bands have been studied at higher resolution (~80 cm^{-1}) by Cvitas[9] and co-workers. This experiment was performed at room temperature giving rise to extensive hot band structure. Thus the vibrational bands found are broad and somewhat overlapping. However it was possible to assign extensive (3 or 4 quanta) vibrational progressions in both spin-orbit states to two of the symmetric normal modes of the molecule; ν_1, the symmetric C-F stretch (~1000 cm^{-1}) and ν_3, the symmetric C-I stretch (~240 cm^{-1}). The vertical ionisation energy was found to be 10.45 eV (84280 cm^{-1}) although structure was observed as low as 10.30 eV (83070 cm^{-1}). Such extended vibrational structure is very different to that of the unfluorinated analogue, CH_3I, which shows a He(I) photoelectron spectrum more consistent with removal of an electron from a non-bonding molecular orbital[8,23].

However the ZEKE-PFI spectrum of methyl iodide[24,25] using two photons direct from the neutral ground state displays a completely different picture from that of the conventional photoelectron spectrum. Long progressions (up to ten quanta) in the C-I stretch (ν_3) and the CH_3 umbrella mode (ν_2) are observed for both spin-orbit components of the ion. The cause of this is the fact that the first photon is resonant with the repulsive A state resulting in extension of the C-I bond (i.e. the molecule is beginning to dissociate). This results in a far wider Franck-Condon region of the ion being accessed by the second photon giving vastly extended vibrational progressions. Other molecules also show a similar effect[26,27], e.g. I_2 and IBr.

4.3. The Coherent Two-Photon One-Colour ZEKE-PFI Spectrum of CF_3I^+ ($^2E_{3/2}$)

4.3.1. Results

In the absence of tuneable vacuum ultraviolet laser radiation the most direct excitation scheme for a ZEKE-PFI experiment is a coherent two-photon one-colour route[24-27] (see figure 4.1). This has the simplicity of not requiring the characterisation of a suitable neutral intermediate state. Such schemes have proved particularly useful for halogen containing species[24-27].

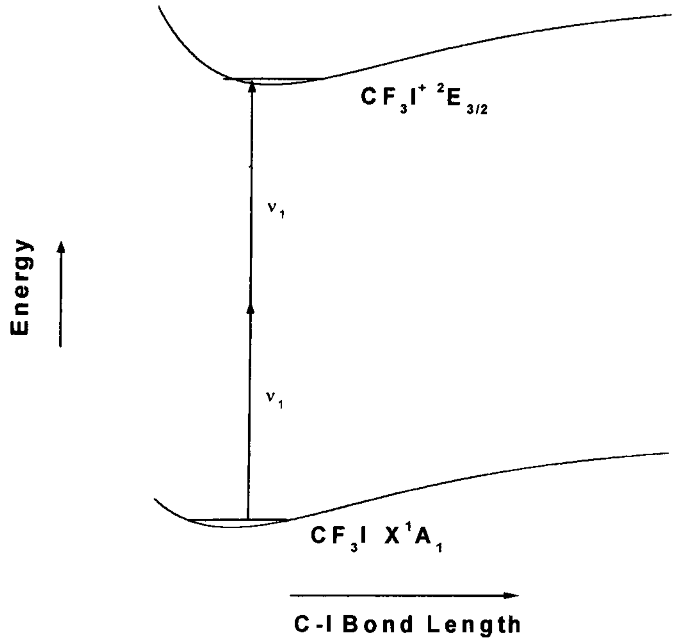

Figure 4.1: Schematic of the coherent two-photon one-colour excitation scheme.

The one-colour two-photon ZEKE-PFI spectrum of the lower spin-orbit state ($^2E_{3/2}$) of CF_3I^+ is shown in figure 4.2. This spectrum was obtained using several laser dyes. No attempt has been made to adjust for the laser power although the transitions are, in general, weak and were only observed near the maximum of dye output.

Vibrational assignments (given in table 4.1) are made by comparison with neutral ground state vibrational frequencies[11,12], He(I) PES[9] and the vibrational frequencies found for Rydberg states[20] and are denoted in the following fashion; X_n^m where X is the normal mode of vibration (1-6) of the ion, n is the neutral ground state vibrational quantum number (equal to 0 in all cases since no hot bands are seen) and m is the ionic state vibrational quantum number. The observed signals are weak but progressions of up to three quanta in all three symmetric modes, and combinations thereof, can be observed. The vibrational frequencies found are ν_1 (974 cm^{-1}), ν_2 (735 cm^{-1}) and ν_3 (206 cm^{-1}). The long vibrational progressions are atypical of ionisation from what is, to a first approximation, a non-bonding orbital. In particular ν_3 (the C-I stretch) is substantially reduced relative to the neutral ground state[11] (286 cm^{-1}) indicating significant bonding character of the iodine lone pair orbitals. A further sign of this effect is the ionisation energy which is substantially increased relative to the unfluorinated species. The adiabatic ionisation energy is found to be 83847 cm^{-1}, an increase of nearly 1 eV relative to that of CH_3I[24] (76932 cm^{-1}). However the electron signals are too weak to allow a full electric field dependence to be carried out (the spectrum in figure 4.2. was obtained with an extraction field of 7 Vcm^{-1} at a delay of 1 μs).

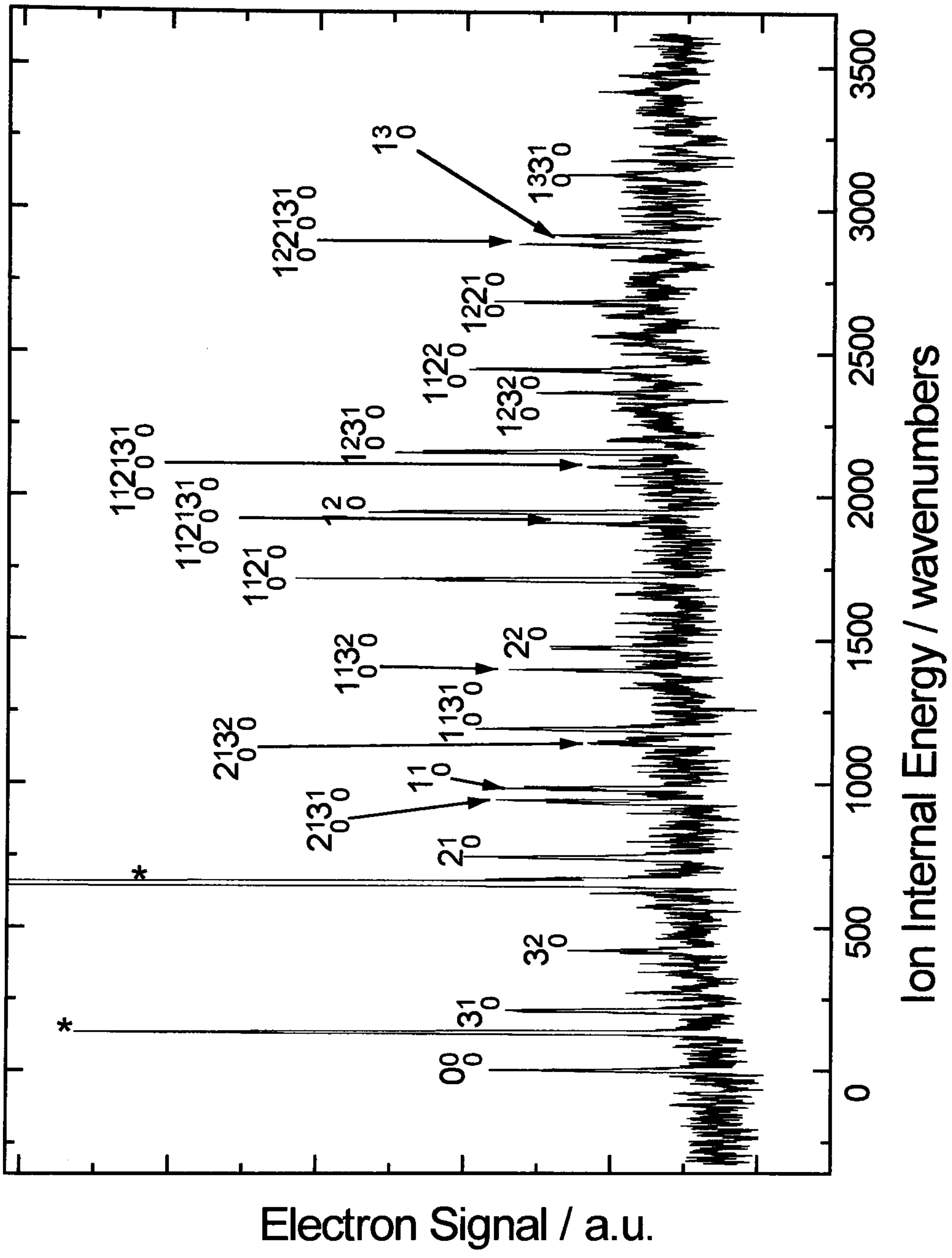

Figure 4.2: Coherent two-photon one-colour ZEKE-PFI spectrum of CF_3I^+ ($^2E_{3/2}$). * indicates atomic iodine transitions (see text). The spectrum is presented relative to the adiabatic ionisation energy (83647 cm^{-1}).

Given the fact that only those high-*n* Rydberg states which lie within ~10 cm^{-1} of the ionisation threshold (the so-called ZEKE or magic region[28]) survive the delay time the field free ionisation energy must lie no more than 10 cm^{-1} higher than the quoted value.

Two additional transitions, which are more intense than the CF_3I signals, are designated with asterisks in figure 4.2. On the basis of previous work these are assigned to two-photon ZEKE-PFI transitions of atomic iodine[24,29]. The first corresponds to the I^+ ($^3P_1$) ←← I ($^2P_{1/2}$) transition while the second is the I^+ ($^3P_2$) ←← I ($^2P_{3/2}$) transition. These result from the one-photon dissociation of CF_3I in the A band[13] followed by two-photon excitation to the high-*n* Rydberg states which are then field ionised. No sign of similar transitions were observed for the second product of photo-dissociation, the CF_3 radical, despite there being a sizeable ionisation cross-section in this energy region[30,31].

Except for these atomic lines the spectrum of figure 4.2. is essentially the same as the conventional He(I) PES[9] with the addition of jet-cooling (no hot bands are observed) and the substantially higher resolution afforded by ZEKE-PFI spectroscopy. However one major difference remains; namely that no sign of the upper spin-orbit state ($^2E_{1/2}$) was seen. The vibrational envelope of the $^2E_{3/2}$ state extends up to nearly 4000 cm^{-1} above the origin. This compares with a spin-orbit splitting of 5900 cm^{-1} (from He(I) PES[9]). Given the energy range of the dyes used it is likely that the $^2E_{1/2}$ state would have been observed if, as in the He(I) PES spectrum[9], it is of comparable intensity to its spin-orbit counterpart. Its absence indicates some specific aspect of ZEKE-PFI spectroscopy and is discussed in the next section.

Ion Internal Energy (cm^{-1})	**Assignment**	**Ion Internal Energy (cm^{-1})**	**Assignment**
0	0^0_0	**1899**	$1^1_0 2^1_0 3^1_0$
206	3^1_0	**1938**	1^2_0
410	3^2_0	**2098**	$1^1_0 2^1_0 3^2_0$
612	3^3_0	**2150**	$1^2_0 3^1_0$
735	2^1_0	**2193**	2^3_0
928	$2^1_0 3^1_0$	**2356**	$1^2_0 3^2_0$
974	1^1_0	**2434**	$1^1_0 2^2_0$
1140	$2^1_0 3^2_0$	**2672**	$1^2_0 2^1_0$
1179	$1^1_0 3^1_0$	**2871**	$1^2_0 2^1_0 3^1_0$
1379	$1^1_0 3^2_0$	**2904**	1^3_0
1463	2^2_0	**3114**	$1^3_0 3^1_0$
1705	$1^1_0 2^1_0$	**3403**	$1^2_0 2^2_0$

Table 4.1: Peak positions and assignments for the (1+1) ZEKE-PFI spectrum of CF_3I^+ ($^2E_{3/2}$). The adiabatic ionisation energy was 83647 cm^{-1} (uncorrected for field effects).

4.3.2. Discussion

The vibrational progressions seen in figure 4.2. indicate that the iodine lone-pair molecular orbitals have a significant amount of bonding character. This is a direct result of the presence of three fluorine atoms in the molecule. For C_{3v} molecules such as CF_3I or CH_3I the CX_3 group forms a set of molecular orbitals of the type a_1 and e along with their anti-bonding counterparts a_1^* and e^*. Figure 4.3. shows a schematic of the molecular orbitals.

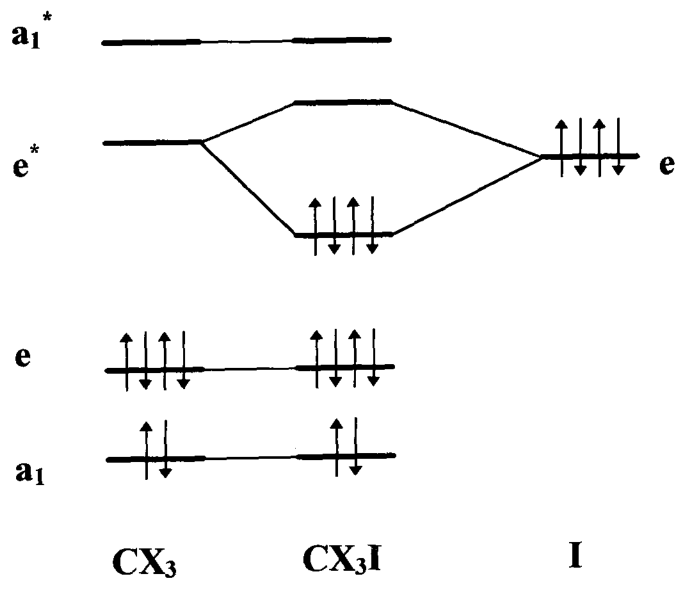

Figure 4.3. Schematic of the molecular orbitals involved in CX_3I. Orbitals involved in the direct bonding between C and I and the fluorine lone pairs have been omitted for clarity.

The bonding orbitals are filled in the neutral ground state. The lone pairs on the iodine atom are also of **e** symmetry and can interact with the anti-bonding **e** orbitals based on the CF_3 fragment resulting in the stabilisation of the lone-pair orbital. Such a mechanism is not restricted to CF_3I, methyl iodide can and does display some stabilisation. In CH_3I the C-I stretch (υ_3) reduces from 533 cm^{-1} to 478 cm^{-1} on ionisation[24,25] (i.e. the ionic frequency is 90% of the neutral). In CF_3I however the reduction is from 286 cm^{-1} to 205 cm^{-1} (72%). The conclusion from this is that the interaction between the anti-bonding orbitals on the CF_3 fragment and the lone-pair orbitals is far greater than that experienced by the unfluorinated species. This is most likely due to the different energetics and spatial extent of fluorine orbitals relative to hydrogen resulting in a higher degree of overlap. Thus CF_3I is an excellent example of the perfluoro effect[1,2] in that the non-bonding orbitals are stabilised by the presence of the fluorine atoms.

The results show further differences between CF_3I and its unfluorinated analogue. Firstly, no evidence for bond stretching at the one-photon level is observed for CF_3I. To explain this the relative one-photon cross-sections for transitions into the repulsive A band must be compared. It is a general feature of perfluorinated alkyl iodides that the ultra-violet absorption cross-section is lower than that of the unfluorinated species[7]. In the case of CF_3I there exists an absorption maximum[13] of 6.0×10^{-19} $cm^2molecule^{-1}$ at 267 nm while for CH_3I the absorption maximum[13] is almost twice as intense (1.1×10^{-18} $cm^2molecule^{-1}$) and is shifted to the blue (258 nm). The net result of this is that the two-photon wavelength for ionisation of CH_3I (260 nm) lies almost exactly at the UV absorption maximum resulting in large scale intermediate effects which are easily observable[24,25]. For the case of CF_3I the ionisation energy has shifted significantly to higher energy (240 nm) with the result that UV cross-section is considerably reduced and so any intermediate effects will be much weaker than in CH_3I. It is likely that any such effects will be too weak to be observed in the current experiment given the rather poor signal to noise ratio of figure 4.2. In previous experiments on IBr[27], where the ionisation energy and UV absorption maximium[32] have a similar relative position to that of CF_3I, the Franck-Condon allowed transitions ($v^+ = 0$-3) are observed followed by a much weaker extended progression (up to $v^+ = 9$) due to the repulsive state. Figure 4.4. summarises the UV absorption data for CF_3I, CH_3I and IBr.

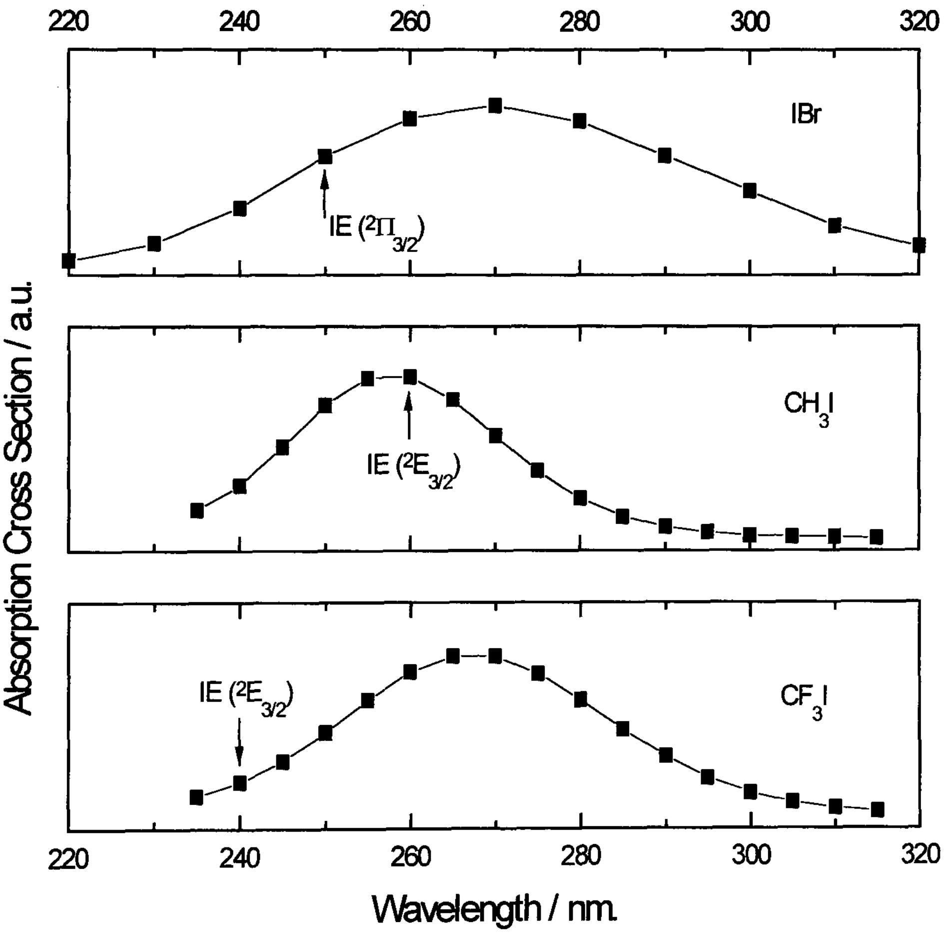

Figure 4.4: Ultra-violet absorption cross-sections and two-photon ionisation energies for CF_3I, CH_3I and IBr. Adapted from references 13, 24, 27 and 32.

In a further difference from CH_3I the upper spin-orbit state ($^2E_{1/2}$) is not observed in the current experiment. For the upper spin-orbit component there exists an additional means of decay for the high-*n* Rydberg states populated by the laser, namely spin-orbit autoionisation[33] into the continuum of the lower component. A schematic of this is shown in figure 4.5.

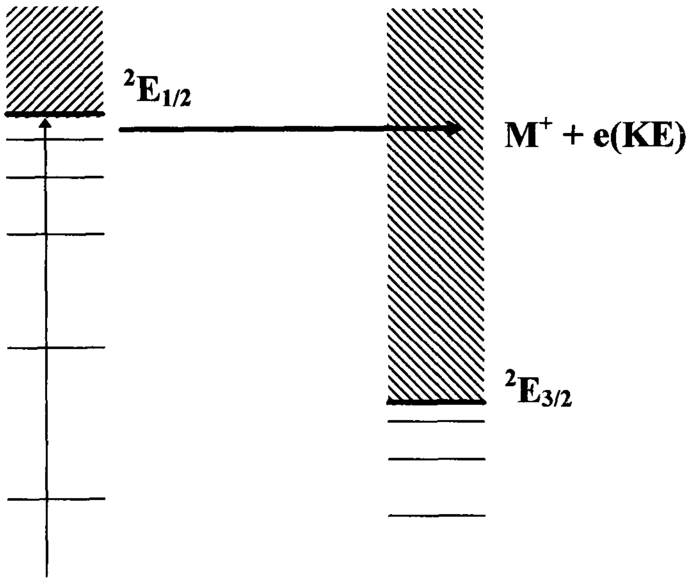

Figure 4.5. Spin-orbit autoionisation.

Such decay has previously been found to be efficient for several halogen containing molecules (e.g. HCl[34], IBr[27] and I_2[26]) and results in the upper spin-orbit component being considerably less intense relative to the lower state. The mechanism involves the interaction of a distant Rydberg electron with the ionic core since the state of the core must change. As the CF_3 group is considerably more polar than its methyl counterpart such interaction may be more efficient for CF_3I than for CH_3I.

In the present case any reduction in intensity would lead to the electron signal falling below the noise level and hence being undetectable. No substantial differences in ion yields were observed in the regions of the two ionisation thresholds indicating that the absence of the upper spin-orbit state is due to a mechanism specific to ZEKE-PFI spectroscopy.

4.4. The (2+1') ZEKE-PFI of CF_3I^+ ($^2E_{3/2}$) via the $[^2E_{3/2}]_c$ 6p Rydberg States

4.4.1. Introduction

The region of the $[^2E_{3/2}]6p$ Rydberg states of CF_3I has been studied previously by Waits et al[19] and by other members of the Edinburgh group[20]. No definitive assignment of the electronic or vibrational structure has yet been made. This section will present (2+1) REMPI spectra of the region and make assignments using ZEKE-PFI spectroscopy. Figure 4.6. shows a schematic of the excitation schemes.

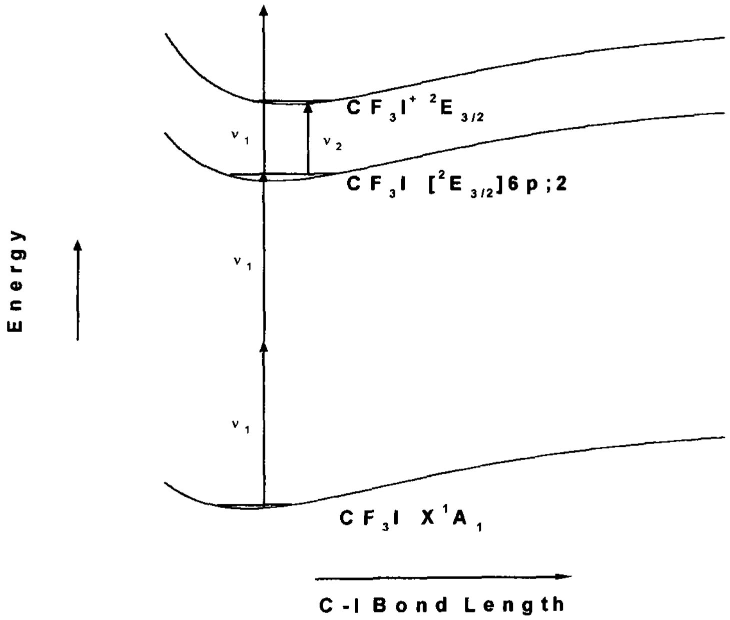

Figure 4.6: Schematic of the (2+1') ionisation scheme.

4.4.2. The (2+1) REMPI spectrum of the 6p Rydberg states

The (2+1) REMPI spectrum of CF_3I in the region of the $[^2E_{3/2}]$ 6p Rydberg states is shown in figure 4.7. Two distinct regions can clearly be seen. Above 66500 cm^{-1} the peaks are broader and weaker than those below this energy. Figure 4.8. shows the higher energy region in more detail using both linear and circularly polarised light. All the broader peaks show a substantial decrease in intensity under circular polarisation. By contrast the sharper peaks to lower energy show an increase in intensity. Theoretical work by Bray and Hochstrasser[35] indicates that the intensity of *all* rotational branches in a two-photon transition in diatomic molecules should *increase* by a factor of 1.5 under circular polarisation relative to linear, with one important exception. The Q-branch of an $\Omega=0 \leftarrow \Omega=0$ transition can exhibit changes in intensity of *up to* a factor of 1.5. Experimental work on heavier molecules (such as I_2 or CH_3I[36,37]) for which only vibrational resolution is possible has shown that the intensity of a $\Delta\Omega=0$ transition is reduced under circular polarisation relative to linear. With this in mind the two-photon transitions which decrease in intensity in figure 4.8. are assigned as being part of a $[^2E_{3/2}]6p;0$ system.

The remaining structure (except for the transition at 65496 cm^{-1}, indicated in figure 4.7., which has been previously assigned as $[^2E_{3/2}]6p;1$ by the dependence of the (3+1) REMPI spectrum on the polarisation of the light[20]) is assigned as $[^2E_{3/2}]6p;2$ although it is not possible to say if all the structure belongs to a single Rydberg state or to several. However it is clear that the 6p region of CF_3I is very different to that of the 6s Rydberg states of CF_3I and to the analogous 6p states of CH_3I[6].

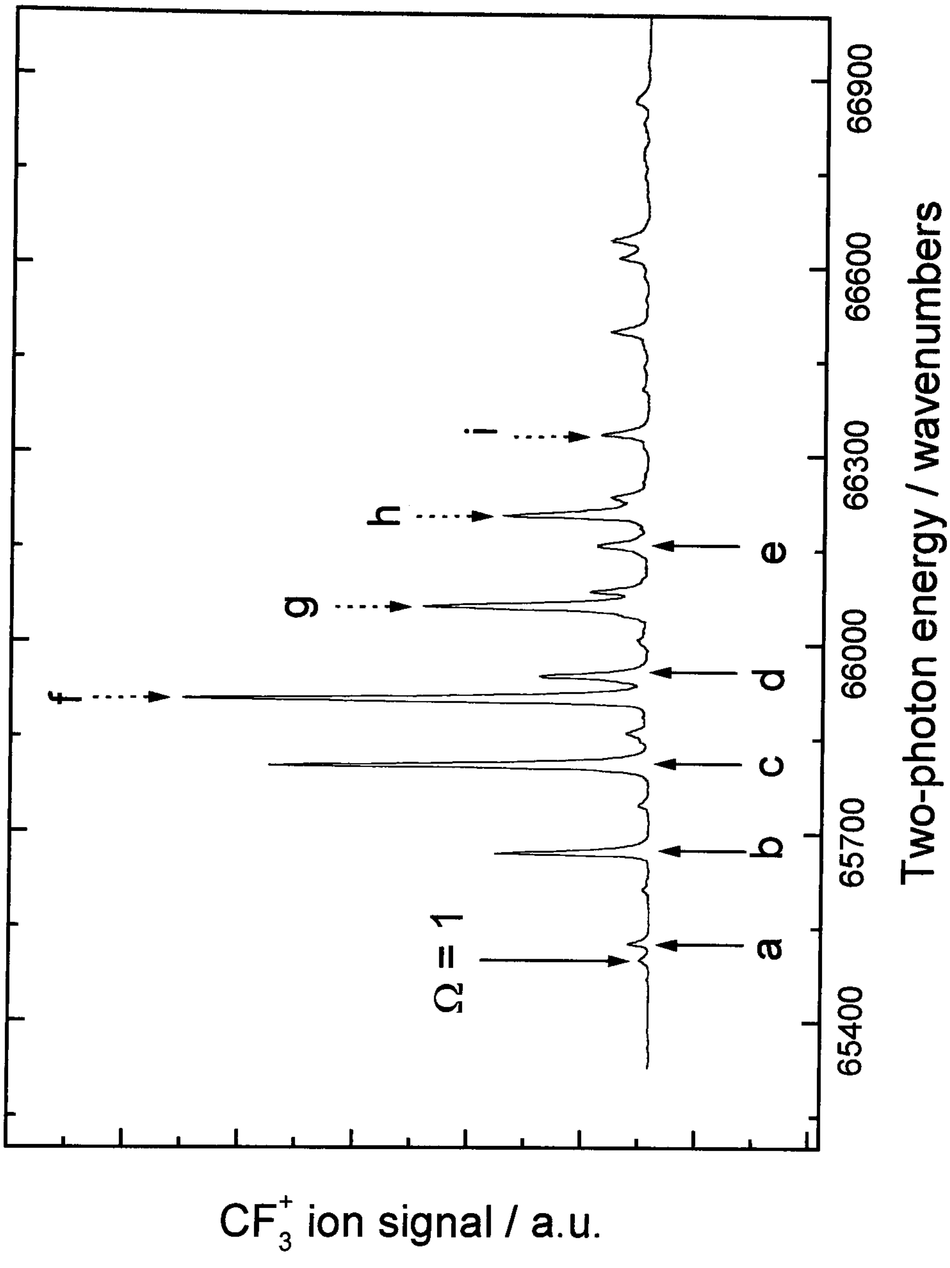

Figure 4.7: (2+1) REMPI of the $[^2E_{3/2}]6p$ Rydberg states of CF_3I. Arrows indicate transitions used in two-colour experiments. The $\Omega = 1$ state has previously been identified by (3+1) REMPI[20].

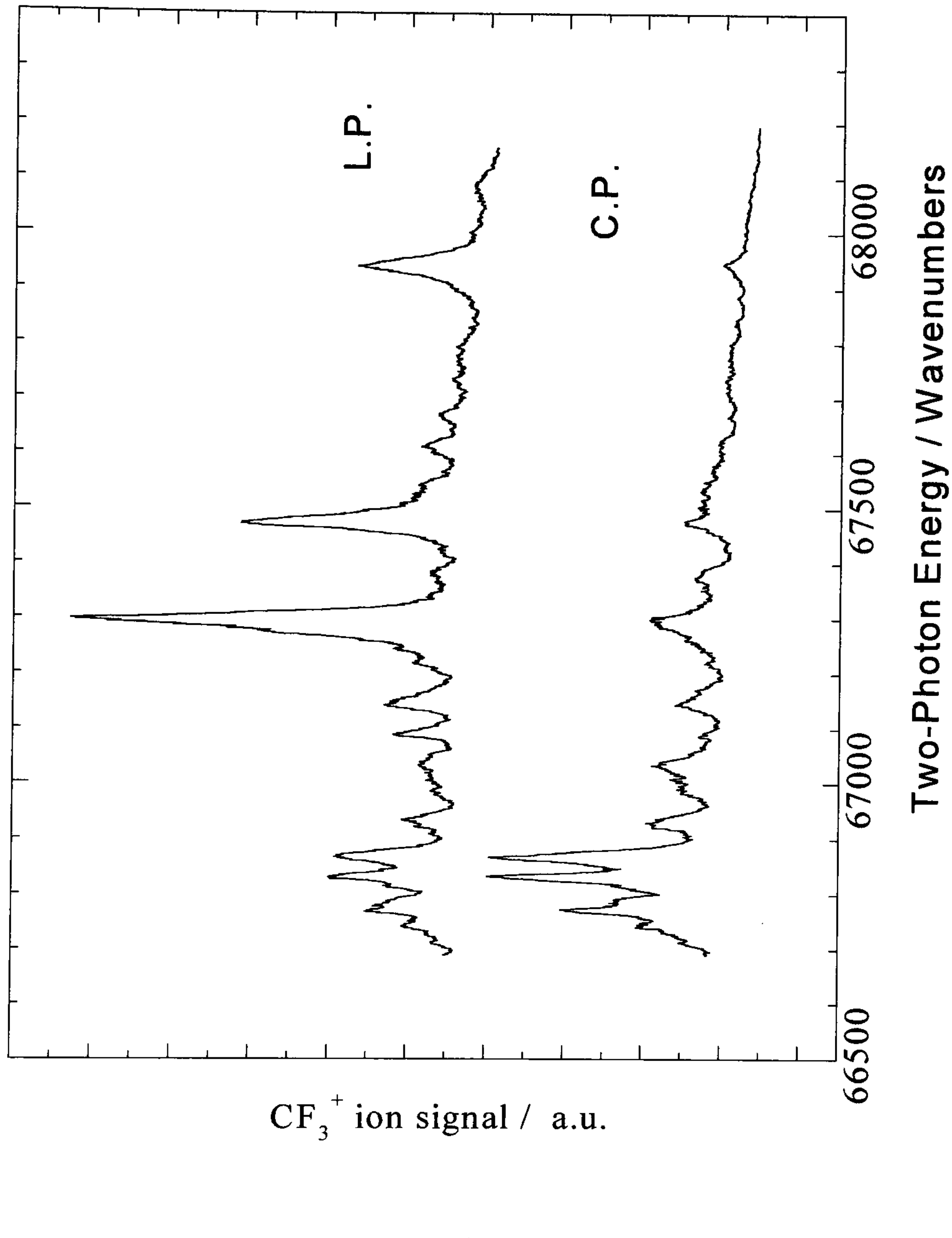

Figure 4.8: (2+1) REMPI spectrum of the $[^2E_{3/2}]6p$ Rydberg states using linearly (LP) and circularly polarised (CP) light.

Figure 4.9. shows this region of the REMPI spectrum measured in both the parent (CF_3I^+) and fragment (CF_3^+) mass channels. It is clear that the transition at 65908 cm^{-1}, while the most intense peak in both spectra, is relatively weaker in the fragment channel when compared to the other transitions. This may indicate two different states having the same overall symmetry. A similar argument was used in the assignment of the 6s Rydberg states[18].

Vibrational assignments could only be made by use of two-colour photoelectron spectroscopy using the 6p Rydberg states as resonant intermediates. The results of such experiments are shown in the following section.

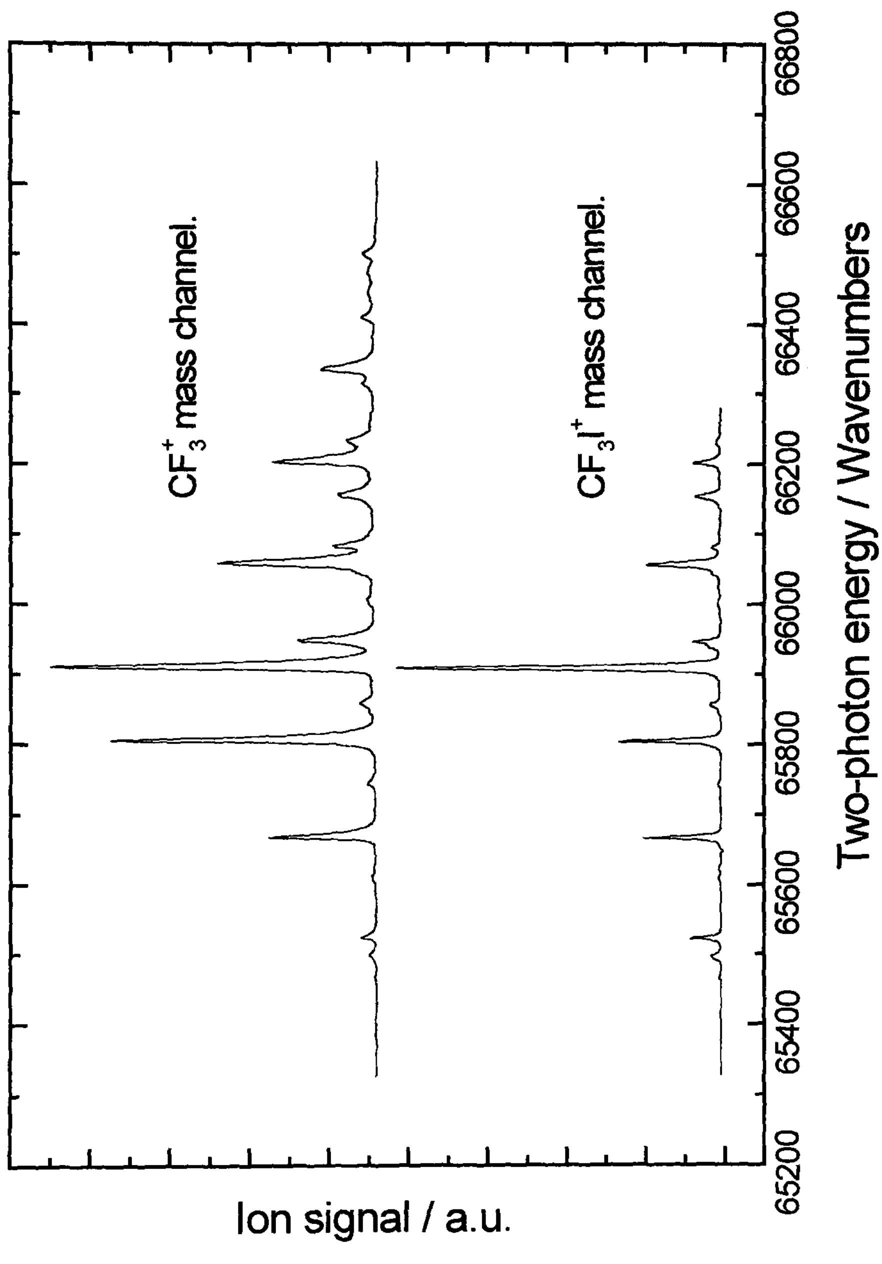

Figure 4.9: (2+1) REMPI of CF_3I in the $[^2E_{3/2}]_c$ 6p:2 region in both the parent (CF_3I^+) and fragment (CF_3^+) mass channels.

4.4.3. (2+1') ZEKE-PFI via the $[^2E_{3/2}]_c$ 6p;2 system

It was possible to record ZEKE-PFI spectra of CF_3I^+ ($^2E_{3/2}$) using nine of the most intense transitions (denoted a to i in figure 4.7.) of the $[^2E_{3/2}]$6p;2 system. These spectra, shown in figures 4.10., 4.11. and 4.12. allow the unambiguous assignment of the majority of the vibrational structure of the intermediate.

In addition the far superior signal to noise ratio relative to the one colour experiment allowed a detailed study of the electric field dependence of the ionisation energy. Figure 4.13 shows the extrapolation to zero field (the experimental spectra were given in chapter 2, figure 2.8.). The excellent straight line fit allows an accurate determination of the adiabatic ionisation energy to be made as 83652±2 cm^{-1}. This compares well with the lower limit obtained from the one-colour experiment (83647 cm^{-1}) and is a considerable improvement over the previous determinations by Rydberg extrapolation[8] and conventional He(I) photoelectron spectroscopy[9].

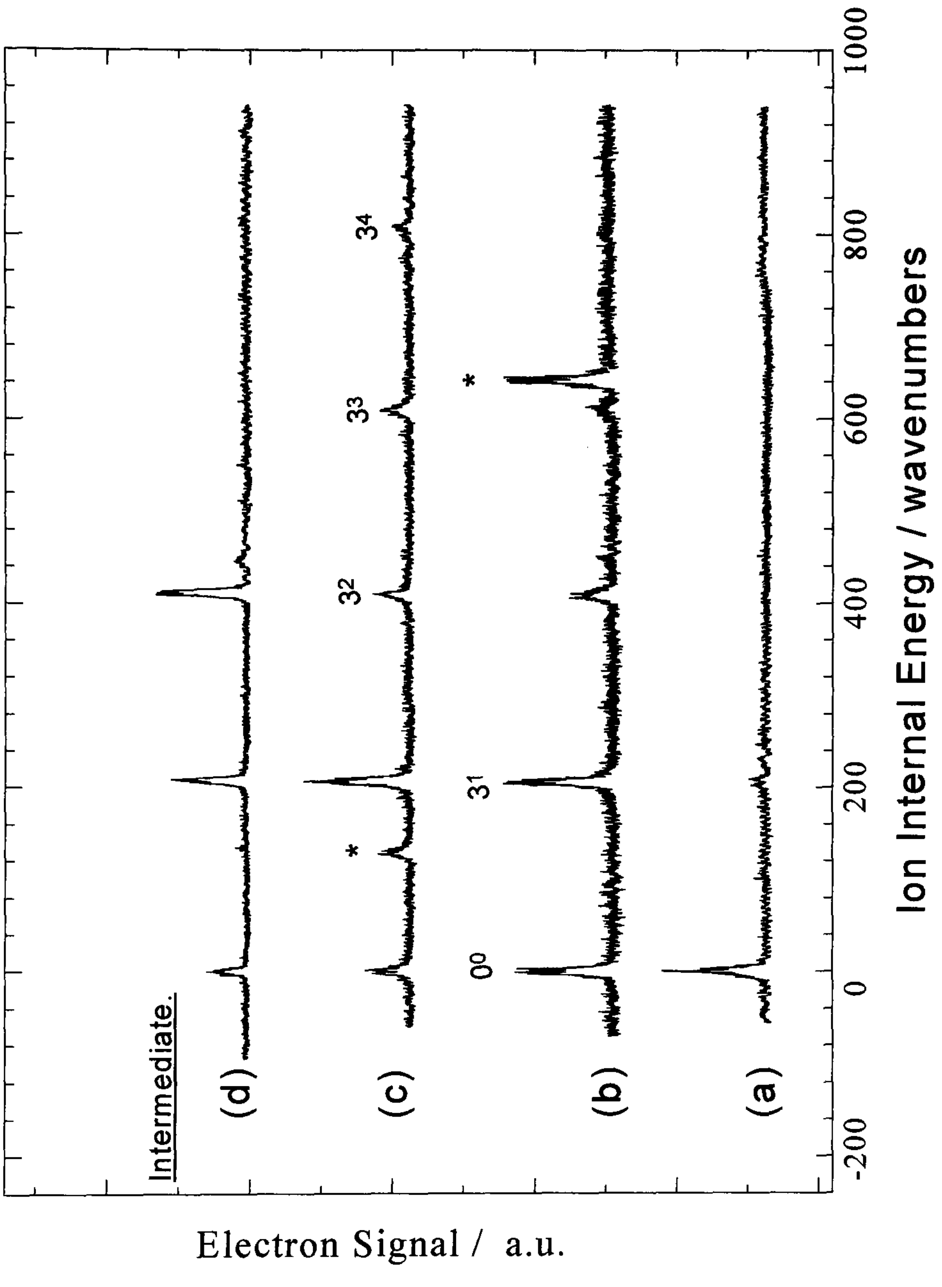

Figure 4.10: (2+1') ZEKE-PFI spectra of CF_3I^+ ($^2E_{3/2}$) via various members (a, b, c & d in figure 4.7) of the [$^2E_{3/2}$]6p;2 Rydberg system. * indicate atomic iodine transitions (see text). The spectra have been shifted relative to the adiabatic ionisation energy (83652 cm^{-1}).

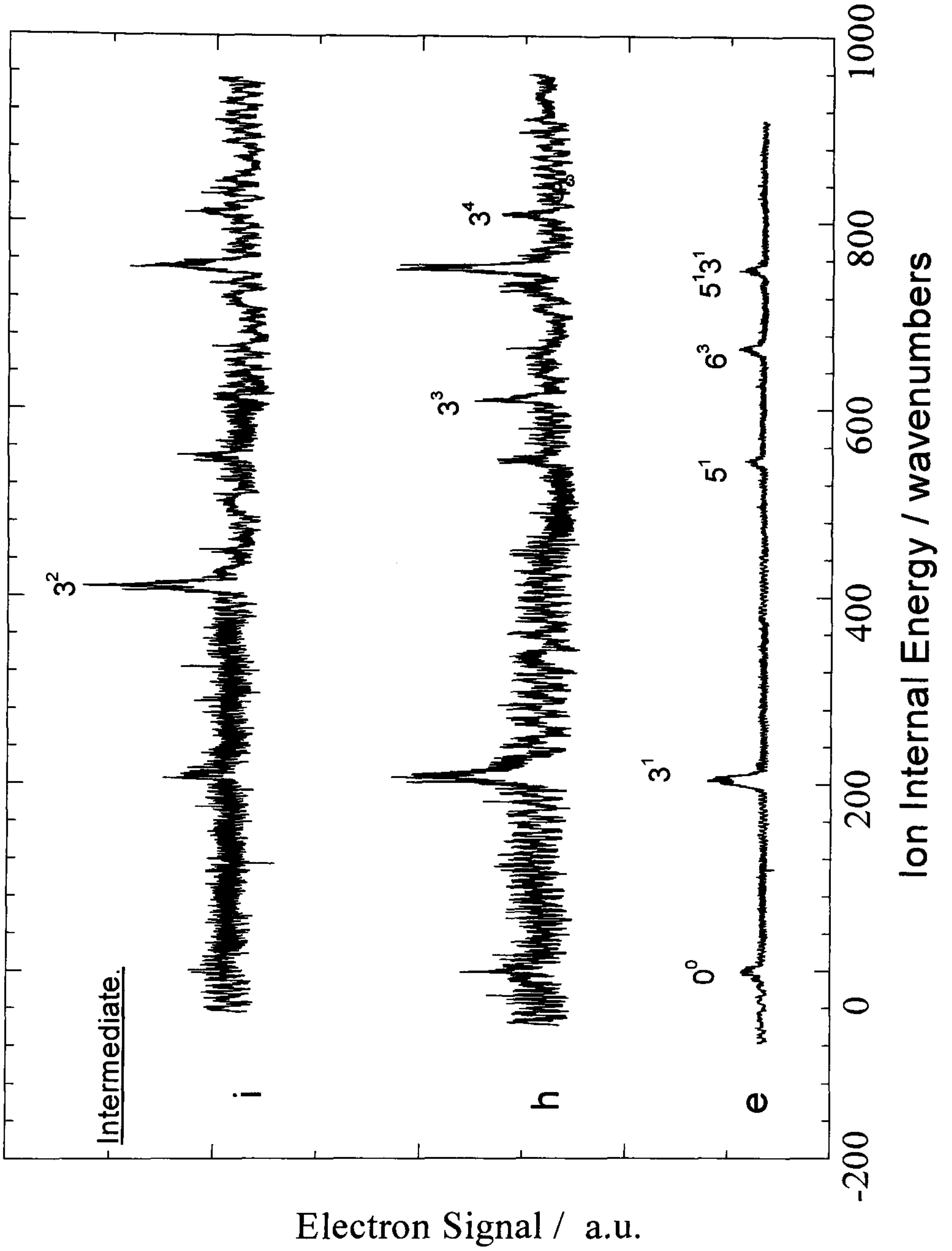

Figure 4.11: (2+1') ZEKE-PFI spectra of CF_3I^+ ($^2E_{3/2}$) via various members of the [$^2E_{3/2}$]6p;2 system (denoted e, h and i in figure 4.7). The spectra have been shifted relative to the adiabatic ionisation energy (83652 cm^{-1}).

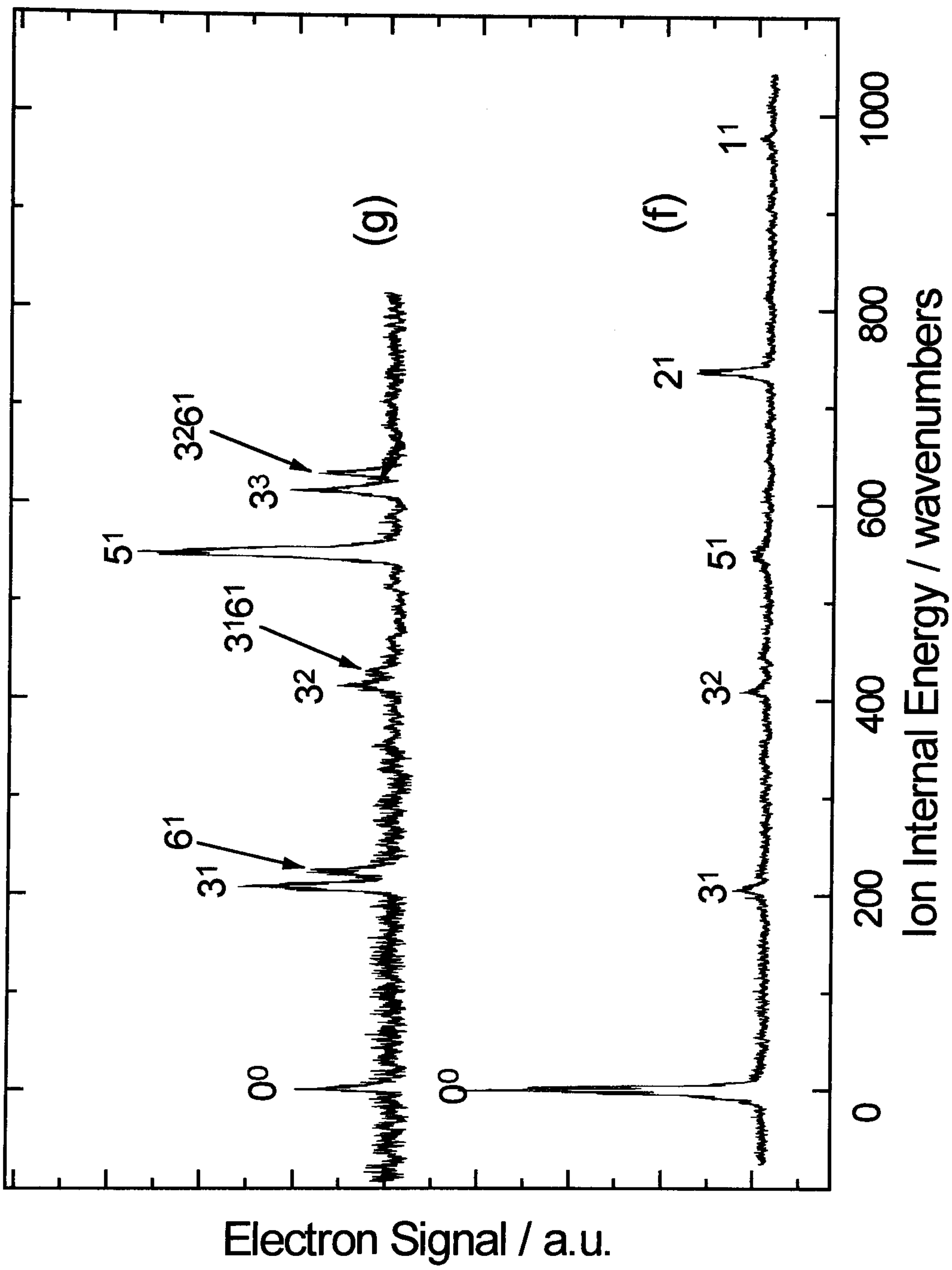

Figure 4.12: (2+1') ZEKE-PFI spectra of CF_3I^+ ($^2E_{3/2}$) via two transitions of the [$^2E_{3/2}$]6p;2 system (denoted f and g in figure 4.7). The spectra have been shifted relative to the adiabatic ionisation energy (83652 cm^{-1}).

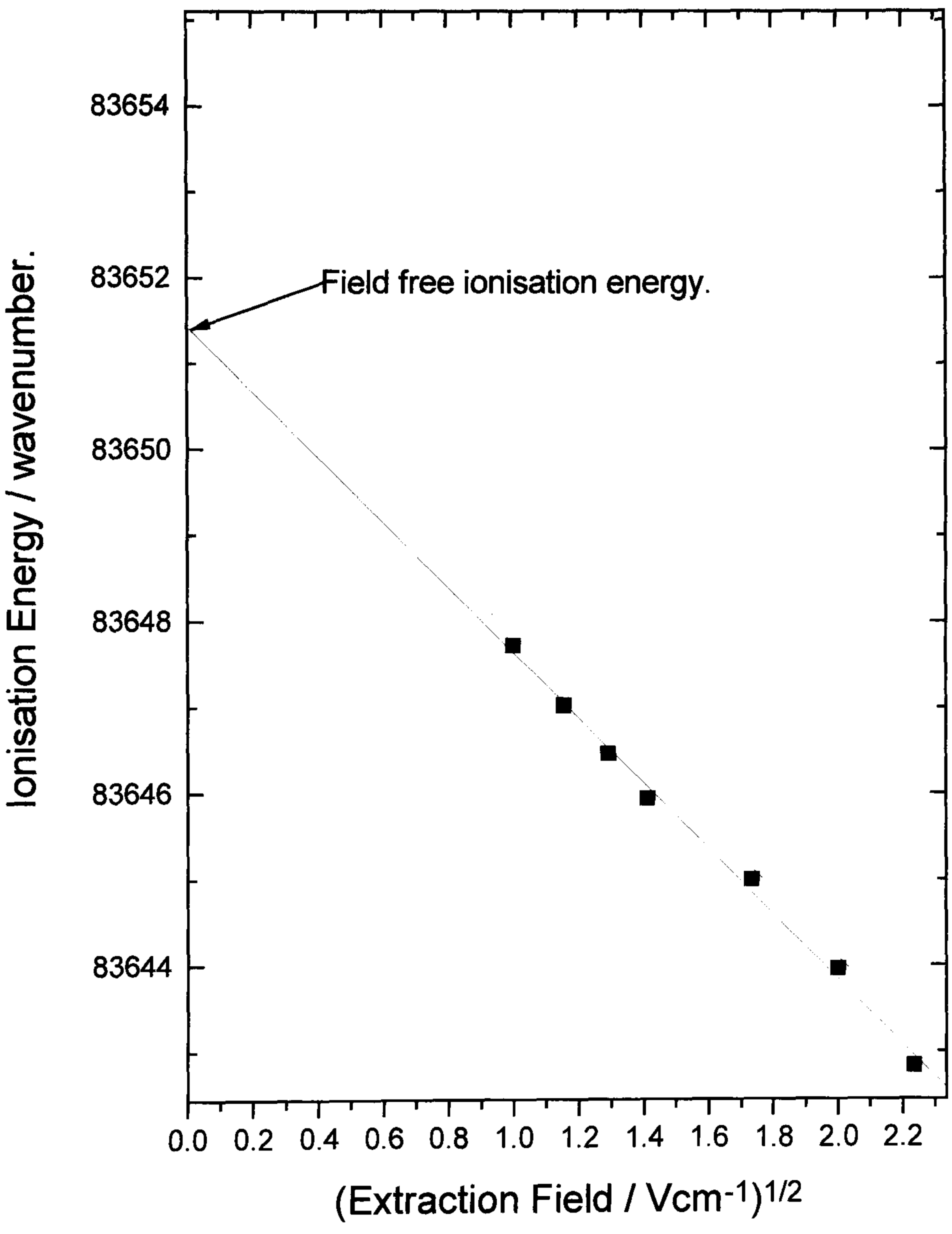

Figure 4.13: Extrapolation to zero field of the ionisation energy of CF_3I^+ ($^2E_{3/2}$). The experimental spectra are shown in figure 2.8.

The assignment of the ionic vibrational structure was crucial to the identification of the intermediate. The (1+1) ZEKE-PFI spectrum in section 4.3. gave the vibrational frequencies for the three totally symmetric normal modes of the $^2E_{3/2}$ state. Figure 4.10. shows the (2+1') ZEKE-PFI spectra via four transitions of the intermediate (denoted a, b, c & d in figure 4.7.). These spectra all show a progression (up to 4 quanta) with a vibrational spacing of 205 cm^{-1} which corresponds to v_3. The two transitions denoted with asterisks are (2+1') ZEKE-PFI transitions of atomic iodine. These occur due to an accidental resonance of the pump photon with the 6p Rydberg states of iodine with a transition energy only a few wavenumbers to the red of the molecular transitions[19,29]. These are so intense that even pumping the wing of the transition results in the observation of a ZEKE-PFI signal. It is a coincidence that two of the ionisation thresholds for atomic iodine[24,25,29] lie in the same region as that of CF_3I. Tuning the pump photon off the molecular transition and onto that of the atomic results in a large increase of the atomic ZEKE-PFI transition. Therefore the four intermediates can be assigned as an electronic origin (two-photon energy 65522 cm^{-1}) and a progression of three quanta of v_3 (65666, 65804 and 65946 cm^{-1}). This results in an initial vibrational spacing (144 cm^{-1}) for the Rydberg state which is substantially reduced from that of the neutral[11,12] (286 cm^{-1}) and the ionic (205 cm^{-1}) ground states indicating a substantial lengthening of the carbon-iodine bond. Another member of this progression can be identified at 66080 cm^{-1} although this was too weak to use in a two-colour experiment.

The remainder of the vibrational structure of the intermediate, however, cannot be so easily and unambiguously assigned. The ZEKE spectra via intermediates e, f, g, h and i all show transitions which cannot be assigned to any combination of the three totally symmetric vibrational modes of the molecule. Therefore they must be due to the non-totally symmetric vibrational modes.

Intermediate e (two-photon energy 66153 cm^{-1}) shows a ZEKE spectrum (figure 4.11.) which has a progression in ν_3 but also has transitions at 547, 668 and 752 cm^{-1} ion internal energy. These are attributed to 5^1, 6^3 and $5^1 3^1$ by comparison with neutral ground state values[11,12]. Intermediate e can therefore be assigned as 6^3_0 giving a value of ν_6 in the Rydberg state of 210 cm^{-1} and 221 cm^{-1} in the ion. Further to this a weak progression in ν_6 can be observed (e.g. 6^2_0 at 65940 cm^{-1}). The determination of the vibrational frequency for ν_6 also allows the identification of several hot bands in the Rydberg state. These lie approximately 50 cm^{-1} to the red of all the main transitions. Such a spacing is in good agreement with the difference between the vibrational frequency of ν_6 in the neutral ground state and the Rydberg state. The remaining spectra in figure 4.11. (intermediates h and i) also show structure in ν_3 and ν_3 in combination with ν_5. Thus these intermediates are assigned as $5^1_0 3^n_0$ and $5^1_0 3^{n+1}_0$. The exact position of 5^1_0 (and the value of n) itself remains a matter of doubt.

There are two possible candidates for the assignment of 5^1_0 in the Rydberg state; intermediates f (two-photon energy 65908 cm^{-1}) and g (66056 cm^{-1}). The ZEKE spectra via these intermediates are shown in figure 4.12. That of intermediate f is dominated by the origin band although weak transitions to the symmetric vibrational modes are observed. In addition a very weak feature at 547 cm^{-1} ion internal energy is assigned to 5^1. The appearance of such a transition may indicate that the intermediate is 5^1_0 or, given the fact that it is so weak, may be the result of coupling between the vibrational mode and the high-*n* Rydberg states upon which ZEKE-PFI spectroscopy depends.

The ZEKE spectrum via intermediate g, on the other hand, shows considerable activity in the non-totally symmetric vibrational modes. 5^1 dominates the spectrum but 6^1 and $6^1 3^1$ are also observed. On the basis of the ZEKE spectra intermediate f is assigned as a second $\Omega = 2$ origin and g is 5^1_0 based on the first origin at 65522 cm^{-1}. This allows assignment of intermediates h and i to $5^1_0 3^1_0$ and $5^1_0 3^2_0$. Such assignments are also compatible with the fragmentation pattern shown in figure 4.9. This results in a value for the vibrational frequency of ν_5 of 534 cm^{-1} in the Rydberg state which is almost identical to that of the neutral ground state[11,12] (540 cm^{-1}). Such a limited change in vibrational frequency would seem to be at odds with the considerable activity seen in ν_5 in the REMPI spectrum. Table 4.2. lists the relative intensities of ZEKE transitions via each intermediate. Table 4.3. lists the energies and assignments of the observed ZEKE transitions.

Examination of the $[^2E_{3/2}]_c$ 6p:0 region of the REMPI spectrum (figure 4.8.) shows a similar appearance to the $\Omega = 2$ region. Hence similar vibronic assignments can be made. This gives a value for the vibrational frequency for ν_3 of 192 cm^{-1} in one of the $\Omega = 0$ states. Final vibronic assignments for the 6p Rydberg states are given in figure 4.14. and table 4.4.

Table 4.5. summarises the vibrational frequencies found in this and several other studies as comparison. It is clear that the 6p Rydberg states are severely distorted relative to both the neutral and ionic ground states. This distortion appears particularly acute for the carbon-iodine symmetric stretch (ν_3) which has approximately half the frequency in the 6p;2 Rydberg state compared to the neutral ground state[11,12].

Intermediate	a	b	c	d	e	f	g	h	i
Ionic transition									
0^0	s	s	m	m	m	s	m	w	-
3^1	w	s	s	s	s	w	s	s	w
6^1	-	-	-	-	-	-	m	-	-
3^2	-	m	m	s	-	w	w	-	s
$6^1 3^1$	-	-	-	-	-	-	w	-	-
5^1	-	-	-	-	w	w	s	w	w
3^3	-	w	m	-	-	-	m	m	-
$6^1 3^2$	-	-	-	-	-	-	m	-	-
6^3	-	-	-	-	m	-	-	-	-
2^1	-	-	-	-	-	m	-	-	-
$5^1 3^1$	-	-	-	-	m	-	-	s	s
3^4	-	-	w	-	-	-	-	w	w
1^1	-	-	-	-	-	w	-	-	-

Table 4.2. Relative intensities of ZEKE transitions via the vibrational levels of the [$^2E_{3/2}$] 6p Rydberg state.

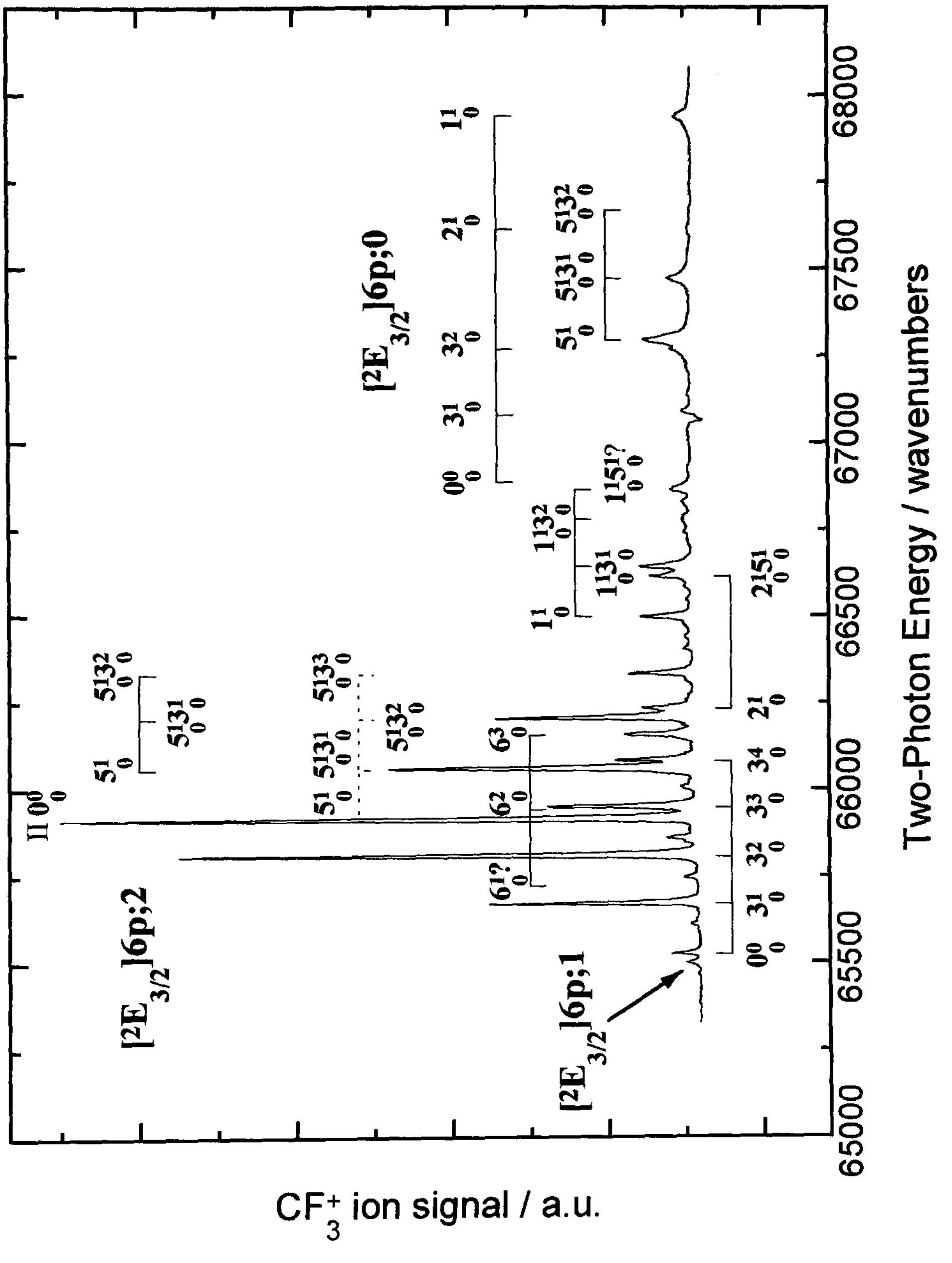

Figure 4.14: (2+1) REMPI of the [$^2E_{3/2}$]6p region of CF_3I with full vibrational assignments. Dotted line represents an alternative assignment (see text). The assignment II 0^0_0 indicates the origin band of a second Ω = 2 state.

Ion Internal Energy (cm^{-1})	Assignment	Ion Internal Energy (cm^{-1})	Assignment
0	0^0	628	$6^1 3^2$
205	3^1	668	6^3
221	6^1	734	2^1
410	3^2	752	$5^1 3^1$
426	$6^1 3^1$	809	3^4
547	5^1	973	1^1
611	3^3		

Table 4.3. Energies of transitions found in the (2+1') ZEKE of CF_3I^+ ($^2E_{3/2}$) via the [$^2E_{3/2}$] 6p Rydberg states. Field corrected adiabatic ionisation energy is 83652 cm^{-1}.

Energy (cm^{-1})	**Assignment [Ω] ν**	**Energy (cm^{-1})**	**Assignment [Ω] ν**
65496	[1]?	**66497**	[2] 1^1_0
65522	[2] 0^0_0	**66613**	[2] $2^1_0 5^1_0$
65666	[2] 3^1_0	**66641**	[2] $1^1_0 3^1_0$
65804	[2] 3^2_0	**66779**	[2] $1^1_0 3^2_0$
65908	[2] (II) 0^0_0 or 5^1_0 (a)	**66864**	[2] $1^1_0 5^1_0$
65940(shoulder)	[2] 6^2_0	**66885(not seen)**	[0] 0^0_0
65946	[2] 3^3_0	**67077**	[0] 3^1_0
66056	[2] 5^1_0 or $5^1_0 3^1_0$ (a)	**67268(shoulder)**	[0] 3^2_0
66080	[2] 3^4_0	**67295**	[0] (II) 0^0_0or 5^1_0 (a)
66153	[2] 6^3_0	**67471**	[0] 5^1_0 or $5^1_0 3^1_0$(a)
66201	[2] $5^1_0 3^1_0$ or $5^1_0 3^2_0$ (a)	**67614**	[0] 2^1_0
66231	[2] 2^1_0	**67668**	[0] $5^1_0 3^1_0$ or $5^1_0 3^2_0$ (a)
66331	[2] $5^1_0 3^2_0$ or $5^1_0 3^3_0$ (a)	**67938**	[0] 1^1_0

Table 4.4. Energies and assignments of the [$^2E_{3/2}$] 6p Rydberg states of CF_3I. (a) represents an alternative assignment (see text).

Mode	$^1A_1$ (a)	$[^2E_{3/2}]$ 6s;1 (b)	$[^2E_{3/2}]$ 6p;2	$[^2E_{3/2}]$ 6p;0	CF_3I^+ ($^2E_{3/2}$)
ν_1 (cm^{-1})	1075	970	974	1053	973
ν_2 (cm^{-1})	743	681	709	730	734
ν_3 (cm^{-1})	286	232	144	192	205
ν_4 (cm^{-1})	1187	1282	-	-	-
ν_5 (cm^{-1})	540	525	534 (386)^c	586 (410)^c	547
ν_6 (cm^{-1})	262	223	210	-	221

Table 4.5. Vibrational frequencies in various states of CF_3I. (a) reference 18, (b) reference 12. c represents an alternative assignment.

4.4.4. Discussion

From the results of the previous section it is clear that the $[^2E_{3/2}]6p;2$ Rydberg states of CF_3I are severely perturbed. The nature of this perturbation is not known although several possibilities exist.

Firstly the 6p states may be undergoing a Jahn-Teller distortion[17] as previously observed for the 6s states[16]. This is a possibility since the assignments show substantial activity in degenerate vibrational modes (ν_5 and ν_6). However dynamic Jahn-Teller coupling[38] usually leads to considerably more complex structure than the relatively straightforward vibrational progressions observed here. The (1+1`) ZEKE-PFI spectrum of benzene[39] is an excellent example of this where the coupling of degenerate vibrational modes with a degenerate electronic state leads to a complex structure which requires rotational resolution to be fully understood. In addition the Jahn-Teller effect appears only weakly in the 6s states[18] of CF_3I and, apparently, not at all in the ionic ground state. A second possibility, namely bond stretching at the one-photon level, can also be discounted since two- and three-photon excitation routes give identical spectra[20] (see section 2).

For the third option the coupling of the Rydberg electron with the ionic core must be considered[40]. Low-*n* Rydberg states in systems with large spin-orbit couplings (such as are found for iodine containing molecules) are best considered as belonging to Hund`s case (c) (see chapter 2). The coupling of an electron in a 6p orbital (electron orbital angular momentum, $\lambda = 0$ (pσ) or ± 1 (pπ) and electron spin of $\pm 1/2$) with a $^2E_{3/2}$ ($\Omega=3/2$) core leads to a number of Rydberg states with four distinct Ω values; 3, 2 (two times), 1 (two times) and $0^{\pm}$. The microconfigurations of such a situation are shown in table 4.6. The lone pair orbitals of iodine are denoted by the 1 and -1 symbols and the spin of the three electrons by + or - superscripts. Hence the $^2E_{3/2}$ state of the ion is described as $|1^+1^-\,-1^+|$ with one filled and one half-filled p-type orbital. The second part of the microconfigurations is the description of the orbital and spin angular momentum of the Rydberg electron.

Microconfiguration. **|core| Ryd.**	**Total Angular momentum.** **(Ω)**	**Spin.**
$|1^+1^-\text{-}1^+|\ 6p\pi^+$	3	Triplet
$|1^+1^-\text{-}1^+|\ 6p\pi^-$	2	Singlet/Triplet
$|1^+1^-\text{-}1^+|\ 6p\sigma^-$	2	Triplet
$|1^+1^-\text{-}1^+|\ 6p\pi^+$	1	Triplet
$|1^+1^-\text{-}1^+|\ 6p\sigma^-$	1	Singlet/Triplet
$|1^+1^-\text{-}1^+|\ 6p\pi^-$	0^+	Singlet/Triplet
$|1^+1^-\text{-}1^+|\ 6p\pi^-$	0^-	Triplet

Table 4.6. Microconfigurations of a $^2E_{3/2}$ core with a 6p Rydberg electron in Hund's case (c).

The selection rules concerning Hund's case (c) have been discussed in chapter 2 but are briefly mentioned here. The total angular momentum (Ω) can change by 0 or ±1 per photon, the overall spin must remain the same (i.e. $\Delta S = 0$) as must the parity of the wavefunction (i.e. transitions of the type $0^+ \leftrightarrow 0^+$ are allowed but $0^- \leftrightarrow 0^+$ is forbidden).

Applying these to the present situation results in the transition to the $\Omega = 3$ state being forbidden. However all the remaining states are allowed by the angular momentum selection rule. Previous work on diatomic halogens has shown that, for two-photon excitation, only those states with substantial singlet character are observed[36]. For the case of the $[^2E_{3/2}]$6p states this implies that one of the $\Omega = 2$ states, one $\Omega = 1$ state and the $\Omega = 0^+$ state should be observed by (2+1) REMPI since the remaining states are pure triplets. In addition the 0^- state should also be forbidden by the parity selection rule. Thus only three Rydberg states based on this state of the ion should be observed in a two-photon excitation process. This seems to be at odds with the most likely explanation for the observed ZEKE-PFI spectra where there are two $\Omega = 2$ states with similar intensities, one of which shows extended vibrational structure while the other shows none (a similar assignment can also be made for the $\Omega = 0$ states). It is possible that Hund's case (c) may not be appropriate in this case. Hund's case (e), in which the spin of the Rydberg electron is no longer coupled to the ionic core and hence the total spin is no longer a good quantum number, may be more applicable[40]. However, given that such a coupling scheme applies to large values of *n*, it should not apply in the case where $n = 6$. A second mechanism which could give singlet character to the pure triplet Rydberg states is spin-orbit coupling of the ionic core. The addition of minor configurations to the ionic core state may result in triplet states gaining singlet character and hence being observed in the two-photon excitation spectrum.

Despite the discrepancy between theory and experiment in the assignment of the Rydberg states it is clear that one of the $\Omega = 2$ states has a vibrational frequency for the C-I stretch which is greatly reduced relative to both the neutral and ionic ground states. The implication of this is that the Rydberg state is distorted by interaction with another electronic state of the molecule.

The characteristic of such a state is that it has a considerably longer C-I bond length than the neutral or ionic ground states (and hence a much lower vibrational frequency). The obvious candidates are ion-pair states. Such states have been observed for the diatomic halogens[41,42,43] and have vibrational frequencies approximately half that of the neutral ground state (for example the ion-pair states of I_2 have frequencies in the region of 100 cm^{-1} compared to 215 cm^{-1} for the neutral ground state). For CF_3I no ion-pair states have been observed experimentally and the only method of locating them is to calculate the thresholds for formation of separated ions using the known C-I bond dissociation energy[44] (~19000 cm^{-1}) and the electron affinities[45] and ionisation energies[44] of CF_3 (~14900 and ~73000 cm^{-1}) and I (E.A. = 24700 cm^{-1} and 84340, 90800 and 91130 cm^{-1} for the spin-orbit components of I^+ (^2P))[29,45]. These are shown in table 4.7.

Dissociation products.	**Threshold Energy. (cm^{-1})**
CF_3^+ ($^1A_1$) + I^- (^1S)	67300
CF_3^- ($^1A_1$) + I^+ ($^3P_2$)	88400
CF_3^- ($^1A_1$) + I^+ ($^3P_0$)	94900
CF_3^- ($^1A_1$) + I^+ ($^3P_1$)	95500

Table 4.7. Calculated dissociation thresholds for ion pair states of CF_3I.

Since CF_3 has a lower ionisation energy than iodine the lowest lying ion-pair state will dissociate to CF_3^+ and I^-. The calculated threshold for this is around 67000 cm^{-1}. This is in the region of the 6p Rydberg states and so close to the dissociation threshold the vibrational spacing of the ion-pair state will be very small (in effect it would be a continuum at the current laser resolution), in fact too small to account for the vibrational spacing observed in the $\Omega = 2$ state. However, it may well account for the observed predissociation of the $\Omega = 0$ state which lies above this threshold. Since the dissociation fragments of this threshold are both filled shells only one ion-pair state will exist with Ω = 0. Hence the coupling of the two states may be large. No sign of I^- was observed experimentally but this could be due to the photodetachment of the electron by the intense laser pulses used to obtain the REMPI spectrum of the $\Omega = 0$ Rydberg state.

The next set of ion-pair states correlate to CF_3^- and I^+ with thresholds of 88000-96000 cm^{-1} depending on the spin-orbit state of I^+. Given the very deep potential wells found for ion-pair states (in the diatomic halogens the well lies some 30-40000 cm^{-1} below the threshold[41-43]) it is possible that such a state will have a potential minimum in the region of the 6p Rydberg cluster. In addition the vibrational frequencies[41] of the ion-pair states of the diatomic halogens tend to be approximately half that of the neutral ground state which is the case in the $[^2E_{3/2}]$ 6p;2 Rydberg state of CF_3I.

Interaction between a Rydberg state and the vibrational levels of an ion-pair state have previously been observed for iodine where the $[^2\Pi_{3/2}]7s$; 1_g Rydberg state (recently reassigned as part of the 5d series[36]) interacts with the β (1_g) ion-pair state. Interaction results in intensity borrowing between the states which allows the observation of the vibrational levels of the ion-pair state when they lie close in energy to the Rydberg transition. The spacing of these levels in I_2 is of the order of 15 cm^{-1} ($v \approx 600$) which is considerably greater than observed for CF_3I where the experimental energy is around the bottom of the ion-pair potential well. However given that the ZEKE-PFI results point to two distinct $\Omega = 2$ Rydberg states only one of them seems to be affected by this interaction.

4.5. Conclusion

The ground ionic state of CF_3I^+ ($^2E_{3/2}$) has been studied by two separate ZEKE-PFI excitation schemes. The one-colour two-photon ZEKE-PFI spectrum was very similar to the conventional He(I) photoelectron spectrum (albeit with substantially higher resolution) and reflects the direct Franck-Condon overlap between the neutral and ionic ground states. No evidence was seen of intermediate effects at the one-photon level due to the weakness of the repulsive state at the one-photon excitation energy. The long vibrational progressions in the three symmetric modes (ν_1, ν_2 and ν_3) are a result of the interaction of the anti-bonding orbitals of the CF_3 fragment with the iodine lone-pairs. In contrast to methyl iodide no evidence for bond stretching at the one-photon level was observed due to the weakness of the absorption band at the wavelength required for two-photon ionisation.

The two-colour ZEKE-PFI spectrum of the same ionic state of CF_3I was obtained using several members of the [$^2E_{3/2}$]6p;2 Rydberg states as resonant intermediates in a (2+1') process. The unusual vibrational structure of the intermediate allowed the degenerate modes of the ion to be accessed (e.g. ν_5 and ν_6). The ZEKE-PFI spectra were also used to assign the vibrational structure of the intermediate. Although some doubt remains over one of the assignments, it is clear that the [$^2E_{3/2}$]6p;2 Rydberg state of CF_3I is severely perturbed with ν_3 (the C-I stretch) greatly reduced from that of the neutral and ionic ground state values. The most likely candidate for such perturbation is an ion-pair state correlating to CF_3^- and I^+.

Overall the experiments reported in this chapter allowed the determination of five of the six normal vibrational modes of the [$^2E_{3/2}$]6p;2 Rydberg state and the ionic ground state ($^2E_{3/2}$). These point to several differences between fluorinated and unfluorinated methyl iodide.

4.6. References

1. C.R. Brundle, M.B. Robin, N.A. Kuebler & H. Basch. *J.Am.Chem.Soc.* 1972, **94**, 1451.
2. C.R. Brundle, M.B. Robin & N.A. Kuebler. *J.Am.Chem.Soc.* 1972, **94**, 1466.
3. A. Gedanken & M.D. Rowe. *Chem.Phys.Lett.* 1975, **34**, 39.
4. A. Gedanken, M.B. Robin & Y. Yafet. *J.Chem.Phys.* 1982, **76**, 4798.
5. M. Kawasaki, H. Sato, T. Kikuchi, S. Kobayashi & T. Arikawa. *J.Chem.Phys.* 1987, **87**, 5739.
6. M.R. Dobber, W.J. Buma & C.A. de Lange. *J.Chem.Phys.* 1993, **99**, 836.
7. R.A.A. Boschi & D.R. Salahub. *Mol.Phys.* 1972, **24**, 735.
8. R.A.A. Boschi & D.R. Salahub. *Can.J.Chem.* 1974, **52**, 1217.
9. T. Cvitas, H. Gusten, L. Klasinc, I. Novadj & H.Vancik. *Z.Naturforsch.* 1978, **33a**, 1528.
10. T. Cvitas, H. Gusten & L. Klasinc. *J.Chem.Phys.* 1977, **67**, 2687.
11. H. Burger, K. Burczyk, H. Hollenstein & M. Quack. *Mol.Phys.* 1989, **55**, 255.
12. G. Herzberg. Molecular Spectra and Molecular Structure. Volume 2. Infrared and Raman Spectra of Polyatomic Molecules. Krieger Publishing (Florida). 1991.
13. O.V. Rattigan, D.E. Shallcross & R.A. Cox. *J.Chem.Soc.Faraday Trans.* 1997, **93**, 2839.
14. A. Gedanken. *Chem.Phys.Lett.* 1987, **137**, 462.
15. L.H. Sutcliffe & A.D. Walsh. *Trans.Faraday Soc.* 1961, **57**, 873.
16. G. Herzberg. *Disc.Faraday Soc.* 1963, **35**, 7.
17. H.A. Jahn & E. Teller. *Proc.Roy.Soc.A.* 1937, **161**, 220.
18. C.A. Taatjes, J.W.G. Mastenbroek, G. van den Hoek, J.G. Snijders & S. Stolte. *J.Chem.Phys.* 1993, **98**, 4355.

19. L.D. Waits, R.J. Horwitz, R.G. Daniel, J.A. Guest & J.R. Appling. *J.Chem.Phys.* 1992, **97**, 7263.
20. J. Hennessy. PhD Thesis. University of Edinburgh. 1999.
21. J.D. Bozek, G.M. Bancroft, J.N. Cutler, K.H. Tan, B.W. Yates & J.S. Tse. *Chem.Phys.* 1989, **132**, 257.
22. R. Bombach, J. Dannacher, J.P. Stadelmann, J. Vogt, L.R. Thorne & J.L. Beauchamp. *Chem.Phys.* 1982, **66**, 403.
23. L. Karlsson, R. Jadrny, L. Mattsson, F.T. Chau & K. Siegbahn. *Phys.Scr.* 1977, **16**, 225.
24. A. Strobel, A. Lochschmidt, I. Fischer, G. Niedner-Schatteburg & V.E. Bondybey. *J.Chem.Phys.* 1993, **99**, 733.
25. A. Strobel, I. Fischer, A. Lochschmidt, K. Muller-Dethlefs & V.E. Bondybey. *J.Phys.Chem.* 1994, **98**, 2024.
26. M.C.R. Cockett, R.J. Donovan & K.P. Lawley. *J.Chem.Phys.* 1996, **105**, 3347.
27. D.A. Beattie, N.A. Macleod, K.P. Lawley & R.J. Donovan. *J.Electron Spectrosc.* 1998, **97**, 191.
28. A. Held, L.Y. Baranov, H.L. Selzle & E.W. Schlag. *J.Chem.Phys.* 1997, **106**, 6848.
29. C.E. Moore. *Atomic Energy Levels, Nat.Stand.Ref.Data.Ser. (US. Nat.Bur.Stand.),* 1971, **35**.
30. C. Lifshitz & W.A. Chupka. *J.Chem.Phys.* 1967, **47**, 3439.
31. M. Horn, M. Oswald, R. Oswald & P. Botschwina. *Ber.Bunsen.Phys.Chem.* 1995, **99**, 323.
32. D.J. Seery & D. Britton. *J.Phys.Chem.* 1964, **68**, 2263.
33. M.C.R. Cockett. *J.Phys.Chem.* 1995, **99**, 16228.
34. N.P.L. Wales, W.J. Buma, C.A. de Lange & H. Lefebvre-Brion. *J.Chem.Phys.* 1996, **105**, 5702.
35. R.G. Bray & R.M. Hochstrasser. *Mol.Phys.* 1976, **31**, 1199.

36. R.J. Donovan, A.C. Flexen, K.P. Lawley & T. Ridley. *Chem.Phys.* 1998, **226**, 217.
37. D.A. Beattie, M.C.R. Cockett, K.P. Lawley & R.J. Donovan. *J.Chem.Soc.Faraday Trans.* 1997, **93**, 4245.
38. H.C. Longuet-Higgins, U. Opik, M.H.L. Pryce & R.A. Sack. *Proc.Roy.Soc.A.* 1958, **244**, 1.
39. High Resolution Laser Photoionization and Photoelectron Studies. Edited by I. Powis, T. Baer & C.Y. Ng. J. Wiley & Sons (London). 1995.
40. G. Herzberg. Molecular Spectra and Molecular Structure, Volume 1: Spectra of Diatomic Molecules. Krieger Publishing (Florida). 1989.
41. R.J. Donovan & K.P. Lawley. *J.Chem.Soc.Faraday Trans.* 1993, **89**, 1885.
42. A.J. Yencha, T. Ridley, R. Maier, R.V. Flood, K.P. Lawley, R.J. Donovan & A. Hopkirk. *J.Phys.Chem.* 1993, **97**, 4582.
43. V.A. Alekseev & D.W. Setser. *J.Chem.Phys.* 1997, **107**, 4771.
44. R.L. Asher & B. Ruscic. *J.Chem.Phys.* 1997, **106**, 210.
45. CRC handbook of Chemistry and Physics. Edited by R.C. Weast. 55th edition (1974). CRC press (Cleveland, Ohio).

Chapter 5

ZEKE-PFI of the Aminobenzotrifluorides

5.1. Introduction

The advent of high resolution photoelectron techniques such as ZEKE-PFI makes the study of large amplitude motion in ions experimentally feasible[1-8]. An understanding of the effects of electronic state on internal rotation is important not only from a theoretical standpoint but also for an understanding of the three dimensional structure of larger more complex molecules[9,10].

The methyl rotor has been extensively studied by a barrage of experimental techniques[9,11-13] (see chapter 2). For ZEKE spectroscopy the rotor has generally been attached to a benzene ring (for example toluene[1] and its derivatives[2-8]) although a two-colour study of acetone via the 6p Rydberg states has been reported[14]. However its fluorinated counterpart, the trifluoromethyl rotor (CF_3) has received considerably less attention although microwave studies of the neutral ground states of such a rotor have been reported[15,16].

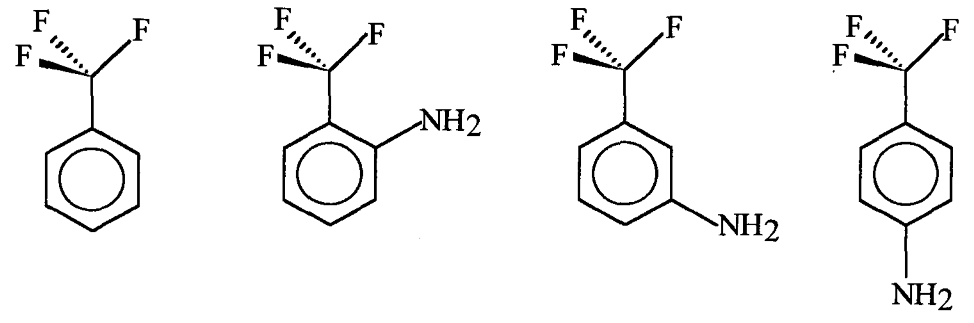

(a) Benzotrifluoride **(b) 2-ABTF** **(c) 3-ABTF** **(d) 4-ABTF**

Figure 5.1. Structures of the molecules of interest.

The parent molecule (benzotrifluoride (figure 5.1a) has been studied by microwave spectroscopy[17] in the neutral ground state (S_0) revealing a barrier to internal rotation of similar type (six-fold symmetry) and scale (V_6 = 3.6 cm^{-1}) to that of toluene[1,18] (4.9 cm^{-1}). Excited states were examined by UV and VUV absorption in the 1950's although no torsional analysis was performed[19,20]. The ionisation energy was found to be 78000 cm^{-1} by extrapolation of a Rydberg series. This is considerably higher (~3500 cm^{-1}) than benzene[21] (74556 cm^{-1}) indicating that the CF_3 group acts to withdraw electron density from the ring. This is the opposite behavior to that of the methyl rotor which is a net electron donor. Hence the ionisation energy of toluene (71199 cm^{-1})[1] is lower than that of benzene.

Benzotrifluoride, however, is not a straightforward candidate for a ZEKE-PFI experiment since the S_1 state lies at an energy less than half that required for ionisation[19,20]. Furthermore both wavelengths required for a two-colour experiment (500-530 nm) require pumping by the third, and weaker, harmonic of the Nd:YAG laser (see chapter 3). Further substitution of the benzene ring allows the study of the CF_3 group to become more experimentally accessible and can lead to considerable changes in the nature of the barrier to internal rotation. Of such substituted benzotrifluorides the most experimentally accessible are the aminobenzotrifluorides (ABTF's) shown in figure 5.1 (b), (c) and (d).

This chapter presents the ZEKE-PFI spectra of the torsional structure of the ionic ground state of the aminobenzotrifluorides excited via the S_1 state. Results on each geometric isomer is presented in turn followed by a discussion of the interesting features. In addition the amine inversion of 4-ABTF will also be examined.

5.2. Previous Work on the Aminobenzotrifluorides

In the early 1990's Hollas and co-workers published a series of papers on the aminibenzotrifluorides[22-27]. Using a combination of infra-red, Raman and fluorescence techniques the torsional structure of all three geometric isomers in the neutral ground state (S_0) and the first excited singlet state (S_1) was determined. Trends in barrier heights and conformations of the rotor were in general agreement with those found for the aminotoluenes[4] and other substituted toluenes[1-3,5-7].

However, the fluorescence excitation spectra of the S_1 state were very different to those of the aminotoluenes. The reason for this lies in the greater mass of the CF_3 group relative to the CH_3 rotor which has the effect of greatly reducing the internal rotation constant, F, from ~5 to ~0.3 cm^{-1} (the reduction is mainly caused by the greater mass (x19) of the fluorine atoms relative to hydrogen). This has two major consequences. Firstly many more torsional levels will lie below the barrier and secondly, that many of these torsional states will be so far below the barrier that tunneling between adjacent minima is negligible[11]. This has the effect of rendering the **a** type symmetry and the **e** type symmetry states (see chapter 2) degenerate (or at least beyond the available laser resolution) although true degeneracy exists only for an infinite barrier. Hence the torsional structure observed by Hollas resembles more a torsional vibration than true internal rotation. States are assigned as τ^n which contains an **a** state ($\mathbf{a}_1$ for even values of n and $\mathbf{a}_2$ for odd values of n) state and a doubly degenerate **e** state for the G_6 symmetry case. For G_{12} molecules each symmetry type has a prime or double prime designation in addition to the subscripts.

Schematic energy diagrams[1,11,12] for both G_6 and G_{12} symmetries are shown in figure 5.2. The splitting between the states becomes greater as the top of the barrier is approached.

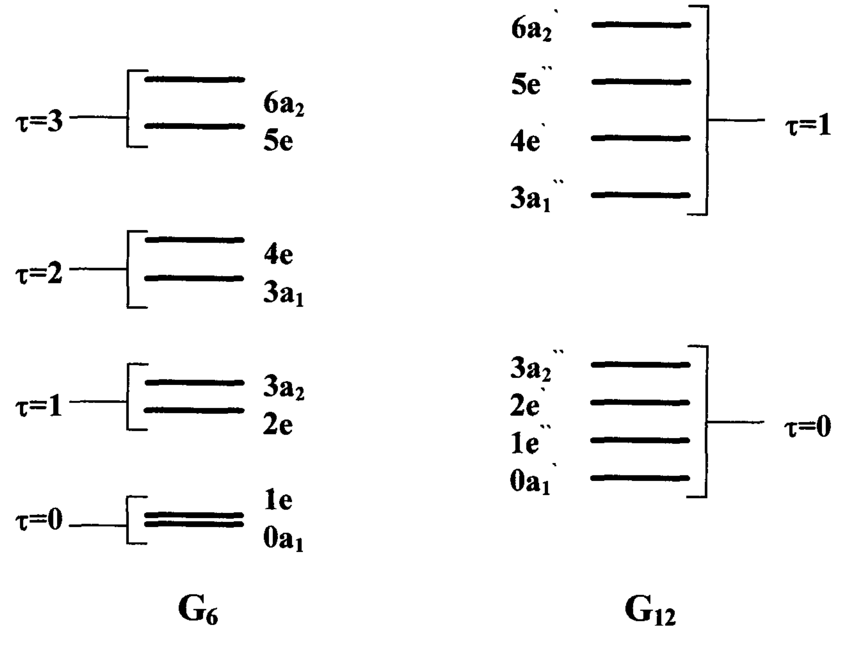

Figure 5.2: Schematic energy diagram for G_6 and G_{12} symmetries.

The torsional structure found has a marked dependence on both the electronic state and the position of the substituent relative to the rotor. The para-isomer[24] (4-ABTF (figure 5.1(d))), in a similar way to analogous toluenes[2,3], displays only small sixfold barriers in both the S_0 and S_1 states due to the high symmetry (G_{12}) of the molecule. In consequence only extremely limited torsional progressions are observed. This has the additional effect of reducing the congestion of the spectra allowing the examination of the other vibrational modes. Of most interest was the amine inversion which Hollas assigned to one of two possible transitions in the predicted energy region.

The ortho[22] (2-ABTF (figure 5.1(b))) and meta[23] (3-ABTF (figure 5.1(c))) isomers, by virtue of their lower overall symmetry (G_6), display three-fold barriers to internal rotation which vary greatly in magnitude from state to state. The ortho-isomer has a large (450 cm^{-1}) barrier in S_0 which is approximately halved in S_1 (240 cm^{-1}). No significant change in the geometry of the CF_3 group was observed on excitation (the internal rotation constant, F, was similar in both states[22]). The meta-isomer displays the opposite behavior with the barrier greatly increasing from S_0 (V_3 = 9 cm^{-1}) to S_1 (V_3 = 155 cm^{-1}). Again no significant change in the geometry of the rotor was found was found[23].

Such dramatic dependence of the barrier to internal rotation on substituent position and electronic state has been previously noted for substituted toluenes[1-8]. This chapter extends the work of Hollas to the ionic ground state by two-colour ZEKE-PFI using the S_1 states as resonant intermediates. Schematics of the ionisation and excitation routes used are shown in figure 5.3. For all three isomers the pump photon was unfocused (<200 μJ, spot size 5 mm) while the probe photon (6-700 μJ) was focused with a 15 cm focal length lens. Further details of the experimental arrangement are given in chapter 3.

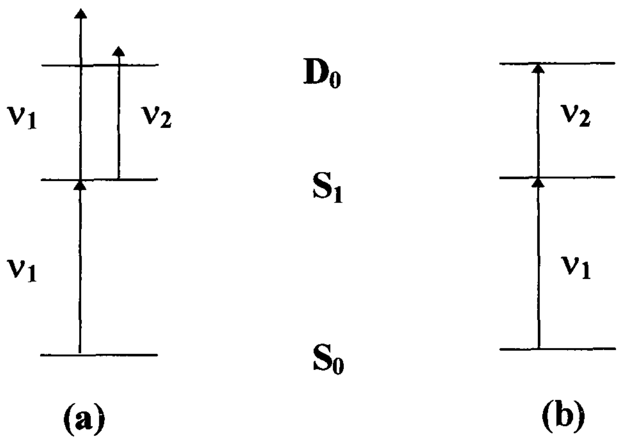

Figure 5.3. Excitation schemes. (a) multiphoton ionisation (MPI) and two-colour photoionisation efficiency (PIE). (b) two-colour ZEKE-PFI.

5.3. 2-Aminobenzotrifluoride

5.3.1. (1+1) MPI of the S_1 state

The one-colour multiphoton ionisation (MPI) spectrum of the S_1 state of 2-ABTF in shown in figure 5.4. It is identical to that obtained by Hollas by fluorescence excitation[22] but with a superior signal to noise ratio. Peak positions and assignments are given in table 5.1. Absolute energies differ slightly from the previous work although torsional spacings are similar. A similar effect has been observed for the aminotoluenes[4] and is ascribed to the difference in ionisation and fluorescence yields over the rotational contour of a band.

Selection rules for torsional excitations have been previously discussed in chapter 2 and in references 1-9,11 & 12. In the case of 2-ABTF this results in changes in the torsional quantum number of 0, ±2, ±4 etc. Thus a progression in the torsional mode (0^0_0, τ^2_0, τ^4_0, τ^6_0 and τ^8_0) is observed. Due to the large barrier to internal rotation in the S_0 state (450 cm^{-1}) the majority of the population resides in the $\tau = 0$ state so any hot bands (i.e. τ^1_1 and τ^3_1 which are allowed by the selection rules) are very weak and unobserved under jet-cooled conditions. Although the selection rules allow **e** ↔ **e** transitions, which should result in odd ↔ even transitions, these are not observed due to the vanishingly small Franck-Condon factors for such transitions when the equilibrium conformation of the rotor remains unchanged.

It is possible that coupling[28,29] of the torsional motion to other degrees of freedom of the molecule (i.e. electronic, vibrational and overall rotation) can give such transitions some intensity but this is clearly not the case in this instance. Hollas obtained a good fit to the experimental features with $V_3 = 240$ cm^{-1}, $V_6 = -67$ cm^{-1} and $F = 0.29$ cm^{-1} for the S_1 state and $V_3 = 450$ cm^{-1}, $V_6 = 83$ cm^{-1} and $F = 0.29$ cm^{-1} for the S_0 state. Calculated Franck-Condon factors for the $S_1 \leftarrow S_0$ transition were in poor agreement with the observed intensities, an effect ascribed to interaction between the two substituent groups.

This interaction is further displayed by the appearance of several weak transitions in figure 5.4. (and in the fluorescence excitation spectrum) which are not part of the torsional sequence. Instead these are assigned to combinations of the torsional motion with other low frequency vibrations of the molecule[25]. Most notable are ν_{43} (the out-of-plane C-CF_3 bend) and ν_{42} (NH_2 torsion). Both these transitions lie very close in energy to the τ^8_0 transition. The 42^1_0 transition, for example, is predicted to lie approximately 5 cm^{-1} to the blue of the CF_3 torsional feature assuming a similar spacing to that of the vibrationless state.

E_{obs} (cm^{-1})	**Assignment**	**Spacing (cm^{-1})**	E_{obs} (cm^{-1})	**Assignment**	**Spacing (cm^{-1})**
33193.2	0^0_0	0	33344.8	$42^1_0\tau^1_0$	151.6
33217.0	τ^2_0	23.8	33350.2	??	157.0
33251.4	τ^4_0	58.2	33372.4	τ^{10}_0	179.2
33291.8	τ^6_0	98.6	33384.0	$42^1_0\tau^3_0$	190.8
33325.0	$43^1_0\tau^1_0$	131.8	33392.5	30^1_0	199.3
33332.7	τ^8_0	139.5			

Table 5.1: Energies and assignments of the S_1 state of 2-ABTF.

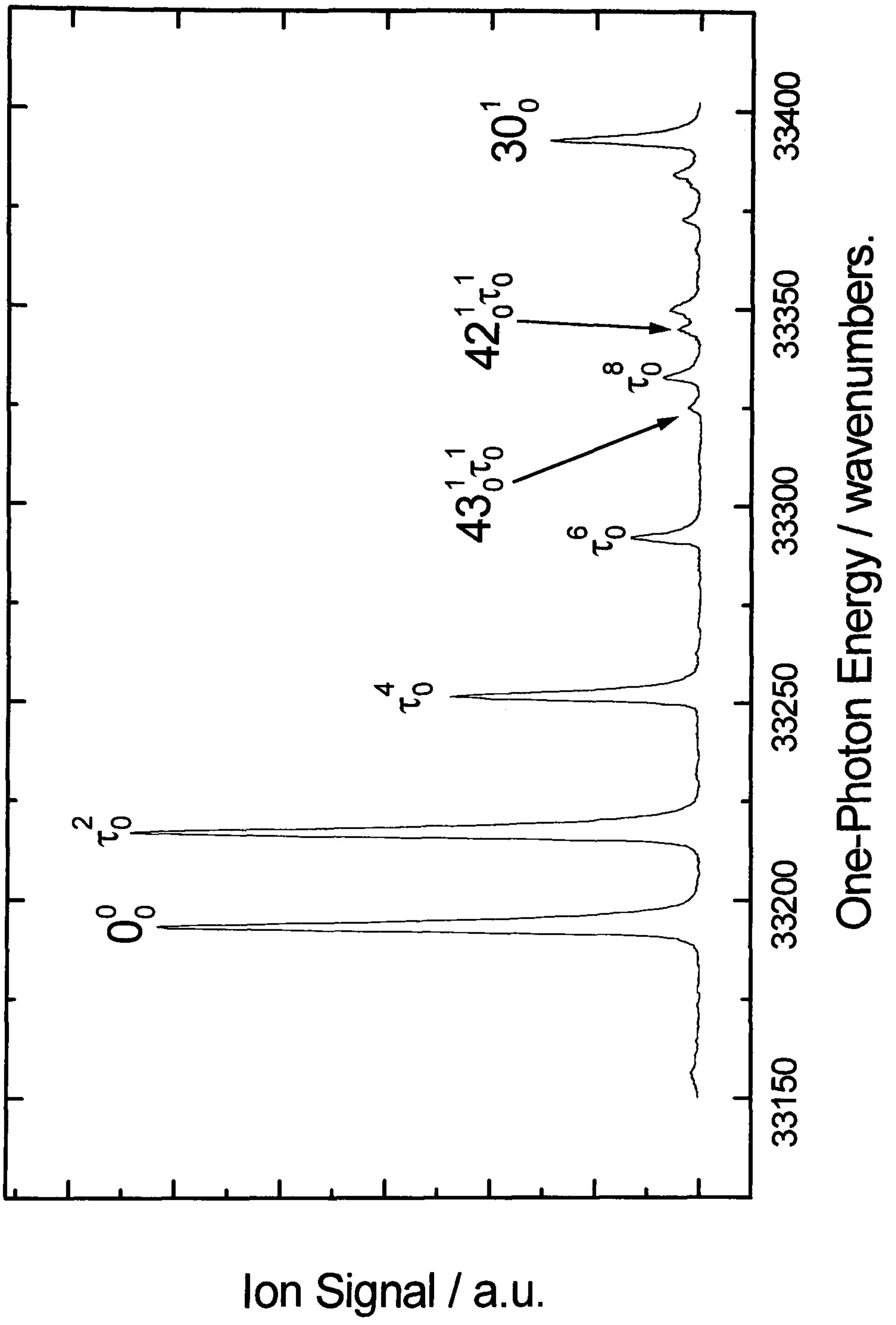

Figure 5.4: (1+1) MPI spectrum of 2-aminobenzotrifluoride.

5.3.2. Ionisation Threshold

To the best of my knowledge no photoelectron or photoionisation study of the aminobenzotrifluorides has been published. This is likely due to the change in the geometry of the amino group on ionisation[30]. The He(I) photoelectron spectrum of the ionic ground state of aniline[31] (which the aminobenzotrifluorides closely resemble in their chemical and spectroscopic behavior) is a broad partially resolved feature. No electron signal was observed at the known ionisation threshold[32] as measured by ZEKE-PFI via the S_1 state (62271 cm^{-1}). A similar situation is found for other substituted anilines[33] and should be expected for the aminobenzotrifluorides. The torsional structure of the ABTF's would only add to the problem by further increasing the density of states of the ion. An approximate value of the ionisation energy for 2-ABTF can be found by considering the ionisation energies of benzotrifluoride[20,31] (78000 cm^{-1}) and 2-aminotoluene[4] (~61000 cm^{-1}) relative to benzene[21] (74556 cm^{-1}) yielding a value in the region of 65000 cm^{-1}.

To obtain an experimental value of the ionisation threshold prior to a ZEKE-PFI experiment a two-colour photoionisation efficiency (PIE) spectrum of 2-ABTF was obtained using the origin of the S_1 state as a resonant intermediate. This is shown in figure 5.5. Sharp rises in ion-yield are observed at total energies of 65260 and 65340 cm^{-1}. The dc electric field used was 270 Vcm^{-1} giving rise to a adiabatic field shift[34] in wavenumbers ($-6.1\sqrt{V}$ where V has units of Vcm^{-1}) of approximately 100 cm^{-1}. A first estimate of the ionisation energy of 2-ABTF is therefore 65360±20 cm^{-1}. The steps can be attributed to additional ionisation channels opening up, in this case the torsional structure of the ion. Similar stepped spectra have been obtained for many molecules notably m-cresol[35] for which the entire torsional structure of both the cis and trans isomers of the ion could be found by this method alone.

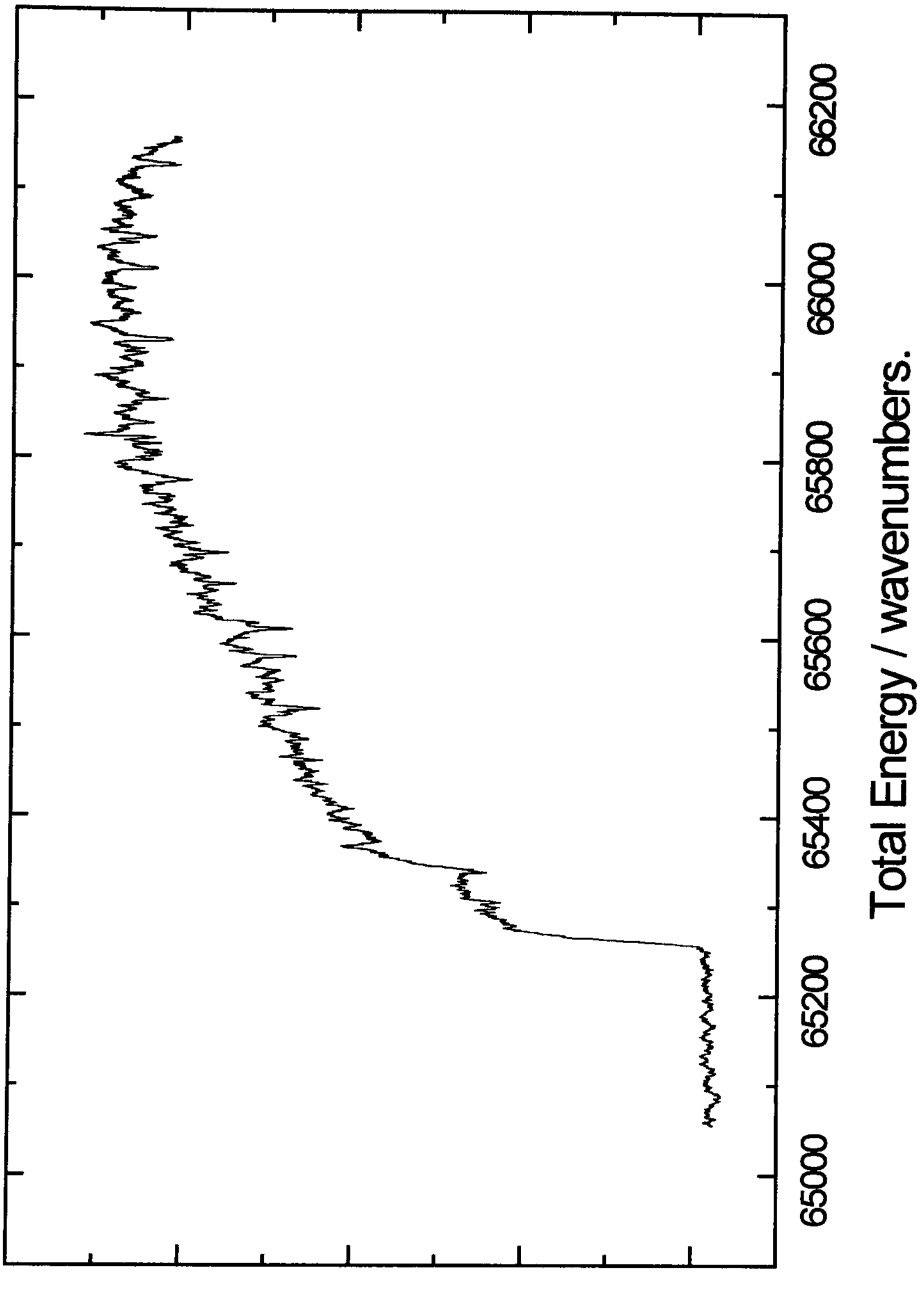

Figure 5.5: (1+1') Photoionisation efficiency spectrum of 2-ABTF via the origin of the S_1 state. The spectrum has not been corrected for the field shift.

5.3.3. Two-Colour ZEKE-PFI

It was possible to use the origin band (0^0_0) and the first four torsional bands (τ^2_0, τ^4_0, τ^6_0 and τ^8_0) of the S_1 state as resonant intermediates in a ZEKE-PFI experiment. The spectra obtained are given in figure 5.6. The field free ionisation energy was measured as 65373±3 cm^{-1} (see appendix 3) in good agreement with the value from the PIE experiment and with the estimate based on ionisation energies. A progression of 12 quanta in the torsional vibration can be assigned with an initial spacing of 43 cm^{-1} indicating a barrier to internal rotation of the CF_3 group of a similar magnitude to that of the S_0 state[22]. No sign of any splitting of the torsional peaks[11] is observed indicating that the barrier is higher than the energy range spanned in the experiment. As with the MPI spectrum the even torsional levels (i.e. 0^0 and τ^2) dominate although weak features can be assigned to the odd levels (i.e. τ^1 and τ^5). The length and spacing of the progression is such that several vibrational modes (for example ν_{28} and ν_{29}) appear amongst, and in fact partially obscure, the torsional structure. (ZEKE spectra of these vibrations are given in appendix 3). Most notable of these vibrational modes is the one which appears at 145 cm^{-1} internal energy and is assigned to one quantum of the NH_2 torsion (ν_{42}). This assignment is made by comparison to the S_0 and S_1 vibrational frequencies[25] although an alternative assignment to mode ν_{43} is also a possibility. This transition (and its combinations with the CF_3 torsion (τ)) are observed via all the resonant intermediates and become more and more apparent as the energy of the intermediate is increased. This is particularly noticeable in the ZEKE spectrum via τ^8_0 where ν_{42} dominates and the only intense CF_3 torsional features are those which lie close in energy to transitions involving ν_{42} (i.e. τ^5 and τ^{10}). Such a situation indicates substantial interaction between the two substituent groups in the ground state of the ion.

Energies and assignments of the ionic ground state of 2-ABTF are given in table 5.2. The transitions all display full widths at half maximum (FWHM) of 7 cm^{-1} in agreement with the range of Rydberg states sampled by the electric field (4 Vcm^{-1} equivalent to 8 cm^{-1} using the diabatic shift of 4√V). Quoted energies are the peak maxima and should be accurate to within 2 cm^{-1}.

Assignment	E_{obs} (cm^{-1})	**Assignment**	E_{obs} (cm^{-1})
0^0	**0**	τ^7	**282**
τ^1	**43**	$42^1\tau^4$or 42^2	**306**
τ^2	**84**	τ^8	**320**
τ^3	**125**	τ^9	**355**
42^1	**145**	$42^1\tau^6$ or $42^2\tau^2$	**382**
τ^4	**165**	τ^{10}	**393**
τ^5	**206**	τ^{11}	**-**
$42^1\tau^2$	**228**	τ^{12}	**461**
τ^6	**244**		

Table 5.2. Energies and assignments of the ion state of 2-ABTF.

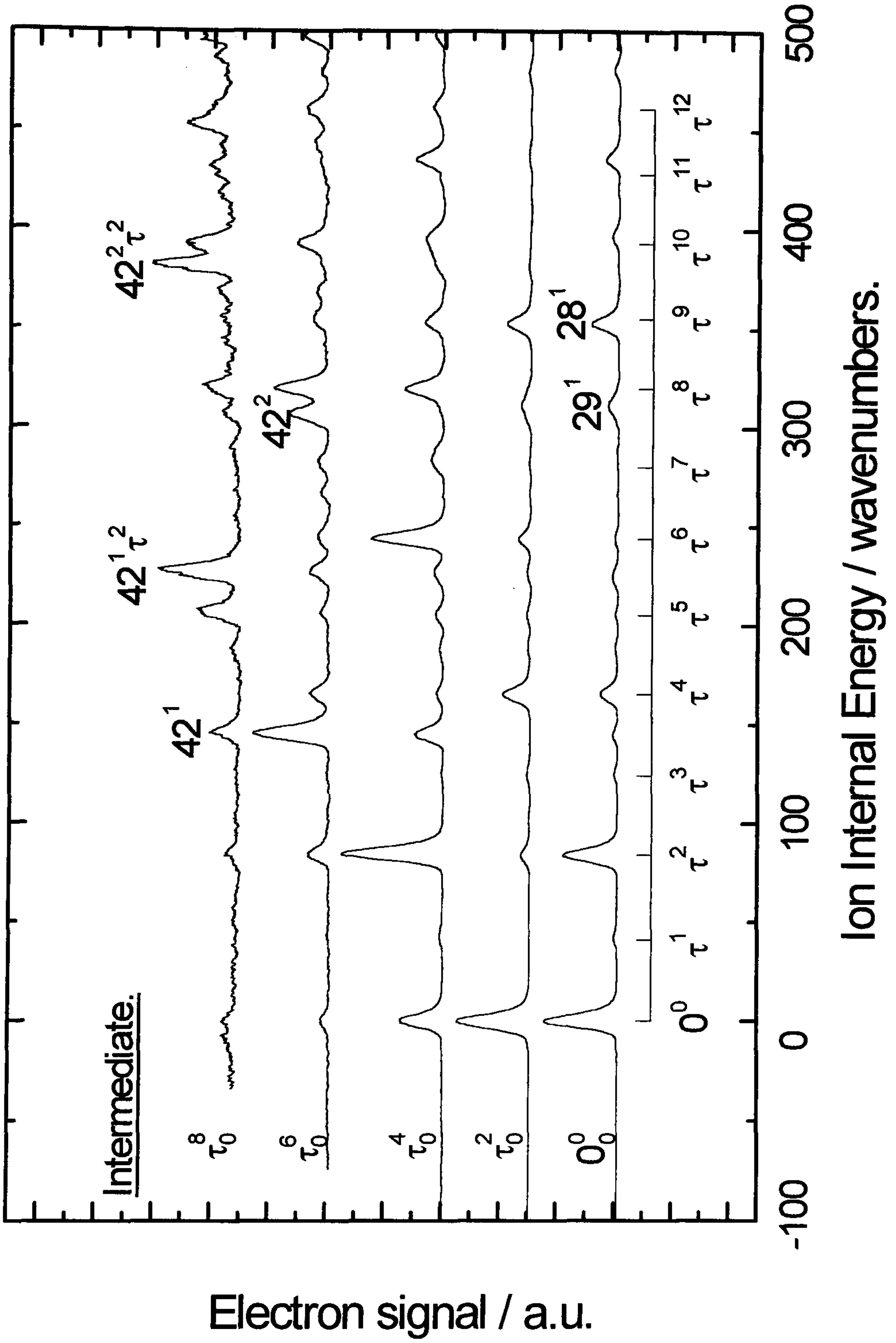

Figure 5.6: Two-colour ZEKE-PFI spectra of 2-ABTF via several torsional levels of the S_1 state.

5.3.4. Calculation of Barrier Height

The experimental torsional levels were fitted by the calculational methods outlined in chapter 2[36-38]. Good fits to the experimental values were found for V_3 = 720±10 cm^{-1}, V_6 = -3±4 cm^{-1} and F = 0.290±0.004 cm^{-1}. Error limits are found by calculating the root-mean-square deviation from observed values. Given the FWHM of the ZEKE transitions the upper limit for the r.m.s. value is 2 cm^{-1}. In addition the energy range spanned in the experiment (~500 cm^{-1}) does not extend up to the barrier and the calculated values only represent the best fit to the area covered. Any unusual behavior of the potential beyond this energy range cannot be accounted for. Calculated and observed energies are given in table 5.3. A pictorial representation of the barriers in all three states (S_0, S_1 and D_0) is shown in figure 5.7. The trend follows that of 2-aminotoluene[4] and of other ortho-substituted toluenes[2,3] in that the barrier decreases from S_0 to S_1 but then increases on ionisation.

τ^+	E_{calc} (cm^{-1})	E_{obs} (cm^{-1})	$E_{calc} - E_{obs}$ (cm^{-1})
0	0	0	0
1	42.3	43	-0.7
2	84.0	84	0
3	125.1	125	+0.1
4	165.4	165	+0.4
5	205.1	206	-0.9
6	244.0	244	0
7	282.2	282	+0.2
8	319.6	320	-0.4
9	356.1	355	+1.1
10	391.7	393	-1.3
11	426.7	-	-
12	460.6	461	-0.4

Table 5.3: Calculated and observed torsional energy levels for the ground ionic state of 2-ABTF. Calculated energies are from the values V_3 = 720 cm^{-1}, V_6 = -3 cm^{-1} and F = 0.290 cm^{-1}.

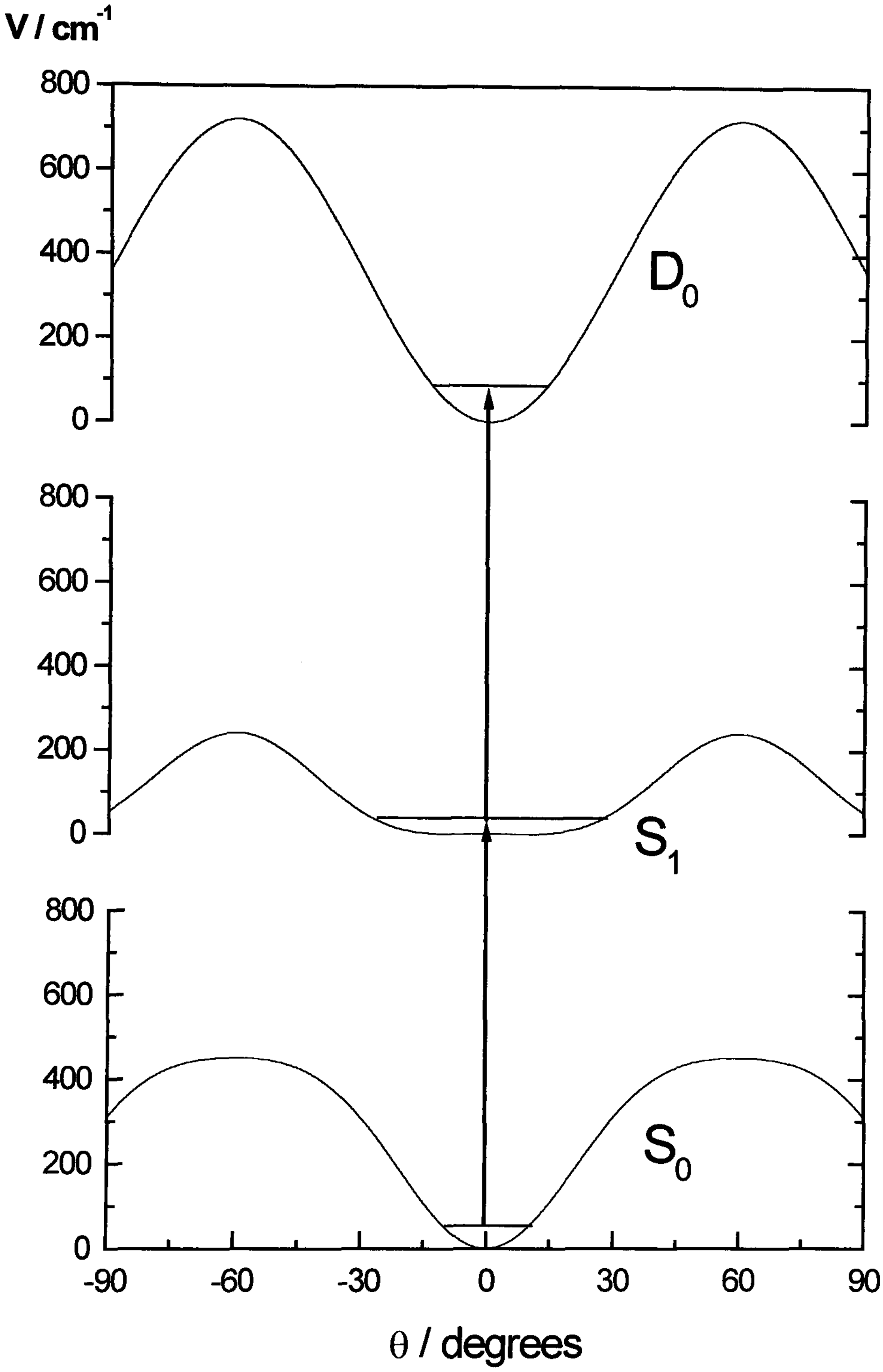

Figure 5.7: Barriers to internal rotation in 2-ABTF in various electronic states. The S_0 and S_1 barriers are from reference 22.

Using the calculated eigenvalues it was possible to determine the Franck-Condon factors for the $D_0 \leftarrow S_1$ transition. Only allowed transitions[11,12] were considered ($\mathbf{a_1} \leftrightarrow \mathbf{a_1}$, $\mathbf{a_2} \leftrightarrow \mathbf{a_2}$ and $\mathbf{e} \leftrightarrow \mathbf{e}$) and only one of the doubly degenerate **e** components was used to allow for the differing nuclear spin statistics of the **a** and **e** torsional states[22-24,39]. Calculated ZEKE spectra (fitted with a Gaussian of 7 cm^{-1} full width at half maximum) are shown in figure 5.8. The conformation of the rotor was found to be unchanged from the S_1 state to that of the ionic ground state.

Agreement between the calculated and experimental spectra is not particularly good. Several obvious differences are noticeable. Firstly, the intensity of the origin bands obtained via τ_0^2, τ_0^4, τ_0^6, and τ_0^8 are far more intense than predicted. Secondly, the odd torsional levels are observed as weak features when the calculated Franck-Condon factors for such transitions are zero. Thirdly, and finally, although the calculated intensity envelopes show at least qualitative agreement with experimental results for the spectra obtained by 0_0^0, τ_0^2, τ_0^4 and τ_0^6 (for example when pumping via τ_0^4, τ^4 in the ion is very weak both experimentally and in theory), the ZEKE spectra obtained via τ_0^8 has no resemblance to that of the calculated spectrum. It was noted previously that this spectrum is dominated by ν_{42} (the NH_2 torsion) and the intermediate lies very close in energy to that of the first quantum of ν_{42}. It is clear from these results that interaction between the CF_3 and NH_2 groups is considerable for both the S_1 state and the ionic ground state of 2-ABTF. This will be further discussed in section 5.6.2.

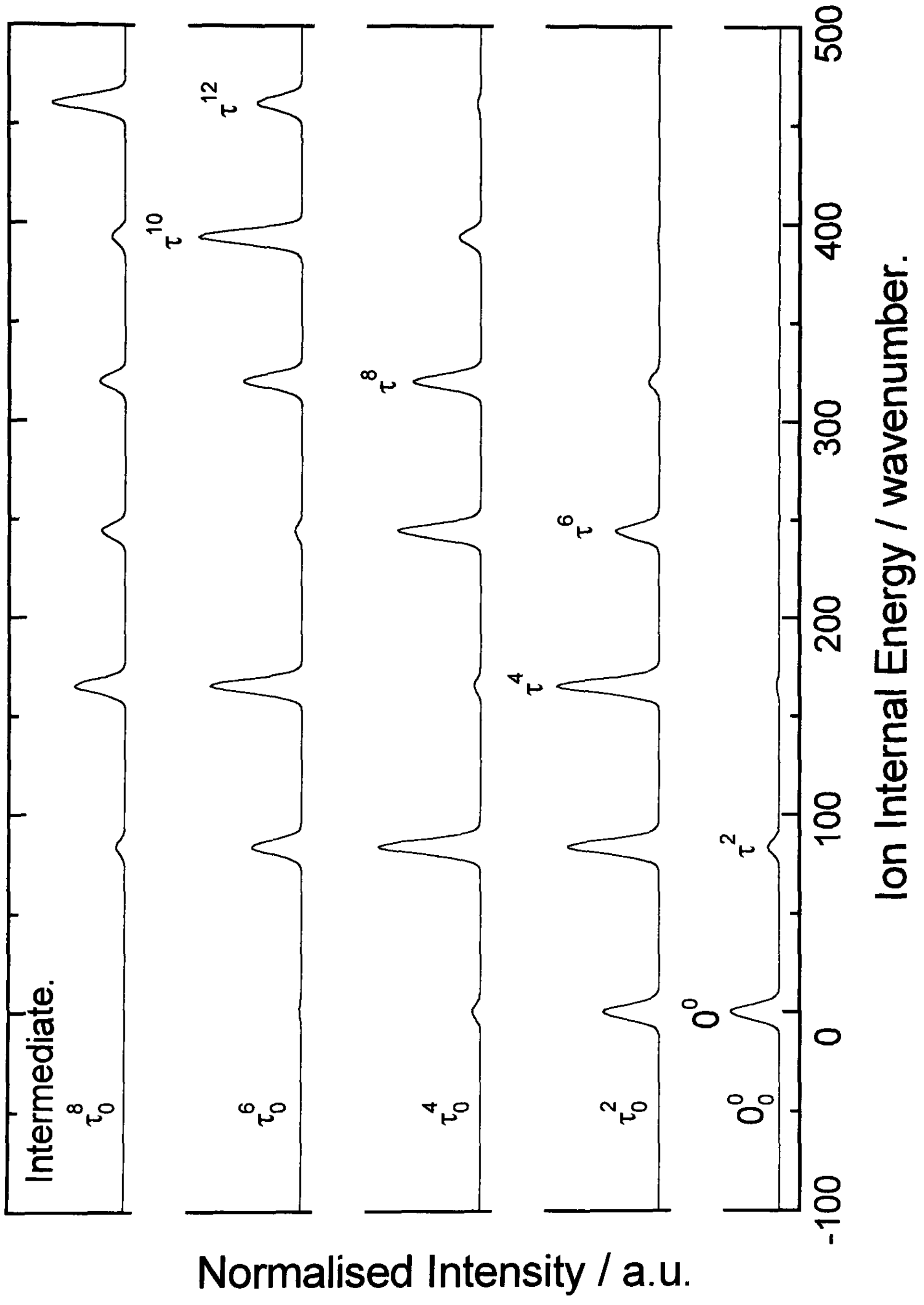

Figure 5.8: Calculated ZEKE spectra for 2-ABTF.

5.4. 3-Aminobenzotrifluoride

5.4.1. (1+1) MPI of the S_1 state

The one-colour multiphoton ionisation spectrum of the S_1 state of 3-ABTF is shown in figure 5.9. As was seen for 2-ABTF the spectrum observed is identical to that obtained by fluorescence[23]. The selection rules for 2-ABTF are equally applicable here. Hollas fitted the experimental data with the following values; V_3 = 155 cm^{-1}, V_6 = -40 cm^{-1} and F = 0.29 cm^{-1} for the S_1 state and V_3 = 9 cm^{-1}, V_6 = -10 cm^{-1} and F = 0.29 cm^{-1} for the S_0 state. Although the barrier to internal rotation in the S_1 state is of similar magnitude to that of the S_1 state of 2-ABTF the observed MPI spectrum is very different in that it is considerably more congested. This is caused by the very small barrier to internal rotation in the neutral ground state (V_3 = 9 cm^{-1}) where the first excited torsional level (τ^1) lies only 1.5 cm^{-1} above the origin. The result of this is that the excited torsional levels of the S_0 state will have substantial population even under jet-cooled conditions. Therefore extensive hot band structure is observed in the MPI spectrum (i.e. τ_1^n where n = 1, 3, 5 etc. and τ_2^m where m = 0, 2, 4 etc.). The nature of these bands is confirmed by their dependence on beam conditions (see chapter 3, figure 3.2.) with transitions such as τ_1^1 and τ_1^3 displaying considerable intensity even under good cooling conditions (typically 750 Torr of helium). For later two-colour experiments involving these hot bands the pressure was lowered (~300 Torr) to optimise observed signals. Energies and assignments are shown in table 5.4.

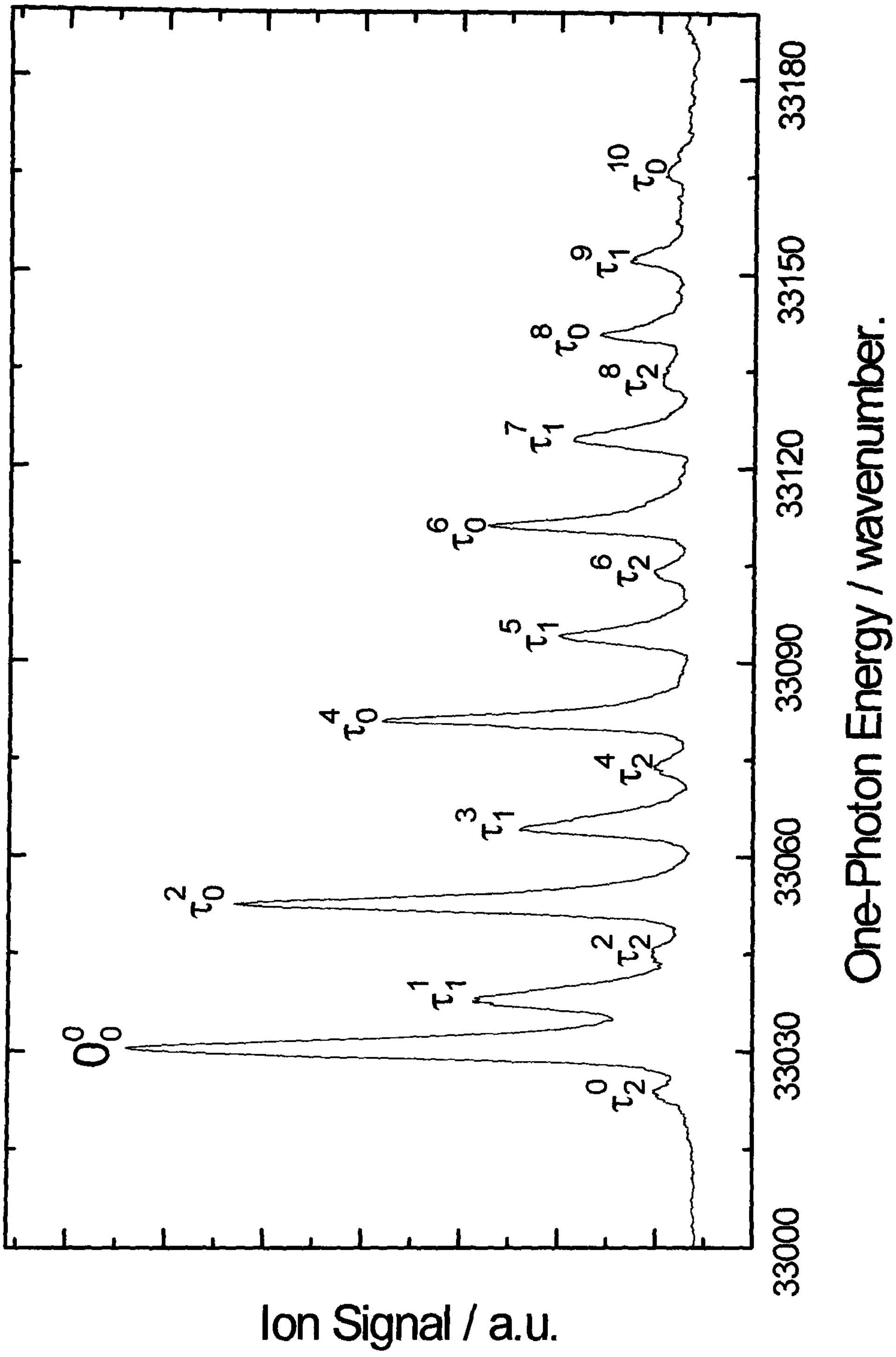

Figure 5.9: (1+1) MPI spectra of the S_1 state of 3-ABTF.

E_{obs} (cm^{-1})	Assignment	Spacing (cm^{-1})	$\mathrm{E_{obs}}$ (cm^{-1})	Assignment	Spacing (cm^{-1})
33023.7	τ_2^0	-6.7	33094.1	τ_1^5	63.7
33030.4	0_0^0	0	33103.9	τ_2^6	73.5
33037.7	τ_1^1	7.3	33111.0	τ_0^6	80.6
33044.9	τ_2^2	14.5	33124.4	τ_1^7	94.0
33052.5	τ_0^2	22.1	33134.2	τ_2^8	103.8
33064.3	τ_1^3	33.9	33140.5	τ_0^8	110.1
33073.9	τ_2^4	43.5	33151.8	τ_1^9	121.4
33080.8	τ_0^4	50.4	33165.6	τ_0^{10}	135.2

Table 5.4. Energies and assignments of the torsional levels of the S_1 state of 3-ABTF.

5.4.2. Ionisation Threshold

The ionisation energy for 3-ABTF was not known previously. Using the same means as for 2-ABTF an estimate of 65000 cm^{-1} can be obtained. Figure 5.10. shows the photoionisation efficiency spectrum via the origin of the S_1 state. It is very different to that found for 2-ABTF (figure 5.5.) in that a long gradual increase in the ion yield was found with a possible onset of 65450 cm^{-1} giving an estimate of the ionisation energy as 65550 cm^{-1} although clearly this could be very inaccurate. The slow onset reflects the poor (or possibly non-existent) Franck-Condon overlap between the origin of the S_1 state and that of the ion indicating a large change in the conformation of the rotor. This is borne out by the ZEKE-PFI spectra presented in the next section. Similar experiments involving meta substituted toluenes show similar behavior[2-4].

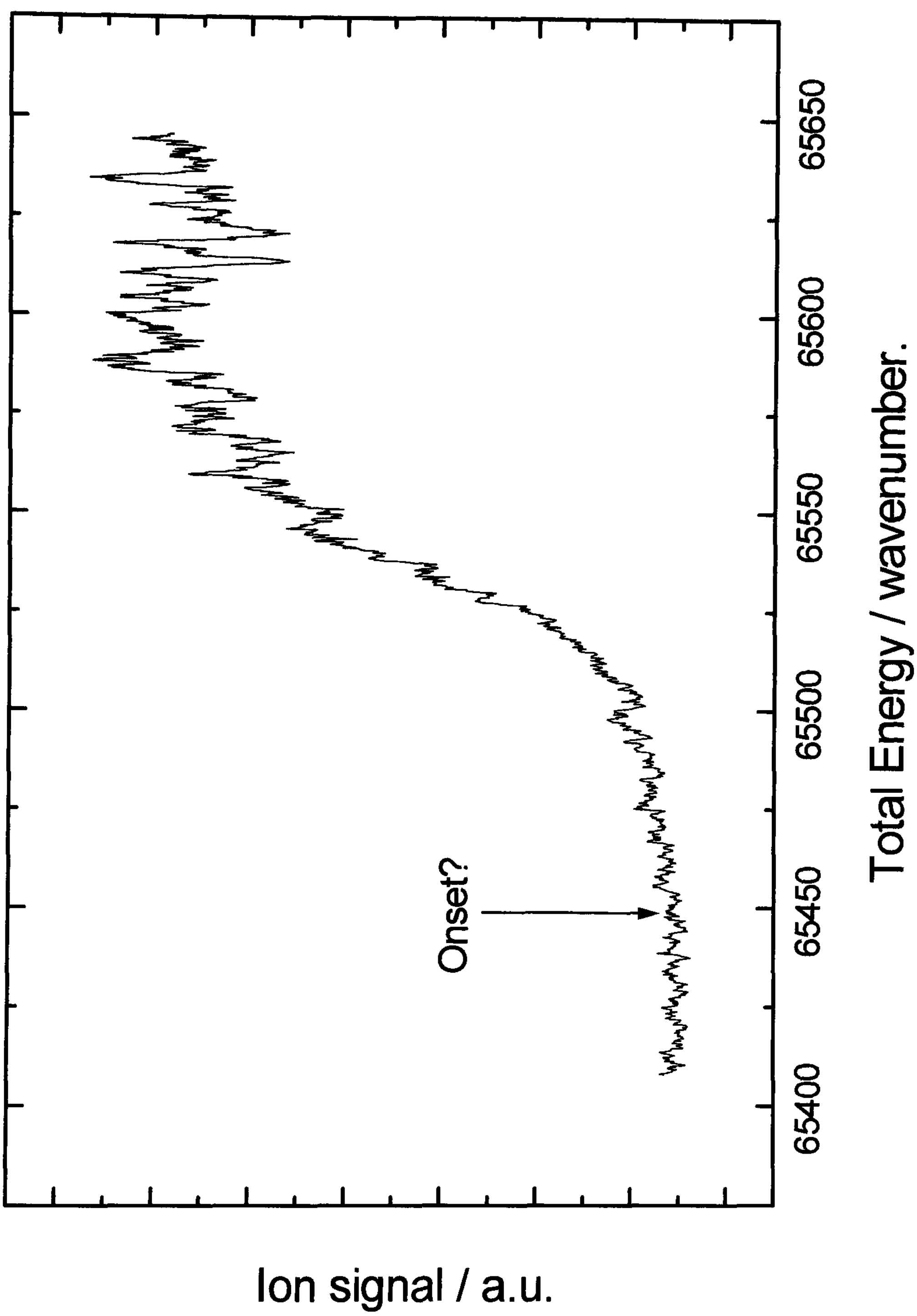

Figure 5.10: Two-colour PIE spectrum of 3-ABTF via the origin of the S_1 state. The spectrum has not been corrected for the field shift.

5.4.3. Two-Colour ZEKE-PFI

The presence of a large number of hot bands in the S_1 state greatly increases the number of resonant intermediates available for a ZEKE-PFI experiment. In particular the odd members of the torsional sequence are available. Figure 5.11. presents ZEKE-PFI spectra obtained via the origin band (0_0^0) and the first eight torsional bands (τ_1^1, τ_0^2, τ_1^3, τ_0^4, τ_1^5, τ_0^6, τ_1^7 and τ_0^8) of the S_1 state. These show a striking pattern distinct from that of 2-ABTF. As the degree of torsional excitation in the intermediate increases ZEKE-PFI transitions are observed at lower and lower energy. The origin band of the ion is not observed using the origin of the S_1 state as a resonant intermediate indicating a large change in the conformation of the rotor on ionisation. Such a change results in the even ↔ odd transitions (or at least the e components of such states) having appreciable Franck-Condon factors. In the absence of any other data the lowest energy transition is assigned as the origin. The field free ionisation energy is 65450±3 cm^{-1} (see appendix 3). The torsional sequence can be followed up to the twelfth quantum with an initial spacing of 22 cm^{-1} indicating a barrier similar in height to that of the S_1 state although the preferred conformations are different. In addition broad unresolved features are observed at higher energies for several intermediates. These are assignable to torsional states above the barrier and will be considered in section 5.4.4.

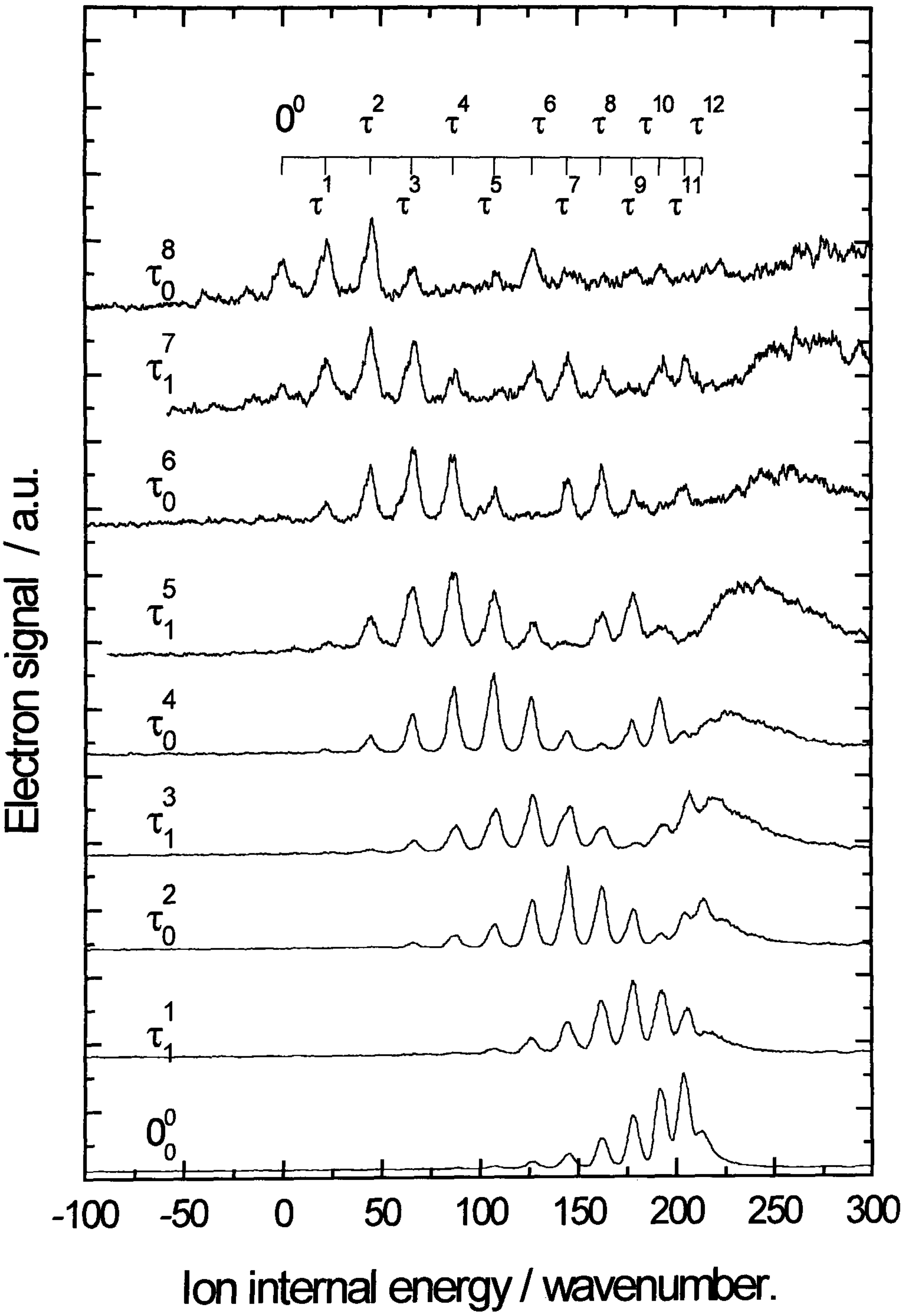

Figure 5.11: Two-colour ZEKE-PFI spectra of 3-ABTF via various torsional levels of the S_1 state.

For the ZEKE-PFI spectrum via the highest possible intermediate (τ_0^8) there are two very weak features below the apparent origin. These exhibit a spacing consistent with the torsional progression (~20 cm^{-1}) but do not match up to the chosen origin. It can be seen from figure 3.2. in chapter 3 that the intermediate used is considerably broader at higher beam temperatures. More detailed analysis of this spectrum reveals the presence of a hot band originating from the third torsional level (τ^3) of the neutral ground state. Hence the two features in the ZEKE-PFI spectrum can be assigned as originating from this level and do not form part of the observed torsional sequence.

Energies and assignments of the ion state of 3-ABTF are given in table 5.5.

τ^+	E_{obs} (cm^{-1})	τ^+	E_{obs} (cm^{-1})
0	0	7	145
1	22	**8**	162
2	45	**9**	178
3	66	**10**	192
4	87	**11**	205
5	108	**12**	214
6	127		

Table 5.5. Energies and assignments of the torsional states of the cation of 3-ABTF.

5.4.4. Calculation of Barrier Height

The torsional energy levels in table 5.5. could be fitted to the values; V_3 = 222±10 cm^{-1}, V_6 = -4±2 cm^{-1} and F = 0.290±0.005 cm^{-1}. Calculated and observed energies are compared in table 5.6. Agreement is excellent and well within experimental limits. In this case the experimental energy range spans the calculated barrier height. This barrier and those of the neutral states (S_0 and S_1) are shown pictorially in figure 5.12. The barrier in the ionic ground state has been shifted by 60° in accordance with the conformation change in meta-substituted toluenes[2-4].

τ^+	E_{calc} (cm^{-1})	E_{obs} (cm^{-1})	$E_{calc} - E_{obs}$ (cm^{-1})
0	0	0	0
1	22.7	22	+0.7
2	44.8	45	-0.2
3	66.3	66	+0.3
4	87.1	87	+0.1
5	107.3	108	-0.7
6	126.6	127	-0.4
7	145.1	145	+0.1
8	162.6	162	+0.6
9	178.8	178	+0.8
10	193.2 (a_1)	192	+1.2
	193.6 (e)		
11	206.2 (a_2)	205	+1.2
	208.6 (e)		
12	213.8 (a_1)	214	-0.2
	217.5 (e)		

Table 5.6: Calculated and observed torsional energies for the ground ionic state of 3-ABTF. The calculated values are from V_3 = 222 cm^{-1}, V_6 = -4 cm^{-1} and F = 0.290 cm^{-1}.

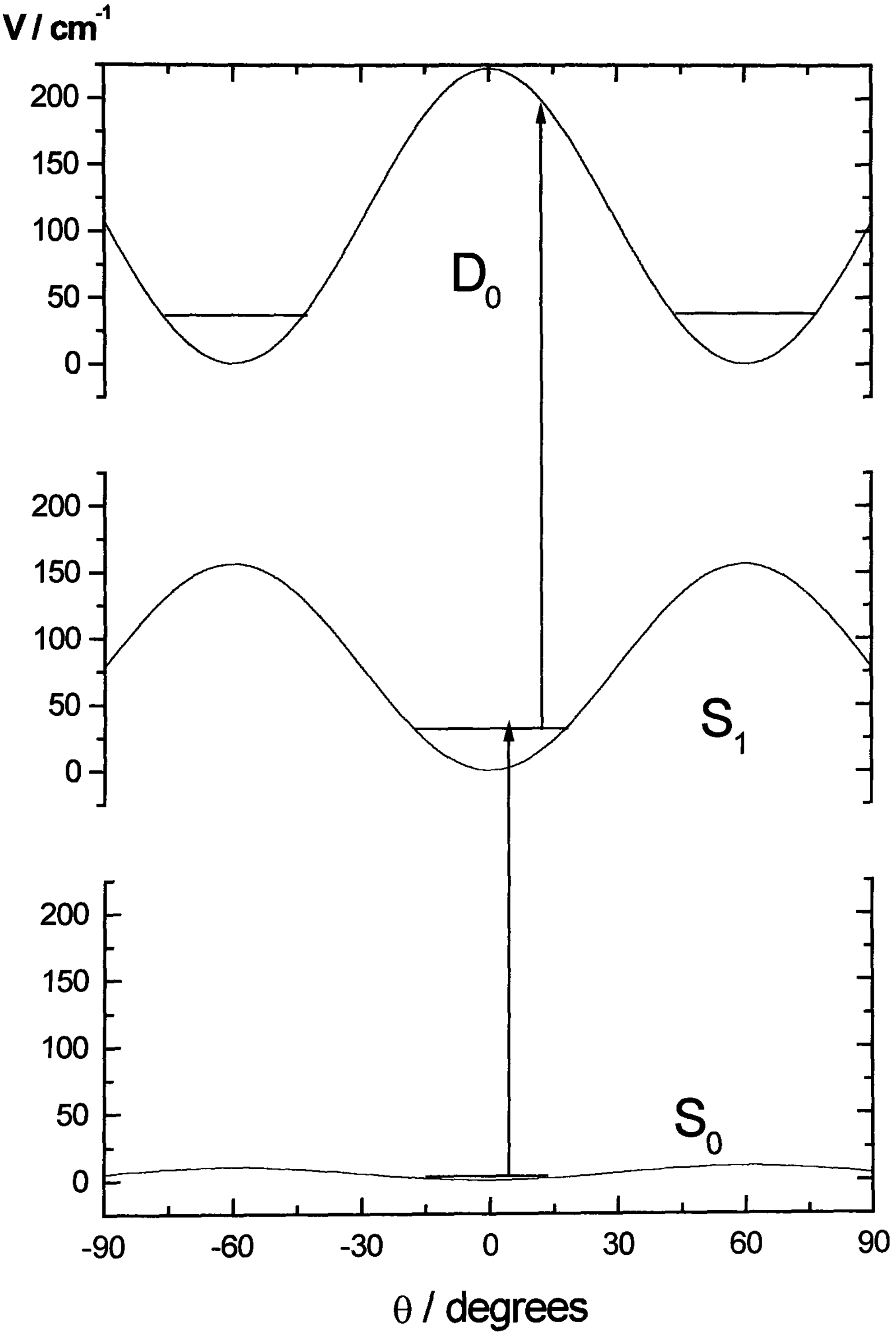

Figure 5.12: Barriers to internal rotation for all three electronic states of 3-ABTF. The barriers in the S_0 and S_1 states are from reference 23.

Calculated and experimental intensities are shown in figure 5.13. for the even intermediates (0_0^0, τ_0^2, τ_0^4, τ_0^6 and τ_0^8) and 5.14. for the odd (τ_1^1, τ_1^3, τ_1^5 and τ_1^7). Agreement was best for a rotor angle in the ion of 60° (π/3 radians) different from that of the S_1 state. The general shape of the experimental intensity envelope can be reproduced but it is noticeable that the calculated envelopes do not display the smooth behavior of the experimental intensities. Instead a distinct oscillation is observed superimposed on such an envelope. For example, when an even torsional level (i.e. 0_0^0 or τ_0^2) in the S_1 state is pumped the calculated intensities for the odd torsional levels of the ion (i.e. τ^1 or τ^3) are smaller than that observed experimentally (figure 5.13.). In a similar way the even torsional levels are calculated to be much weaker when pumping via an odd intermediate (figure 5.14.).

The calculation also shows considerable activity to higher energy for several of the intermediates. These correspond to transitions to torsional states above the barrier where internal rotation is unhindered. Such transitions are predicted to have an intensity comparable to that of the states below the barrier in good agreement with the experimental spectra. For example for the spectra via τ_1^5 the **e** component of $\tau = 14$ (calculated ion internal energy of 247 cm^{-1}) is calculated to have an intensity approximately the same as τ^4 which is the most intense feature which is fully resolved. It is clear from figure 5.11. that this is observed experimentally with a broad unresolved hump around 250 cm^{-1} internal energy.

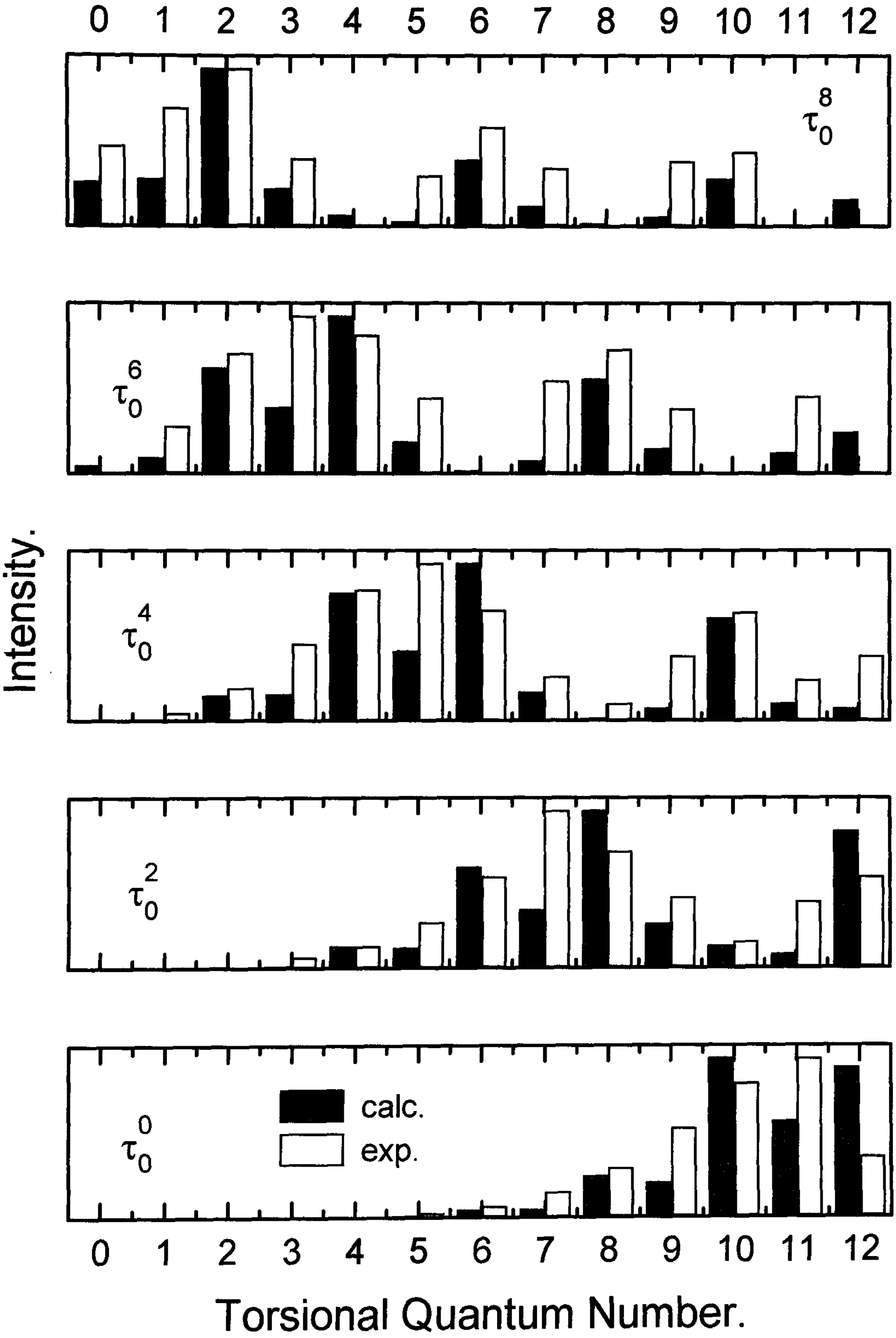

Figure 5.13: Calculated and observed intensities for 3-ABTF obtained via the even torsional levels of the S_1 state.

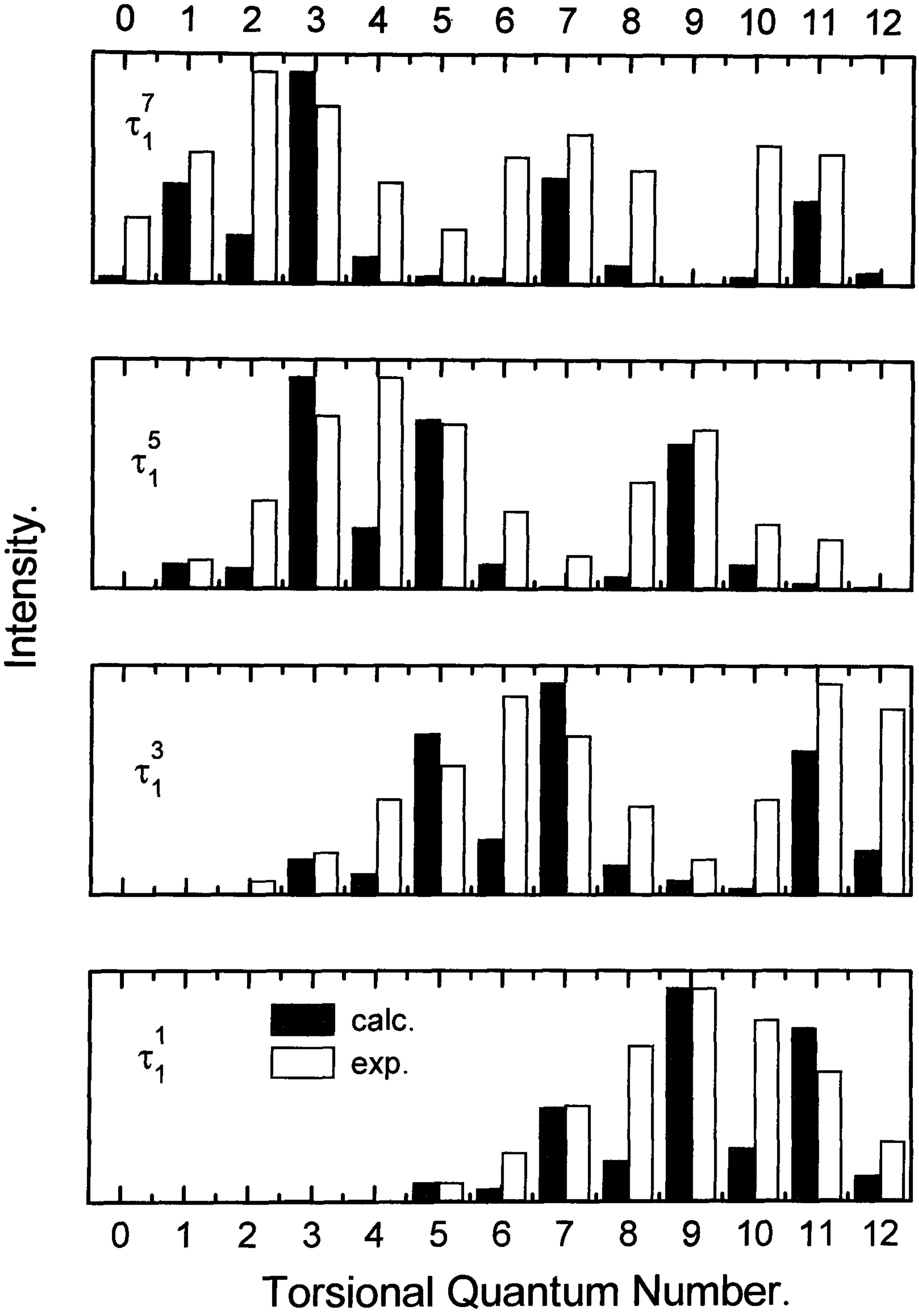

Figure 5.14: Calculated and observed intensities for 3-ABTF obtained via the odd torsional levels of the S_1 state.

It appears as if some factor is missing from the Franck-Condon calculation which is present experimentally. Examination of figure 5.2. reveals that the odd torsional levels have states of **e** and $\mathbf{a_2}$ symmetry while the even levels are of **e** and $\mathbf{a_1}$ symmetry. In the absence of coupling between the torsional vibration[28,29] and the other degrees of freedom of the molecule $\mathbf{a_1} \leftrightarrow \mathbf{a_2}$ transitions are forbidden. Such transitions can gain intensity by several mechanisms but the one which is relevant here arises from the details of the technique used to study the ion[1,3], namely Pulsed-Field-Ionisation (PFI). The excitation of high-*n* Rydberg states and their subsequent field-ionisation can have a substantial effect on the intensity pattern of a photoelectron spectrum[40,41]. Interaction between the high-*n* Rydberg states and the torsional motion can result in $\mathbf{a_1} \leftrightarrow \mathbf{a_2}$ transitions gaining some intensity[1-7]. As a measure of this figures 5.15. and 5.16. show the calculated and experimental intensities when only transitions between **e** symmetry levels is considered. The smooth envelopes of the experimental spectra are reproduced well. Thus there is considerable coupling between the torsional levels of the ion and the high-*n* Rydberg states. This will be discussed further in section 5.6.3.

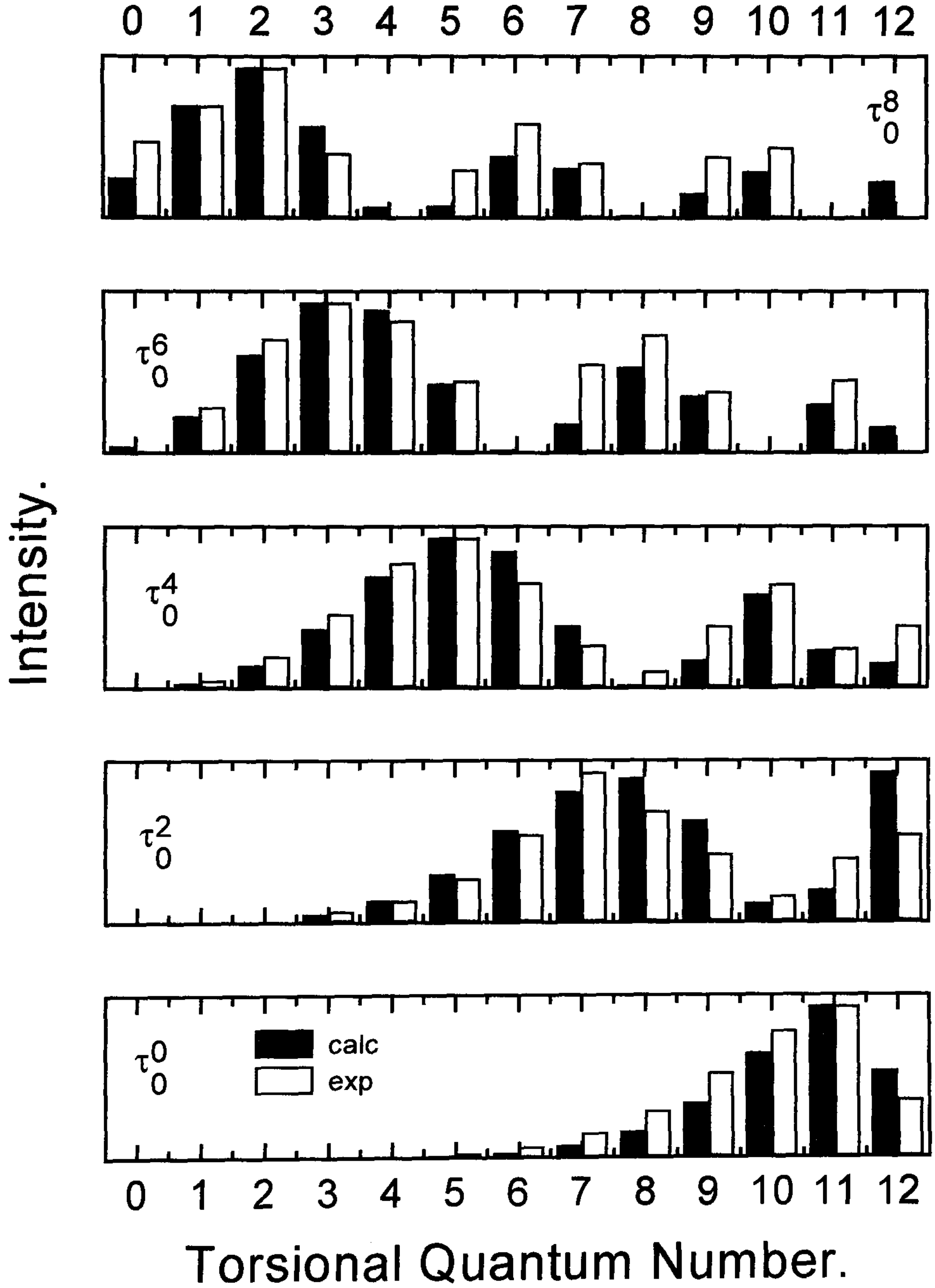

Figure 5.15: Experimental and calculated intensities for the $D_0 \leftarrow S_1$ transition via the even torsional intermediates of the S_1 state. The calculated intensities include transitions between levels of e type symmetry only.

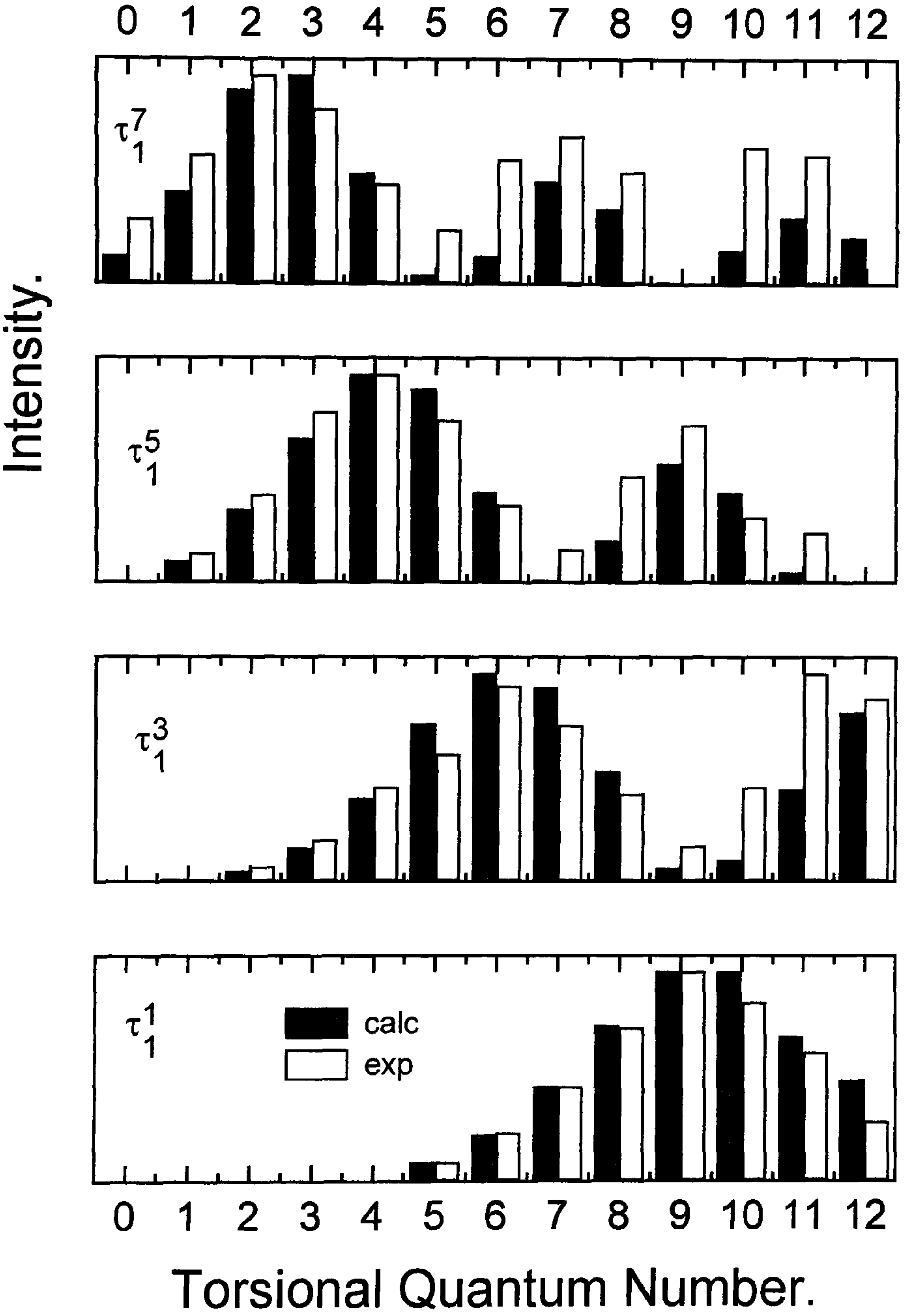

Figure 5.16: Experimental and calculated intensities for the $D_0 \leftarrow S_1$ transition via the odd torsional intermediates of the S_1 state. The calculated intensities include transitions between levels of e type symmetry only.

5.5. 4-Aminobenzotrifluoride

5.5.1. (1+1) MPI of the S_1 State

The one-colour multiphoton ionisation spectrum of the origin band of the S_1 state of 4-aminobenzotrifluoride is shown in figure 5.17. Only very limited torsional structure is observed with the origin band the dominant feature[24]. This is typical of the para-substituted toluenes[2-7] (and of toluene[1] itself) where the barrier to internal rotation has sixfold symmetry due to the symmetry of the molecule. Weak features at 15 and 26 cm^{-1} to the blue of the origin band can be assigned to the first and second torsional levels. Energies and assignments are given in table 5.7. Hollas fitted the observed energies with the constants $V_6 = 33$ cm^{-1} and $F = 0.38$ cm^{-1}.

E_{obs} (cm^{-1})	**Assignment**	**Spacing (cm^{-1})**
34233.8	0_0^0	0
34242.4	τ_1^1	8.6
34248.9	τ_0^1	15.1
34259.3	τ_0^2	25.5

Table 5.7: Energies and assignments of the torsional levels of the S_1 state of 4-ABTF.

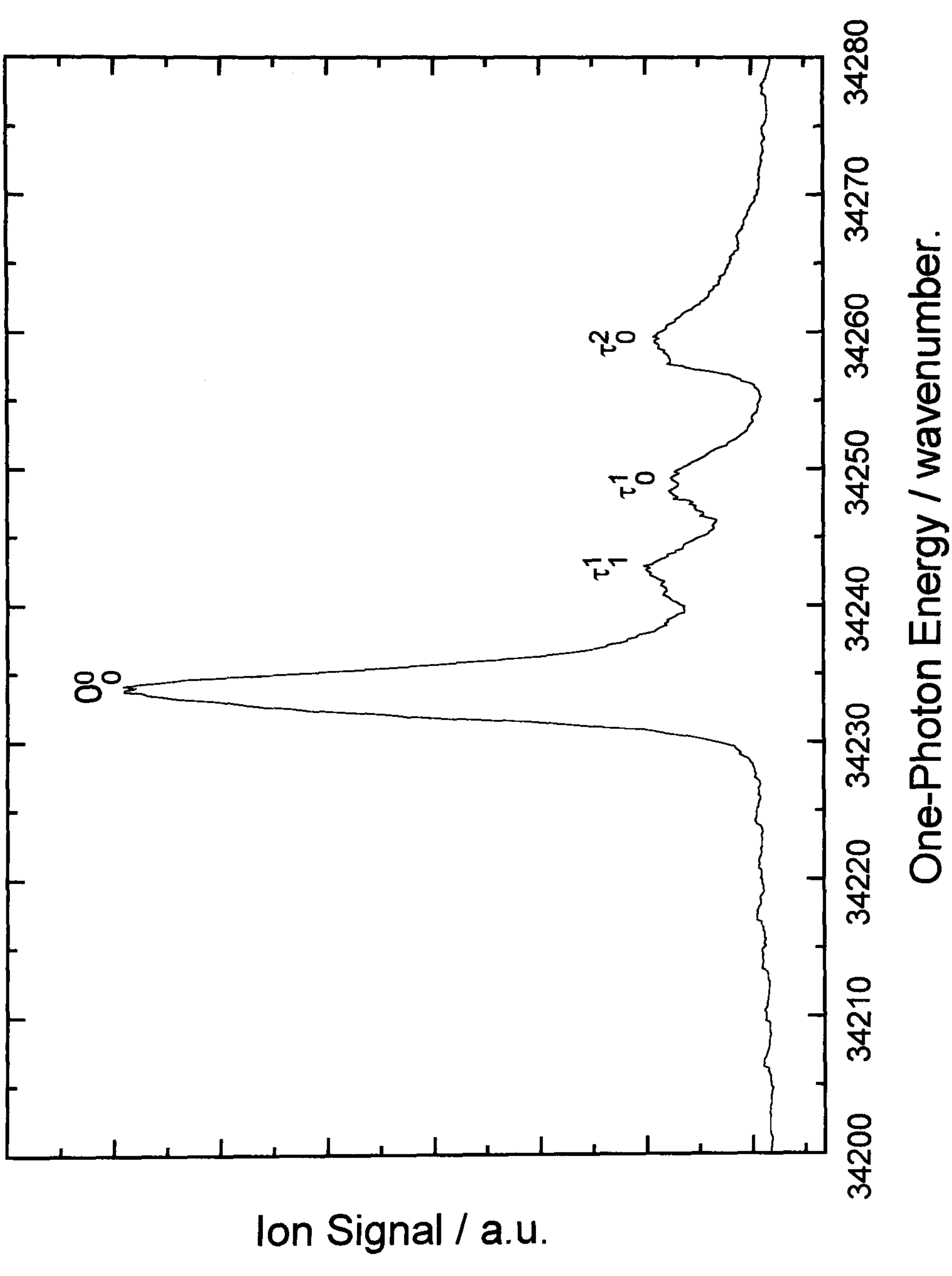

Figure 5.17: (1+1) MPI spectrum of the S_1 state of 4-ABTF.

5.5.2. Ionisation Threshold

The two-colour photoionisation efficiency spectrum of 4-ABTF via the origin band of the S_1 state is shown in figure 5.18. A reasonably sharp onset is observed at 65775 cm^{-1} giving an estimate of 65875 cm^{-1} for the ionisation energy. Some evidence of a limited step structure is observed. This indicates little or no change in the conformation of the rotor.

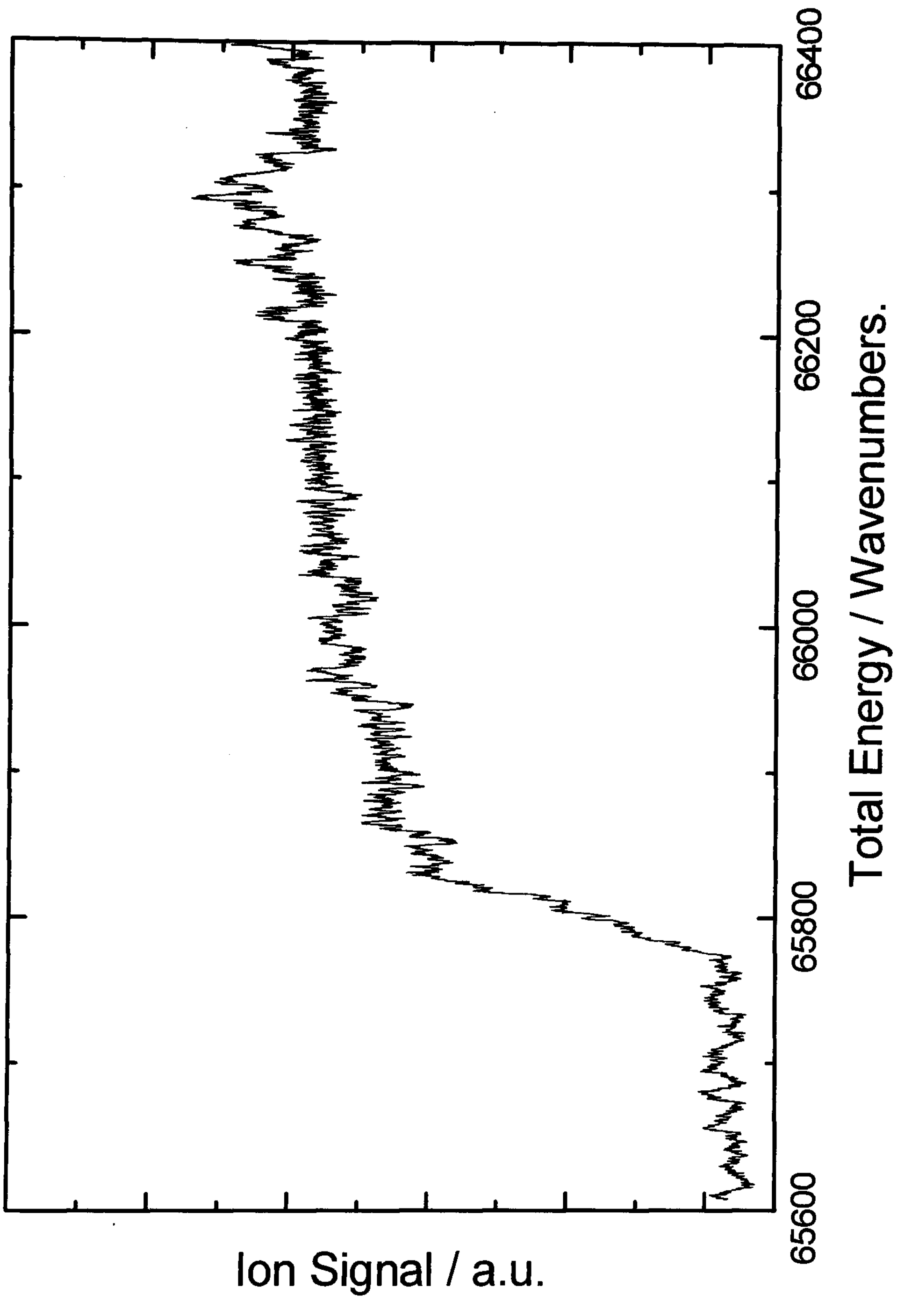

Figure 5.18: Two-colour photoionisation efficiency spectrum of 4-ABTF via the origin of the S_1 state. The spectrum has not been corrected for the field shift.

5.5.3. Two-Colour ZEKE-PFI

The short torsional progression of the S_1 state effectively limits the number of intermediate states for two-colour ZEKE-PFI experiments to one, namely the origin band. The ZEKE-PFI spectrum obtained by pumping this intermediate is shown in figure 5.19. The field corrected ionisation energy is 65886±3 cm^{-1} (see appendix 3). Three definite peaks and one possible peak are observed with the third exhibiting a considerably larger half-width. The torsional spacing is 7 cm^{-1} indicating a small barrier to internal rotation. Energies and assignments are given in table 5.8.

τ^+	E_{obs} (cm^{-1})
0	0
1	7
2	14 (broad)
3	30 (broad)

Table 5.8: Energies and assignments of the torsional levels of the ionic ground state of 4-ABTF.

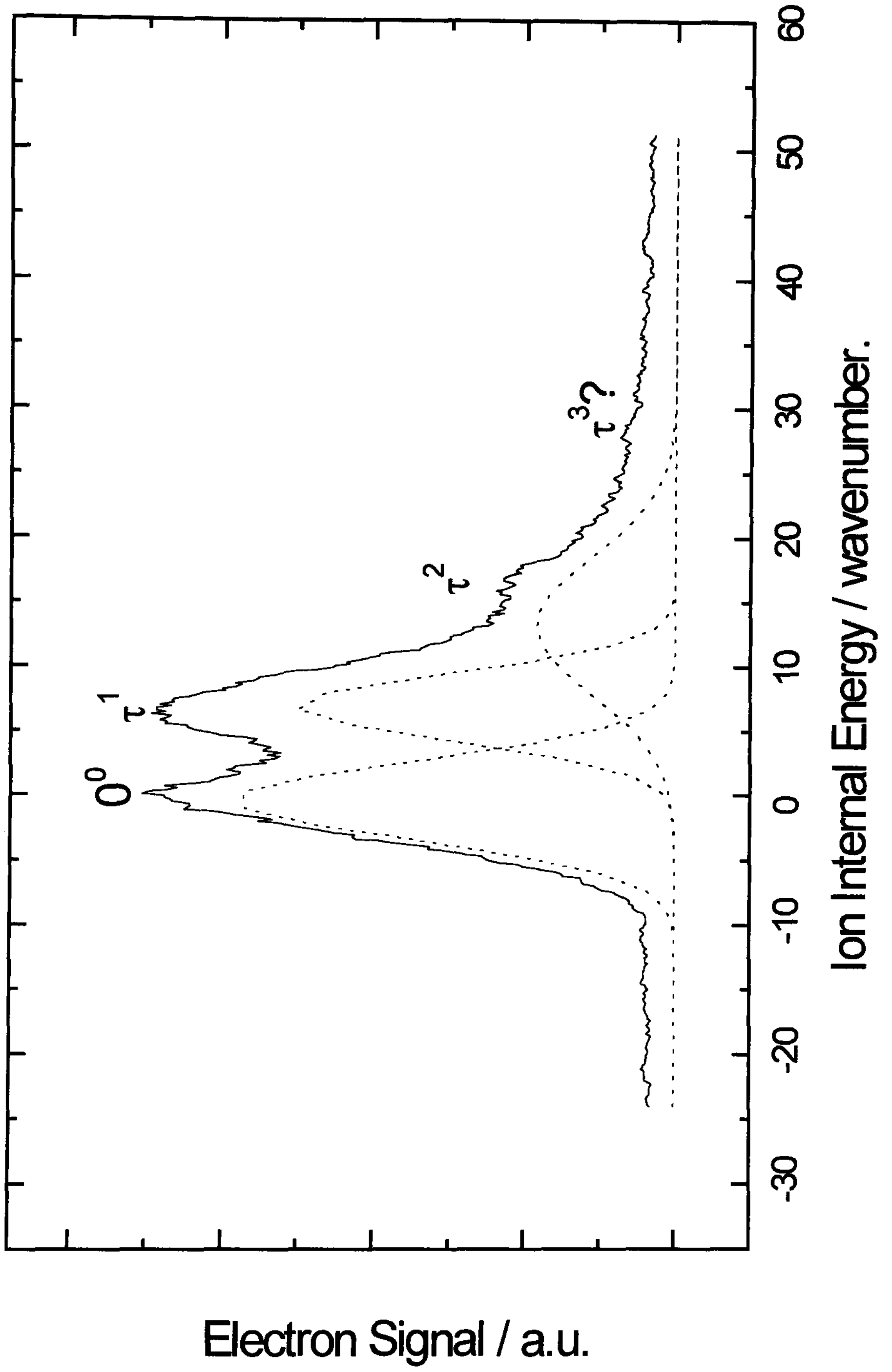

Figure 5.19: (1+1') ZEKE-PFI of 4-ABTF via the origin band of the S_1 state. Dotted lines represent a gaussian fit to the experimental data.

5.5.4. Calculation of Barrier Height

As 4-ABTF is classified under the G_{12} molecular symmetry group[24] and has a small barrier to internal rotation the calculation of torsional energy levels and Franck-Condon factors is a little more complex than for the other two isomers. For an infinite barrier the lowest torsional state ($\tau = 0$) is sixfold degenerate[11] ($\mathbf{0a}_1'$, $\mathbf{1e}''$, $\mathbf{2e}'$ and $\mathbf{3a}_2''$ (see figure 5.2.)). In the S_1 state Hollas calculated[24] that transitions to such states lie within 1.5 cm^{-1} of each other. With this in mind it is assumed that all the torsional states in $\tau = 0$ of the S_1 state are populated by the pump laser. The observed torsional structure of the ion can then be fitted with $V_6 = 12$ cm^{-1} and $F = 0.32$ cm^{-1}. Given the limited torsional structure these values are relatively inaccurate. In addition increasing V_6 and decreasing F can also give a good fit to the data. What is clear is that the barrier height is lower than that of the S_1 state. Table 5.9. shows calculated energy levels and Franck-Condon factors. It is noticeable that τ^1 has a calculated intensity much lower than observed experimentally. No change in the equilibrium conformation of the rotor was necessary. In line with previous work on para-substituted toluenes V_6 is assumed to be negative[2-4,24]. Hence the rotor is staggered with respect to the benzene ring by 30°. Figure 5.20. shows the barriers in all three electronic states.

Transition ($D_0 \leftarrow S_1$)	**Calculated Energy / cm^{-1}**	**Calculated Intensity**	**Experimental Energy / cm^{-1}**
$0a_1' \leftarrow 0a_1'$	0	0.95	0
$3a_1'' \leftarrow 0a_1'$	6.9	(a)	7
$6a_1' \leftarrow 0a_1'$	14.1	0.05	14
$1e'' \leftarrow 1e''$	0.1	0.93	0
$2e' \leftarrow 1e''$	0.7	(a)	-
$4e' \leftarrow 1e''$	7.4	(a)	7
$5e'' \leftarrow 1e''$	10.8	0.04	-
$7e'' \leftarrow 1e''$	16.4	0.03	14
$8e' \leftarrow 1e''$	23.4	(a)	-
$1e'' \leftarrow 2e'$	0.1	(a)	-
$2e' \leftarrow 2e'$	0.8	0.98	0
$4e' \leftarrow 2e'$	7.4	0.01	7
$5e'' \leftarrow 2e'$	10.8	(a)	-
$7e'' \leftarrow 2e'$	16.4	(a)	14
$8e' \leftarrow 2e'$	23.4	0.01	-
$0a_1' \leftarrow 3a_2''$	0	(a)	0
$3a_2'' \leftarrow 3a_2''$	1.0	0.99	0
$6a_2' \leftarrow 3a_2''$	12.7	(a)	14
$9a_2'' \leftarrow 3a_2''$	27.5	0.01	30?

Table 5.9. Calculated torsional energy levels and Franck-Condon factors for the ionic ground state of 4-ABTF. (a) indicates transitions allowed through coupling between the torsional motion and the other degrees of freedom of the molecule.

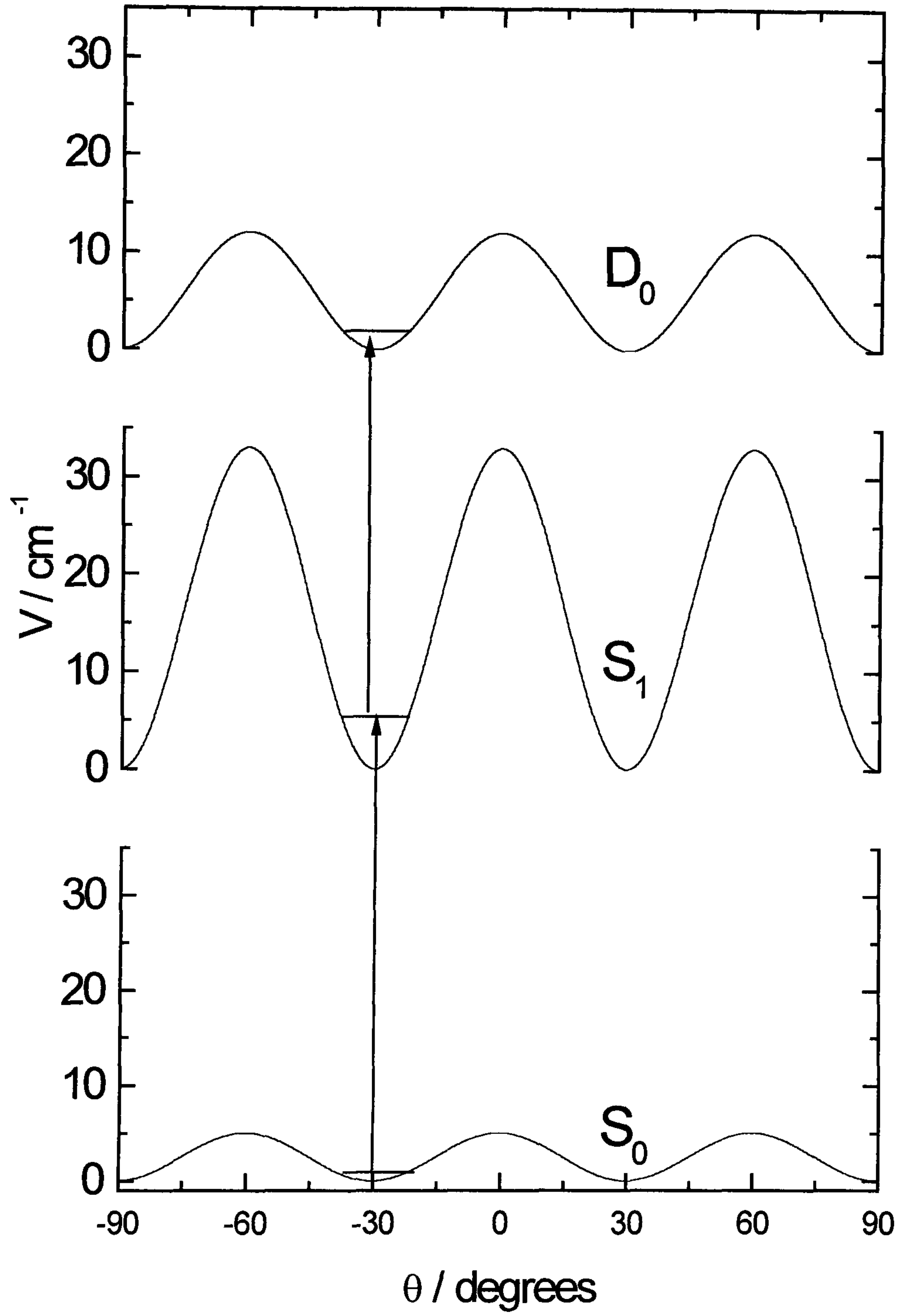

Figure 5.20: Barriers to internal rotation for all three electronic states of 4-ABTF. Barriers for the S_0 and S_1 states are from reference 24.

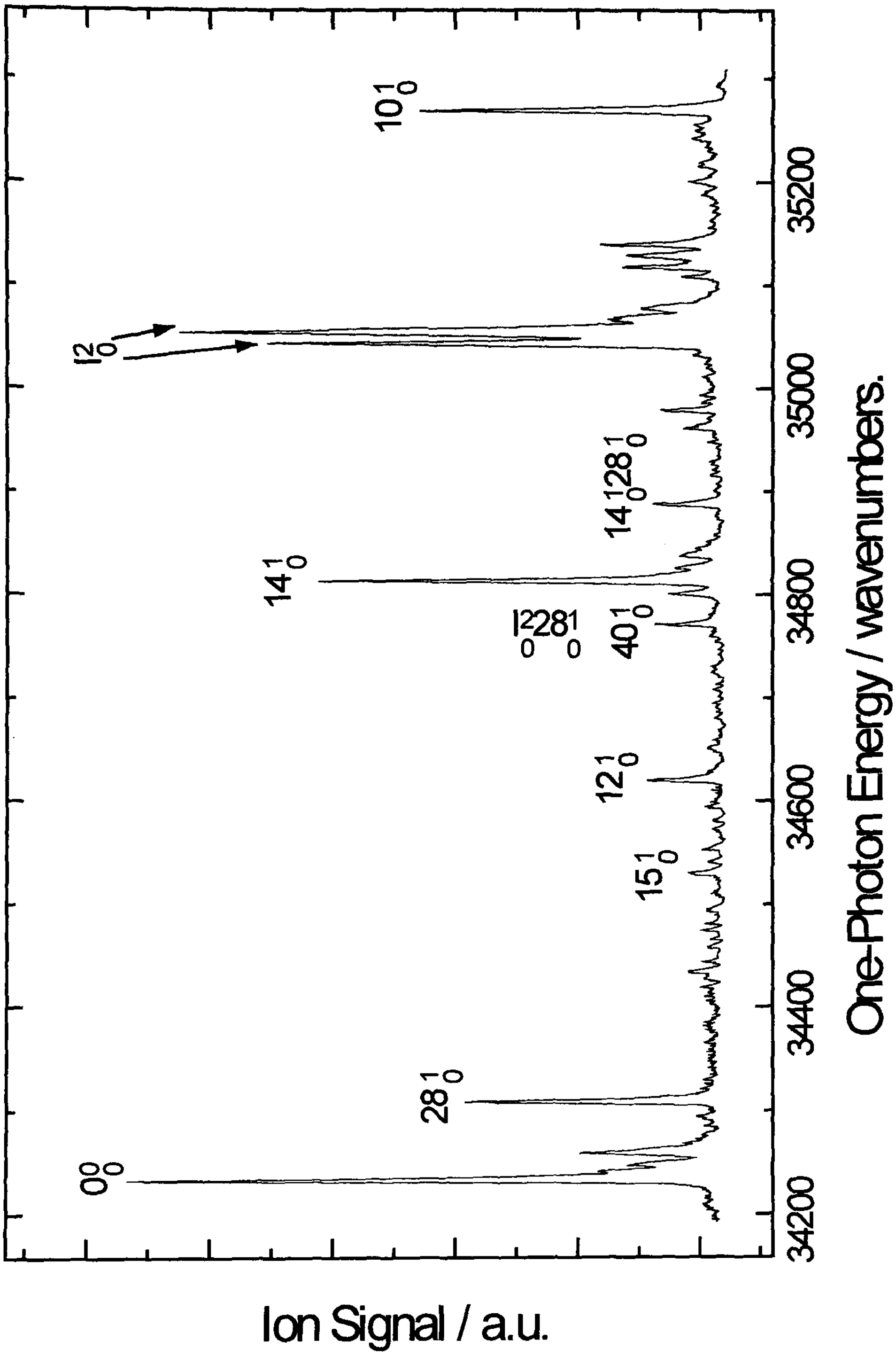

Figure 5.21: (1+1) MPI spectrum of the S_1 state of 4-ABTF. Assignments are from reference 27 and by comparison with ZEKE data.

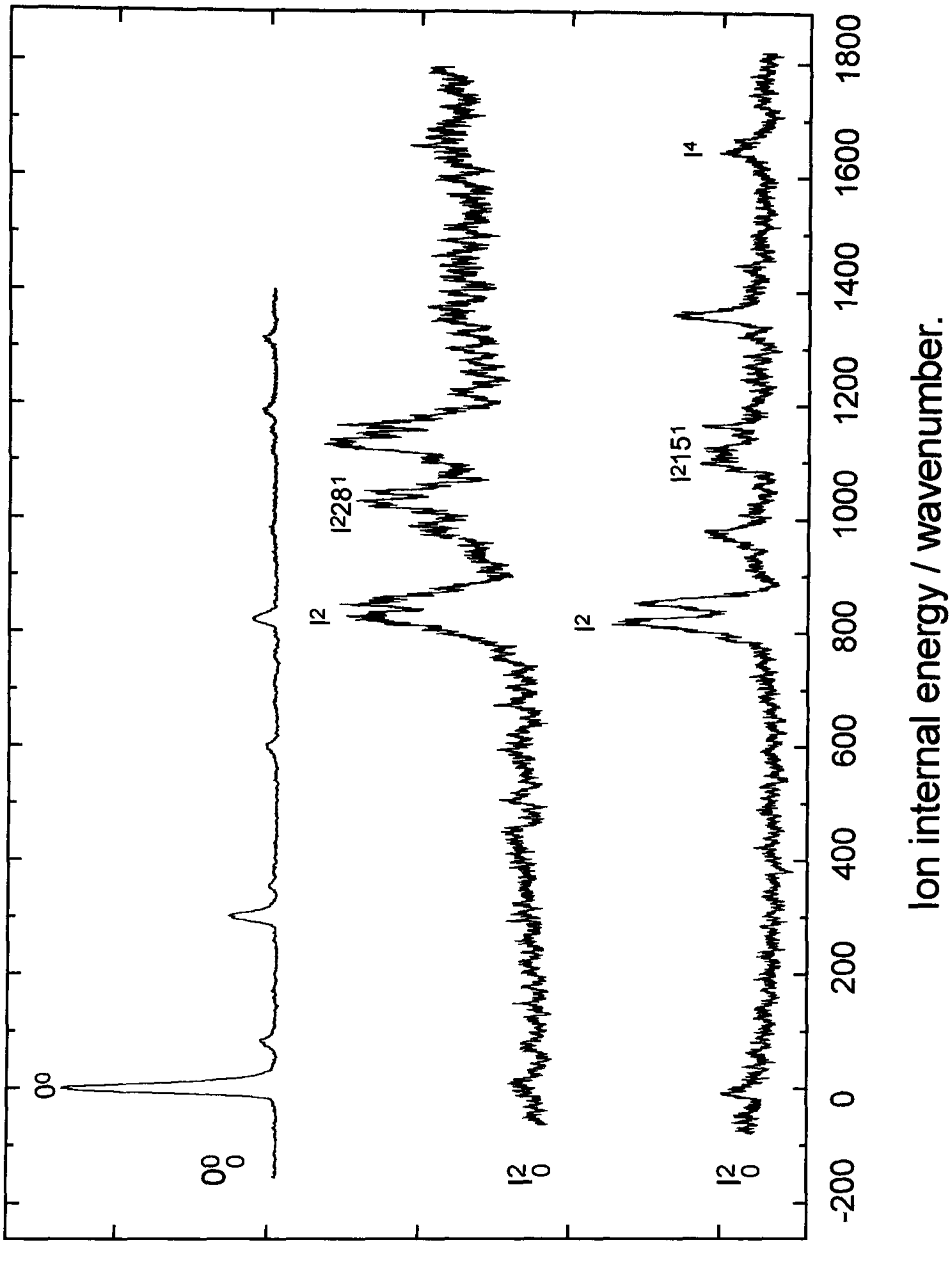

Figure 5.22: (1+1') ZEKE-PFI spectra of 4-ABTF via the origin band and two intermediates of the S_1 state.

5.6. Discussion

5.6.1. Introduction

Calculated barrier heights for each of the isomers in all three electronic states are given in table 5.10. along with the aminotoluenes as comparison. Similar trends are noted for both sets of molecules indicating the same basic causes of barriers to internal rotation (see chapter 2). This section will discuss the interesting features of each isomer in turn.

Molecule (state)	**V_3 (cm^{-1})**	**V_6 (cm^{-1})**	**F (cm^{-1})**	**reference**
2-ABTF.				
S_0	450	83	0.29	22
S_1	240	-67	0.29	22
D_0	720	-3	0.29	this work
2-AT.				
S_0	703	62	5.28	4
S_1	40	-11	5.40	4
D_0	649	19	5.20	4
3-ABTF.				
S_0	9	-10	0.29	23
S_1	155	-40	0.29	23
D_0	222	-4	0.29	this work
3-AT.				
S_0	9	-10	5.37	4
S_1	340	-22	4.77	4
D_0	248	-13	5.20	4
4-ABTF.				
S_0	-	5	0.38	24
S_1	-	33	0.38	24
D_0	-	12	0.32	this work
4-AT				
S_0	-	5.6	5.473	42
S_1	-	44	5.408	42
D_0	-	-	-	-

Table 5.10. Barrier heights of the aminobenzotrifluorides and the aminotoluenes.

5.6.2. 2-Aminobenzotrifluoride

From the results presented in section 5.3. it is clear that the experimental intensities of the ZEKE-PFI spectra of 2-ABTF cannot be accurately reproduced using the calculational procedure used[36]. Two obvious discrepancies were previously noted; firstly the appearance of Franck-Condon forbidden odd torsional levels. These appear as a consequence of interaction between the torsional vibration and other degrees of freedom of the molecule[1,28,29] as outlined in chapter 2. Similar (but far more obvious) results were observed for 3-ABTF and this effect will be discussed in section 5.6.3.

The second discrepancy, and one which is unique to 2-ABTF, concerns the interaction between the two substituent groups. Considerable activity in the torsional motions of both CF_3 and NH_2 in combination indicates substantial coupling between these groups. Hollas came to a similar conclusion[22] in his fluorescence study of the S_1 state although the effects appear to be more apparent in the ion than in the neutral molecule. The appearance of formally forbidden transitions is more common in ZEKE-PFI spectroscopy than in neutral state spectroscopic techniques such as resonance ionisation or fluorescence excitation[40,41]. No such effect has been observed in the corresponding aminotoluene[4].

As a further indication of this the barrier heights of 2-ABTF and 2-AT in table 5.10. can be compared. Although the trend is the same for both molecules with a large decrease in V_3 on excitation to the S_1 state the reduction is considerably greater in 2-AT (a factor of approximately 18)[4] than in 2-ABTF (a factor of 2)[22]. In addition the barrier in the ionic ground state is considerably greater in 2-ABTF than in 2-AT. This points to some extra source of stabilisation in the case of the CF_3 rotor. Interaction between the substituent groups can account for this. That such an effect is absent for the CH_3 case can be explained by taking note of the electronic properties of the three substituents. Both amino and methyl are net electron donors to the ring while trifluoromethyl acts as an electron withdrawing group. This can be seen in the ionisation energies of aniline[32] (62271 cm^{-1}), toluene[1] (71199 cm^{-1}) and benzotrifluoride[20,31] (78000 cm^{-1}) relative to benzene[21] (74556 cm^{-1}). The consequence of this is that only in the case of molecules containing the CF_3 group will there be resonance structures with significant weighting that have a partial negative charge on the fluorine atoms. Electrostatic attraction between fluorine and the acidic protons of the amino group will result in the formation of a hydrogen bond between the substituents. Such interaction will favour one conformation of the rotor over the other resulting in a higher barrier to internal rotation than would be observed in the absence of such an interaction. Internal rotation now corresponds to breaking the intramolecular hydrogen bond.

The presence of another low frequency vibration can have a substantial effect on the Franck-Condon factors. This has been studied by Moule[43] and co-workers in their study of thioacetaldhyde where considerable coupling between the torsional modes of the CH_3 and aldehylic groups was observed. A multidimensional potential needs to be considered to obtain agreement between calculated and observed intensities. The rigid rotor model becomes less appropriate as the energy of the intermediate approaches the first quantum of ν_{42}. Hence the effects are most apparent for the spectrum via τ^8 which is nearly degenerate with 42^1.

Previous experimental and theoretical studies of the toluenes[1-7,44] has revealed that 2-substituted toluenes have the same preferred conformation in all three electronic states, a trend which 2-ABTF agrees with. Calculations on the neutral and ionic ground states of the halotoluenes[44] indicate that the lowest energy structure is the psuedo-trans in which one C-H bond lies in the same plane as the benzene ring on the opposite side of the other substituent. This is shown in figure 5.23. along with the psuedo-cis conformer. It is not known which conformer 2-aminotoluene adopts or whether 2-ABTF displays similar behavior.

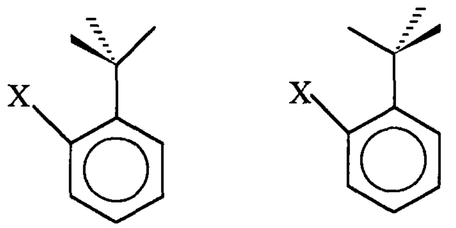

Pseudo trans. **Pseudo cis.**

Figure 5.23. Conformations of a 2-substituted toluene.

2-fluorotoluene adopts the pseudo-trans conformation in the S_0 state due mainly to steric repulsion between the substituents. Theoretical studies by Wiesshaar and co-workers[44] showed that these dominate over a weak hydrogen bond between fluorine and the protons of the methyl group. In 2-ABTF this may be reversed with a much stronger hydrogen bond present stabilising the pseudo-cis conformation. Calculations on a similar scale to those on the fluorotoluenes would be necessary to resolve this question.

5.6.3. 3-Aminobenzotrifluoride

The ZEKE-PFI spectra of both 2- and 3-ABTF show evidence for transitions involving the torsional structure of the CF_3 rotor which are formally forbidden to a first approximation. This effect is considerably more apparent in the case of 3-ABTF and hence is discussed here rather than in the previous section. The appearance of transitions in ZEKE-PFI spectra which are either symmetry or Franck-Condon forbidden is a common occurrence[40,41] and has been ascribed to the mechanism underpinning the pulsed-field-ionisation variant of ZEKE spectroscopy, namely the excitation and subsequent field ionisation of high principal quantum number Rydberg states converging on the ionic thresholds[45].

Coupling of the torsional vibration with such Rydberg states has been discussed previously[1] (see chapter 2) and has been used by several groups to explain the presence of weak forbidden transitions in ZEKE-PFI spectra[1-7]. Such a mechanism can also account for the weak odd torsional features in the ZEKE-PFI spectra of 2-ABTF. However, in the case of 3-ABTF the forbidden transitions appear to be of a similar intensity to the fully allowed ones. Thus it is possible that a further mechanism is required to fully account for the observed spectra, namely autoionisation.

In a PFI experiment this mechanism is more accurately termed field-induced or forced autoionisation[45] since it involves interaction of a low-*n* Rydberg state converging on a higher core of the ion with the high-*n* Rydberg or ZEKE states converging on a lower core state. This is shown in figure 5.24.

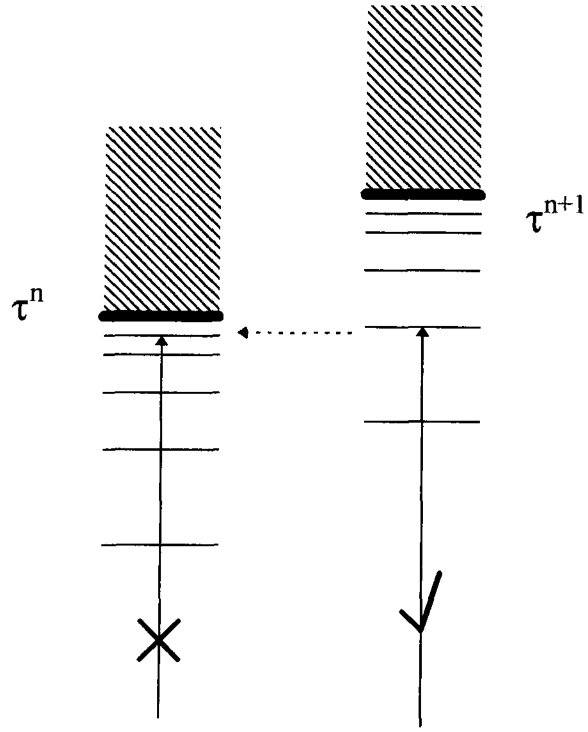

Figure 5.24. Schematic of field-induced autoionisation. The tick and cross indicate allowed and forbidden transitions to the Rydberg states converging on the various ionisation thresholds. The dotted arrow shows the process of autoionisation resulting in the appearance of symmetry forbidden transitions (see text).

In the case of 3-ABTF the situation is an excellent example in that the lower torsional state of the ion (τ^n) contains a forbidden transition (i.e. $\mathbf{a_1} \leftrightarrow \mathbf{a_2}$ denoted by the cross in figure 5.24) while the transition to the upper state is fully allowed ($\mathbf{a_1} \leftrightarrow \mathbf{a_1}$ or $\mathbf{a_2} \leftrightarrow \mathbf{a_2}$ and $\mathbf{e} \leftrightarrow \mathbf{e}$ denoted by the tick in figure 5.24). Thus a low-*n* Rydberg state converging on the upper state will have a much greater transition probability than the transition to isoenergetic Rydberg states converging on the lower core. The low-*n* Rydberg state can act as a window state allowing the population of the ZEKE states which have little or no direct transition intensity. For such a mechanism to occur two conditions must be satisfied. Firstly the Rydberg states must lie close to each other in energy. In 3-ABTF this is the case since the initial torsional spacing of the ion is only 22 cm^{-1} and hence the possibility of a coincidence is very high since the ZEKE states lie within 5-10 cm^{-1} of the ionisation threshold[3,40]. Comparing the density of torsional states for the ionic ground states of 3-ABTF and 3-aminotoluene this can be clearly seen. In 3-AT states up to the **7e** level lie within the first 300 cm^{-1} of the ionisation energy amounting to 10 torsional levels in total[4]. 3-ABTF, on the other hand, shows detail up to τ^{12} which comprises the **18a₁** and **19e** torsional levels. This amounts to 26 torsional states in the 200 cm^{-1} above the adiabatic ionisation energy, a considerably higher density of torsional states than its methyl counterpart. This is due to the much more massive CF_3 rotor with its dramatically smaller F value.

The second prerequisite is that there is substantial coupling between the two Rydberg series involved. This involves a change in the torsional state of the ionic core and hence must involve the interaction of the Rydberg electron with the core. In the case of a molecule containing a CX_3 rotor such interaction may be greater when X is the more electronegative fluorine than with hydrogen. The greater charge separation in 3-ABTF relative to 3-AT results in a more polarised ionic core and hence a larger effect on the Rydberg electron[46]. Hence both the mass and electronic nature of the CF_3 group contribute to the appearance of forbidden transitions in 3-ABTF.

5.6.4. 4-Aminobenzotrifluoride

4-ABTF displays only a limited amount of torsional structure with the barriers to internal rotation in line with those found for other para-substituted toluenes[2-4]. For the same reasons outlined in the previous section the first torsional peak of the ion is far more intense experimentally than can be accounted for by consideration of allowed transitions from the origin of the S_1 state. In addition the first hot band of the S_1 state lies very close in energy to that of the origin (see figure 5.17.) and may also be pumped in the ZEKE experiment. Since the transition from such a state to the first torsional level of the ion is allowed and diagonal this may also be the cause of the unusual intensity distribution.

The splitting of the amine inversion has been previously observed for 4-aminotoluene[47] and was ascribed to interaction between the two substituent groups. Since the amine group is essentially planer in the S_1 and D_0 states, amine inversion can be visualised as a "flapping" motion of the two protons. For a para substituted aniline this is shown in figure 5.25.

Figure 5.25. The amine inversion in a para substituted aniline.

The threefold nature of the CF_3 rotor means that the NH_2 group is in a different environment at the extremes of its motion. Yan and Spangler observed a quartet splitting of I_0^2 and attributed this to the twofold nature of the NH_2 group and the fact that the methyl torsion has transitions from both **a** type and **e** type symmetry levels. Hence there are four closely spaced transitions observed in the S_1 state of 4-

aminotoluene. In 4-ABTF only a doublet structure is observed in both the S_1 and D_0 states. This is caused by the much greater mass of CF_3 relative to methyl which has the effect of making the energy spacing between the **a** and **e** states much less. Hence a doublet structure is observed with each peak containing an unresolved doublet.

The two substituent groups are far enough apart in space that any steric effects or through space interactions are negligible. Interaction must be mediated by the π-system of the benzene ring. The splitting is greater for the ionic ground state since complete removal of an electron results in a more dynamic pattern of electron density over the ring. Hence the two groups are more efficiently coupled in this state.

5.7. Conclusion

Two-colour (1+1') ZEKE-PFI spectra of the ground ionic state of the aminobenzotrifluorides have been obtained using the S_1 state as a resonant intermediate. Both the torsion of the CF_3 group and the amine inversion have been studied. Barriers to internal rotation of the CF_3 group in the ion were calculated using a one-dimensional rigid rotor model. These were found to display similar trends to those of the toluenes, in particular the aminotoluenes, although some interesting differences were found.

Substantial interaction between the two substituent groups can be seen for 2-ABTF indicating a intramolecular hydrogen bond. This results in a higher barrier to internal rotation in the S_1 and ionic ground state compared to that of 2-aminotoluene. This effect can be ascribed to the electronic nature of the trifluoromethyl group which acts as an electron withdrawer. Since the methyl group is an electron donating group no such effect would be expected for 2-aminotoluene.

The amine inversion of 4-ABTF was found to be split in both the S_1 and ionic ground states. This can be explained by the interaction between the two substituent groups which is mediated by the π-system of the benzene ring.

For all three isomers there is substantial coupling between the high-*n* Rydberg states and the torsional vibration of the molecule. This is manifested as the appearance of forbidden transitions in the ZEKE-PFI spectra and is particularly noticeable for 3-ABTF. This is ascribed to the electronic nature of the CF_3 group and to the effects of decreasing the internal rotation constant (F) by replacing the protons of the rotor with fluorine. This greatly increases the probability of a coincidence between the high-*n* Rydberg states and low-*n* Rydberg states converging on a higher torsional state of the ionic core.

5.8. References

1. K.T. Lu, G.C. Eiden & J,C. Weisshaar. *J.Phys.Chem.* 1992, **96**, 9742.
2. K. Takazawa, M. Fujii & M. Ito. *J.Chem.Phys.* 1993, **99**, 3205.
3. High Resolution Laser Photoionization and Photoelectron Studies. Edited by I. Powis, T. Baer & C.Y. Ng. J. Wiley & Sons (London). 1995.
4. H. Ikoma, K. Takazawa, Y. Emura, S. Ikeda, H. Abe, H. Hayashi & M. Fujii. *J.Chem.Phys.* 1996, **105**, 10201.
5. K. Okuyama, M.C.R. Cockett & K. Kimura. *J.Chem.Phys.* 1992, **97**, 1649.
6. R.A. Walker, E.C. Richard, K.T. Lu & J.C. Weisshaar. *J.Phys.Chem.* 1995, **99**, 12422.
7. R.A. Walker, E.C. Richard & J.C. Weisshaar. *J.Phys.Chem.* 1996, **100**, 7333.
8. T. Vondrak, S.I. Sato, V. Spirko & K. Kimura. *J.Phys.Chem.A.* 1997, **101**, 8631.
9. Internal Rotation in Molecules. Edited by W.J. Orville-Thomas. J. Wiley & Sons, London. 1974.
10. H. Demene & I.P. Sugar. *J.Phys.Chem.A.* 1999, **103**, 4664.
11. L.H. Spangler. *Annu.Rev.Phys.Chem.* 1997, **48**, 481.

12. Jet Spectroscopy and Molecular Dynamics. Edited by J.M. Hollas and D. Phillips. Blackie, London. 1995.
13. D.A. Long. *J.Mol.Struct.* 1985, **126**, 9.
14. R.T. Wiedmann, L. Goodman & M.G. White. *Chem.Phys.Lett.* 1998, **293**, 391.
15. W.M. Tolles, E.T. Handelman & W.D. Gwinn. *J.Chem.Phys.* 1965, **43**, 3019.
16. A.P. Cox, C.A. Rego & R. Stevens. *J.Mol.Struct.* 1990, **223**, 185.
17. T. Ogata & A.P. Cox. *J.Mol.Spectrosc.* 1976, **61**, 265.
18. W.A. Kreiner, H.D. Rudolph & B.T. Tan. *J.Mol.Spectrosc.* 1973, **48**, 86.
19. W.T. Cave & H.W. Thompson. *Disc.Faraday Soc.* 1950, **9**, 35.
20. V.J. Hammond, W.C. Price, J.P. Teegan & A.D. Walsh. *Disc.Faraday Soc.* 1950, **9**, 53.
21. R.G. Neuhauser, K. Siglow & H.J. Neusser. *J.Chem.Phys.* 1997, **106**, 896.
22. R.D. Gordon, J.M. Hollas, P.J.A. Ribeiro-Claro & J.J.C. Teixeira-Dias. *Chem.Phys.Lett.* 1993, **211**, 392.
23. R.D. Gordon, J.M. Hollas, P.J.A. Ribeiro-Claro & J.J.C. Teixeira-Dias. *Chem.Phys.Lett.* 1991, **183**, 377.
24. R.D. Gordon, J.M. Hollas, P.J.A. Ribeiro-Claro & J.J.C. Teixeira-Dias. *Chem.Phys.Lett.* 1991, **182**, 649.
25. P.J.A. Ribeiro-Claro, J.J.C. Teixeira-Dias, R.D. Gordon & J.M. Hollas. *J.Mol.Spectrosc.* 1993, **162**, 426.
26. P.J.A. Ribeiro-Claro, J.J.C. Teixeira-Dias, R.D. Gordon & J.M. Hollas. *J.Mol.Spectrosc.* 1991, **150**, 46.
27. P.J.A. Ribeiro-Claro, J.J.C. Teixeira-Dias, R.D. Gordon & J.M. Hollas. *J.Mol.Spectrosc.* 1991, **149**, 34.
28. R.A. Walker, E. Richard, K.T. Lu, E.L.Sibert III & J.C. Weisshaar. *J.Chem.Phys.* 1995,**102**, 8718.
29. A.Q. Zhao, C.S. Parmenter, D.B. Moss, A.J. Bradley, A.E.W. Knight & K.G. Owens. *J.Chem.Phys.* 1992, **96**, 6362.
30. J.M. Hollas, M.R. Howson, T. Ridley & L. Halonen. *Chem.Phys.Lett.* 1983, **98**, 611.

31. Molecular Photoelectron Spectroscopy. D.W. Turner, C. Baker, A.D. Baker & C.R. Brundle. J. Wiley & Sons, London. 1970.
32. X. Song, M. Yang, E.R. Davidson & J.P. Reilly. *J.Chem.Phys.* 1993, **99**, 3205.
33. Principles of Ultraviolet Photoelectron Spectroscopy. J.W. Rabalais. John Wiley & Sons (London). 1977.
34. W.A. Chupka. *J.Chem.Phys.* 1993, **98**, 4520.
35. H. Mizuno, K. Okuyama, T. Ebata & M. Ito. *J.Phys.Chem.* 1987, **91**, 5589.
36. K.P. Lawley. *J.Mol.Spectrosc.* 1997, **183**, 25.
37. N.C. Shand, C.L. Ning, M.R.F. Siggel, I.C. Walker & J. Pfab. *J.Chem.Soc.Faraday Trans.* 1997, **93**, 2883.
38. J.D. Lewis, T.B. Malloy, T.H. Chao & J. Laane. *J.Mol.Struct.* 1972, **12**, 427.
39. L.H. Spangler & D.W. Pratt. *J.Chem.Phys.* 1986, **84**, 4789.
40. K. Muller-Dethlefs & E.W. Schlag. *Angew.Chem.Int.Ed.* 1998, **37**, 1346.
41. M.C.R. Cockett. *J.Phys.Chem.* 1995, **99**, 16228.
42. X.Q. Tan & D.W. Pratt. *J.Chem.Phys.* 1994, **100**, 7061.
43. D.C. Moule, H.A. Bascal, Y.G. Smeyers, D.J. Clouthier, S. Karolczak & A. Nino. *J.Chem.Phys.* 1992, **97**, 3964.
44. K.T. Lu, F. Weinhold & J.C. Weisshaar. *J.Chem.Phys.* 1995, **102**, 6787.
45. M.C.R. Cockett, R.J. Donovan & K.P. Lawley. *J.Chem.Phys.* 1996, **105**, 3347.
46. A. Held, L.Y. Baranov, H.L. Selzle & E.W. Schlag. *Chem.Phys.Lett.* 1997, **267**, 318.
47. S. Yan & L.H. Spangler. *J.Chem.Phys.* 1992, **96**, 4106.

Chapter 6

ZEKE-PFI of 4-Fluorobiphenyl

6.1. Introduction

Biaryl type molecules, of which biphenyl is the classic example, exhibit large changes in the relative conformation of the two rings dependant on the electronic state of the molecule. A large body of work exists on the neutral states of such molecules with biphenyl (and its derivatives) among the most widely studied[1-15].

The neutral ground state of biphenyl (S_0) has a conformation where the two rings are twisted at an angle of approximately 45° in the gas phase[16] while the S_1 state has a planar conformation[3-5]. These are shown in figure 6.1.

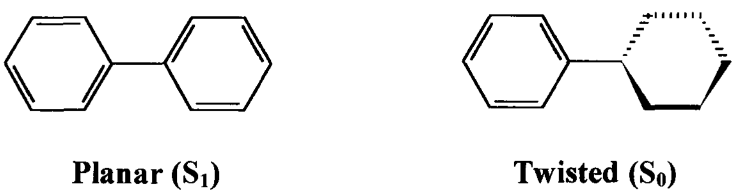

Planar (S_1) Twisted (S_0)

Figure 6.1. Conformation of biphenyl in the S_0 and S_1 states.

In addition the condensed phase conformations are different[6,7]. In the solid phase the molecule is found to be planar[6] while solution studies[7] reveal a twisted geometry of approximately 20°. It is clear that the conformation of the molecule depends greatly on the local chemical environment.

At present very little work has been performed on the ionic ground state (D_0) of biphenyl or its derivatives to gauge the effects of completely removing an electron from the molecule rather than simply rearranging the electron configuration[17-19]. This chapter presents two-colour ZEKE-PFI spectra of 4-fluorobiphenyl via the S_1 state. Experimental conditions are similar to those for the aminobenzotrifluorides with the addition of a heated nozzle to allow a high enough vapour pressure of the sample to be generated[20,21]. The 4-fluorobiphenyl sample (melting point 72-74 °C) was heated to approximately 70 °C.

6.2. Previous Work on the Biphenyls

6.2.1. Neutral States

Biphenyl is one of the simplest molecules which contains more than one benzene ring and has attracted considerable interest in terms of its spectroscopy[1-8]. In addition polymers of substituted biphenyls are of interest for their liquid crystal properties[22,23]. The molecular orbital diagram of the frontier π-orbitals of biphenyl is shown in figure 6.2. The HOMO is antibonding with respect to the inter-ring bond while the LUMO is bonding[24].

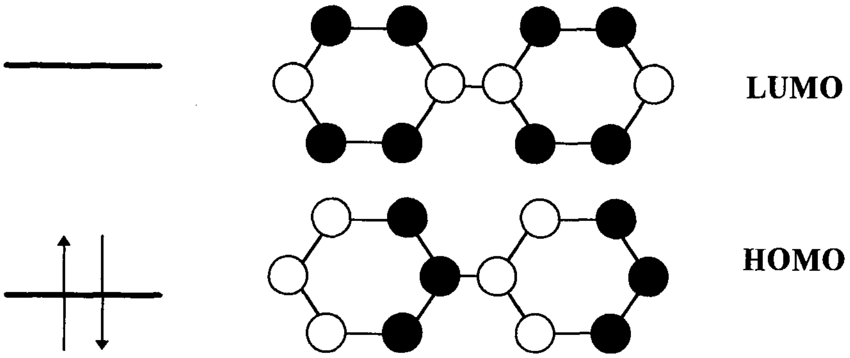

Figure 6.2. Schematic of the frontier orbitals of biphenyl.

Early studies on biphenyl were carried out using absorption techniques at room temperature[1,2]. These showed a broad feature in the UV assignable to the S_1 state. In the 1980's several groups studied biphenyl and its derivatives using jet-cooling coupled with fluorescence or ionisation techniques[3-5] to determine the torsional spacing of the S_1 and S_0 states. In addition there has been considerable interest in biaryl molecules where a benzene ring is joined to a heterocyclic ring such as pyridine[8-15].

Such studies show a common trend in barriers to internal rotation with the S_0 state twisted away from planarity while the S_1 state is planar. This large change in the conformation of the molecule has lead to some problems in the assignment of the torsional structure of the S_1 state with the exact location of the electronic origin being a particular problem. Two groups have reported multiphoton ionisation spectra of the S_1 state of biphenyl with differing conclusions[3,4]. Im and Bernstein[3] assigned the lowest observed transition as the electronic origin and calculated that the S_0 state was twisted at an angle of 44°. Takei and co-workers[4] also assigned the same transition as the origin but used an angle of 38° for the S_0 state based on ab-initio calculations.

Other ab-initio studies[25,26] of the S_0 state have found angles which vary from 37-44° depending on the basis set and method of calculation utilised. However, electron diffraction data[16] agrees with the work of Im and Bernstein that the angle is approximately 45°. Since this is a more direct measurement of the molecular geometry it should be considered more reliable than those from Franck-Condon simulations.

6.2.2. Ionic States

In contrast to the neutral molecules the cations of biphenyl and its derivatives have had relatively little study. Conventional He(I) PES[17] reveals broad unresolved bands indicating a significant change in molecular conformation between the neutral and ionic ground states. Maier and Turner obtained PES spectra[17] for a wide variety of substituted biphenyls (including halogens, amino etc.) and were able to determine a correlation between two of the ionisation energies (Π_1 and Π_4) and the angle of twist in the S_0 state. For para (or 4) substituted biphenyls this angle was found to be between 40 and 50° in agreement with electron diffraction studies of the neutral molecules[16,27,28]. The ortho (or 2) analogues, however, showed a considerably greater angle (~70-80°) which was dependant on the steric bulk of the substituent.

Recent ab-initio studies of the biphenyl radical cation[26] have found that the rings are twisted at an angle of approximately 20° and that the inter-ring bond is shortened significantly indicating that the barrier to internal rotation in the ion is affected by electronic factors. The ZEKE-PFI spectrum of biphenyl has been briefly mentioned by Cockett and Kimura[19] although the torsional structure was not resolved.

The torsional structure of a biaryl type molecule in the ionic ground state has only been resolved in one case; namely 9,10-dihydrophenathrene[18] (figure 6.3.). The ethyl linker prevents the rings from adopting a conformation with a large twist angle and results in a limited torsional progression in the $S_1 \leftarrow S_0$ transition. The ZEKE-PFI spectra obtained via this structure allow the observation of the torsional structure of the ionic ground state. The angle of twist was found to decrease from S_0 to S_1 (i.e. the molecule is trying to be more planar in the S_1 state) but increases again on ionisation. The angle in the ion was smaller than that of the neutral ground state. The calculated potentials were all harmonic over the range of energies sampled. This is in agreement with experimental and theoretical work on biphenyl itself[3,26]. It was also noticeable that the ionisation energy from the ZEKE experiment was substantially higher than that from conventional PES. This discrepancy can be attributed to the drawbacks of conventional PES outlined in chapter 2.

However 9,10-dihydrophenanthrene is not a typical representative of substituted biphenyls for the very reason that makes it experimentally accessible, the limited rotation of the rings. For that reason the molecule studied in this chapter is 4-fluorobiphenyl for which the rings may rotate freely.

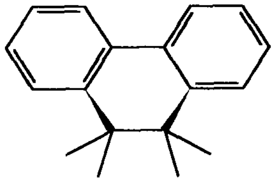

Figure 6.3. Structure of 9,10-dihydrophenanthrene.

6.3. (1+1) MPI of the S_1 State

6.3.1. Experimental Results

The (1+1) MPI spectrum of the S_1 state of 4-fluoribiphenyl (4-FB) is shown in figure 6.4. and shows a long progression in the torsional vibration. The spectrum has been normalised to the laser intensity. The maximum intensity is observed around τ_0^{18} or τ_0^{19} following previous assignments[3,4] with the exact position difficult to distinguish due to the broad nature of the Franck-Condon envelope. A second progression in the torsional mode can also be seen to the blue of the first sequence (~10 cm^{-1}). Several assignments of such structure are feasible and include a progression originating from a hot band of the S_0 state, a combination band of the torsional vibration and another low frequency mode or the torsional progression of another electronic state (S_2). Of these the first can be discounted by the fact that the intensity of the unidentified progression relative to the main torsional progression is unaffected by the temperature of the molecular beam. Figure 6.5. shows the S_1 region of 4-FB under two different backing pressures of helium. The remaining two possibilities cannot be distinguished by one-colour methods alone but two-colour methods such as ZEKE-PFI can be used for this purpose and are discussed in section 6.4.

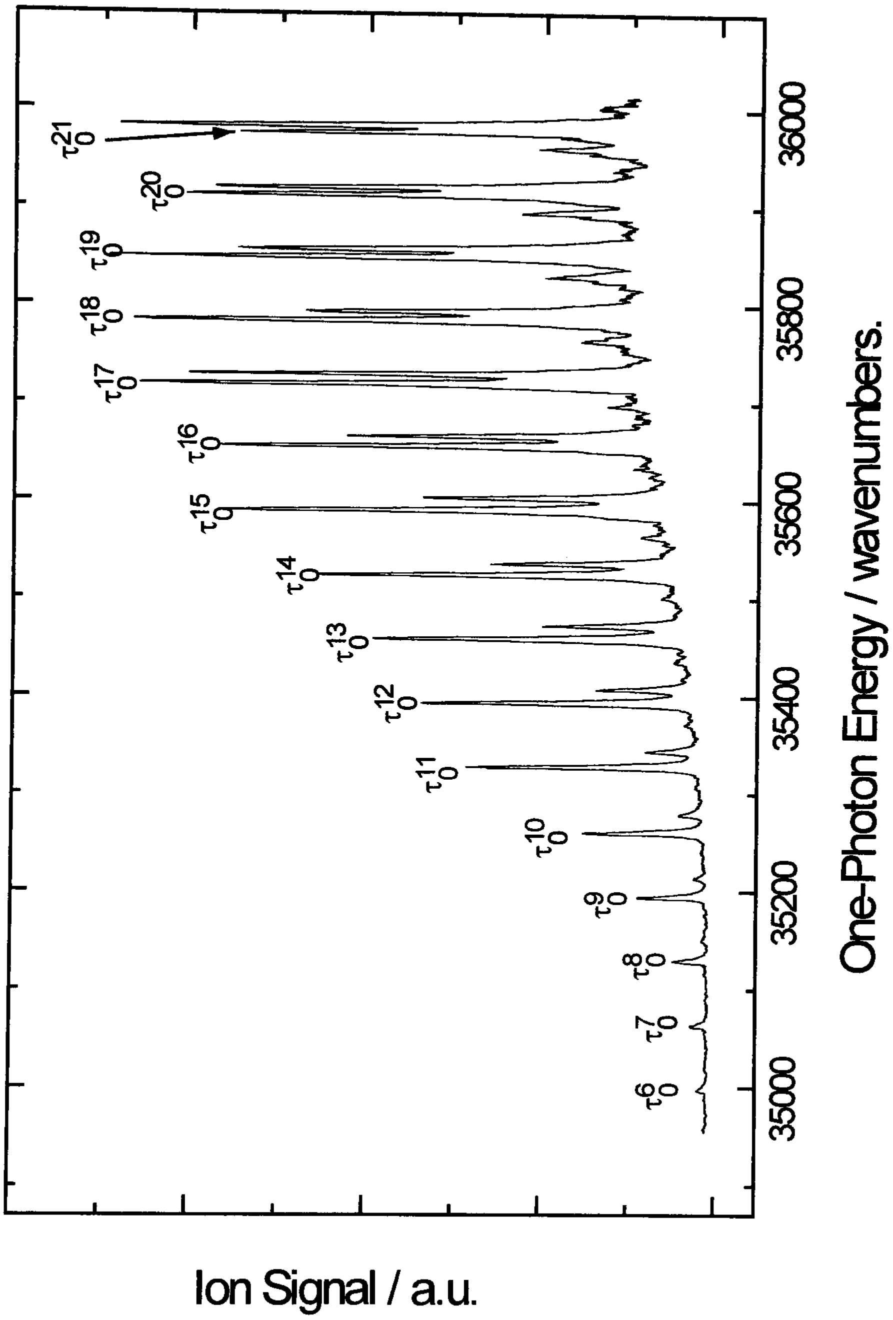

Figure 6.4: The (1+1) MPI spectrum of the S_1 state of 4-fluorobiphenyl. The spectrum has been normalised to the laser power. Assignments are those of Im and Bernstein[3].

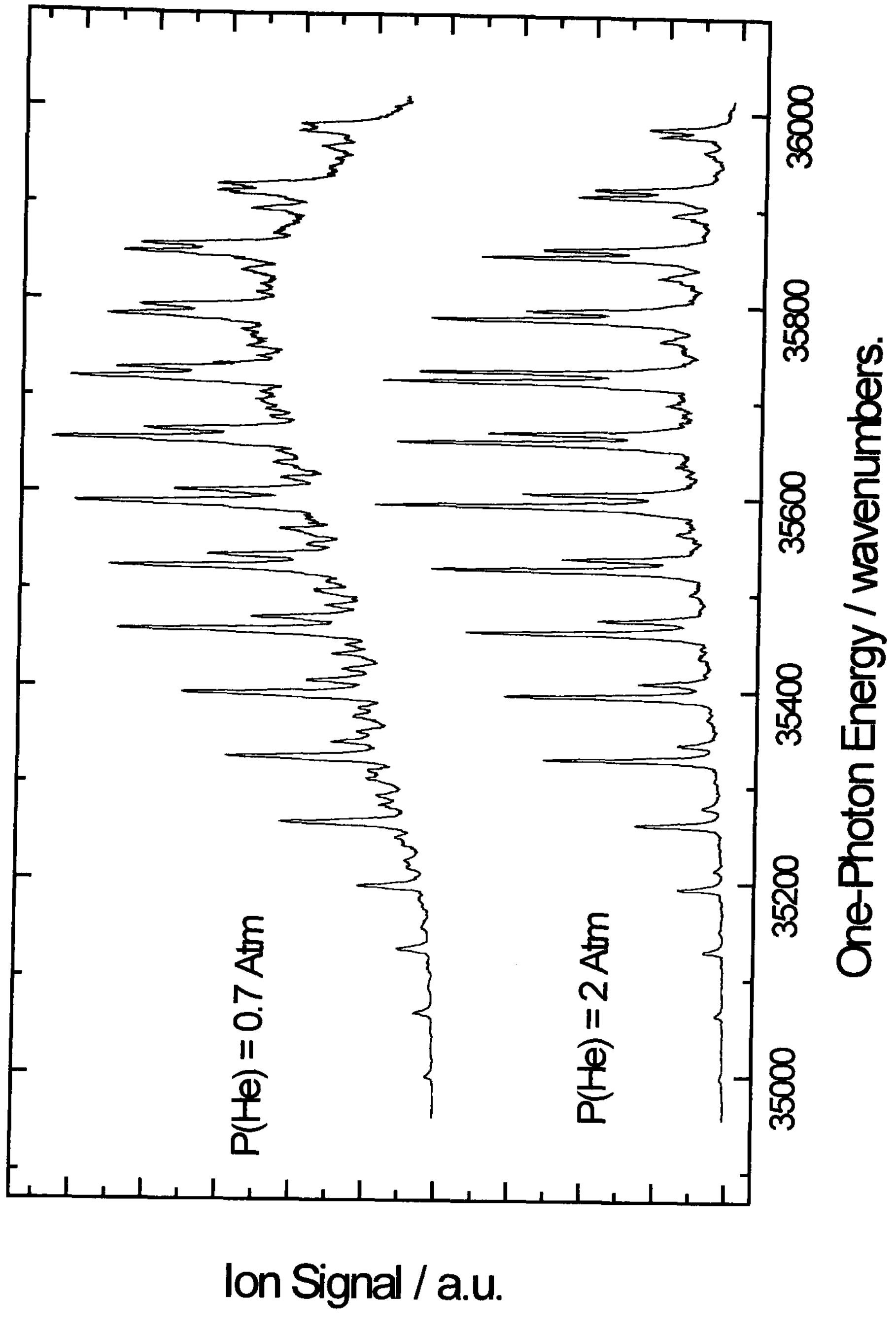

Figure 6.5: The (1+1) MPI spectrum of 4-FB under different beam conditions. The spectra have not been normalised to the laser intensity.

6.3.2. Calculation of the Barrier Height

In their paper Im and Bernstein[3] calculated the S_1 torsional potential of biphenyl with the constants $V_2 = 1195\ \mathrm{cm}^{-1}$, $V_4 = -190\ \mathrm{cm}^{-1}$, $V_6 = 18\ \mathrm{cm}^{-1}$ and $F = 0.387\ \mathrm{cm}^{-1}$ and a change in the relative phases of the two states of 44°. This calculates an apparent torsional spacing of 60-65 cm^{-1}. In 4-FB a similar spacing is observed so a calculation using the same potential would seem to be appropriate. The calculation was carried out using the method of Lawley[29] and is shown in table 6.1. along with the observed values. Good agreement is found for the lower torsional states (up to approximately $\tau = 14$) but as the calculated barrier energy (~1200 cm^{-1}) is approached the calculated spacing between adjacent torsional levels begin to decrease. This is not observed experimentally indicating that the actual barrier is far higher than that calculated by Im and Bernstein. In fact a completely different approach is required

τ	$E_{calc.}$ (cm^{-1})	E_{obs} (cm^{-1})	τ	$E_{calc.}$ (cm^{-1})	E_{obs} (cm^{-1})
0	0	0	**11**	713.8	713
1	61.5	65	**12**	778.9	778
2	124.2	128	**13**	843.1	844
3	187.8	189	**14**	906.1	910
4	252.3	253	**15**	967.6	975
5	317.5	320	**16**	1027.1	1042
6	383.2	383	**17**	1084.0	1104
7	449.3	449	**18**	1136.9	1170
8	515.6	515	**19**	1181.3	1234
9	581.9	579	**20**	1216.9	1297
10	648.1	645	**21**	1263.1	1362

Table 6.1. Calculated and observed torsional energies for the S_1 state of 4-fluorobiphenyl using the calculated potential of Im and Bernstein (V_2 = 1195 cm^{-1}, V_4 = -190 cm^{-1}, V_6 = 18 cm^{-1} and F = 0.387 cm^{-1})^3. Experimental values are relative to the origin band (34614 cm^{-1}).

For a two-fold rotor such as found in 4-FB the angle between the two rings is θ and is shown in figure 6.6. θ is defined as the difference between the angles of the two rings (θ_1 and θ_2 respectively).

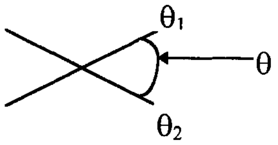

Figure 6.6. Definition of ring angles for a biphenyl type molecule.

The angles of the rings (θ_1 and θ_2) can each range from 0 to 360° so θ itself varies from -360° to +360°. Im and Bernstein[3] use a different value for the relative angle of the rings (denoted γ) which is equal to half the value of θ. Since the energy level are calculated with respect to the second derivative ($\partial^2/\partial\theta^2$) of the potential it is necessary to scale the internal rotation constant by a factor of 4 to obtain a true value of the barrier. This was not done by Im and Bernstein hence their calculated barriers are incorrect. In addition work on 2-phenylindole by Hollas[8] and co-workers found a similar torsional spacing for the S_1 state but calculated a barrier to internal rotation of between 3000 and 5000 cm^{-1}.

Given that the active space of the system is from -360° to +360° this also has an affect on the symmetries of the torsional levels. For a system where V_4 is the largest term the potential has eight minima and hence each torsional state far below the barrier is eightfold degenerate. These consist of two **e** type states (doubly degenerate) and four non-degenerate states, $\mathbf{a_1}$, $\mathbf{a_2}$, $\mathbf{b_1}$ and $\mathbf{b_2}$. Such a situation is found for the neutral ground state of biphenyls. For the situation where V_2 is much greater than V_4 the potential has minima every 180° and hence has four minima in the active range. Thus the torsional energy levels are fourfold degenerate with an **e** type symmetry level and two others ($\mathbf{a_1}/\mathbf{b_1}$ for τ even or $\mathbf{a_2}/\mathbf{b_2}$ for τ odd). This is the case for the S_1 state of biphenyl. The energy spacing of the lines is found to be regular and decreases as the barrier is approached. The final case is when V_2 is the largest term in the potential but V_4 is of a significant magnitude and negative. The result is a potential which has a small double minimum (or at least a very flat bottom to the potential well) but is essentially the same symmetry as the second case. The energy spacing increases to a limiting value as the torsional state is increased. Figure 6.7. shows the relative energy levels for all three cases.

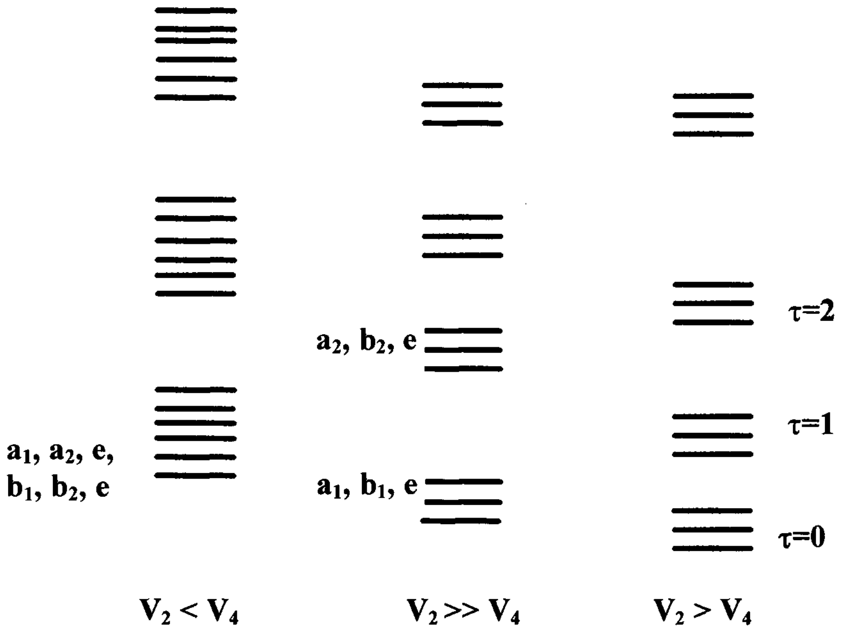

Figure 6.7. Energy spacings for a C_{2v} rotor with various potentials.

Using the information in figure 6.7. it is possible to discuss the $S_1 \leftarrow S_0$ spectrum of 4-FB. The selection rules allow transitions between states of the same symmetry (i.e. $a_1 \leftrightarrow a_1$) and allows transitions from the ground torsional level of the S_0 state to both the odd and even torsional levels of the S_1 state. This is shown in figure 6.8. Hence the calculation of Im and Bernstein[3], which essentially only calculates states of a_1 symmetry, is incorrect and the barrier to internal rotation in the S_1 state of 4-FB (and other biphenyls) is considerably greater.

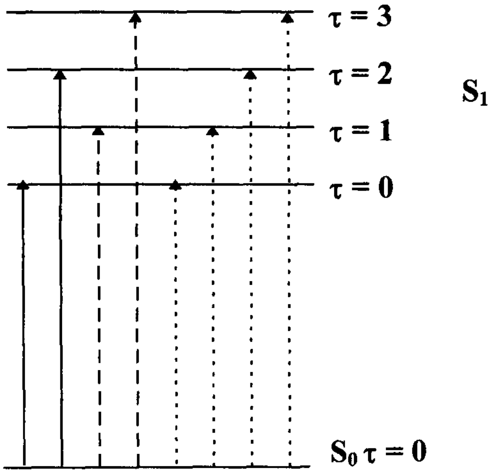

Figure 6.8. Allowed transitions in the $S_1 \leftarrow S_0$ transition of biphenyls. Solid lines indicate transitions from states of a_1 and b_1 symmetry, dashed line are a_2/b_2 symmetry and dotted lines are e type.

The conclusion is that since the calculational procedure separately calculates the different symmetry states the torsional spacing for a_1 states that must be considered is twice that considered by Im and Bernstein[3]. For 4-FB this amounts to approximately 130 cm^{-1} rather than 65 cm^{-1}. This results in a far higher barrier than that found previously. A similar procedure has been found for 4-cyanobiphenyl[30]. Recent work by Simons and co-workers[14] have shown a similar situation using depletion measurements. These show that the odd torsional levels of the S_1 state originate from different levels of the S_0 state than the even transitions.

Assuming such a situation the observed torsional energies of the S_1 state of 4-FB can be fitted with the constants V_2 = 3890 cm^{-1}, V_4 = -255 cm^{-1}, V_6 = -35 cm^{-1} and F = 0.387 cm^{-1}. Calculated and observed values are shown in table 6.2. Clearly the calculated barrier height is far higher than the range sampled by the experiment and should be regarded with some scepticism.

τ	$E_{calc.}$ (cm^{-1})	E_{obs} (cm^{-1})	τ	$E_{calc.}$ (cm^{-1})	E_{obs} (cm^{-1})
0	0	0	**11**	710.8	713
1	63.3	65	**12**	776.3	778
2	126.9	128	**13**	841.8	844
3	191.0	189	**14**	907.6	910
4	255.3	253	**15**	972.8	975
5	319.9	320	**16**	1038.2	1042
6	384.6	383	**17**	1103.6	1104
7	449.6	449	**18**	1169.0	1170
8	514.8	515	**19**	1234.2	1234
9	580.0	579	**20**	1299.3	1297
10	645.4	645	**21**	1364.3	1362

Table 6.2. Calculated and observed torsional energy levels for the S_1 state of 4-FB using the values given in the text.

Using the potential for the S_0 state found by electron diffraction (V_2 = 30 cm^{-1}, V_4 = 900 cm^{-1} and F = 0.387 cm^{-1}) the Franck-Condon factors for the $S_1 \leftarrow S_0$ transition can be calculated. The calculated MPI spectrum is shown in figure 6.9. for several rotor angles. For an angle of 45° a wide envelope is found with a maximum intensity around τ = 25 or 26. This is not in agreement with that found experimentally where the maximum intensity is found at τ = 18 or 19. Using a smaller phase shift it is possible to obtain a calculated spectrum which has a maximum around the experimental value. Best agreement is found for an angle of approximately 39°. This is in agreement with the work of Takei and co-workers on biphenyl[4]. However such a situation is in disagreement with the electron diffraction study which is more direct measurement of the molecular geometry of the S_0 state[27]. The conclusion must be that the lowest observed transition is not the electronic origin of the S_1 state. A similar argument can also be applied to other similar molecules[8-15]. The only reason it was assigned in this way is that there is no indication of any other transitions to lower energy. From the Franck-Condon calculation it appears as if the transition assigned as the origin of the S_1 state is in fact better assigned as a higher member of the torsional progression given that the maximum intensity is calculated to lie between τ_0^{24} and τ_0^{27}. Assignments can be made by the two-colour ZEKE-PFI spectra shown in the next section.

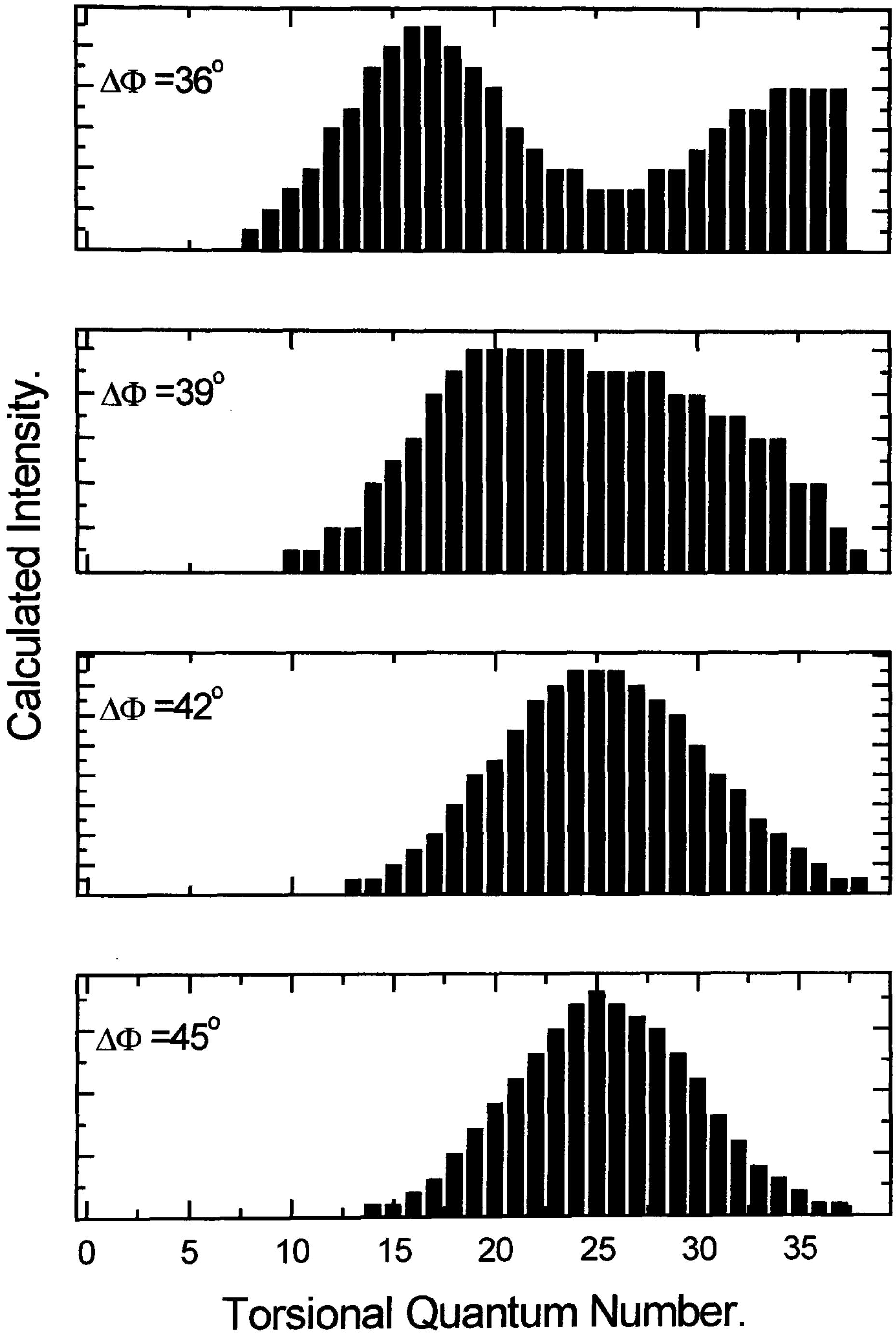

Figure 6.9: Calculated MPI spectrum of the S_1 state of 4-FB using several phase angles for the S_0 state.

6.4. (1+1`) ZEKE-PFI

6.4.1. Experimental Results

The two-colour (1+1`) ZEKE-PFI spectra of 4-FB via eighteen torsional levels of the S_1 state are shown in figures 6.10., 6.11. and 6.12. The lowest usable intermediate was τ_0^4 as assigned by Bernstein and Im[3]. Each intermediate displays a similar spectrum that shifts in energy as the intermediate is changed. The lowest observed level of the ion is assigned as the origin of the ion. The ionisation energy for this transition is 66202 cm^{-1}. No field correction was possible due to the weakness of the transition. From previous studies the field free ionisation energy can be predicted to be 66207 cm^{-1}. The error in this value is considerable due to the weakness of the observed signal. Table 6.3. lists the energies of the observed torsional levels. The zero energy is given as τ^4 (total energy of 66324 cm^{-1}) since this was the lowest level observed with a large intensity.

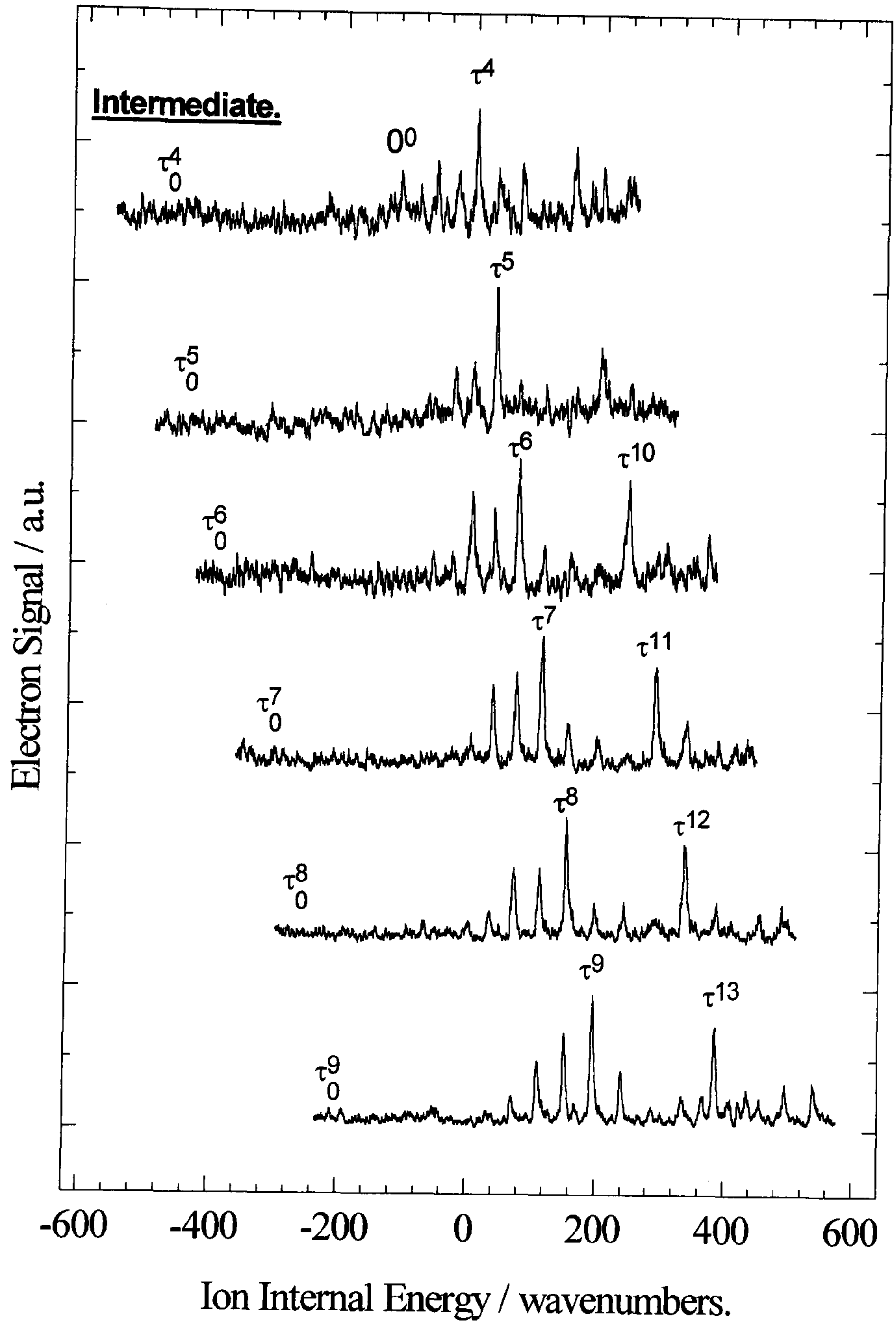

Figure 6.10: (1+1') ZEKE-PFI spectra of 4-FB via several torsional levels of the S_1 state. Intermediate assignments are from previous work. The spectra are displayed relative to τ^4 of the ion (total energy of 66324 cm^{-1}).

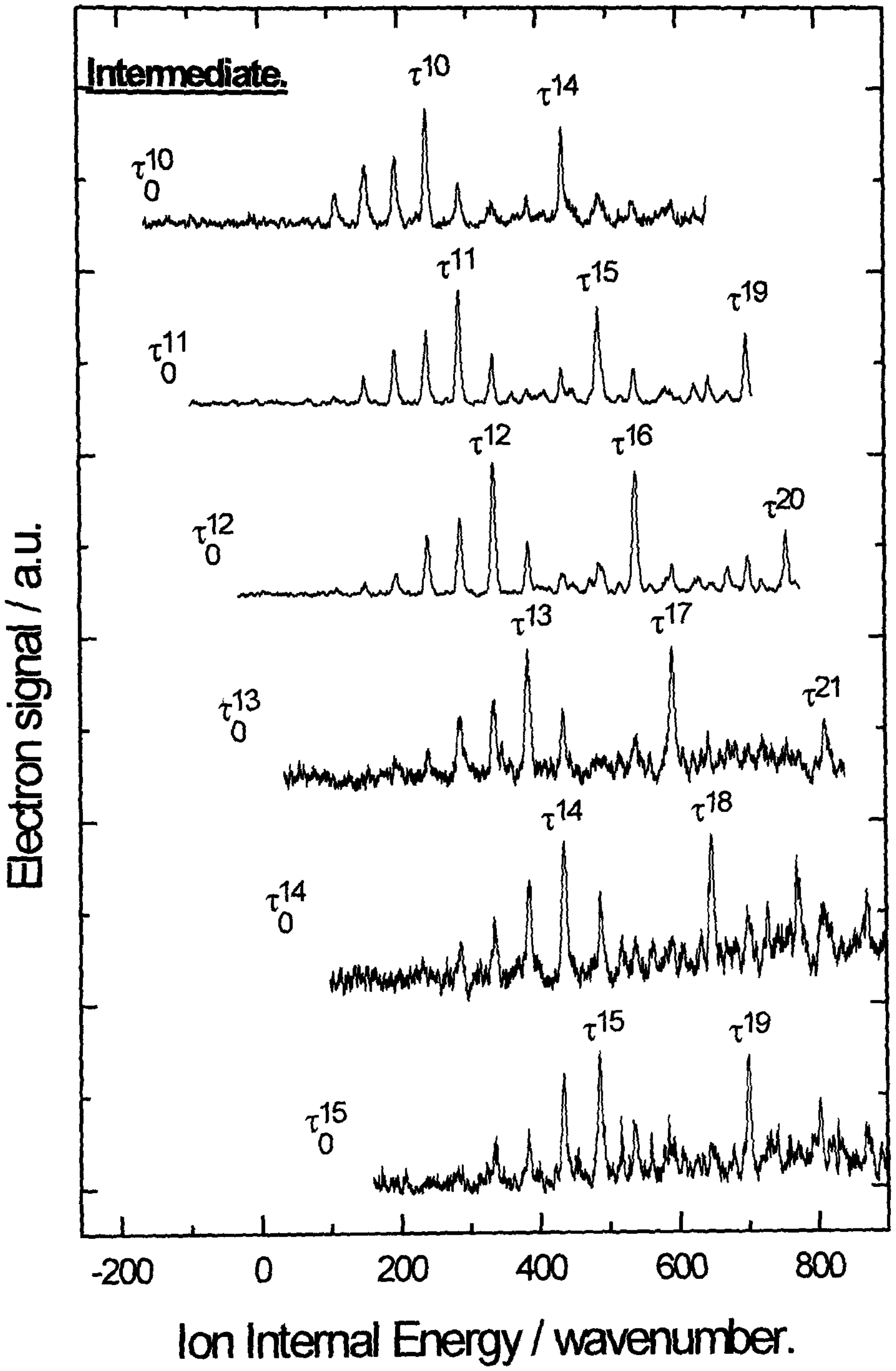

Figure 6.11: (1+1') ZEKE-PFI spectra of 4-FB via several torsional levels of the S_1 state. Intermediate assignments are from previous work. The spectra are displayed relative to τ^4 of the ion (total energy of 66324 cm^{-1}).

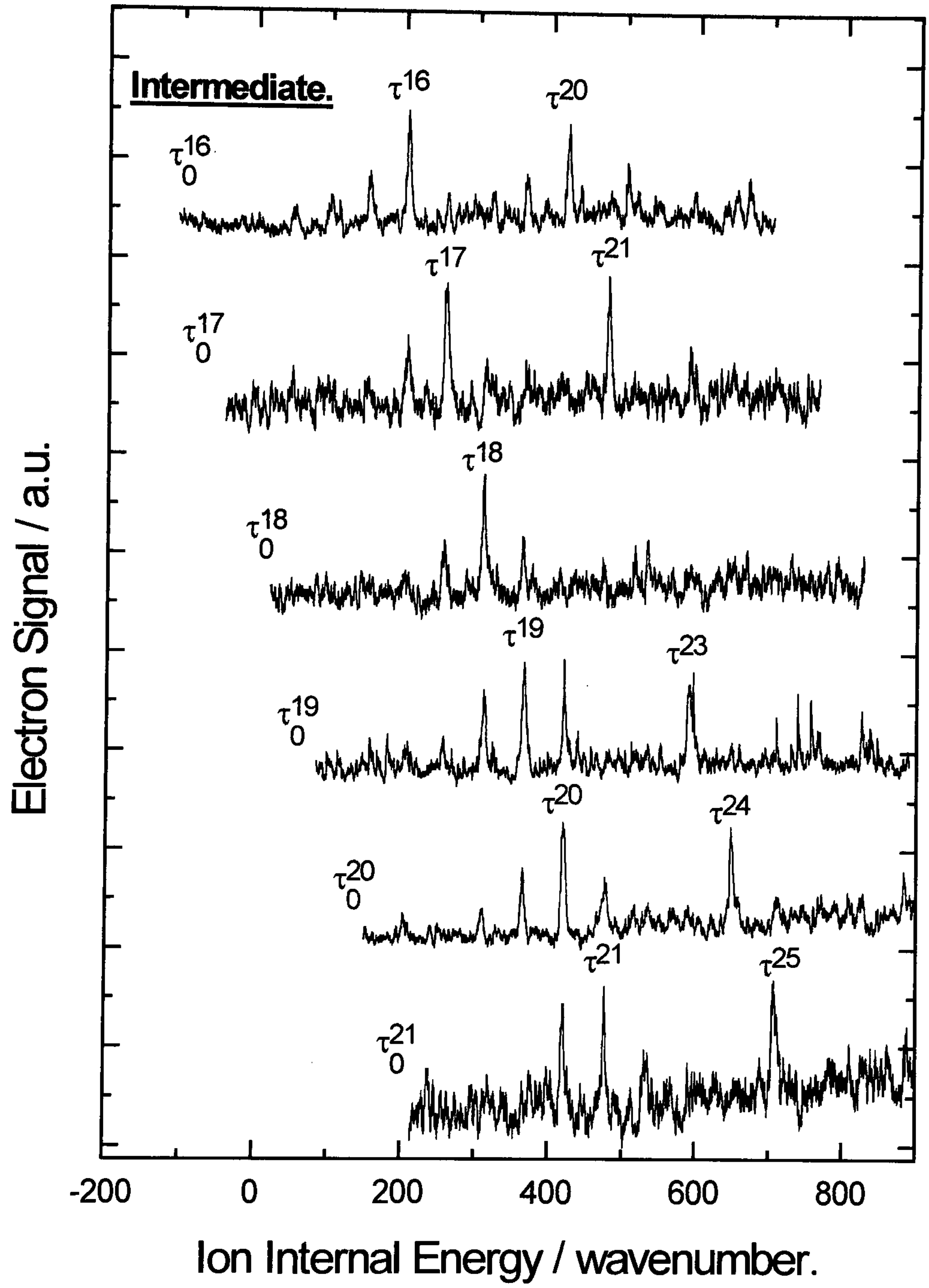

Figure 6.12: (1+1') ZEKE-PFI spectra of 4-FB via several torsional levels of the S_1 state. Intermediate assignments are from previous work. The spectra are displayed relative to τ^4 of the ion (total energy of 66324 cm^{-1}).

τ^+	Energy (cm^{-1})	τ^+	Energy (cm^{-1})
0	-117	**14**	435
1	-91	**15**	487
2	-61	**16**	538
3	-29	**17**	590
4	0	**18**	646
5	34	**19**	700
6	71	**20**	756
7	111	**21**	812
8	152	**22**	869
9	196	**23**	925
10	241	**24**	983
11	287	**25**	1042
12	335	**26**	-
13	385	**27**	-

Table 6.3. Energies of the torsional levels of the ionic ground state of 4-fluorobiphenyl. The zero level is given as τ^4 (66324 cm^{-1}).

In addition it was possible to record ZEKE spectra via some of the transitions of the S_1 state which lie to the blue of the main torsional progression. Two such spectra are shown in figure 6.13. and allow these intermediates to be assigned as a progression of the torsional mode based on a vibrational mode of the molecule. From figure 6.13. this vibration has a vibrational frequency of between 200 and 300 cm^{-1}.

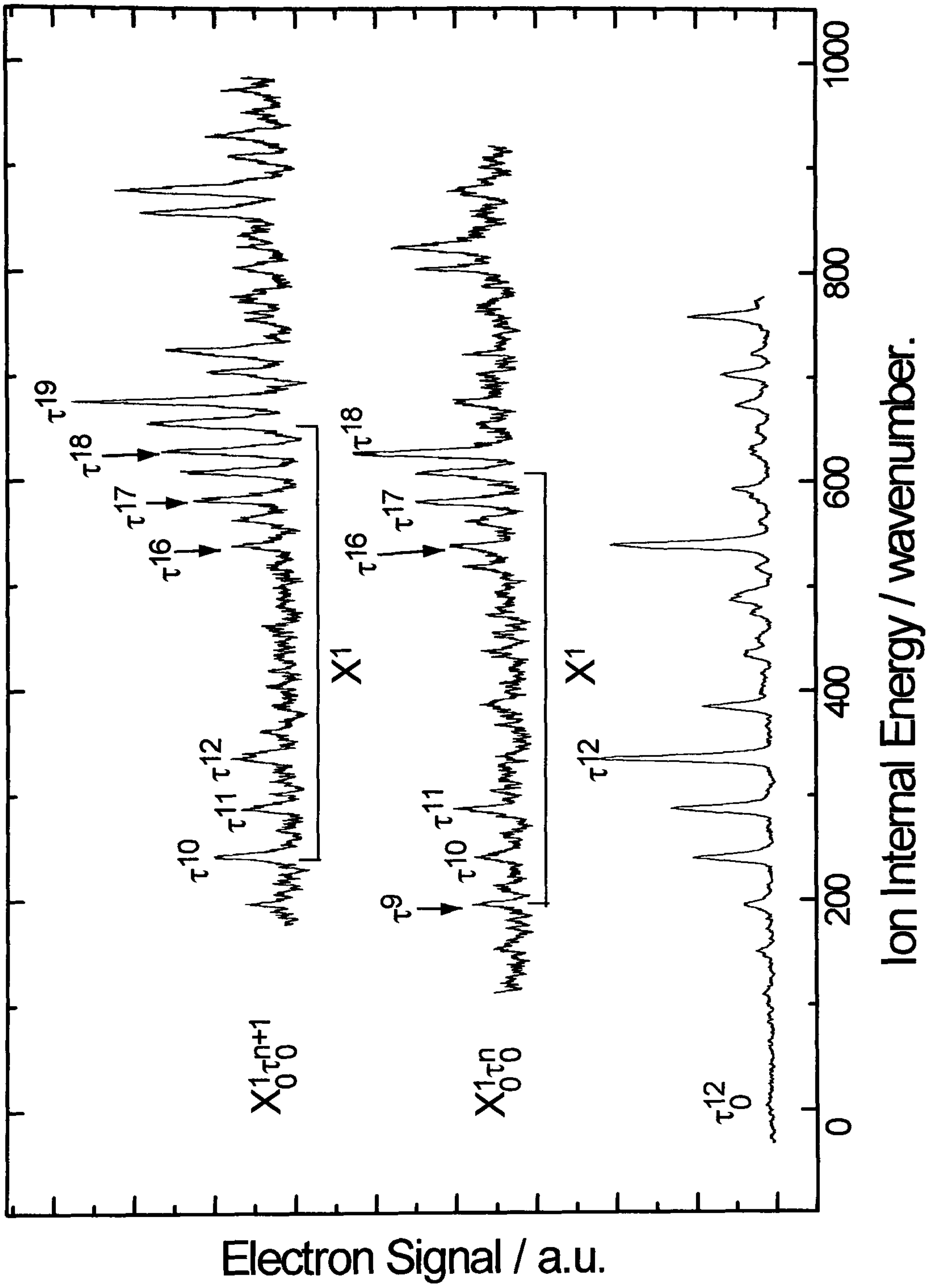

Figure 6.13: The (1+1') ZEKE-PFI spectra of 4-FB via two transitions of the S_1 state.

6.4.2. Calculation of the Barrier Height

The torsional energy levels of the ionic ground state of 4-FB display a very different behaviour from those of the S_1 state in that the spacing between adjacent levels increases as the torsional quantum number increases. The first spacing is 26 cm^{-1} which increases to 56 cm^{-1} between τ^{20} and τ^{21}. From examination of figure 6.7. this corresponds to the situation where V_4 is large and negative. The energy levels can be fitted with the constants $V_2 = 3490$ cm^{-1}, $V_4 = -910$ cm^{-1}, $V_6 = -30$ cm^{-1} and $F = 0.393$ cm^{-1}. Calculated and experimental energies are given in table 6.4. The fit is relatively poor and is further hampered by the fact that V_2 and V_4 are strongly correlated. It is clear from table 6.5. that the potential fits better for some parts of the experimental range than others. This may be due to the weakness of some transitions (for example the origin and first two torsional bands) or may be due to the potential itself. Higher order terms (V_8, V_{10} etc.) may be required or it may be that a simple cosine function does not adequately describe the real potential. As an example of this altering the potential could improve one portion of the fit but would worsen another. The calculated potential used is a compromise with the region of best experimental signal (τ^+ = 4-21) used as a benchmark. Spline functions, where different regions of the potential are fitted with different functions, may give a better fit to the experimental data[29].

The calculated potential has the effect that the torsional levels are four-fold degenerate with the even torsional levels having states of $\mathbf{a_1}$, $\mathbf{b_1}$ and **e** symmetry and the odd levels having $\mathbf{a_2}$, $\mathbf{b_2}$ and **e** symmetry. Since transitions of the type **e** ↔ **e** are formally allowed but have essentially zero Franck-Condon factors if the conformation of the rotor does not change this should result in odd ↔ even transitions being forbidden. This is not observed experimentally where the same torsional levels are accessed by both odd and even intermediates. Calculated spectra for the $D_0 \leftarrow S_1$ system are shown in figures 6.14, 6.15 and 6.16. Ignoring the odd ↔ even transitions good agreement between experiment and theory can be found although this becomes less reliable for the spectra via the lower intermediates. For such agreement it is necessary to assign the S_1 transition labelled the origin by Im and Bernstein[3] as τ_0^4. However for continuity the intermediates are labelled as for previous work.

τ^+	E_{obs} (cm^{-1})	E_{calc} (cm^{-1})	E_{obs}-E_{calc} (cm^{-1})	τ^+	E_{obs} (cm^{-1})	E_{calc} (cm^{-1})	E_{obs}-E_{calc} (cm^{-1})
0	-117	-99.3	-17.7	**14**	435	436.6	-1.6
1	-91	-86.9	-4.1	**15**	487	487.0	0
2	-61	-61.5	0.5	**16**	538	538.2	-0.2
3	-29	-32.7	3.7	**17**	590	590.1	-0.1
4	0	0	-	**18**	646	642.8	3.2
5	34	35.7	-1.7	**19**	700	696.0	4.0
6	71	73.8	-2.8	**20**	756	749.9	6.1
7	111	114.0	-3.0	**21**	812	804.2	7.8
8	152	156.0	-4.0	**22**	869	859.1	9.9
9	196	199.6	-3.6	**23**	925	914.3	10.7
10	241	244.6	-3.6	**24**	983	970.0	13.0
11	287	291.0	-4.0	**25**	1042	1026.0	16.0
12	335	338.5	-3.5	**26**	-	1082.4	-
13	385	387.0	-2.0	**27**	-	1139.0	-

Table 6.4. Calculated and experimental torsional energy levels for the ionic ground state of 4-FB.

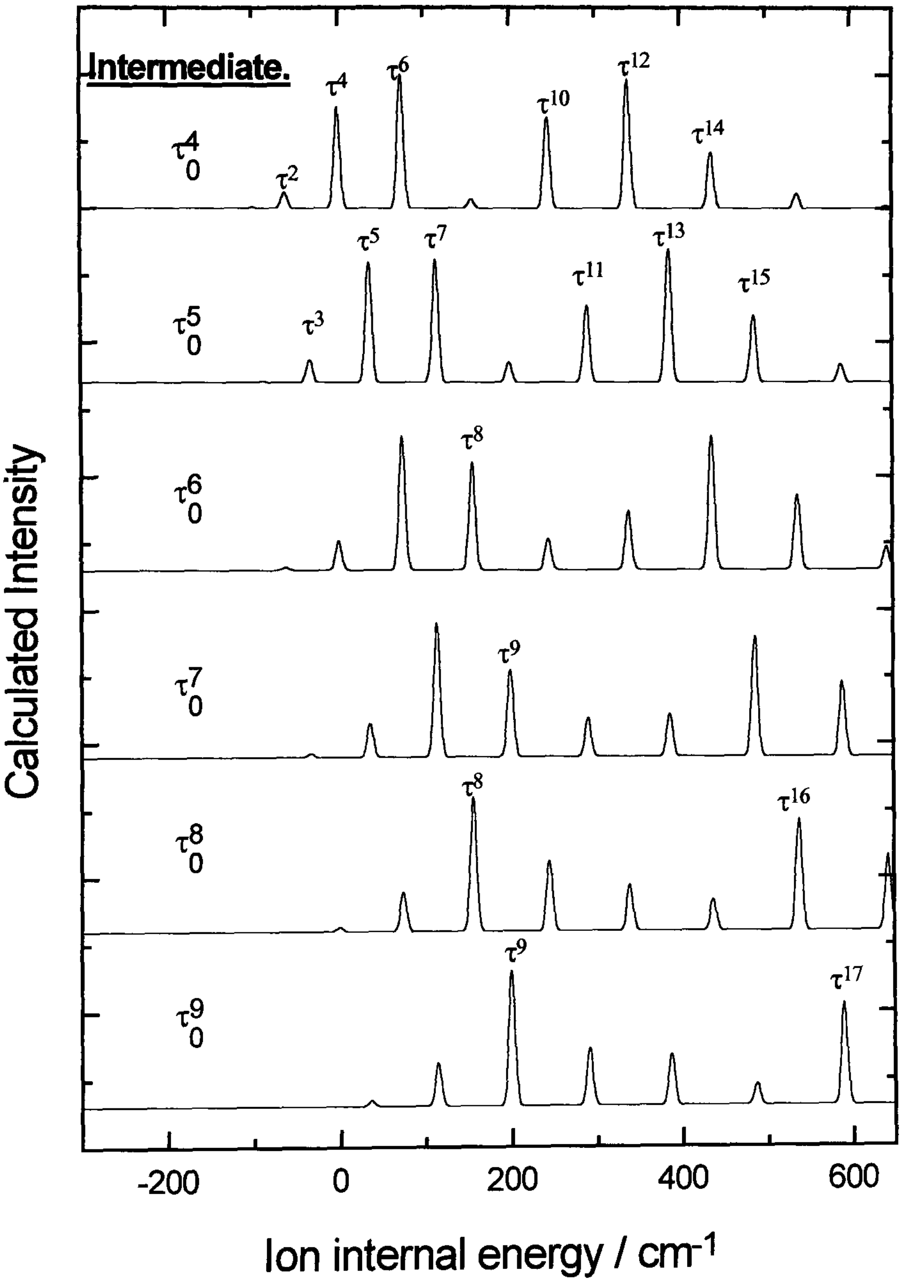

Figure 6.14: Calculated ZEKE spectra for 4-Fluorobiphenyl. The spectra are displayed relative to τ^4 of the ion. Intermediate assignments are from previous work and should have four quanta added to them (i.e. τ^4_0 is actually τ^8_0).

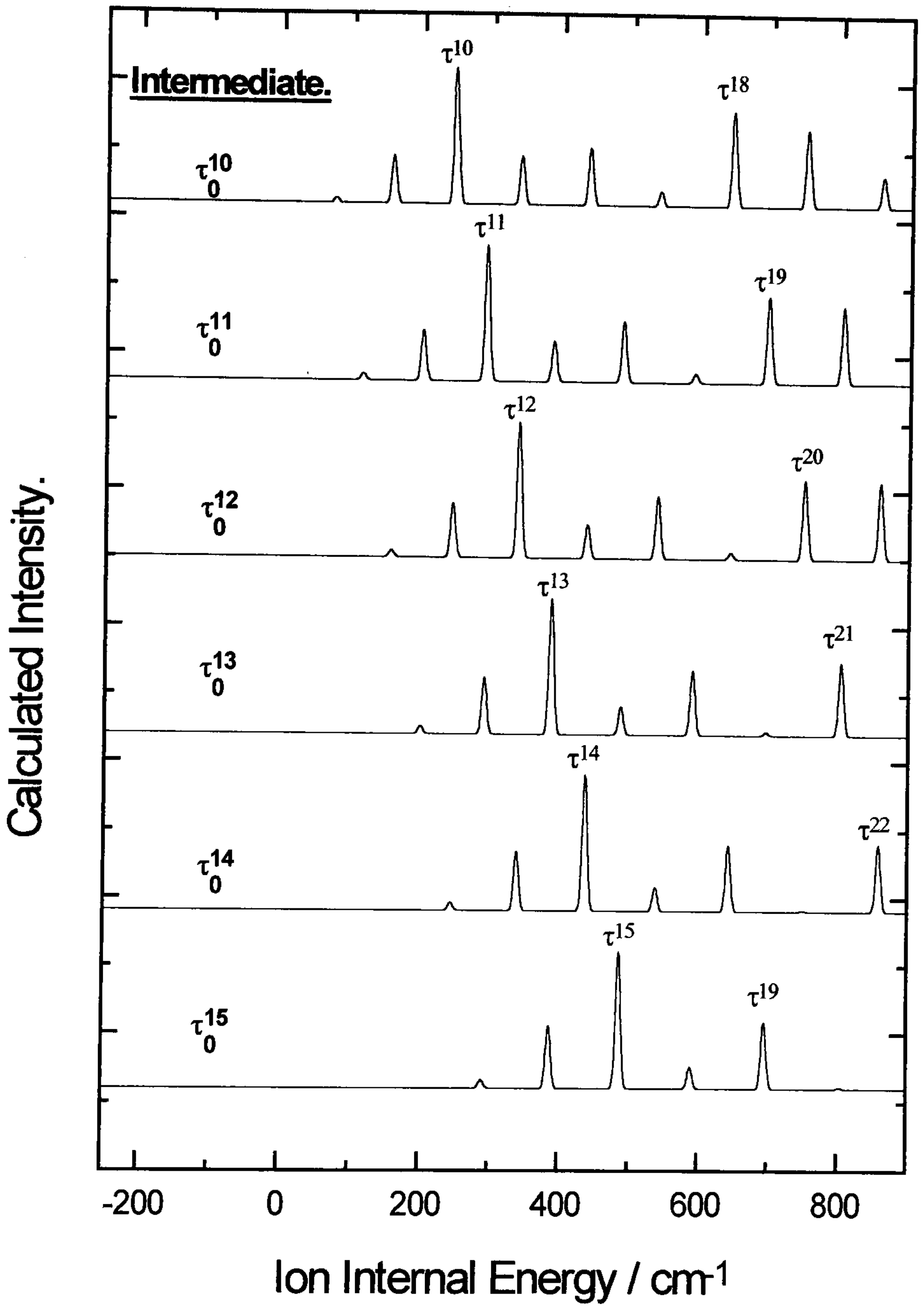

Figure 6.15: Calculated ZEKE spectra for 4-Fluorobiphenyl. The spectra are displayed relative to τ^4 of the ion. Intermediate assignments are from previous work and should have four quanta added to them (i.e. τ^4_0 is actually τ^8_0).

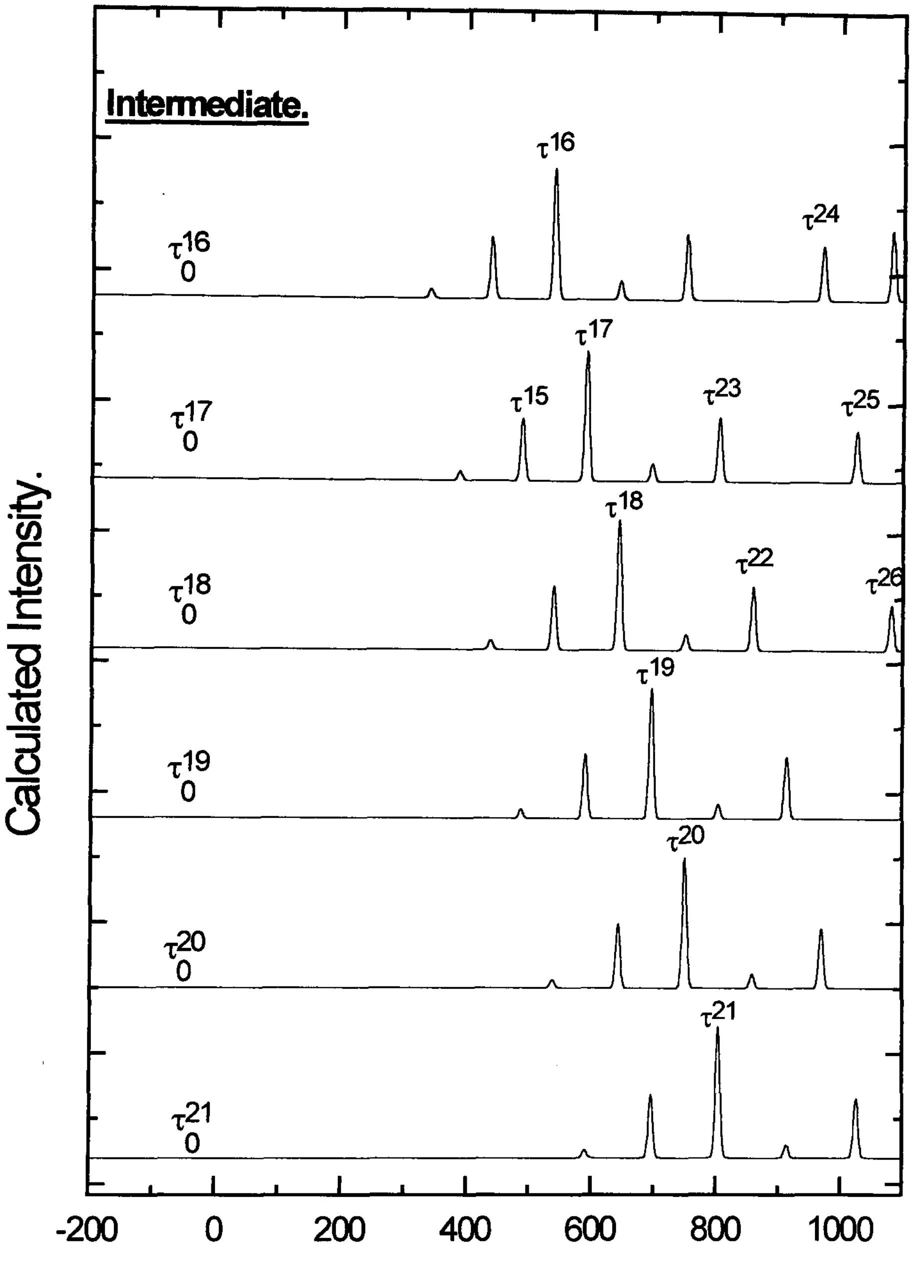

Figure 6.16: Calculated ZEKE spectra for 4-Fluorobiphenyl. The spectra are displayed relative to τ^4 of the ion. Intermediate assignments are from previous work and should have four quanta added to them (i.e. τ^4_0 is actually τ^8_0).

Figure 6.17. shows calculated and experimental ZEKE spectra via τ_0^{16} of the S_1 state (previously assigned as τ_0^{12} by Im and Bernstein) in more detail. Although the exact intensities are not precisely reproduced there is good agreement for the even to even transitions. The odd levels have zero intensity in the calculation which is in complete contrast to the experimental observations.

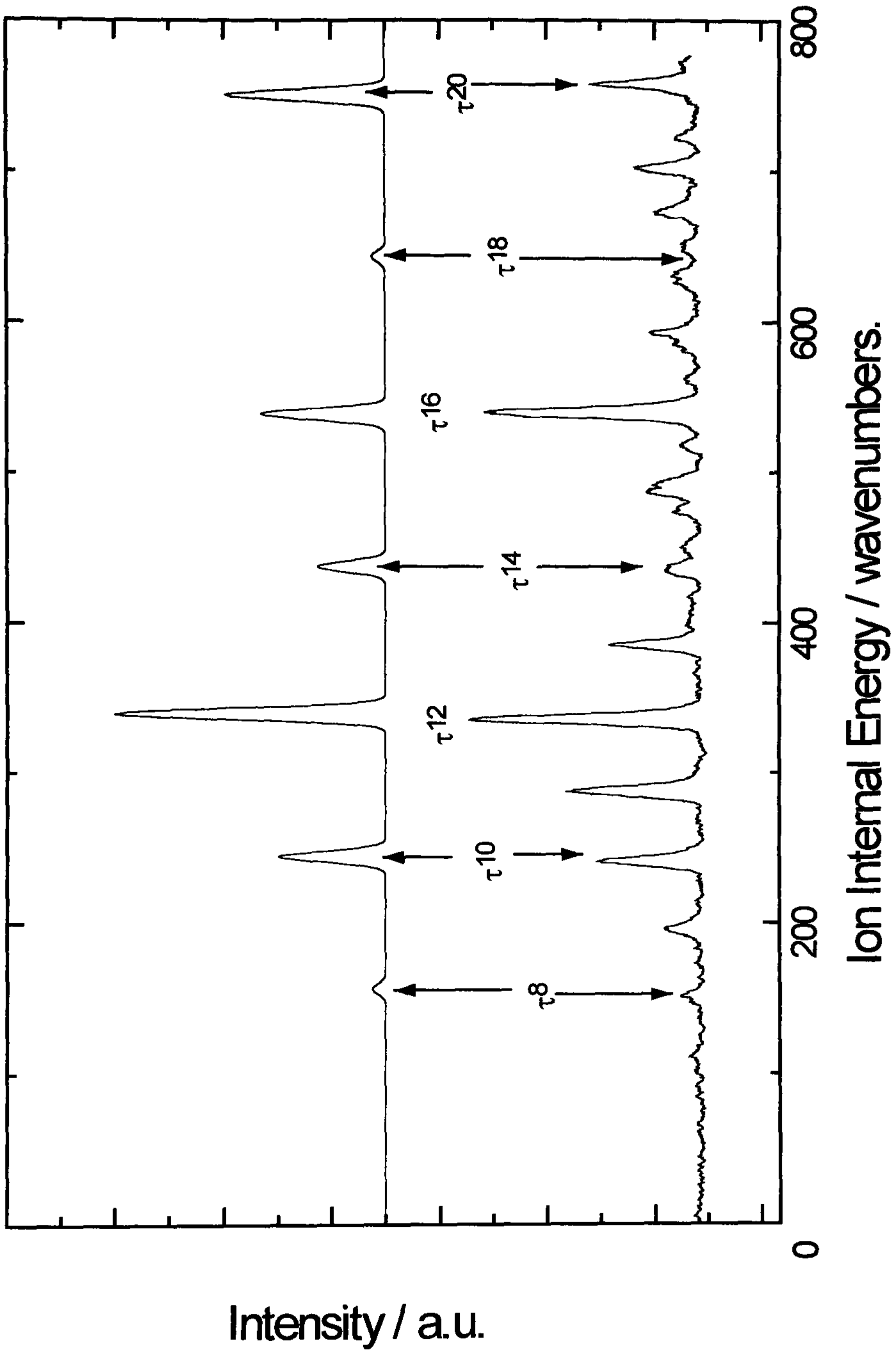

Figure 6.17: Calculated and experimental ZEKE spectra via τ_0^{16} of the S_1 state. The intermediate used was previously assigned as τ_0^{12}.

The reassignment of the S_1 state is shown in table 6.5. along with the calculated energy levels using the potential $V_2 = 3890 cm^{-1}$, $V_4 = -265 cm^{-1}$, $V_6 = -42 cm^{-1}$ and $F = 0.387 cm^{-1}$. The energy levels display such a regular spacing that very little adjustment of the potential used previously is required to obtain an adequate fit. The calculated MPI spectrum is shown in figure 6.18 for an angle of 44°. This results in a maximum around $\tau = 24$-26 in fair agreement with the experimental observation.

τ	E_{obs} (cm^{-1})	E_{calc} (cm^{-1})	$E_{obs}-E_{calc}$ (cm^{-1})	τ	E_{obs} (cm^{-1})	E_{calc} (cm^{-1})	$E_{obs}-E_{calc}$ (cm^{-1})
0	-		-	**13**	579	581.7	-2.7
1	-		-	**14**	645	646.9	-1.9
2	-		-	**15**	713	712.2	0.8
3	-		-	**16**	778	777.4	0.6
4	0	0	-	**17**	844	842.6	1.4
5	65	63.8	1.2	**18**	910	907.8	2.2
6	128	127.9	0.1	**19**	975	972.9	2.1
7	189	192.2	-3.2	**20**	1042	1037.9	4.1
8	253	256.8	-3.8	**21**	1104	1102.8	1.2
9	320	321.5	-1.5	**22**	1170	1167.5	2.5
10	383	386.4	-3.4	**23**	1234	1232.2	1.8
11	449	451.4	-2.4	**24**	1297	1296.6	0.4
12	515	516.5	-1.5	**25**	1362	1360.9	1.1

Table 6.5. Calculated and experimental energies for the S_1 state of 4-FB using the new assignment.

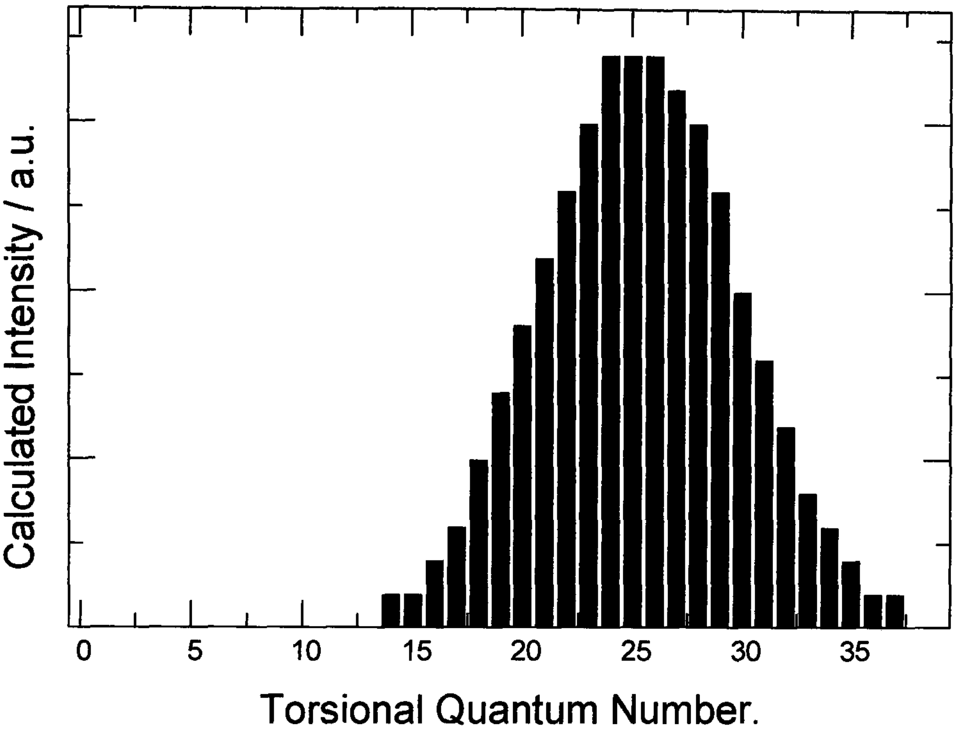

Figure 6.18: The calculated MPI spectrum of the S_1 state of 4-FB using a phase angle of 44° in the S_0 state.

6.5. Discussion

6.5.1. Analysis of the Results

The results presented in this chapter are dependant on the correct level of theory utilised. Previous work, most particularly that of Im and Bernstein[3], has been found to be wrong in that the calculated potentials do not concur with experimental observations either in terms of torsional energies or in Franck-Condon factors. For example the calculated barrier for the S_0 state of biphenyl is supposed to model a spacing[4] of 58 cm^{-1}. Im and Bernstein`s barrier does not satisfy this. However there remain several outstanding points which require some comment.

Firstly it is necessary to reassign the S_1 torsional progression to allow better agreement with the experimental spectrum. Previous work had assigned the lowest observed transition as the electronic origin for no other reason than the fact that it was the lowest energy transition[3,4]. The analysis of this chapter is that the lowest observed transition is not the origin. A similar conclusion can be reached for biphenyl itself and it is clear that a reassessment of the S_1 state potentials may be required for substituted biphenyls in general[1-15]. The exact position of the electronic origin of the S_1 state is difficult to establish from the MPI spectrum alone since the region of peak intensity occurs over several quanta of the torsional vibration. The calculated potential can be made to fit the experimental results by altering the angle between the two rings (see figure 6.10.). Hence there are two unknowns to be fitted. The assignment of the S_1 origin presented in this chapter is made by comparison with the ZEKE-PFI spectra obtained via the S_1 state.

The assignment of the torsional levels of the ion also requires some comment. The origin of the ion is assumed to be the lowest observed transition (the same assumption as made in previous studies[3,4] of the S_1 state). Such an assignment appears to be confirmed by the Franck-Condon calculations although there are several features of the calculation which require some explanation. Firstly the calculated potential has

V_2 as its main term with the result that even torsional levels consist of different torsional symmetries from odd levels (see figure 6.7). This means that only transitions to even states should be observed from even intermediates and vice-versa (although both odd and even states contain an e type symmetry level transitions between such levels have zero Franck-Condon overlap for an odd to even transition when the relative phases of the potentials remain unchanged). However, the experimental spectra show evidence of both odd and even transitions. There can be two explanations for this; the calculated potential is wrong or the pulsed-field-ionisation mechanism is allowing forbidden transitions to occur.

It is possible that the experimental energies could be fitted using a much larger value of V_4 (and a smaller value for V_2) to obtain a situation where the odd and even levels have the same symmetries. Such a potential would be twisted away from the planar conformation and hence would appear more like that of the neutral ground state. This explanation can be discounted for two main reasons. Firstly, the conventional He(I) photoelectron spectrum of this molecule indicates a large change in the angle of the two potentials and secondly the calculated intensities of a transition from the S_1 state to such a potential would not match those observed in the ZEKE spectra. In addition such a large (>3000 cm^{-1}) value of V_4 would indicate a large repulsion between the two rings. Such a situation could occur if the protons of the rings gain enough partial charge to make electrostatic effects important. Although removal of an electron does increase the partial charge of the protons it is unlikely that this could reach a high enough level to be so dominant.

This leaves the second mechanism, namely some effect of the Rydberg states populated in the ZEKE-PFI experiment. The most obvious explanation would be the field-induced autoionisation mechanism[21,31,32] used to explain the ZEKE spectra of 3-aminobenzotrifluoride (chapter 5). However, there are several problems with such an explanation. The calculated and observed ZEKE spectra via τ_0^{16} of the S_1 state show these up clearly (figure 6.17.). The formally forbidden transition to τ^{11} of the ion can gain intensity from interaction with the Rydberg series converging on τ^{12}. Such

Rydberg series will have a significant transition probability and so autoionisation can result in the forbidden transition gaining substantial intensity. However, in the same spectrum, τ^{13} also displays considerable intensity. For the resonant mechanism to be present here the Rydberg series would have to be one converging on a much higher torsional level (τ^{16}). Hence the density of Rydberg states around τ^{13} would be much lower than that found for τ^{11} with the result that a coincidence is not so likely. For a typical torsional spacing in 4-FB (50 cm^{-1}) the spacing between Rydberg states of the same series is ~2 cm^{-1}. For a gap of two torsional levels (100 cm^{-1}) the spacing between adjacent Rydberg states is 3 cm^{-1}. Given the bandwidth of the ZEKE transitions (~6 cm^{-1}) the chance of coincidence is still high. Such a pattern is repeated for each of the intermediates. A further possibility is that other mechanisms are contributing to the observed spectra.

Several mechanisms for the appearance of Franck-Condon forbidden transitions in threshold photoelectron spectroscopy have been discussed[33-37]. The first is that proposed by Guyon[33] to explain the non Franck-Condon behavior of the TPES of N_2O and is essentially an extension of the resonant mechanism previously mentioned. The coupling of a low-*n* Rydberg state to a high-*n* state converging on a lower state of the ionic core was mediated by a dissociative state. The criterion was that the two Rydberg states were close in energy in a similar way to field induced autoionisation in ZEKE-PFI experiments. In more recent work on the ZEKE spectra[34-36] of O_2 and NO_2 it was necessary to use a slightly modified version of this mechanism in which a low-*n* Rydberg state was not required. The interaction is direct between the repulsive state and the high-*n* Rydberg states. This was necessary since the intensity of ZEKE transitions was not linked to the proximity of autoionising Rydberg states. The effect can be widespread since the repulsive arm of the dissociative state coincides with the bound state over a wide energy range.

In the case of 4-FB such a mechanism is more difficult to conceive since the torsional motion does not correspond to a dissociative vibration such as found for the stretching vibrations of diatomic and triatomic molecules. A second possibility is that photoelectrons are picked up by ions in the excitation volume. This is essentially an electron scattering process and has been observed for benzene[37]. However it was found to only account for a very small amount of the ZEKE signal (~3%).

For the present case it may be that all three mechanisms are present although it is likely that the first mechanism (resonant autoionisation) is the major contribution.

6.5.2. Sources of Barriers to Internal Rotation

Calculated potentials for all three electronic states of 4-fluorobiphenyl are shown in figure 6.19. The S_0 barrier is taken from electron diffraction data of reference 27. Each state displays a different shape of barrier which reflects the relative magnitude of the two main sources of hindering potentials in biphenyls; steric repulsion between the rings and electronic conjugation. These two effects are in opposition and it is the balance between them that determines the shape of the potential barrier[1-15,18].

Steric repulsion between the rings (specifically the protons at the ortho position relative to the ring-ring bond) has the effect of twisting the rings away from planarity. In the absence of any other effects this would result in the two rings being perpendicular. Such a geometry would render the π system of the two rings orthogonal. This is shown in figure 6.20. This is the dominant factor in the S_0 state where the rings are twisted at an angle of 45° relative to each other (interaction between the rings is enough to make the 90° conformation a maximum in the potenial). This means that the potential repeats after 90° and V_4 is the dominant term. Such a conformation is also aided by the highest occupied molecular orbital which has a nodal pattern that is anti-bonding between the rings. Hence the S_0 state can be considered as two benzene rings linked by a single bond and internal rotation is not hindered by the breaking of a π-bond

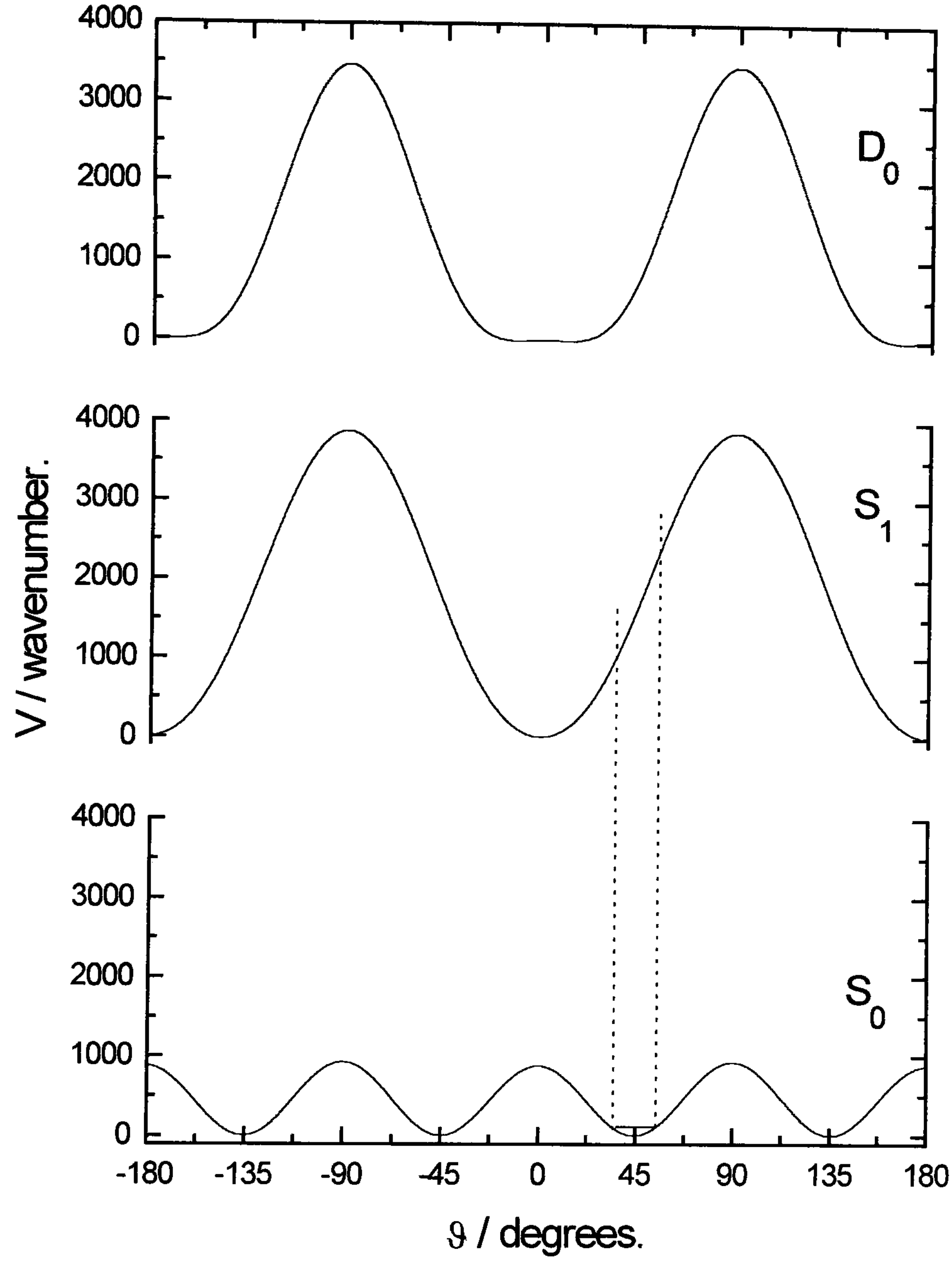

Figure 6.19: Calculated potentials for all three states of 4-fluorobiphenyl. The dotted line shows the width of the Franck-Condon window for the ground torsional level of the S_0 state.

Excitation of an electron to the lowest unoccupied molecular orbital (the π-π^* transition) radically alters the balance between steric and electronic effects[24,25] with the result that the S_1 state has a very different potential to that of the S_0 state. The π^* orbital is bonding with respect to the inter-ring bond. This greatly increases the double bond character of this bond with the result that the molecule adopts a planar conformation. The potential now repeats after 180° and V_2 is the dominant term. Internal rotation now corresponds to the breaking of a carbon-carbon double bond and is very much hindered.

Finally, the ionic ground state shows a third type of behaviour in that both V_2 and V_4 are sizeable although V_2 is greater. Removal of an electron from the HOMO reduces the antibonding nature of the inter-ring bond which allows the molecule to be planar. In addition the resonance from shown in figure 6.21. favours the planar structure particularly if the substituent at the 4 position can donate electrons into the ring. The electron donating ability of fluorine is relatively weak but is enough that the molecule is essentially planar. (An interesting extension of this experiment would be the substitution of biphenyl at the 4 position by fragments which are more strongly electron donating (e.g. NH_2 or OH) or, in contrast, more strongly electron withdrawing (e.g. CN)). However the steric effects are still present and try to twist the molecule from planarity. Such interaction is actually increased since the inter-ring bond is considerably shorter in the planar conformation[25,26]. Furthermore the removal of an electron from the molecule renders the C-H bonds of the ring more polar. This has the effect of adding a coulombic repulsion to the steric effect. (This effect could be measured by carrying out ZEKE experiments on biphenyls which are substituted at the 2 position). The net result is a potential that repeats every 180° but which has a very flat potential well (V_4 is large enough that there is a small double minimum here).

It is clear that the conformation of 4-fluorobiphenyl is the result of a subtle balance between opposing forces. Similar effects were seen by Knee and co-workers[18] in their study of 9,10-dihydrophenanthrene. Although the two rings are linked in this case and cannot take up any conformation, the angle between the rings decreases from the S_0 state to the S_1 state but then increases again on ionisation. The ionic angle, however, is still less than that of the neutral ground state which is in agreement with the conclusions reached here. This molecule and 4-fluorobiphenyl are the only derivatives of biphenyl for which torsionally resolved photoelectron spectra have been obtained. A wide number of other such derivatives remain unstudied (although the S_1 state has received considerable attention[3-5]) and would help to quantify the relative magnitude of the steric and electronic effects. Furthermore more work is required on the S_0 state to fully quantify the torsional potential there.

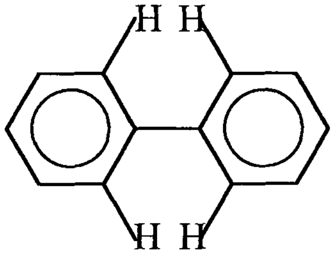

Figure 6.20. Steric repulsion between the two rings of biphenyl.

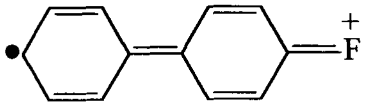

Figure 6.21. Conjugation in the ionic ground state of 4-fluorobiphenyl.

6.6. Conclusion

The torsional structure of 4-fluorobiphenyl has been studied in the S_1 and D_0 states by a combination of multiphoton ionisation (MPI) and Zero-Kinetic-Energy Pulsed-Field-Ionisation (ZEKE-PFI) photoelectron spectroscopy. Barriers to internal rotation were calculated using a one-dimensional rigid rotor model. A comprehensive reassignment of the S_1 spectrum was necessary to obtain agreement between theory and experiment. The transition previously assigned as the electronic origin of the S_1 state is reassigned as τ_0^4. This was made possible by the use of the S_1 state as a resonant intermediate in a two-colour photoelectron study.

Calculated barriers to internal rotation show a subtle balance between steric and electronic effects. Both the S_1 and D_0 states are planar while the S_0 state is twisted at an angle of approximately 45°. The ZEKE spectra also show interesting features in that formally forbidden transitions are observed with intensities comparable to the allowed transitions. This can be attributed to autoionisation although the phenomenon may be too widespread to be due solely to resonant autoionisation. Coupling between the high-*n* Rydberg states and a dissociative valence state may also be involved.

The results detailed in this chapter cover only one derivative of biphenyl. A more comprehensive study is required to understand the relative magnitudes of the steric and electronic effects which lead to the potential barriers.

6.8. References

1. N. Wenzel. *J.Chem.Phys.* 1953, **21**, 403.
2. H.H. Jaffe & M. Orchin. Theory and Applications of Ultraviolet Spectroscopy. John Wiley & Sons (London). 1962.
3. H.S. Im & E.R. Bernstein. *J.Chem.Phys.* 1988, **88**, 7337.
4. Y. Takei, T. Yamaguchi, Y. Osamura, K. Fuke & K. Kaya. *J.Phys.Chem.* 1988, **92**, 577.
5. J.I. Murakami, M. Ito & K. Kaya. *J.Chem.Phys.* 1981, **74**, 6505.
6. R.M. Hochstrasser & H.N. Sung. *J.Chem.Phys.* 1977, **66**, 3265.
7. E.C. Lim & Y.H. Li. *J.Chem.Phys.* 1970, **52**, 6416.
8. W.E. Sinclair, H. Yu, D. Phillips & J.M. Hollas. *J.Chem.Phys.* 1997, **106**, 5797.
9. R. Zimmermann, C. Weickhardt, U. Boesl & E.W. Schlag. *J.Mol.Struct.* 1994, **327**, 81.
10. K. Okuyama, Y. Numata, S. Odawara & I. Suzuka. *J.Chem.Phys.* 1998, **109**, 7185.
11. M. Takayanagi, T. Gejo & I. Hanazaki. *J.Phys.Chem.* 1994, **98**, 12893.
12. T. Tsuji, Y. Hayashi, H. Sekiya, H. Hamabe, Y. Nishimura, H. Kawakami & A. Mori. *Chem.Phys.Lett.* 1997, **278**, 49.
13. T. Chakraborty & M Chowdhury. *Chem.Phys.Lett.* 1991, **177**, 223.
14. M.R. Hockridge, E.G. Robertson & J.P. Simons. *Chem.Phys.Lett.* 1999, **302**, 538.
15. H.T. Jonkman & D.A. Wiersma. *Chem.Phys.Lett.* 1983, **97**, 261.
16. A. Almenningen, O. Bastiansen, L. Fernholt, B.N. Cyvin, S.J. Cyvin & S. Samdal. *J.Mol.Struct.* 1985, **128**, 59.
17. J.P. Maier & D.W. Turner. *Faraday Disc.* 1972, **54**, 149.
18. J.M. Smith & J.L. Knee. *J.Chem.Phys.* 1993, **99**, 38.
19. M.C.R. Cockett & K. Kimura. Annual Review. Institute for Molecular Science (Okazaki). 1992.

20. J.G. Goode. PhD Thesis. University of Edinburgh. 1995.
21. D.A. Beattie. PhD Thesis. University of Edinburgh. 1998.
22. F.M. Menger. *Angew.Chem.Int.Ed.* 1991, **30**, 1086.
23. L.P.A. Siebbeles & B. Movaghar. *J.Chem.Phys.* 1999, **110**, 10162.
24. Theory and Applications of Ultraviolet Spectroscopy. H.H. Jaffe & M. Orchin. John Wiley & Sons (London). 1962.
25. A. Karpfen, C.H. Choi & M. Kertesz. *J.Phys.Chem.* 1997, **101**, 7429.
26. K. Furuya, H. Torri, Y. Furukawa & M. Tasumi. *J.Mol.Struct.(THEOCHEM).* 1998, **424**, 225.
27. A. Almenningen, O. Bastiansen, S. Gundersen, S. Samdal & A. Skancke. *J.Mol.Struct.* 1985, **128**, 95.
28. A. Almenningen, O. Bastiansen, L. Fernholt, S. Gundersen, E. Kloster-Jensen, B.N. Cyvin, S.J. Cyvin & S. Samdal. *J.Mol.Struct.* 1985, **128**, 77.
29. K.P. Lawley. *J.Mol.Spectrosc.* 1997, **183**, 25.
30. A. Jones, P. Richardson, P. Donaldson & K.P. Lawley. Unpublished work.
31. M.C.R. Cockett, J.G. Goode, K.P. Lawley & R.J. Donovan. *J.Chem.Phys.* 1995, **102**, 5226.
32. M.C.R. Cockett, R.J. Donovan & K.P. Lawley. *J.Chem.Phys.* 1996, **105**, 3347.
33. P.M. Guyon, T. Baer & I. Nenner. *J.Chem.Phys.* 1983, **78**, 3665.
34. W. Kong & J.W. Hepburn. *Can.J.Phys.* 1994, **72**, 1284.
35. H. Matsui, J.M. Behm & E.R. Grant. *J.Phys.Chem.* 1997, **101**, 6717.
36. W.A. Chupka & E.R. Grant. *J.Phys.Chem A.* 1999, **103**, 6127.

37. C. Alt, W.G. Scherzer, H.L Selzle & E.W. Schlag. *Chem.Phys.Lett.* 1994, **224**, 366.

Chapter 7

Conclusions and Future Work

This thesis has presented the high resolution photoelectron spectra of a number of polyatomic molecules. The ionic ground state of CF_3I has been studied by two distinct excitation schemes. Together with polarisation studies these allow the assignment of the majority of the vibronic structure of the $[^2E_{3/2}]6p$ Rydberg manifold. Such work reveals evidence for interaction of the Rydberg states with an isoenergetic ion-pair state. This results in a greatly reduced frequency for the C-I stretch (ν_3) and substantial activity in the non-totally symmetric vibrational modes[1].

The remainder of the work focused on the internal rotation of larger polyatomics. All three of the aminobenzotrifluorides have been studied in a two-colour study using the S_1 valence state as a resonant intermediate. The torsional potentials were found to be similar to that of substituted toluenes[2-4] although some interesting differences appear. For 2-ABTF there is evidence of substantial interaction between the two substituent groups. This has an effect on the intensities of the photoelectron transitions. Transitions involving combinations of the CF_3 and NH_2 torsions were observed with substantial activity. For all three isomers activity was noticed in photoelectron transitions which are symmetry forbidden. In particular the ZEKE-PFI spectra of 3-ABTF show formally forbidden transitions with intensities comparable to that of the fully allowed transitions. This can be ascribed to field-induced autoionisation[5] between the high-*n* Rydberg states and low-*n* states converging on a higher ionic core state. The spacing of the torsional structure (~20 cm^{-1}) means that there is a very high chance of such states being isoenergetic. For 2-ABTF, where the torsional spacing is of the order of 40 cm^{-1}, only very weak forbidden transitions are observed.

The torsional structure of 4-ABTF was very limited. This allowed the vibrational structure of both the S_1 and ionic ground states to be studied. The amine inversion could be identified and was found to be split into a doublet in both states. This is due to interaction between the two substituent groups.

The torsional structure of 4-fluorobiphenyl was also studied. The barrier to internal rotation was found to be a subtle balance between steric repulsion and electronic effects[6,7]. The ionic ground state was found to be planer but with a flat-bottomed well. In addition substantial activity was observed in formally forbidden transitions by a similar mechanism to that for the aminobenzotrifluorides.

There remains a considerable amount of further work to be done both for the aminobenzotrifluorides and in particular for the biphenyls. For the ABTF's it would be interesting to study the effects of other substituents such as fluorine or chlorine although such studies would most likely be similar to that found previously for the toluenes[2-4].

The biphenyls, on the other hand, have had relatively little detailed study. In particular the ionic ground state has only been studied at a resolution sufficient to resolve torsional structure in one other study (9,10-dihydrophenanthrene[6]). There exists a wide range of substituted biphenyls which are readily available and should allow the balance between steric and electronic factors to be examined. In particular substitution at the 4 position with species that are better or worse electron donors than fluorine should allow the electronic effects to be quantified while steric effects could be monitored by substitution at the 2 position.

The calculation of barriers and their fitting to observed values was done manually[8]. This is a slow and tedious process which could be made more automatic. This would speed up the process and should give better fits to barriers with several significant terms such as were found for the ionic ground state of 4-fluorobiphenyl.

The molecules studied in this thesis are of a reasonable size from a spectroscopic viewpoint and display features such as non-bonded interactions and electron delocalisation[9]. An understanding of such interactions is vital for the understanding of larger, biologically important species (proteins, DNA, etc.) which cannot be easily studied spectroscopically.

The experimental and theoretical arrangements are now in place to study low frequency motion in large molecules. The heated nozzle arrangement allows the use of samples with sufficient vapour pressure at 130°C. This allows a wide number of species to be studied at a resolution sufficient to observe such motions. The main limiting factor is the volatility of the molecule under study.

References

1. N.A. Macleod, S. Wang, J. Hennessy, T. Ridley, K.P. Lawley & R.J. Donovan. *J.Chem.Soc.Faraday Trans.* 1998, **94**, 2689.
2. High Resolution Laser Photoionization and Photoelectron Studies. Edited by I. Powis, T. Baer & C.Y. Ng. John Wiley & Sons (London). 1995.
3. H. Ikoma, K. Takazawa, Y. Emura, J. Ikeda, H.Abe, H. Hayashi & M. Fujii. *J.Chem.Phys.* 1996, **105**, 10201.
4. K.T. Lu, F.Weinhold & J.C. Weisshaar. *J.Chem.Phys.* 1995, **102**, 6787.
5. M.C.R. Cockett, R.J. Donovan & K.P. Lawley. *J.Chem.Phys.* 1996, **105**, 3347.
6. J.M. Smith & J.L. Knee. *J.Chem.Phys.* 1993, **99**, 38.
7. H.S. Im & E.R. Bernstein. *J.Chem.Phys.* 1988, **88**, 7337.
8. K.P. Lawley. *J.Mol.Spectrosc.* 1997, **183**, 25.
9. L.H. Spangler & D.W. Pratt. *Internal rotation dynamics from electronic spectroscopy in supersonic jets and beams.* Jet Spectroscopy and Molecular Dynamics. Edited by J.M. Hollas & D. Phillips. Blackie Academic (London). 1995.

Appendix 1
Hund's Coupling Cases

The concept of different coupling schemes for the spin and orbital angular momentum was given in chapter 2 section 2.2.1. with Hund's case (c) as example. The four other coupling cases are given in this appendix[1-4].

The coupling of case (a) is given in figure A.1.1. The angular momentum of the electrons combine to give orbital (L) and spin (S) components. The coupling between these is small and in consequence the major interaction is between L and S with the internuclear axis to form projections Λ and Σ. These in turn combine to from Ω (the total angular momentum without nuclear rotation). The coupling of this with the angular momentum of the nuclear rotation (R) forms the total angular momentum of the system (J). Thus the good quantum numbers are S, Λ, Σ, Ω and J. Hund's case (a) applies to systems where the interaction between the spin and orbital components is relatively weak and is generally found for species containing first and second row elements.

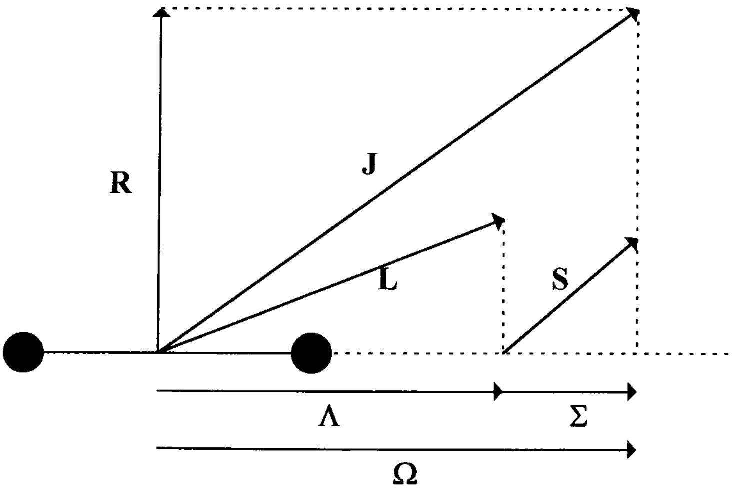

Figure A.1.1. Hund's coupling case (a).

The coupling scheme for Hund's case (b) is shown in figure A.1.2. In contrast to case (a) the spin angular momentum is not coupled to the orbital component or to the internuclear axis. L is coupled to the axis to form Λ which is in turn coupled with R to form a resultant angular momentum (N). This interacts with S to form the total angular momentum (J). Λ, N, S and J are good quantum numbers. This case covers light systems with large rotational constants.

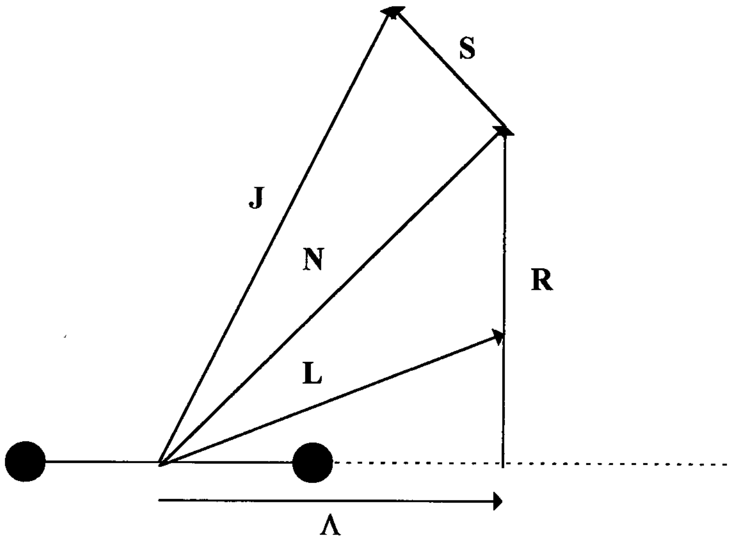

Figure A.1.2. Hund's coupling case (b).

Figure A.1.3. shows the coupling scheme for case (d). In contrast to the first three cases neither L or S are strongly coupled to the nuclear axis. L is coupled with R to give a resultant (N) which is coupled in turn with S to give the total angular momentum of the system (J). J, S, N and R are all good quantum numbers. Such coupling has been found to be a good model for high-*n* Rydberg states.

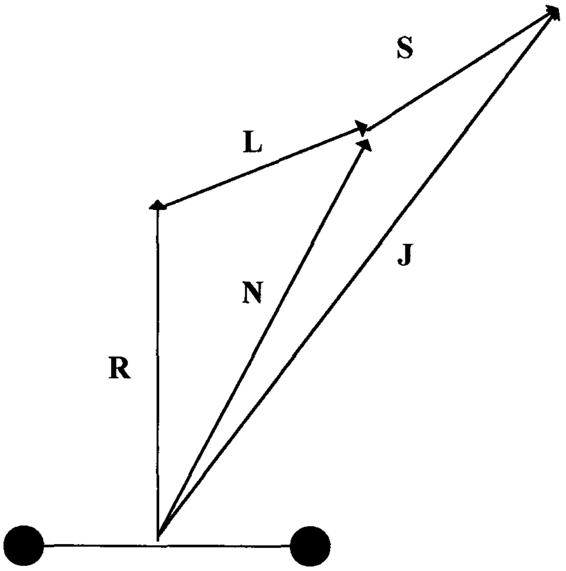

Figure A.1.3. Hund's coupling case (d).

The final coupling scheme, case (e), is shown in figure A.1.4. L and S are strongly coupled to form a resultant angular momentum, J_a which combines with the nuclear angular rotation, R, to form the total angular momentum of the system, J. Good quantum numbers are R, J_a and J. This case applies to high-*n* Rydberg states although it is not very common.

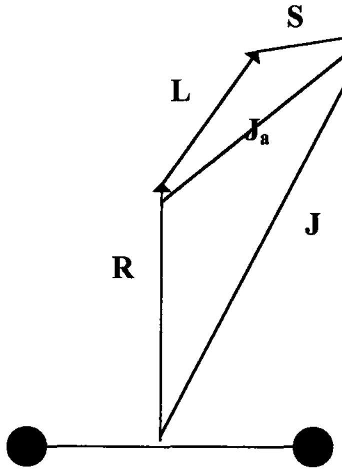

Figure A.1.4. Hund's coupling case (e).

References

1. G. Herzberg. Molecular Spectra and Molecular Structure. Volume 1: Spectra of Diatomic Molecules. Krieger Publishing (Florida). 1989.
2. G. Herzberg & C. Jungen. *J.Mol.Spectrosc.* 1972, **41**, 425.
3. H. Lefebvre-Brion, A. Giusti-Suzor & G. Raseev. *J.Chem.Phys.* 1985, **83**, 1557.
4. A. Mank, M. Drescher, T. Huth-Fehre, N. Bowering, U. Heinzmann & H. Lefebvre-Brion. *J.Chem.Phys.* 1991, **95**, 1676.

Appendix 2

Programs for torsional calculations

Torsional energy levels and Franck-Condon factors were calculated using the discrete variable approach of Lawley (see section 2.5.5.). Separate programs were used for the threefold and twofold cases.

Program ROTOR3_bal calculates the energy levels and Franck-Condon factors for a threefold system while ROTORC2v_bal does the same for the twofold case.

```
PROGRAM ROTOR3_bal
C Calculates a band of energy levels in the periodic potential V(x) specified
C analytically by a sum of harmonic terms, 0.5(1-cos(3n*phi). The case of a balanced
C rotor is treated, in which the moment of inertia is independent of phi, which is a
C special case of the program ROTOR3. The kinetic energy op. is now just
C G0*d**2/d(phi)**2

C Both the potential V(x) and the eigenvectors WAV(x) are tabulated from
C x=STEP to x=PI-STEP, not from 0 to PI. x=0 and x=PI are either nodes
C (in the A2 and one of each E pair of states) of the eigenfunctions or maxima/minima
C (in the A1 states and the other E partner ). The various classes of solution are
C tackled separately by imposing the nodal pattern.

C ROTOR3 deals specifically with a polar potential with a 3-fold axis of
C symmetry. The angular range is from 0 to 2*PI/NDIV, with nodes and anti-node
C combinations being selected at the two boundaries - node/node (nn), node/anti
C-node (na) etc. To cover all the symmetry species, first put NDIV=2 (0 to 180
C deg) which will automatically apply the nn and aa terminations. All the symmetry
C species will then appear; one member of each degenerate pair in nn, the other in
C aa, the A1 species will appear only in the aa list and the A2 in the nn list.
C Next, reduce the angular range to 120 deg by putting NDIV=3 in the input file;
C this will apply the nn, aa and now the na termination. The latter will select only
C one member of each degenerate pair (the one that has a nodal plane through 0-180 deg),
C and so this combination should be used for FC factors involving degenerate states.
C Finally, reduce the range to 0 to 60 deg C (NDIV=6), when the degenerate
C levels will disappear and the aa list will contain only the A1 species, the nn
C list only the A2 species. This combination could be used for FC factors
C involving the A1 and A2 species, because contamination with any very close-lying E
C states is removed .


   IMPLICITDOUBLE PRECISION(A-H,O-Z)
   DOUBLEPRECISION I44
   EXTERNAL N2COUNT
   PARAMETER(NDIM=3000)
   DIMENSION V(NDIM),Y(NDIM),H(NDIM)
C The final eigenvalues are held in separate arrays for nn aa and na states
   DIMENSION EIGEN_nn(0:100),EIGEN_aa(0:100),EIGEN_na(0:100)
   DIMENSION FDET(0:NDIM),BDET(1:NDIM+1),WAV(NDIM),WAV_init(NDIM)
   CHARACTER REPLY*3,FNAME*20,CASE*2,CASE1*2
C CASE1 contains the symmetry for the previously prepared initial state, nn, aa or na

   COMMON/POT/G0,V3,V6,V9
   COMMON/VECTORS/H  !the diagonal entries, V(n)+2, properly terminated
```

```
      COMMON/PARMS/FRAC,STEP,ESP,NMAX
      COMMON/NORMS/NODE,WNORM(0:100) !Stores partial normalization of corresponding
                                      !eigenvector

      OPEN(UNIT=1,FILE='rotor3_bal.in')
      OPEN(UNIT=7,FILE='rotor3_bal.results')
      WRITE(6,'(A,$)')'Are Franck-Condon factors to be calculated ?'
      READ(*,*)REPLY
      IF(REPLY.EQ.'yes'.OR.REPLY.EQ.'YES'.OR.REPLY.EQ.'Y')THEN
            REPLY='yes'
C           WRITE(6,'(A,$)')'Enter file name of initial state wave fn: '
        OPEN(UNIT=8,FILE='rotor3_bal.wave')
C           READ(*,*)FNAME
C           OPEN(UNIT=2,FILE=FNAME)
            read(8,'(a)')CASE1 !the input wave function will be headed by aa or nn


            DO 9 I=1,NDIM
              READ(UNIT=8,FMT=105,END=10)WAV_init(I)
9        CONTINUE
      ENDIF
      GOTO 11
10          print*,'Input wave file must contain',NDIM,'entries'
            STOP
11     READ(1,*)V3,V6,V9  !the parameters of the potential
      READ(1,*)G0    !the parameters of the g-function
      READ(1,*)NDIV     !the angular range is 0 to 2*PI/NDIV
      READ(1,*)PREC     !the precision of bisection in cm-1

      tiny = PREC

      WRITE(7,'(A,$)')'The internal rotor problem with '
      WRITE(7,'(A)')'a threefold axis of symmetry'
      WRITE(7,'(A,1X,I3,$)')'The angular range is from 0 to',360/NDIV
      WRITE(7,'(A)')' degrees'
      WRITE(7,'(/,A,I5,/)')'Grid dimension ',NDIM
      WRITE(7,100)V3,V6,V9
      WRITE(7,101)G0

      STEP=3.141592653d0/NDIM
      NMAX=2*NDIM/NDIV  !The length of the eigenvectors before expansion
                                      !by symmetry through WAVEXTEND
      FAC=STEP**2
      PREC=PREC/G0
      V3=V3/G0
      V6=V6/G0
      V9=V9/G0

      PREC=FAC*PREC
      WRITE(6,'(A,$)')'Lower limit of energy band (cm-1) :'
      READ(5,*)ETL
      ETL=ETL*FAC/G0
      WRITE(6,'(A,$)')'Upper limit of energy band (cm-1) :'
      READ(5,*)ETU
      ETU=ETU*FAC/G0

      X=0.5d0*STEP
      V_min=1.0D6
      V_max=-1.0D6
      DO 1 I=1,NMAX
            V_temp=POTL(X)
            IF(V_temp.LT.V_min)V_min=V_temp
            IF(V_temp.GT.V_max)V_max=V_temp
            V(I)=V_temp*FAC
            X=X+STEP
      CONTINUE
            print*,'V_min = ',V_min*G0
            WRITE(7,'(A,F8.3,2X,A,F8.3)')'V_min = ',V_min*G0,'V_max = ',
     &      V_MAX*G0
            IF(ABS(V_min).GE.tiny)THEN !Potential minimum is shifted to zero
```

```
              V_shift=V_min*FAC
              DO 5 I=1,NMAX
                V(I)=V(I)-V_shift
5          CONTINUE
        ENDIF
      DO 2 I=1,NMAX !the diagonal elements of the Hamiltonian
                        !are filled
2       H(I)=2.0d0+V(I)

C Termination for ungerade solutions
      CASE='nn'
      H1_hold=H(1)
      H(1)=H1_hold+1
      H_hold=H(NMAX)
      H(NMAX)=H_hold+1.0d0
      print*,'HN ungerade ',H(NMAX)
      print*,'H1 ...... ',H(1)

      NL=N2COUNT(ETL,H,NMAX)
      NU=N2COUNT(ETU,H,NMAX)
      print*,'NL = ',NL
      print*,'NU = ',NU
6     IF(NL.EQ.NU)THEN
            print*,'Too narrow an energy range specified'
            WRITE(*,'(A,$)')'Enter new value of lower limit '
            WRITE(*,'(A,$)')'(negative value to stop) :'
            READ(*,*)ETL
            ETL=ETL*FAC/G0
            IF(ETL.LT.0)STOP
            WRITE(*,'(A,$)')'Enter new value of upper limit :'
            READ(*,*)ETU
            ETU=ETU*FAC/G0
            NL=N2COUNT(ETL,H,NMAX)
            NU=N2COUNT(ETU,H,NMAX)
            GOTO 6
      ENDIF
      ESP=(ETU-ETL)/(NU-NL)  ! The average spacing of states
      ETU_hold=ETU
      ETL_hold=ETL  ! Retains old lower limit, which is changed by
                    ! BISECT
      ETL=ETU-ESP  !Crude attempt at fixing a lower limit for
                    ! highest eigenstate, corrected within BISECT
      DO 3 NQ=NU,NL+1,-1
      CALL BISECT(ETL,ETU,NQ,PREC,E,N2COUNT)
            EIGEN_nn(NQ)=E
C           ETU=E-PREC          !To bring new ETU just below E(NQ)
        ETU=ETL
            IF(NQ-NL+1.GT.0)THEN
            ESP=(ETU-ETL_HOLD)/(NQ-NL+1) !up-date average spacing
            ENDIF
C           ETL=ETU-ESP         !First estimate of new lower limit
3     CONTINUE

      WRITE(7,'(/,A,/)')'Eigenvalues for node-node termination'
            WRITE(6,'(6X,A,6x,A,6x,A)')' n','E(n)','Nodal planes'
            WRITE(7,'(6X,A,6x,A,6x,A)')' n','E(n)','Nodal planes'
            DO 8 NQ=NU,NL+1,-1
              WRITE(6,104)NQ,EIGEN_nn(NQ)*G0/FAC,NDIV/2*(NQ)
          WRITE(7,104)NQ-1,EIGEN_nn(NQ)*G0/FAC,NDIV/2*(NQ)
C The count of the nodal planes will include the one passing through
C 0/PI.

8     CONTINUE

C Antinode-antinode termination
      CASE='aa'
      H(1)=H1_hold-1.0d0
      H(NMAX)=H_hold-1.0d0
      ETL=ETL_hold
      ETU=ETU_hold
```

```
      NL=N2COUNT(ETL,H,NMAX)
                NU=N2COUNT(ETU,H,NMAX)
                IF(NL.EQ.NU)THEN
                print*,'Too narrow an energy range specified'
                print*,'Lower limit changed to Te'
                   ETL=0
                   NL=N2COUNT(ETL,H,NMAX)
                ENDIF
                ESP=(ETU-ETL)/(NU-NL)  !
                 ETL=ETU-ESP

                 DO 4 NQ=NU,NL+1,-1
                   CALL BISECT(ETL,ETU,NQ,PREC,E,N2COUNT)
           EIGEN_aa(NQ)=E
                   ETU=E-PREC

                   IF(NQ-NL+1.GT.0)THEN
                   ESP=(ETU-ETL_HOLD)/(NQ-NL+1)
                   ENDIF
C                  ETL=ETU-ESP
 4        CONTINUE
      WRITE(6,'(/,A)')'Eigenvalues for antinode-antinode termination'
      WRITE(7,'(/,A)')'Eigenvalues for antinode-antinode termination'
      WRITE(6,'(6X,A,6x,A,6x,A)')' n','E(n)','Nodal planes'
      WRITE(7,'(6X,A,6x,A,6x,A)')' n','E(n)','Nodal planes'
      DO 7 NQ=NU,NL+1,-1
                 WRITE(6,104)NQ,EIGEN_aa(NQ)*G0/FAC,NDIV/2*(NQ-1)
        WRITE(7,104)NQ-1,EIGEN_aa(NQ)*G0/FAC,NDIV/2*(NQ-1)
 7     CONTINUE

      IF(NDIV.EQ.3)THEN
      CASE='na'
      H(1)=H1_hold+1d0
      H(NMAX)=H_hold-1d0
      ETL=ETL_hold
      ETU=ETU_hold
      NL=N2COUNT(ETL,H,NMAX)
      NU=N2COUNT(ETU,H,NMAX)
      print*,'NL = ',NL
      print*,'NU = ',NU
13     IF(NL.EQ.NU)THEN
                print*,'Too narrow an energy range specified'
                WRITE(*,'(A,$)')'Enter new value of lower limit '
                WRITE(*,'(A,$)')'(negative value to stop) :'
                READ(*,*)ETL
                ETL=ETL*FAC/G0
                IF(ETL.LT.0)STOP
                WRITE(*,'(A,$)')'Enter new value of upper limit :'
                READ(*,*)ETU
                ETU=ETU*FAC/G0
                NL=N2COUNT(ETL,H,NMAX)
                NU=N2COUNT(ETU,H,NMAX)
                GOTO 13
     ENDIF
     ESP=(ETU-ETL)/(NU-NL)  ! The average spacing of states
     ETU_hold=ETU
     ETL_hold=ETL  ! Retains old lower limit, which is changed by
                                 ! BISECT
     ETL=ETU-ESP   !Crude attempt at fixing a lower limit for
                                 ! highest eigenstate, corrected within BISECT
      DO 14 NQ=NU,NL+1,-1
     CALL BISECT(ETL,ETU,NQ,PREC,E,N2COUNT)
               EIGEN_na(NQ)=E
C              ETU=E-PREC              !To bring new ETU just below E(NQ)
       ETU=ETL
               IF(NQ-NL+1.GT.0)THEN
               ESP=(ETU-ETL_HOLD)/(NQ-NL+1) !up-date average spacing
               ENDIF
C              ETL=ETU-ESP              !First estimate of new lower limit
14     CONTINUE
```

```
      WRITE(7,'(/,A,/)')'Eigenvalues for node-antinode termination'
            WRITE(6,'(6X,A,6x,A,6x,A)')' n','E(n)','Nodal planes'
            WRITE(7,'(6X,A,6x,A,6x,A)')' n','E(n)','Nodal planes'
            DO 15 NQ=NU,NL+1,-1
              WRITE(6,104)NQ,EIGEN_na(NQ)*G0/FAC,NDIV/2*(NQ)
         WRITE(7,104)NQ-1,EIGEN_na(NQ)*G0/FAC,NDIV/2*(NQ)
C The count of the nodal planes will include the one passing through
C 0/PI.
15   CONTINUE

      ENDIF

16   WRITE(6,'(/,2A,$)')'Wave function stored for',
     &'which symmetry state, aa, nn, or na ?'
      READ(*,'(A2)') CASE
      IF(CASE.NE.'aa'.AND.CASE.NE.'nn'.AND.CASE.NE.'na')STOP
      WRITE(8,'(A)')CASE
      WRITE(6,'(/,A,$)')'Which quantum number ?'
      READ(*,*)NQ
      IF(CASE.EQ.'nn')THEN
      NSYM=-1   !A node will be introduced at 2*PI/NDIV in the
                        !extended wave function
      H(1)=H1_hold+1.0d0
      H(NMAX)=H_hold+1.0d0
      E=EIGEN_nn(NQ)
      ELSEIF(CASE.EQ.'aa')THEN
      NSYM=1    !An antinode will be introduced at multiples of
                        !2*PI/NDIV in the extended wave function
      H(1)=H1_hold-1.0d0
      H(NMAX)=H_hold-1.0d0
      E=EIGEN_aa(NQ)
      ELSE
            NSYM=1
        H(1)=H1_hold+1d0
            H(NMAX)=H_hold-1d0
            E=EIGEN_na(NQ)
      ENDIF

      CALL GRADET(E,FDET,BDET,GRAD,NMAX)
      print*,'GRADET= ',GRAD
      print*,'FDET = ',FDET(NMAX)
      print*,'bdet =',bdet(1)
      E=E+FDET(NMAX)/GRAD
      call GRADET(E,FDET,BDET,GRAD,NMAX)
      print*,'GRADET= ',GRAD
              print*,'FDET = ',FDET(NMAX)
                        print*,'bdet =',bdet(1)
      E=E+FDET(NMAX)/GRAD
      call GRADET(E,FDET,BDET,GRAD,NMAX)
      print*,'GRADET= ',GRAD
              print*,'FDET = ',FDET(NMAX)
                        print*,'bdet =',bdet(1)

      CALL WAVER(FDET,BDET,WAV,NMAX)
       OPEN(UNIT=8,FILE='rotor3_bal.wave')
      CALL WAVEXTEND(NDIV,NSYM,WAV,CASE,REPLY)
      close(UNIT=8)!only the latest wave function is stored for reference
C The Chosen wave function is now in WAV
      IF(REPLY.EQ.'yes')THEN
            IF(CASE.NE.CASE1)THEN
              PRINT*,'The two states have different symmetry'
              goto 16
        ENDIF
            CALL OVERLAP(WAV,WAV_init,FC)
            WRITE(7,'(/,3A,I3,$)')'Symm = ',CASE,' qu. no = ',NQ
            WRITE(6,'(A,D12.4)')'Overlap = ',FC
            WRITE(7,'(2X,A,D12.4)')'Overlap = ',FC
            GOTO 16
      endif
```

```
   STOP

100  FORMAT(2X,'V3 = ',F8.3,2X,'V6 = ',F8.3,2X,'V9 = ',
   &2X,F8.3)
101  FORMAT(2X,'G0 = ',F8.3,' (the rotational constant)')
102  FORMAT(2X,'Moment of intertia = ',F8.3,' amu A**2')
104  FORMAT(5X,I3,3X,F11.6,8X,I3)
105  FORMAT(D14.8)
   END

        FUNCTION N2COUNT(E,A,NMAX)
C Counts the number of sign changes in the sequence of forward DETS
C of the modified tridiagonal form in which the squares of the
C off-diagonal entries are stored in the array B.
        IMPLICITDOUBLEPRECISION(A-H,O-Z)
        PARAMETER(NDIM=3000)
        DIMENSION A(NDIM)
        N=0
        OR=1/(A(1)-E)
        IF(OR.LT.0)N=N+1
        DO 1 I=2,NMAX
                R=A(I)-E-OR
                IF(R.LT.0)N=N+1
        OR=1/R
C       print*,OR
1       CONTINUE
        N2COUNT=N
        RETURN
        END


        SUBROUTINE BISECT(ETL,ETU,NQ,TOL,EOUT,NCOUNT)
C Finds the root with NQ sign changes in the lambda-det.
C Carries out bisection between initial limits ETL and ETU which are
C progressively narrowed until their difference is LE TOL. The number
C of sign changes in the lambda-det is found by calls of NCOUNT and
C the number of bisections is stored in NBIS.
        IMPLICITDOUBLEPRECISION(A-H,O-Z)
        EXTERNAL NCOUNT
        PARAMETER(NDIM=3000)
        COMMON/VECTORS/C(NDIM)
        COMMON/PARMS/FRAC,STEP,ESP,NMAX
        NBIS=0
2       NL=NCOUNT(ETL,C,NMAX)
        NU=NCOUNT(ETU,C,NMAX)
C       print*,'NL=',NL,' NU =',NU
        IF(NL.GE.NQ)THEN
          ETL=ETL-ESP
          GOTO 2
     ELSEIF(NU.LT.NQ)THEN
          ETU=ETU+ESP
          GOTO 2
     ENDIF
        ETEST=0.5*(ETL+ETU)
   NEW=NU
1       NODE=NEW
        NEW=NCOUNT(ETEST,C,NMAX)
        OETEST=ETEST
        NBIS=NBIS+1
        IF(NEW.LT.NQ)THEN
                ETL=ETEST
                ETEST=0.5*(ETL+ETU)
                IF(DABS(OETEST-ETEST).GT.TOL)GOTO 1
C               IF(NQ-NEW.EQ.2)GOTO 1
                IF(ABS(NEW-NODE).GT.1)GOTO 1
                EOUT=ETEST
C               print*,'NBIS = ',NBIS
                RETURN
        ELSE
                ETU=ETEST
```

```
                ETEST=0.5*(ETU+ETL)
                IF(DABS(ETEST-OETEST).GT.TOL)GOTO 1
                IF(ABS(NEW-NODE).GT.1)GOTO 1
                IF(NEW-NQ.EQ.1)GOTO 1

                EOUT=ETEST
        ENDIF
c       print*,'NBIS = ',NBIS
        RETURN
        END


    FUNCTION POTL(X)
    IMPLICITDOUBLEPRECISION(A-H,O-Z)
    COMMON/POT/G0,V3,V6,V9
    POTL=0.5d0*(V3*(1-COS(3*X))+V6*(1-COS(6*X))
   & +V9*(1-COS(9*X)))
    RETURN
    END

    SUBROUTINE GRADET(E,FDET,BDET,GRAD,NMAX)
    IMPLICITDOUBLE PRECISION(A-H,O-Z)
    PARAMETER(NDIM=3000)
    DIMENSION FDET(0:NDIM),BDET(1:NDIM+1)
    COMMON/VECTORS/H(NDIM)

    FDET(0)=1d0
    FDET(1)=H(1)-E
    DO 1 I=2,NMAX
          FDET(I)=(H(I)-E)*FDET(I-1)-FDET(I-2)
1    CONTINUE
    BDET(NMAX+1)=1d0
    BDET(NMAX)=H(NMAX)-E
    DO 2 I=NMAX-1,1,-1
          BDET(I)=(H(I)-E)*BDET(I+1)-BDET(I+2)
2    CONTINUE

    GRAD=BDET(2)
    DO 3 I=2,NMAX-1
          GRAD=GRAD+FDET(I-1)*BDET(I+1)
3    continue
    GRAD=GRAD+FDET(NMAX-1)
    RETURN
    END

    SUBROUTINE WAVER(FDET,BDET,WAV,NMAX)
    IMPLICITDOUBLE PRECISION(A-H,O-Z)
    PARAMETER(NDIM=3000)
    COMMON/NORMS/NODE,WNORM(0:100)
    DIMENSION FDET(0:NDIM),BDET(1:NDIM+1),WAV(NDIM)

    ISIGN=1
    NODE=0
    TNORM=DABS(BDET(2)) !The normalization integral is accumulated
    WAV(1)=TNORM
    WAV_1=WAV(1)
    WAV_2=1D-6
    WAV_max=0d0
    DO 1 I=2,NMAX-1  !the square of the wave fn is calculated
          WAV_t=DABS(FDET(I-1)*BDET(I+1))
          IF(WAV_t.GT.WAV_max)WAV_max=WAV_t
          TNORM=TNORM+WAV_t
          WAV(I)=WAV_t
1   CONTINUE
          WAV_t=DABS(FDET(NMAX-1))
     IF(WAV_t.GT.WAV_max)WAV_max=WAV_t
          TNORM=TNORM+WAV_t
          WAV(NMAX)=WAV_t

   TNORM=1/SQRT(TNORM)
```

```
            WAV(1)=SQRT(WAV(1))*TNORM
            IFLAG=1
       DO 2 I=2,NMAX-1           !Putting in the nodes and normalising over the interval
                                 !0 to NMAX
            WAV_0=WAV(I)
            IF(WAV_0.GT.WAV_1.AND.WAV_2.GT.WAV_1)THEN
              ISIGN=-ISIGN
              NODE=NODE+1
              IF(WAV_0.GT.WAV_2)THEN
              WAV(I-1)=-WAV(I-1)
              IFLAG=-1
              ENDIF
              TWAV=ISIGN*sqrt(WAV_0)*TNORM
              GWAV0=WAV(I-1)-WAV(I-2)
              GWAV1=TWAV-WAV(I-1)
              IF(DABS((GWAV1-GWAV0)/GWAV1).GT.1D-2)THEN
                ISIGN=-ISIGN
                IF(IFLAG.EQ.-1)THEN
                WAV(I-1)=-WAV(I-1)
                ENDIF
                NODE=NODE-1
         ENDIF
            ENDIF
            IFLAG=1
            WAV(I)=ISIGN*sqrt(WAV_0)*TNORM
            WAV_2=WAV_1
            WAV_1=WAV_0
C           print*, wav(i)
2    CONTINUE
     WAV(NMAX)=ISIGN*SQRT(WAV(NMAX))*TNORM

     RETURN
     END

     SUBROUTINE WAVEXTEND(NDIV,NSYM,WAV,CASE,REPLY)
     IMPLICITDOUBLEPRECISION(A-H,O-Z)
     CHARACTER CASE*2,REPLY*3
C Extends the wavefunction associated in WAV to occupy the
C full angular range 0-PI, i.e. to an array NDIM in length
C The full wave function is also normalised, using the partially
C accumulated normalisation in the appropriate WNORM(NROOT)
C array plus that of the symmetry-extended portion.

     PARAMETER(NDIM=3000)
     COMMON/NORMS/NODE,WNORM(0:100)
     COMMON/PARMS/FRAC,STEP,ESP,NMAX

     DIMENSION WAV(NDIM)

     DEG=180D0/NDIM
     NODE_t=0
          WRITE(8,'(A)')CASE
     IF(NSYM.EQ.-1)NODE_t=1 !The extra node passing though 0 & PI
     IF(NDIV.EQ.2)THEN !No extension to WAV is needed and the normalisation
                               !already extends from 0 to PI
     IF(REPLY.NE.'yes')WRITE(8,101)WAV(1)
          WAV_1=WAV(1)
     IF(REPLY.NE.'yes')THEN
       DO 1 I=2,NDIM
        WAV_0=WAV(I)
        IF(WAV_0/WAV_1.LT.0)NODE_t=NODE_t+1
        WAV_1=WAV_0
         WRITE(8,101)WAV(I)
1      CONTINUE
     ELSE
          DO 7 I=2,NDIM
            WAV_0=WAV(I)
            IF(WAV_0/WAV_1.LT.0)NODE_t=NODE_t+1
            WAV_1=WAV_0
7    CONTINUE
```

```
      ENDIF
      print*,'Node count = ',NODE_t

      RETURN
      ENDIF

      IF(NDIV.EQ.3)THEN !The normalisation only extends to 2*PI/3
      N=NDIM-NMAX
       TNORM=0
      DO 2 I=1,N
               WAV(NMAX+I)=NSYM*WAV(NMAX-I+1)
               TNORM=TNORM+WAV(NMAX+I)**2 !the additional contribution to
                                                  !the normalisation integral
2      CONTINUE
      TNORM=1/SQRT(1+TNORM)
      WAV_1=WAV(1)*TNORM
      WAV(1)=WAV_1
      IF(REPLY.NE.'yes')THEN
      WRITE(8,101)WAV(1)
      DO 3 I=2,NDIM
               WAV_0=WAV(I)*TNORM
               IF(WAV_0/WAV_1.LT.0)NODE_t=NODE_t+1
               WAV(I)=WAV_0
               WAV_1=WAV_0
               WRITE(8,101)WAV_0
3      CONTINUE
       ELSE
       DO 8 I=2,NDIM
                WAV_0=WAV(I)*TNORM
                IF(WAV_0/WAV_1.LT.0)NODE_t=NODE_t+1
                WAV(I)=WAV_0
                WAV_1=WAV_0
8               CONTINUE
       ENDIF
       print*,'Node count = ',NODE_t
       RETURN
       ENDIF

       TNORM=0
       IF(NDIV.EQ.6)THEN
               N=2*NMAX
               DO 4 I=NMAX+1,N
                 WAV(I)=NSYM*WAV(N-I+1)
           TNORM=TNORM+WAV(I)**2
4         CONTINUE
               PRINT*,'NORM2 = ',TNORM
               N=3*NMAX
               N4=4*NMAX
               DO 5 I=2*NMAX+1,N
                 WAV(I)=NSYM*WAV(N4-I+1)
                 TNORM=TNORM+WAV(I)**2

5         CONTINUE
         PRINT*,'NORM3= ',TNORM
       TNORM=1/SQRT(1+TNORM)
               WAV_1=WAV(1)*TNORM
               WAV(1)=WAV_1
               IF(REPLY.NE.'yes')THEN
        WRITE(8,101)WAV(1)
                 DO 6 I=2,NDIM
            WAV_0=WAV(I)*TNORM
            IF(WAV_0/WAV_1.LT.0)NODE_t=NODE_t+1
            WAV_1=WAV_0
                   WAV(I)=WAV_0
                WRITE(8,101)WAV_0
6       CONTINUE
       ELSE
                DO 9 I=2,NDIM
                 WAV_0=WAV(I)*TNORM
                 IF(WAV_0/WAV_1.LT.0)NODE_t=NODE_t+1
```

```
            WAV_1=WAV_0
            WAV(I)=WAV_0
9     CONTINUE
      ENDIF
      print*,'Node count = ',NODE_t

      ENDIF

100  FORMAT(2X,F8.2,2X,D12.6)
101  FORMAT(D14.8)
      RETURN
      END

      SUBROUTINE OVERLAP(WAV1,WAV2,FC)
      IMPLICITDOUBLEPRECISION(A-H,O-Z)
      PARAMETER(NDIM=3000)
      DIMENSION WAV1(NDIM),WAV2(NDIM)

      FC=0
      DO 1 I=1,NDIM
            FC=FC+WAV1(I)*WAV2(I)
1     CONTINUE
      print*,'FC= ',FC
      RETURN
      END
```

```
PROGRAM RotorC2v_bal
C Calculates a band of energy levels in the periodic potential V(x) specified
C analytically by a sum of harmonic terms of the from 1/2Vn(1+cos2n*PHI). The
C inertial factor G is angle independent for a balanced rotor. n runs from 1 to
NPOT, so the two term potential V2 & V4 would require NPOT=2.

C Since the potential V(PHI) has C2v symmetry, it repeats after PHI=PI/2 and so
C both the potential V(x) and the eigenvectors WAV(x) are tabulated from
C x=STEP to x=PI/2-STEP, not from 0 to PI. x=0 and x=PI/2 are either nodes
C or antinodes (a); the combination a/a generates A1 species, a/n gives B1, n/n
C A2 and n/a B2.  Each termination requires a modification of the first and last
C diagonal entries of the Hamiltonian matrix (stored in the arrays H1 and H2 for
C initial and final states)

C
C ROTOR2_fc is based on ROTOR2, but simulates a fluorescence/absorption spectrum
C from a band of levels of the initial state to a band of eigenstates on the final
C surface. The initital state is designated (1), the final (2) and the eigenenergies
C are stored in EIGEN1 and EIGEN2 respectively. The array EIGEN1 is filled to full
Cprecision, but no wave functions are stored until required for the FC calculations,
C when they are re-calculated for each row of the Deslandres table.
```

```
      IMPLICITDOUBLE PRECISION(A-H,O-Z)
      EXTERNAL N2COUNT
      PARAMETER(NDIM=1500) !Number of quadrature points
      PARAMETER(NLEVEL=100) !Maximum number of tortional levels
      PARAMETER(NPOT=4)    !The number of parameters in the potential

      DIMENSION EIGEN1(50),EIGEN2(50),FC12(50),DE1(0:50),DE2(0:50)
      DIMENSION FDET(0:NDIM),BDET(1:NDIM+1),WAV1(NDIM),WAV2(NDIM)
      CHARACTER SYM1*1,SYM2*1,S_word*3

      COMMON/POT1/VP1(NPOT)
      COMMON/POT2/VP2(NPOT)
      COMMON/PARMS/FAC,STEP,ESP,NMAX
      COMMON/VECTORS1/H1(NDIM)
      COMMON/VECTORS2/H2(NDIM)
      COMMON/NORMS/NPOS(NLEVEL),WNORM     !Stores normalization and position of nodes
      DIMENSION AVCOS2_1(NLEVEL),AVCOS4_1(NLEVEL)!Stores average value of
                    ! cos(2*phi) and cos(4*phi) in each level of state (1)
      DIMENSION AVCOS2_2(NLEVEL),AVCOS4_2(NLEVEL) !and in state (2)

C     The reading list for the input file C2v.in is the character n or a (for node
C     or antinode at phi=0 and pi/2 respectively) on lines 1
C     and 2, followed by a list of the Vn coeffs, then the rotational constant and
C     finally the precision for root finding (start with .01 unless two roots of
C     the same symmetry are closer than this) The second block of input data, read
C     after the upper state eigenvalues have been calculated, consists of the Vn
C     and G value for the second state (the symmetry conditions are automatically
C     transferred)
      OPEN(UNIT=1,FILE='C2v.in')
      OPEN(UNIT=7,FILE='C2v.results')

      READ(1,'(A)')SYM1
      READ(1,'(A)')SYM2
      print*,SYM1,SYM2
      IF(SYM1.NE.'a'.AND.SYM1.NE.'n')THEN
      PRINT*,'Unrecognised symmetry instruction'
      PRINT*,'Input must be headed by a a or a n etc'
      STOP
      ENDIF
      S_word=SYM1//'/'//SYM2
11    READ(1,*)(VP1(I),I=1,NPOT) !the parameters of the initial potential
      READ(1,*)G1 !the initial g value
      READ(1,*)PREC     !the precision of bisection in cm-1

      PI=3.1415926536d0
      tiny = PREC

      PHIMAX=PI/2.0d0  !The angular range is 0-PI/2
      MAXDEG=NINT(PHIMAX/PI*180d0)
      WRITE(7,'(A,$)')'The internal rotor problem with '
      WRITE(7,'(A)')'a twofold axis of symmetry'
      WRITE(7,'(3A)')'Solutions for ',S_word,' case'
      WRITE(7,'(A,1X,I3,$)')'The angular range is from 0 to',MAXDEG
      WRITE(7,'(A)')' degrees'
      WRITE(7,'(/,A,I5,/)')'Grid dimension ',NDIM
      WRITE(7,'(2A)')'Coeffs V(1)-V(NPOT) for first state potential',
     &' are ;'
      WRITE(7,100)VP1
      WRITE(7,'(A,F7.4)')'Inertial constant for state (1) ',G1
      STEP=PHIMAX/NDIM
      HSTEP=STEP/2d0
      NMAX=NDIM
      FAC=STEP**2
      RG1=1d0/G1
      PREC=PREC*RG1
      DO 12 I=1,NPOT  !The potential parameters are scaled by the rotational
                      ! constant
        VP1(I)=VP1(I)*RG1
12    CONTINUE
      PREC=FAC*PREC
```

```
      X=0.5d0*STEP
      HX=STEP
      V_min=POTL1(0d0,VP1)
      V_2=POTL1(X,VP1)     !V(-x)=V(x)
      V_1=V_min
      V_max=-1.0D6
      IMIN=0         !Counter for number of minima in V(x)
      IMAX=0         !Counter for number of maxima in V(x)
      MIN=0
      DO 1 I=1,NMAX
             V_0=POTL1(X,VP1)
             IF(V_0.LT.V_min)THEN
               V_min=V_0
               N_min=I
               ENDIF
             IF(V_0.GT.V_max)THEN
               V_max=V_0
               N_max=I
        ENDIF
             IF(V_0.GT.V_1.AND.V_1.LE.V_2)THEN
               MIN=I-1
               IMIN=IMIN+1
             ENDIF
             IF(V_0.LT.V_1.AND.V_1.GE.V_2) IMAX=IMAX+1

             H1(I)=V_0*FAC+2d0
             V_2=V_1
             V_1=V_0
             X=X+STEP
1      CONTINUE
             print*,'final HX= ',HX-STEP
             V_0=V_1
             V_2=V_1
             V_1=POTL1(PHIMAX,VP1)
             IF(V_0.GT.V_1.AND.V_1.LE.V_2)IMIN=IMIN+1
             IF(V_1.LT.V_min)THEN
               V_min=v_1
               N_min=NMAX
        ENDIF
             IF(V_0.LT.V_1.AND.V_1.GE.V_2)IMAX=IMAX+1
             IF(V_1.GT.V_max)THEN
               V_max=V_1
               N_max=NMAX
               ENDIF

             print*,'V_min = ',V_min/RG1
             print*,'V_max = ',V_max/RG1
       WRITE(7,'(/,A,2X,I3,A)')'The first state potential :'
             WRITE(7,103)'V_min = ',V_min/RG1,' at alpha = ',
      &(N_min+0.5)*step/PI*180d0,' deg.'
       WRITE(7,103)'V_max = ', V_max/RG1,' at alpha = ',
      &(N_max+0.5)*step/PI*180d0,' deg.'
             print*,' No. of minima = ',IMIN
             print*,'No. of maxima = ',IMAX
             print*,'MIN=',MIN
             IF(MIN.NE.0)THEN
                WRITE(7,'(A,F8.2)')'Barrier at alpha=0 :',
      &         POTL1(0,VP1)/RG1
             ENDIF
             IF(ABS(V_min).GE.tiny)THEN !Potential minimum is shifted to zero
             print*,'V_min is shifted by ',V_min
               V_shift=V_min*FAC
               DO 5 I=1,NMAX
                 H1(I)=H1(I)-V_shift
5         CONTINUE
        ENDIF

       H1_hold=H1(1)
       H_hold=H1(NMAX)
```

```
C Termination for gerade solutions
     IF (SYM1.EQ.'n')THEN
       H1(1)=H1_hold+1d0
     ELSE
       H1(1)=H1_hold-1d0
     ENDIF
     IF(SYM2.EQ.'n')THEN
       H1(NMAX)=H_hold+1d0
     ELSE
            H1(NMAX)=H_hold-1d0
     ENDIF
       print*,'HN ungerade ',H1(NMAX)
       print*,'H1 ...... ',H1(1)


     WRITE(6,'(A,$)')'Lower limit of energy band (cm-1) '
     WRITE(6,'(A,$)')'in first state :'
     READ(5,*)ETL
     ETL=ETL*FAC*RG1
     WRITE(6,'(A,$)')'Upper limit of energy band (cm-1) '
     WRITE(6,'(A,$)')'in first state :'
     READ(5,*)ETU
     ETU=ETU*FAC*RG1
     NL1=N2COUNT(ETL,H1,NMAX)
     NU1=N2COUNT(ETU,H1,NMAX)
     print*,'NL1 = ',NL1
     print*,'NU1 = ',NU1
10     IF(NL1.EQ.NU1.AND.NL1.EQ.0)THEN
            print*,'Too narrow an energy range specified'
            WRITE(*,'(A,$)')'Enter new value of upper limit :'
            READ(*,*)ETU
            ETU=ETU*FAC*RG1
            NL1=N2COUNT(ETL,H1,NMAX)
            NU1=N2COUNT(ETU,H1,NMAX)
     print*,'NU1 = ',NU1,' NL1 = ',NL1
            GOTO 10
            ENDIF

     IF(NU1.EQ.NL1)THEN
            ETL=ETU-ETU/NU1
            NL1=NU1-1
            ELSE
              ESP=(ETU-ETL)/(NU1-NL1)
     ENDIF


            DO 6 NQ=NU1,NL1+1,-1
       CALL BISECT(ETL,ETU,NQ,PREC,H1,E,N2COUNT)
       CALL GRADET1(E,FDET,BDET,GRAD,NMAX)
       E=E+FDET(NMAX)/GRAD
       CALL GRADET1(E,FDET,BDET,GRAD,NMAX)
       E=E+FDET(NMAX)/GRAD
       CALL GRADET1(E,FDET,BDET,GRAD,NMAX)
              E=E+FDET(NMAX)/GRAD
              if(ABS(fdet(NMAX)-BDET(1))/ABS(BDET(1)).LT.0.1)THEN
               CALL GRADET1(E,FDET,BDET,GRAD,NMAX)
               E=E+FDET(NMAX)/GRAD
       ENDIF
C     print*,'GRADET1= ',GRAD
C     print*,'FDET = ',FDET(NMAX)
C     print*,'bdet =',bdet(1)
       EIGEN1(NQ)=E  !The array of first state energies is filled
              ETU=E-PREC
6    CONTINUE


C End of first state calculation. The band of lower states is now tackled

    READ(1,*)(VP2(i),I=1,NPOT) !the parameters of the second state potential
```

```
      READ(1,*)G2              !the G-parameter of the  second state
      WRITE(7,'(/,A,F7.4,A)')'Inertial constant for state (2) ',G2,
     &' cm-1'

      WRITE(7,'(/,A,I1,3A)')'Coeffs V(1)-V(',NPOT,')',
     &' for second state potential are ;'
      WRITE(7,100)VP2

      RG2=1/G2
      DO 15 I=1,6
        VP2(I)=VP2(I)*RG2
 15    CONTINUE

      X=0.5d0*STEP
      V_min=POTL1(0d0,VP2)
      V_2=POTL1(X,VP2)      !V(-x)=V(x)
      V_1=V_min
      V_max=V_min
      IMIN=0          !Counter for number of minima in V(x)
      IMAX=0           !Counter for number of maxima in V(x)
      MIN=0
      DO 17 I=1,NMAX
            V_0=POTL1(X,VP2)
            IF(V_0.LT.V_min)THEN
        V_min=V_0
        N_min=I
              ENDIF

            IF(V_0.GT.V_max)THEN
              V_max=V_0
              N_max=I
       ENDIF
            IF(V_0.GT.V_1.AND.V_1.LE.V_2)THEN
              MIN=I-1
              IMIN=IMIN+1
              ENDIF

            IF(V_0.LT.V_1.AND.V_1.GE.V_2)IMAX=IMAX+1
            H2(I)=V_0*FAC+2d0
            V_2=V_1
            V_1=V_0
            X=X+STEP
 17   CONTINUE

            V_0=V_1
            V_2=V_1
            V_1=POTL1(PI,VP2)
            IF(V_0.GT.V_1.AND.V_1.LE.V_2)IMIN=IMIN+1
            IF(V_1.LT.V_min)THEN
              V_min=v_1
              N_min=NMAX
       ENDIF
            IF(V_0.LT.V_1.AND.V_1.GE.V_2)IMAX=IMAX+1
            IF(V_1.GT.V_max)THEN
              V_max=V_1
              N_max=NMAX
              ENDIF

            print*,'V_min = ',V_min/RG2

     WRITE(7,'(/,A,2X,I3,A)')'The second state potential :'
            WRITE(7,103)'V_min = ',V_min/RG2,' at alpha = ',
    &(N_min+0.5)*step/PI*180d0,' deg.'
     WRITE(7,103)'V_max = ', V_max/RG2,' at alpha = ',
    &(N_max+0.5)*step/PI*180d0,' deg.'

            print*,' No. of minima = ',IMIN
            print*,'No. of maxima = ',IMAX
            IF(MIN.NE.0)THEN
              write(7,'(A,F8.2)')'Barrier at phi= 0 ;',
```

```
  &(POTL1(0d0,VP2)+V_min)/RG2
         endif
         IF(ABS(V_min).GE.tiny)THEN !Potential minimum is shifted to zero
          print* ,'Zero of energy of state (2) shifted by ',V_min/RG2
          WRITE(7,'(2A,F8.3,A)')'Zero of energy of state (2)',
  &       ' shifted by ',V_min/RG2,'cm-1'
          V_shift=V_min*FAC
          DO 18 I=1,NMAX
            H2(I)=H2(I)-V_shift
18     CONTINUE
    ENDIF

   H1_hold=H2(1)
   H_hold=H2(NMAX)

   IF (SYM1.EQ.'n')THEN
    H2(1)=H1_hold+1d0
   ELSE
    H2(1)=h1_hold-1d0
   ENDIF
   IF(SYM2.EQ.'n')THEN
    H2(NMAX)=H_hold+1d0
   ELSE
         H2(NMAX)=H_hold-1d0
   ENDIF

   WRITE(6,'(A,$)')'Lower limit of energy band (cm-1) '
   WRITE(6,'(A,$)')'in ground state :'
   READ(5,*)ETL
   ETL=ETL*FAC*RG2
   WRITE(6,'(A,$)')'Upper limit of energy band (cm-1) '
   WRITE(6,'(A,$)')'in ground state :'
   READ(5,*)ETU
   ETU=ETU*FAC*RG2
   NL2=N2COUNT(ETL,H2,NMAX)
   NU2=N2COUNT(ETU,H2,NMAX)
   print*,'NL2 = ',NL2
   print*,'NU2 = ',NU2
20  IF(NL2.EQ.NU2)THEN
        print*,'Too narrow an energy range specified'
        WRITE(*,'(A,$)')'Enter new value of lower limit '
        WRITE(*,'(A,$)')'(negative valuc to stop) :'
        READ(*,*)ETL
        IF(ETL.LT.0)STOP
        ETL=ETL*FAC*RG2
        WRITE(*,'(A,$)')'Enter new value of upper limit :'
        READ(*,*)ETU
        ETU=ETU*FAC*RG2
        NL2=N2COUNT(ETL,H2,NMAX)
        NU2=N2COUNT(ETU,H2,NMAX)
        GOTO 20
  ENDIF

  ESP=(ETU-ETL)/(NU2-NL2)  ! The average spacing of states
  ETU_hold=ETU
  ETL_hold=ETL  ! Retains old lower limit, which is changed by
                ! BISECT
  ETL=ETU-ESP  !Crude attempt at fixing a lower limit for
                ! highest eigenstate, corrected within BISECT

  WRITE(7,'(/,A)')'       The FC factor table'
  WRITE(7,'(2X,A,50(I2,6X,$))')'n1 ',(I-1,I=NL1+1,NU1)
  WRITE(7,'(2X,A)')'  Sum FC'
  WRITE(7,'(A)')'n2'

  DO 21 NQ=NU2,NL2+1,-1
C  print*,'ETL = ',ETL,'ETU = ',ETU
  CALL BISECT(ETL,ETU,NQ,PREC,H2,E,N2COUNT)
        EIGEN2(NQ)=E
        ETU=E-PREC          !To bring new ETU just below E(NQ)
```

```
          IF(NQ-NL2+1.GT.0)THEN
          ESP=(ETU-ETL_HOLD)/(NQ-NL2+1) !up-date average spacing
          ENDIF
          ETL=ETU-ESP         !First estimate of new lower limit
21    CONTINUE


   EIGEN1(NL1)=EIGEN1(NL1+1)
   EIGEN2(NL2)=EIGEN2(NL2+1)

   DO 22 NQ2=NL2+1,NU2
     SI_tot=0d0   !counts sum of FC factors over all transitions
     E=EIGEN2(NQ2)
     CALL GRADET2(E,FDET,BDET,GRAD,NMAX)
     E=E+FDET(NMAX)/GRAD
     CALL GRADET2(E,FDET,BDET,GRAD,NMAX)
     E=E+FDET(NMAX)/GRAD
     EIGEN2(NQ2)=E
          CALL GRADET2(E,FDET,BDET,GRAD,NMAX)
     CALL NORMER(FDET,BDET,NQ2,AVCOS2_2,AVCOS4_2)
          NPOS(NQ2)=0
          N2=N2COUNT(E,H2,NDIM) ! Fixes positions of nodes in lower state
                                          ! wave function, stored in NPOS array
     CALL WAVER(FDET,BDET,NQ2,WAV2)
    NDIFF=NQ2-1
    DE2(NQ2)=(E-EIGEN2(NDIFF))/(RG2*FAC)
          DO 23 NQ1=NL1+1,NU1
            E=EIGEN1(NQ1)
            CALL GRADET1(E,FDET,BDET,GRAD,NMAX) !fills FDET and BDET for
                                                !current level of state (1)

            IF(NQ2.LT.NU1)THEN
              CALL STORMER(FDET,BDET,NQ1)
            ELSE !the average angles are calculated the last time round
              CALL NORMER(FDET,BDET,NQ1,AVCOS2_1,AVCOS4_1)
            ENDIF
            N2=N2COUNT(E,H1,NDIM)
            CALL WAVER(FDET,BDET,NQ1,WAV1)
            FC12(NQ1)=FC(WAV1,WAV2)
            SI_TOT=SI_tot+FC12(NQ1)
            NDIFF=NQ1-1
      DE1(NQ1)=(E-EIGEN1(NDIFF))/(RG1*FAC)
23    CONTINUE
   print*,'Sum FC = ',SI_tot
   WRITE(6,'(I2,2X,50(F5.3,3X),/)')NQ2-1,(FC12(I),I=NL1+1,NU1)
   WRITE(7,'(I2,2X,50(F5.3,3X),/)')NQ2-1,(FC12(I),I=NL1+1,NU1)
  &,SI_tot
22    CONTINUE

   WRITE(7,'(/,3A)')'Eigenvalues for ',S_word,
  &' termination, state (1)'
          WRITE(6,'(6X,A,3(6x,A))')' n','E(n)','E(n)-E(n-1)'
  &'<cos(2*(phi)>'
          WRITE(7,'(6X,A,2(6x,A),2(2x,A))')' n','E(n)','E(n)-E(n-1)'
  &'<cos(2*(phi)>','<cos4*phi>'
   WRITE(6,104)(NQ-1,EIGEN1(NQ)/(RG1*FAC),DE1(NQ),
  &AVCOS2_1(NQ),AVCOS4_1(NQ),NQ=NL1+1,NU1)
   WRITE(7,104)(NQ-1,EIGEN1(NQ)/(RG1*FAC),DE1(NQ),
  &AVCOS2_1(NQ),AVCOS4_1(NQ),NQ=NL1+1,NU1)
   WRITE(7,'(/,3A)')'Eigenvalues for ',S_word,
  &' termination state (2)'
   WRITE(7,'(6X,A,2(6x,A),2(2x,A))')' n','E(n)','E(n)-E(n-1)'
  &'<cos(2*(phi)>'
   print*,AVCOS2_2(NU2)
   WRITE(6,104)(NQ-1,EIGEN2(NQ)/(RG2*FAC),DE2(NQ),
  &AVCOS2_2(NQ),AVCOS4_2(NQ),NQ=NL2+1,NU2)
   WRITE(7,104)(NQ-1,EIGEN2(NQ)/(RG2*FAC),DE2(NQ),
  &AVCOS2_2(NQ),AVCOS4_2(NQ),NQ=NL2+1,NU2)
```

```
100  FORMAT(2X,6(F8.3,2x))
101  FORMAT(5(2X,'(',I2,')',F6.3))
102  FORMAT(2X,'Moment of intertia = ',F8.3,' amu A**2')
103  FORMAT(X,A,F8.3,2X,A,F6.1,A)
104  FORMAT(5X,I3,3X,F9.4,6X,F7.3,4X,F8.3,7X,F7.3)
105  FORMAT(D13.6)
106  FORMAT(5X,I3,3X,F9.4,6X,F7.3,6x,D10.4,6X,I3,/)
107  FORMAT(5X,I3,3X,F9.4,6X,F7.3,6X,I3,/)
    END

          FUNCTION N2COUNT(E,A,NMAX)
C Counts the number of sign changes in the sequence of forward DETS
C of the modified tridiagonal form in which the squares of the
C off-diagonal entries are stored in the array B.
          IMPLICITDOUBLEPRECISION(A-H,O-Z)
          PARAMETER(NLEVEL=100)
    COMMON/NORMS/NPOS(NLEVEL),WNORM
          PARAMETER(NDIM=1500)
          DIMENSION A(NDIM)
          N=0
          J=1 !counter for node positions
          OR=1/(A(1)-E)
          IF(OR.LT.0)N=N+1
          DO 1 I=2,NMAX
                    R=A(I)-E-OR
                    IF(R.LT.0)THEN
                    N=N+1
                    NPOS(J)=I
                    J=J+1
                    ENDIF
          OR=1/R
1         CONTINUE
          N2COUNT=N
          RETURN
          END


          SUBROUTINE BISECT(ETL,ETU,NQ,TOL,C,EOUT,NCOUNT)
C Finds the root with NQ sign changes in the lambda-det.
C Carries out bisection between initial limits ETL and ETU which are
C progressively narrowed until their difference is < TOL. The number
C of sign changes in the lambda-det is found by calls of NCOUNT and
C the number of bisections is stored in NBIS.
          IMPLICITDOUBLEPRECISION(A-H,O-Z)
          EXTERNAL NCOUNT
          PARAMETER(NDIM=1500)
          DIMENSION C(NDIM)
          COMMON/PARMS/FAC,STEP,ESP,NMAX
          NBIS=0
2         NL=NCOUNT(ETL,C,NMAX)
          NU=NCOUNT(ETU,C,NMAX)
          IF(NL.GE.NQ)THEN
            ETL=ETL-ESP
            GOTO 2
    ELSEIF(NU.LT.NQ)THEN
            ETU=ETU+ESP
            GOTO 2
    ENDIF
          ETEST=0.5D0*(ETL+ETU)
1         NODE=NEW
          NEW=NCOUNT(ETEST,C,NMAX)
          OETEST=ETEST
          NBIS=NBIS+1
          IF(NEW.LT.NQ)THEN
                    ETL=ETEST
                    ETEST=0.5D0*(ETL+ETU)
                    IF(ABS(OETEST-ETEST).GT.TOL)GOTO 1
                    IF(ABS(NEW-NODE).GT.1)GOTO 1
                    EOUT=ETEST
                    RETURN
```

```
        ELSE
                ETU=ETEST
                ETEST=0.5D0*(ETU+ETL)
                IF(ABS(ETEST-OETEST).GT.TOL)GOTO 1
                IF(ABS(NEW-NODE).GT.1)GOTO 1

                EOUT=ETEST
        ENDIF
        RETURN
        END


   FUNCTION POTL1(X,V)
         PARAMETER(NPOT=4)
  IMPLICITDOUBLEPRECISION(A-H,O-Z)
  DIMENSION V(NPOT)
  TPOT=0
  DO 1 I=1,NPOT
    TPOT=TPOT+0.5d0*V(I)*(1-cos(2*I*X))
1  CONTINUE
  POTL1=TPOT
  RETURN
  END


  SUBROUTINE GRADET1(E,FDET,BDET,GRAD,NMAX)
  IMPLICITDOUBLE PRECISION(A-H,O-Z)
  PARAMETER(NDIM=1500)
  DIMENSION FDET(0:NDIM),BDET(1:NDIM+1)
  COMMON/VECTORS1/H(NDIM)

  fdet(0)=1d0
  FDET(1)=H(1)-E
  DO 1 I=2,NMAX
        FDET(I)=(H(I)-E)*FDET(I-1)-FDET(I-2)
1  CONTINUE
  BDET(NMAX+1)=1d0
  BDET(NMAX)=H(NMAX)-E
  DO 2 I=NMAX-1,1,-1
        BDET(I)=(H(I)-E)*BDET(I+1)-BDET(I+2)
2  CONTINUE

  GRAD=BDET(2)
  DO 3 I=2,NMAX-1
        GRAD=GRAD+FDET(I-1)*BDET(I+1)
3  continue
  GRAD=GRAD+FDET(NMAX-1)
  RETURN
  END

  SUBROUTINE GRADET2(E,FDET,BDET,GRAD,NMAX)
  IMPLICITDOUBLE PRECISION(A-H,O-Z)
  PARAMETER(NDIM=1500)
  DIMENSION FDET(0:NDIM),BDET(1:NDIM+1)
  COMMON/VECTORS2/H(NDIM)

  fdet(0)=1d0
  FDET(1)=H(1)-E
  DO 1 I=2,NMAX
        FDET(I)=(H(I)-E)*FDET(I-1)-FDET(I-2)
1  CONTINUE
  BDET(NMAX+1)=1d0
  BDET(NMAX)=H(NMAX)-E
  DO 2 I=NMAX-1,1,-1
        BDET(I)=(H(I)-E)*BDET(I+1)-BDET(I+2)
2  CONTINUE

  GRAD=BDET(2)
  DO 3 I=2,NMAX-1
        GRAD=GRAD+FDET(I-1)*BDET(I+1)
```

```
3    continue
     GRAD=GRAD+FDET(NMAX-1)
     RETURN
     END

     SUBROUTINE STORMER(FDET,BDET)
C The normalisation constant of the current eigenvector stored in FDET,BDET
C is laced in WNORM
     IMPLICITDOUBLE PRECISION(A-H,O-Z)
     PARAMETER(NDIM=1500)
     PARAMETER(NLEVEL=100)
     COMMON/NORMS/NPOS(NLEVEL),WNORM
     COMMON/PARMS/FAC,STEP,ESP,NMAX
     DIMENSION FDET(0:NDIM),BDET(1:NDIM+1)

     NODE=0
     TNORM=ABS(BDET(2))
     WAV_max=0d0
     DO 1 I=2,NMAX-1  ! Psi**2 array is filled
            WAV_t=ABS(FDET(I-1)*BDET(I+1))
            IF(WAV_t.GT.WAV_max)WAV_max=WAV_t
            TNORM=TNORM+WAV_t   !The normalization integral is accumulated
1    CONTINUE
            WAV_t=ABS(FDET(NMAX-1))
       IF(WAV_t.GT.WAV_max)WAV_max=WAV_t
            TNORM=TNORM+WAV_t
     TNORM=1/sqrt(TNORM)
     WNORM=TNORM
     RETURN
     END

     SUBROUTINE NORMER(FDET,BDET,NROOT,AVCOS2,AVCOS4)
CThe normalisation constant of the current eigenvector split between FDET and
C BDET is found, and also the average values of cos(2*PHI) and cos(4*PHI), which
C are placed at the position NROOT in the arrays AVCOS2 and AVCOS4

     IMPLICITDOUBLE PRECISION(A-H,O-Z)
     PARAMETER(NDIM=1500)
     PARAMETER(NLEVEL=100)
     COMMON/NORMS/NPOS(NLEVEL),WNORM
     COMMON/PARMS/FAC,STEP,ESP,NMAX
     DIMENSION FDET(0:NDIM),BDET(1:NDIM+1),AVCOS2(NLEVEL)
     DIMENSION AVCOS4(NLEVEL)

     NODE=0
     TNORM=ABS(BDET(2))
     WAV_max=0d0
     TCOS2=COS(STEP)*TNORM
     TCOS4=COS(2*STEP)*TNORM
     DO 1 I=2,NMAX-1  ! Psi**2 array is filled
            WAV_t=ABS(FDET(I-1)*BDET(I+1))
            COS2_phi=COS((2*I-1)*STEP)
            COS4_phi=2*COS2_phi**2-1d0 !cos(4*phi)
       TCOS2=TCOS2+COS2_phi*WAV_t  !The average of cos(alpha) is
                                              !calculated by Simpson's rule
            TCOS4=TCOS4+COS4_phi*WAV_t
            IF(WAV_t.GT.WAV_max)WAV_max=WAV_t
            TNORM=TNORM+WAV_t   !The normalization integral is accumulated
1    CONTINUE
            WAV_t=ABS(FDET(NMAX-1))
       IF(WAV_t.GT.WAV_max)WAV_max=WAV_t
            TNORM=TNORM+WAV_t
            COS2_phi=COS((2*NMAX-1)*STEP)
            TCOS2=TCOS2+COS2_phi*WAV_t
            TCOS4=TCOS4+(2d0*COS2_phi**2-1d0)*WAV_t
     AVCOS2(NROOT)=TCOS2/TNORM
     AVCOS4(NROOT)=TCOS4/TNORM
     TNORM=1/sqrt(TNORM)
     WNORM=TNORM
     RETURN
```

```
      END

      SUBROUTINE WAVER(FDET,BDET,NROOT,WAV)
      IMPLICITDOUBLE PRECISION(A-H,O-Z)
      PARAMETER(NDIM=1500)
      PARAMETER(NLEVEL=100)
      COMMON/NORMS/NPOS(Nlevel),WNORM
      COMMON/PARMS/FAC,STEP,ESP,NMAX
      DIMENSION FDET(0:NDIM),BDET(1:NDIM+1),WAV(NDIM)

      J=1    !counter for node position
      NODE=0
      ISIGN=1
      TNORM=WNORM
      WAV_2=ABS(BDET(2))
      WAV(1)=SQRT(WAV_2)*TNORM
      WAV_1=ABS(FDET(1)*BDET(3))
      WAV(2)=SQRT(WAV_1)*TNORM
      K=NPOS(1)
      DO 2 I=3,NMAX-1              !Putting in the nodes
C     IF(I.GT.K+2)THEN  !To make up for a missed node
C NPOS(J)=0
C J=J+1
C K=NPOS(J)
C IF(K.EQ.0)K=NDIM
C     ENDIF
              WAV_0=ABS(FDET(I-1)*BDET(I+1))
              IF(WAV_0.GT.WAV_1.AND.WAV_2.GT.WAV_1)THEN
C         print*,'NODES', I,'  marker ',K
C     if(ABS(I-K).LE.2)THEN
                 ISIGN=-ISIGN
                 R=(WAV_2-WAV_1)/(WAV_1-WAV_0)
                 X=(R+1)/(R-1)
            IF(X.LT.0)THEN
                  WAV(I-1)=-WAV(I-1)
                 ENDIF
                        NPOS(J)=0
                  J=J+1
                        K=NPOS(J)
                        IF(K.EQ.0)K=NDIM
                  NODE=NODE+1
C     ENDIF
        ENDIF
              WAV(I)=ISIGN*sqrt(WAV_0)*TNORM
              WAV_2=WAV_1
              WAV_1=WAV_0
2     CONTINUE
      WAV(NMAX)=ISIGN*SQRT(ABS(FDET(NMAX-1)))*TNORM
      NPOS(NROOT)=0
C     WRITE(6,'(A,I3,/)')'No. of nodes counted = ',NODE
100   FORMAT(2x,F10.4,2x,D12.4)
      RETURN
      END

      FUNCTION FC(WAV1,WAV2)
      IMPLICITDOUBLE PRECISION(A-H,O-Z)
      PARAMETER(NDIM=1500)
      DIMENSION WAV1(NDIM),WAV2(NDIM)
      COMMON/PARMS/FAC,STEP,ESP,NMAX
      S=0d0
      DO 1 I=1,NDIM
            S=S+WAV1(I)*WAV2(I)
1     CONTINUE
      FC=S**2
      RETURN
      END
```

Appendix 3. Additional spectra of the Aminobenzotrifluorides

A.3.1. Introduction

The work on the ABTF's presented in chapter 5 does not show all the spectra obtained during the experimental work. This appendix presents the remaining spectra and includes both the torsional and the vibrational structure of all three isomers. The vibrational modes studied all show torsional structure similar to that of the origin band and are presented here rather than as a separate chapter for that reason.

A.3.2. 2-Aminobenzotrifluoride

A.3.2.1. The Ionic Ground State

The ionisation energy of the origin band of the D_0 state of 2-ABTF is shown in figure A.3.1. using a variety of extraction voltages. Extrapolation to zero field gives an adiabatic ionisation energy of 65373±3 cm^{-1}.

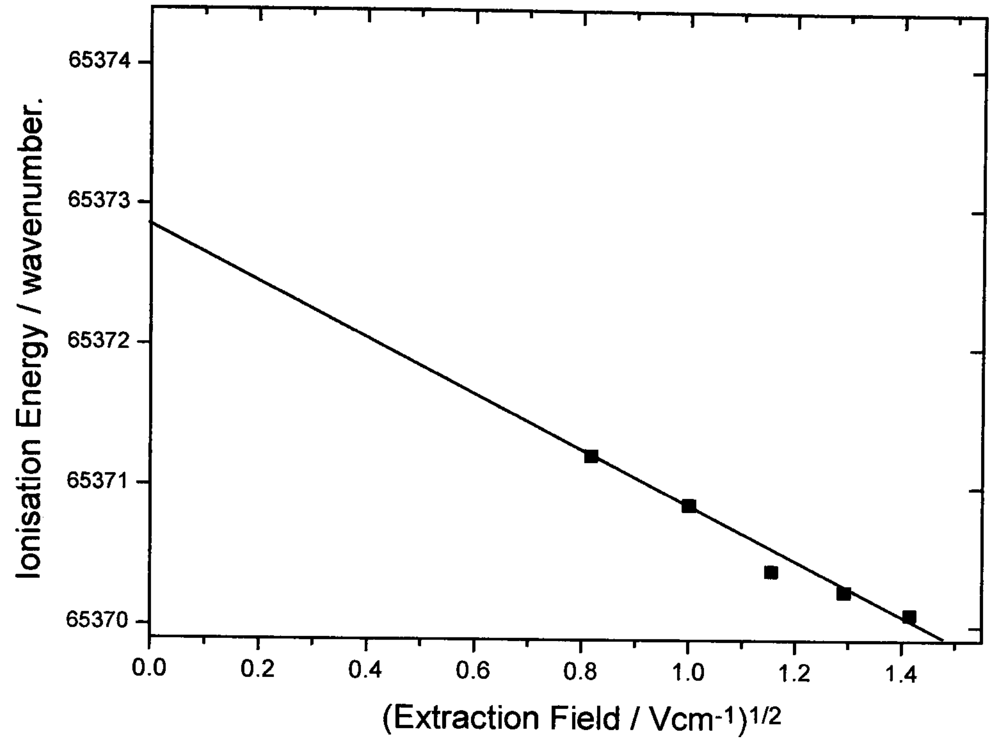

Figure A.3.1 : The ionisation energy of the ionic ground state of 2-ABTF using several values of extraction field. The field free ionisation energy is 65373 cm^{-1} as shown by extrapolation to zero field.

A.3.2.2. Vibrational Structure

The (1+1) MPI spectrum of the S_1 state of 2-ABTF is shown in figure A.3.2. and shows the vibrational modes of the molecule.These are assigned to the totally symmetric normal modes by comparison with previous work by Hollas and co-workers[1]. This assumes the molecule has overal C_s symmetry by treating the CF_3 group as an atom. Each vibrational state shows similar torsional structure to that of the origin band.

Figure A.3.3. and show the (1+1') ZEKE-PFI spectra via a number of these bands. The torsional structure is again very similar to that of the vibrationless state. Table A.3.1. lists the vibrational frequencies of the observed modes in the S_0, S_1 and ionic ground states.

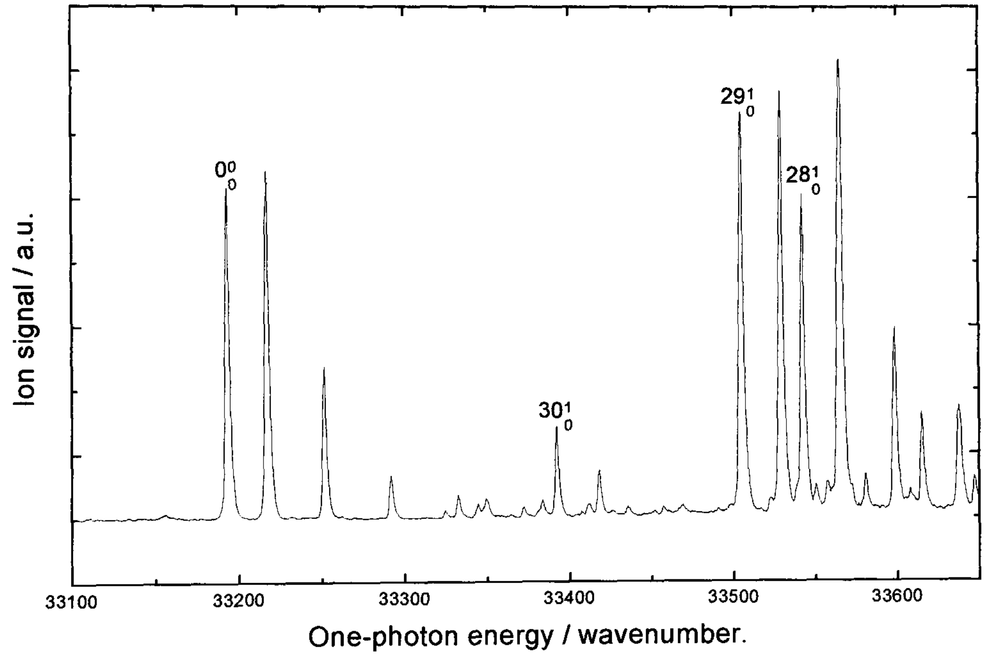

Figure A.3.2: (1+1) MPI spectrum of the S_1 state of 2-ABTF showing the vibrational modes. The torsional structure based on modes 28 and 29 is overlapped.

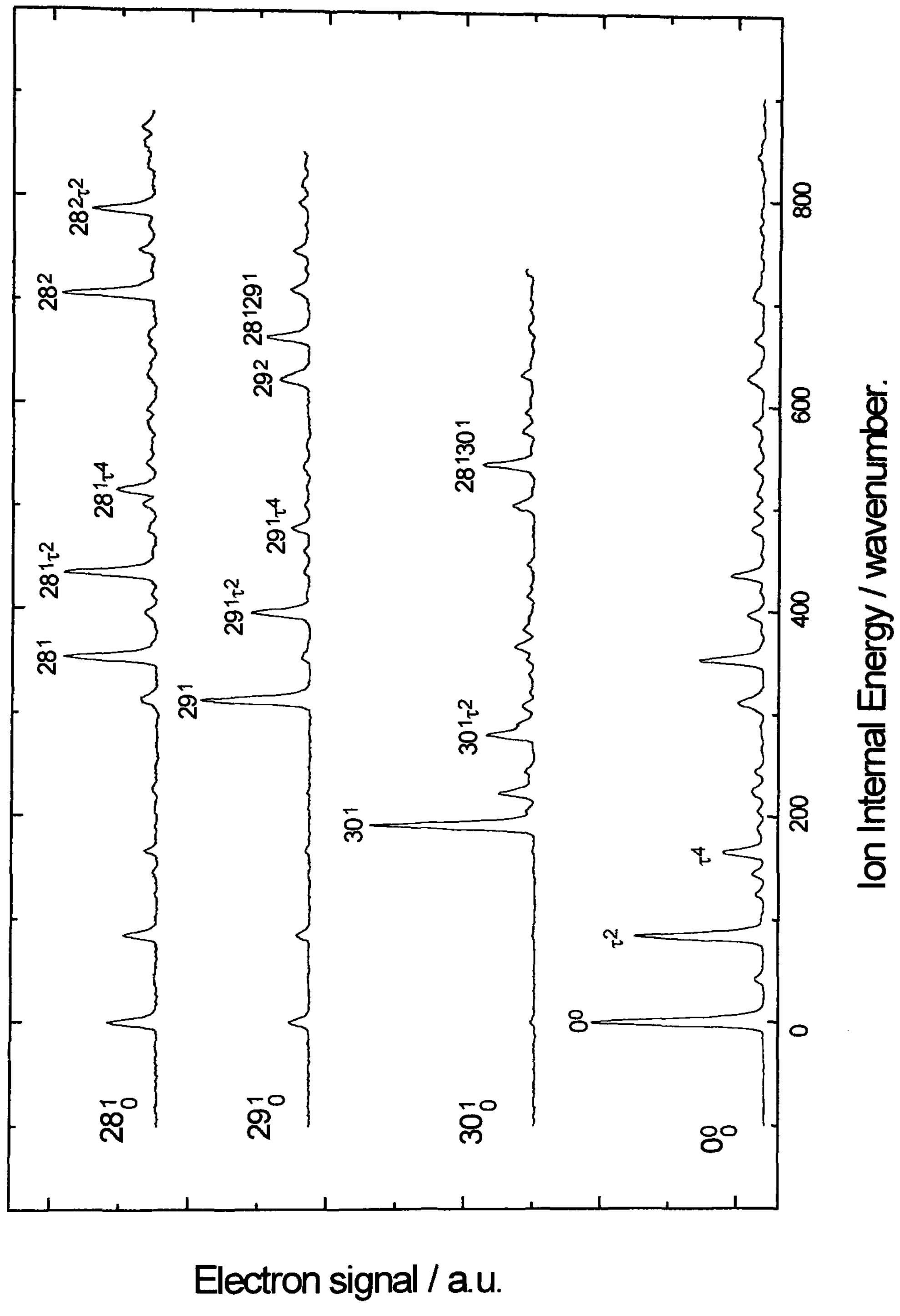

Figure A.3.3: (1+1') ZEKE-PFI spectra of the ionic ground state of 2-ABTF via several vibrational levels of the S_1 state.

Mode.	**Description**	**Sym.**	**S_0 $(\text{cm}^{-1})^a$**	**S_1 (cm^{-1})**	**D_0 (cm^{-1})**
ν_{28}	CF_3 rock	a'	352	349	354
ν_{29}	C-CF_3 stretch	a'	320	312	311
ν_{30}	C-CF_3 in-plane bend	a'	199	199	190
ν_{42}	NH_2 torsion	a''	-	145?	145

Table A.3.1. Vibrational frequencies for 2-ABTF in all three electronic states. (a) from reference 1.

A.3.3. 3-Aminobenzotrifluoride

A.3.3.1. The Ionic Ground State

The origin band of the ionic ground state of 3-ABTF is too weak for a full field dependence to be obtained. However such a procedure could be carried out for one of the higher torsional levels (τ^{11}). This is shown in figure A.3.4. The field free ionisation energy for this transition is 65655 cm^{-1}. Hence the ionisation energy for the origin band is 65450±3 cm^{-1}.

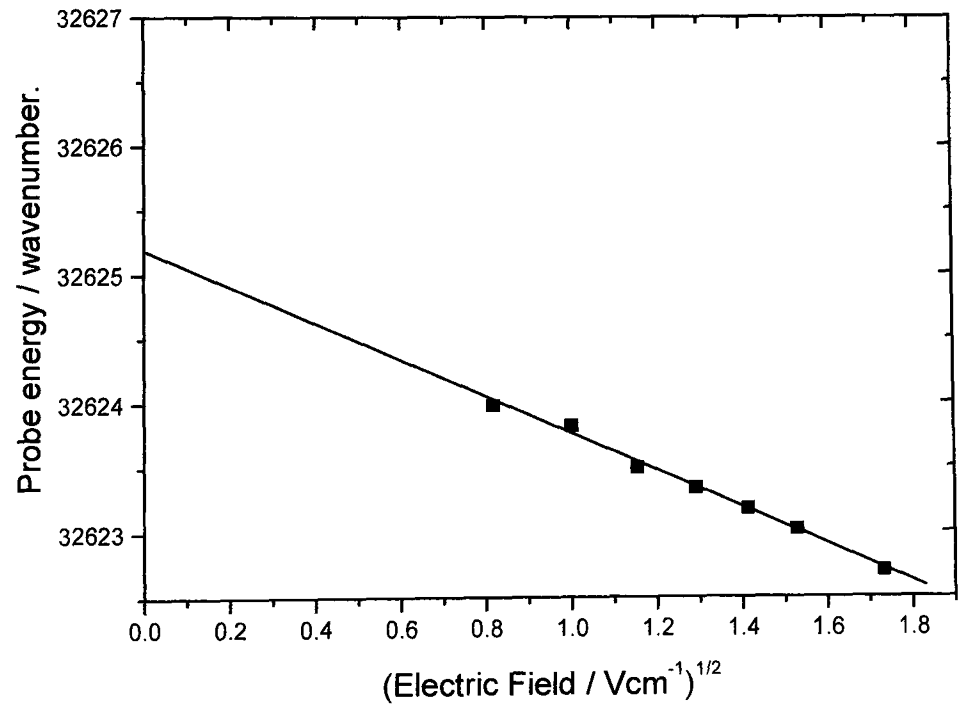

Figure A.3.4: The ionisation energy of τ^{11} of the ionic ground state of 3-ABTF at different extraction voltages.

A.3.3.2. Vibrational Structure

The (1+1) MPI spectrum of the S_1 state of 3-ABTF is shown in figure A.3.5. The vibrational modes observed are similar to those of the 2-isomer. The torsional structure of the vibrational levels is essentially identical to that of the origin band. This results in a very crowded spectrum[2].

Figure A.3.6. shows the two-colour ZEKE spectra via several vibrational levels of the S_1 state. Again the torsional structure is very similar to that of the vibrationless level although the spectra via ν_{29} (the C-CF_3 stretch) shows a smaller (and partially unresolved) torsional spacing. In addition the spectra via this intermediate shows considerable activity in the vibrational mode with both the origin and the first overtone having considerable intensity.

Table A.3.2. lists the vibraional frequencies of the vibrational modes observed for all three electronic states.

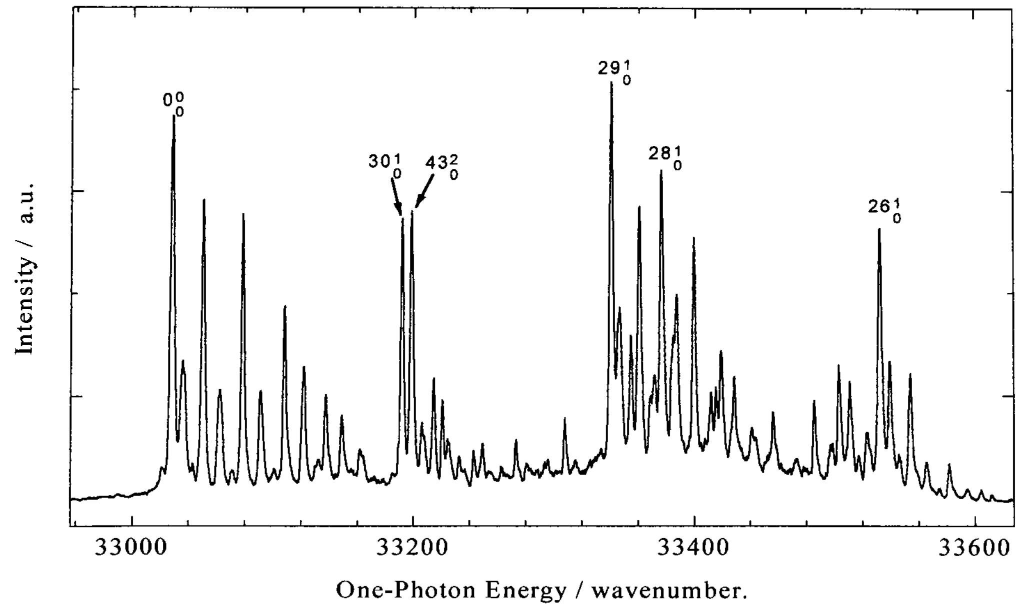

Figure A.3.5: The (1+1) MPI spectrum of 3-ABTF showing the vibrational structure of the S_1 state.

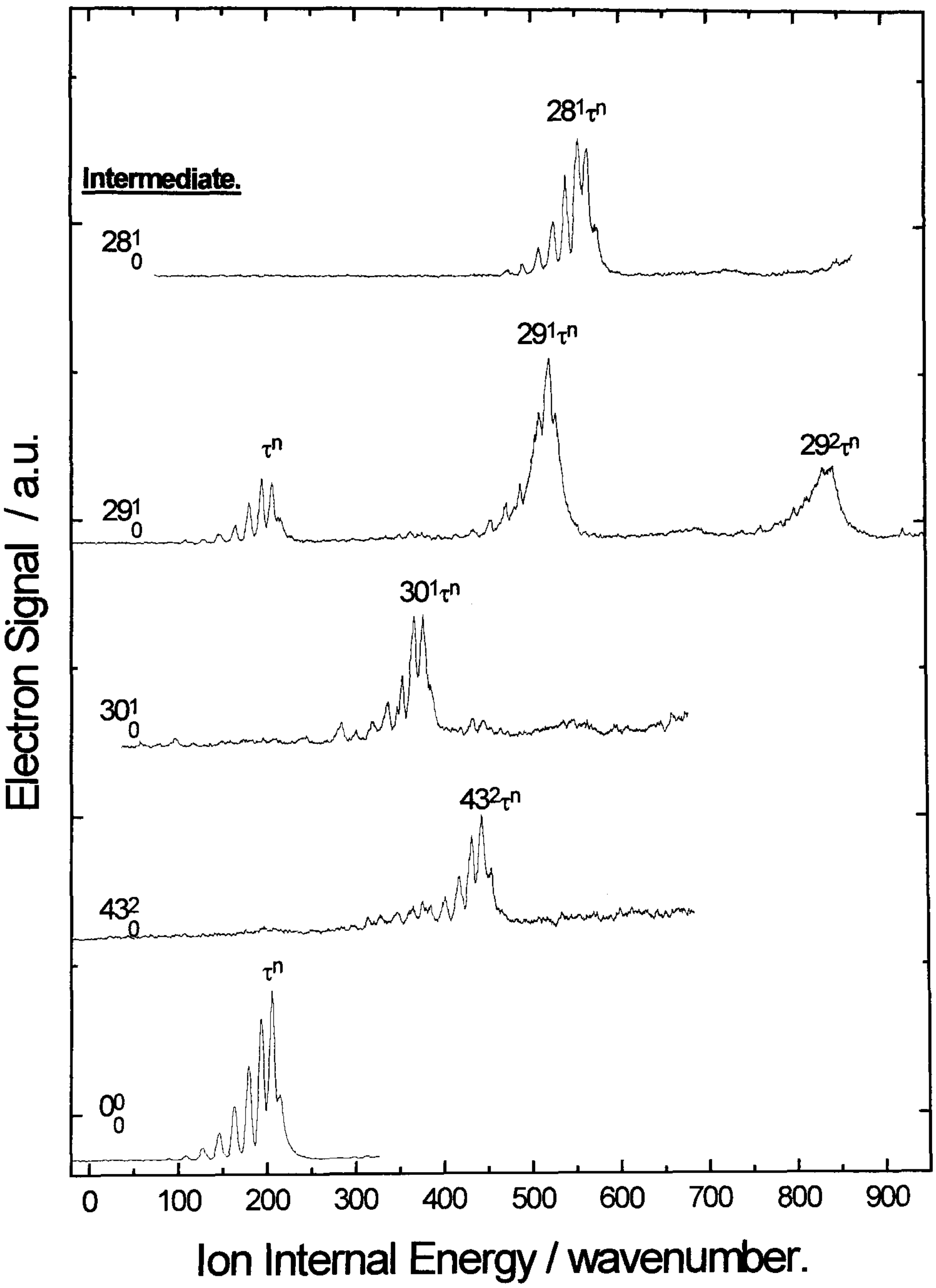

Figure A.3.6: The (1+1') ZEKE-PFI spectra of 3-ABTF via several vibrational levels of the S_1 state.

Mode.	**Description**	**Sym.**	**S_0 (cm^{-1})^a**	**S_1 (cm^{-1})**	**D_0 (cm^{-1})**
ν_{28}	CF_3 rock	a'	349	348	359
ν_{29}	C-CF_3 stretch	a'	324	312	316
ν_{30}	C-CF_3 in-plane bend	a'	170	163	172
ν_{43}	C-CF_3 out of plane bend	a''	123	85	119

Table A.3.2. Vibrational frequencies for 3-ABTF in all three electronic states. (a) from reference 2.

A.3.4. 4-Aminobenzotrifluoride

A.3.4.1. The Ionic Ground State

The ionisation energy of the origin band of the neutral ground state of 4-ABTF at a variety of extraction voltages is shown in figure A.3.7. The field free ionisation energy is 65886±3 cm^{-1}.

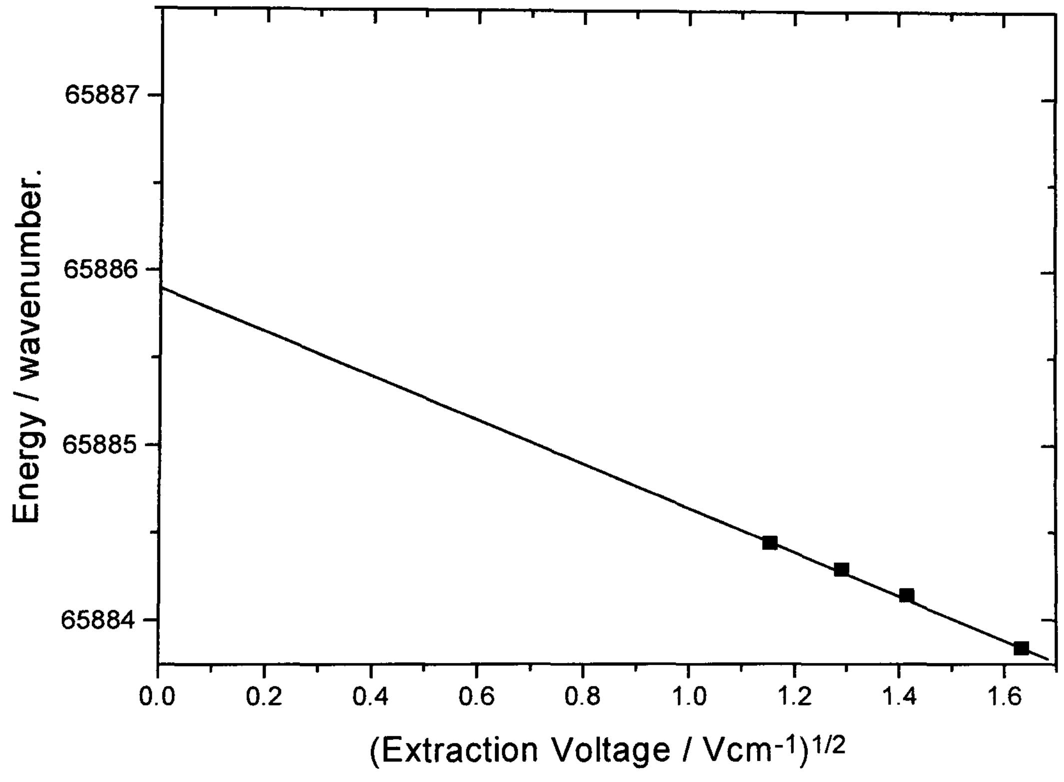

Figure A.3.7: The ionisation energy of the origin band of the ionic ground state of 4-ABTF at a variety of extraction voltages.

A.3.4.2. Vibrational Structure

The (1+1) MPI spectrum of the S_1 state of 4-ABTF was shown in figure 5.21. The vibrational structure observed is different to that of the other isomers since 4-ABTF can be classified under C_{2v} symmetry[3]. The limited torsional structure also allows the vibrational structure to be more clearly resolved particuarly in the region of the amine inversion (see chapter 5). Several non-totally symmetric modes (ν_{28} and ν_{40} for example) appear as a consequence of the small torsional spacing. These modes are actually hot bands of the torsional vibration in combination with the vibration[3].

Figures A.3.8. and A.3.9. show the ZEKE spectra via a number of these vibrational intermediates. The extraction field was such that the torsional structure was not resolved (see chapter 3). Table A.3.3. lists the vibrational frequencies for the observed normal modes in all three electronic states.

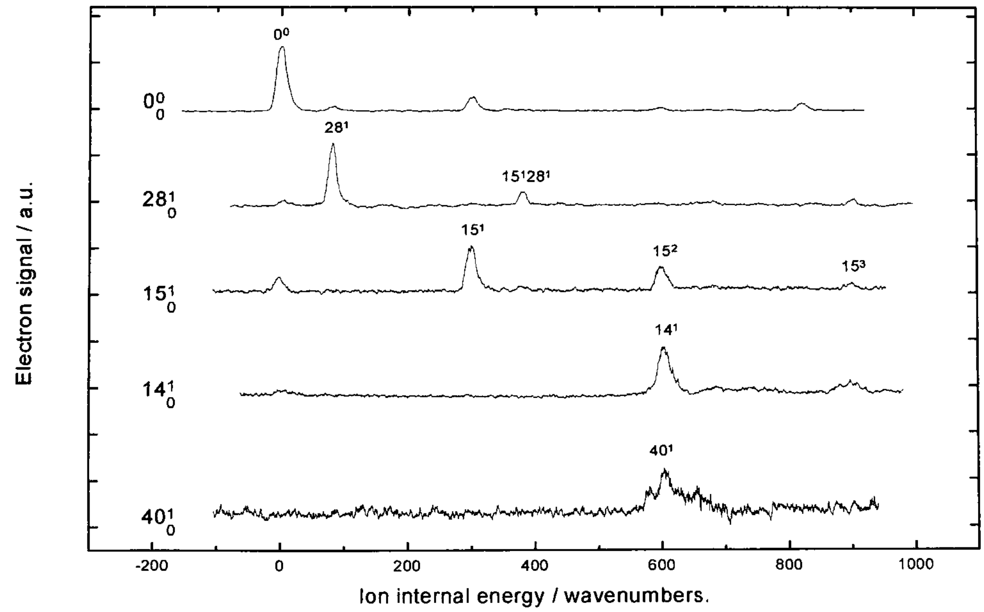

Figure A.3.8: The (1+1') ZEKE-PFI spectra of 4-ABTF via a number of the vibrational levels of the S_1 state.

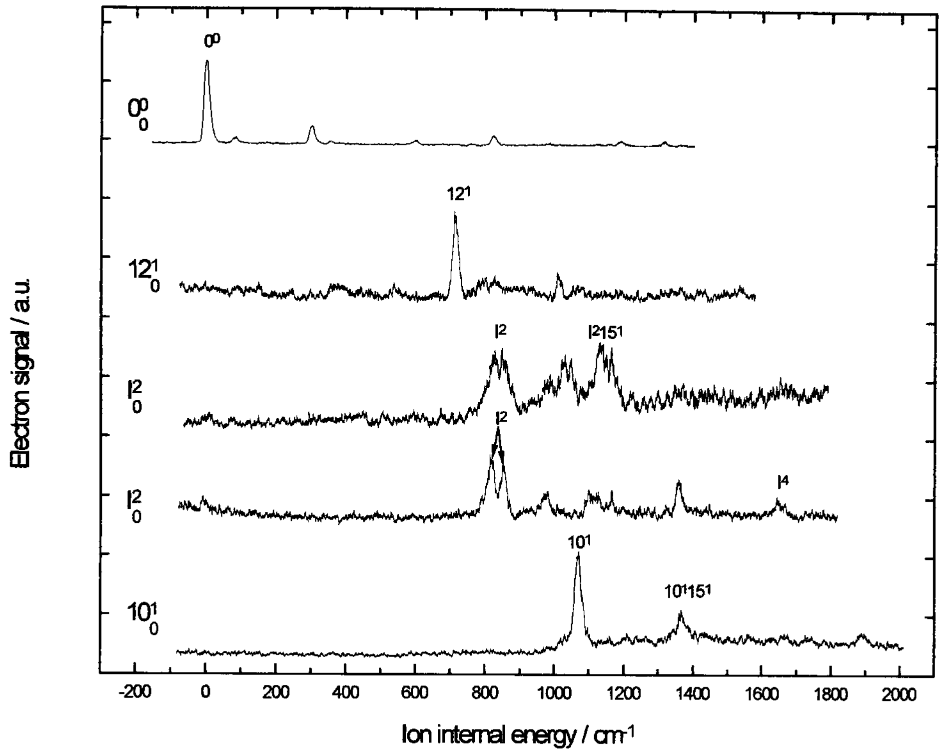

Figure A.3.9: The (1+1') ZEKE-PFI spectra of 4-ABTF via a number of the vibrational levels of the S_1 state.

Mode.	**Description**	**Sym.**	**S_0 (cm^{-1})^a**	**S_1 (cm^{-1})**	**D_0 (cm^{-1})**
ν_{10}	C-C stretch	a_1	1065	1036	1070
ν_{12}	ring in-plane bending	a_1	835	387	715
ν_{14}	ring in-plane bending	a_1	604	580	600
ν_{15}	C-CF_3 stretch	a_1	310	298	300
ν_{28}	C-CF_3 in-plane bending	b_1	90	76	81
ν_{40}	ring in-plane bending	b_2	639	538	600
I (ν_{29})	NH_2 inversion	b_1	72?	405/410	409/426

Table A.3.3. Vibrational frequencies for 4-ABTF in all three electronic states. (a) from reference 3.

A.3.5. Discussion

In general all three isomers display vibrational spectra which have a torsional structure very similar to that of the vibrationless state. The main exception appears to be the C-CF_3 stretch (ν_{29}) of 3-ABTF where a smaller torsional spacing is found. Since the existence of a barrier to internal rotation in this molecule depends on the hyperconjugation of the molecular orbitals of the rotor with that of the π-system of the ring[4] it is not surprising that a motion which involves the rotor-ring bond stretching has such an effect. For the other two modes such an effect is absent since steric effects are the major cause of the barrier to internal rotation.

A.3.6. References

1. P.J.A. Ribeiro-Claro, J.J.C. Teixeira-Dias, R.D. Gordon & J.M. Hollas. *J.Mol.Spectrosc.* 1993, **162**, 426.
2. P.J.A. Ribeiro-Claro, J.J.C. Teixeira-Dias, R.D. Gordon & J.M. Hollas. *J.Mol.Spectrosc.* 1991, **150**, 46.
3. P.J.A. Ribeiro-Claro, J.J.C. Teixeira-Dias, R.D. Gordon & J.M. Hollas. *J.Mol.Spectrosc.* 1991, **149**, 34.
4. K.T. Lu, F. Weinhold & J.C. Weisshaar. *J.Chem.Phys.* 1995, **102**, 6787.

Appendix 4. Lectures and Conferences.

Lectures.

"Advanced Spectroscopic and Dynamical Techniques"

Dr. P.R.R. Langridge-Smith. (10 lectures).

"2nd EPSRC Laser Spectroscopy Summer School"

East-Anglia, September 1997. (25 lectures).

"Short Course on Resonance Ionisation"

UMIST, June 1998. (4 lectures).

Physical Section Seminars. October 1996-June 1999.

Conferences.

International Workshop on Photoionisation Dynamics, Rydberg States and Large-Amplitude Motion. York. November 1996.

Ultra-fast Spectroscopy. East-Anglia. September 1997.

European Research Conference on Very High Resolution Spectroscopy with Photoelectrons. Emmetten, Switzerland. September 1997.

RSC Faraday Discussion 108. Sussex. December 1997.

Resonance Ionisation Spectroscopy 1998. UMIST. June 1998.

Physical Section Annual Meeting. Firbush Point Centre. 1997-99.

Appendix 5. Publications.

Publications.

Ionic and Rydberg states of CF_3I studied by high-resolution (ZEKE-PFI) and resonance-enhanced multiphoton-ionisation spectroscopy.

N.A. Macleod, S. Wang, J. Hennessy, T. Ridley, K.P. Lawley & R.J. Donovan. *J.Chem.Soc.Faraday Trans.* 1998, **94**, 2689.

High resolution photoelectron (ZEKE-PFI) spectrum of IBr: the role of repulsive intermediate states.

D.A. Beattie, N.A. Macleod, K.P. Lawley & R.J. Donovan. *J.Electron Spectrosc.Relat.Phenom.* 1998, **97**, 191.

Posters.

Coherent two-photon ZEKE-PFI of IBr.

European Research Conference on Very High Resolution Spectroscopy with Photoelectrons. Emmetten, Switzerland. September 1997.

REMPI and ZEKE studies of CF_3I.

RSC Faraday Discussion 108. Sussex. December 1997.

High Resolution Photoelectron (ZEKE-PFI) Study of Trifluoromethyl Iodide (CF_3I).

Physical Section Annual Meeting. Firbush Point Center. August 1998.

Appendix 6. List of Tables and Figures

Tables.

Figures.